# Stochastic Analysis of Dense Nonaqueous Phase Liquid Dissolution in Naturally Heterogeneous Subsurface Systems

by

Xin Fu

B.S., Tsinghua University (1997)
M.S., University of Delaware (1999)

Submitted to the Department of Civil and Environmental Engineering
in partial fulfillment of the requirements for the degree of

Doctor of Philosophy

at the

MASSACHUSETTS INSTITUTE OF TECHNOLOGY

Feburary 2003





Signature of Author.....
Department of Civil and Environmental Engineering
22 November 2002

Certified by.....
Lynn W. Gelhar
Professor, Civil and Environmental Engineering
Thesis Superviser

Accepted by.....
Oral Buyukozturk
Chairperson, Department Committee on Graduate Students

# Stochastic Analysis of Dense Nonaqueous Phase Liquid Dissolution in Naturally Heterogeneous Subsurface Systems

by

Xin Fu

Submitted to the Department of Civil and Environmental Engineering
on 22 November 2002, in partial fulfillment of the
requirements for the degree of
Doctor of Philosophy

## Abstract

Field-scale Dense Nonaqueous Phase Liquid (DNAPL) dissolution in three-dimensional heterogeneous subsurface systems is investigated using a stochastic approach that treats the variability of flow properties as three-dimensional random fields. A steady-state, quasi-static DNAPL saturation distribution in a source zone is derived, based on the previous research to describe the field-scale nonuniform residual DNAPL distribution. A local-scale dissolution model is generalized from the laboratory experimental results. Effective transport and dissolution properties are obtained by a stochastic analysis, which includes nonstationarity in the concentration field to address both boundary and downstream effects. An extrapolation of the effective properties is performed for the large spatial variability of hydraulic and dissolution parameters. The extrapolation is evaluated using a unique two-zone model that simplifies the continuous DNAPL distribution to two components: low permeability lens zone with high DNAPL saturation and a surrounding permeable zone with low DNAPL saturation. The agreement between the two-zone model results with stochastic solutions demonstrates the adequacy of the extrapolation of the latter. Four field sites with different geological settings and hydraulic characteristics are evaluated using effective properties: the Borden site, the Cape Cod aquifer, the Savannah River Site and the Hanford site. The theoretical prediction is compared with the DNAPL concentration data from the Hanford site, where millions of pounds carbon tetrachloride were dumped in disposal facilities. In spite of the error and uncertainty involved in the field data, there is reasonable agreement between the field observations and the predicted mean DNAPL concentration field. It is concluded that the dominant factor affecting the field-scale DNAPL dissolution is the variability of the dissolution rate coefficient, which is a function of spatial distribution of DNAPL and permeability. The bypassing effect, reflecting the diversion of water flow around zones of high DNAPL saturation with low aqueous relative permeability, is another important factor that can reduce the effective dissolution rate significantly. The limitations of the study are discussed regarding the data collection and further evaluation of the extrapolation.

Thesis Superviser: Lynn W. Gelhar
Title: Professor, Civil and Environmental Engineering

# Acknowledgment

This research was supported in part by the National Science Foundation through Grant No. BES-9616947.

I would like to thank my advisor Lynn Gelhar for his patience, tolerance and support during the my three and half year here at MIT. I feel very lucky to have a chance to work with Lynn. The insight he has in this field guides me into the deep part of the research. And the way he guides students is an art reflecting a great personality. I also like to thank my other committee members: Dennis McLaughlin, Phil Gschwend and Charley Harvey. The discussions with them are very helpful for me to understand the different aspects of the problem. I like to thank Paul Imhoff for providing the data of the laboratory dissolution experiments. Virginia Rohay and Raz Khaleel provide valuable information about the Hanford site. Thanks also go to Bruce Jacobs and Quanlin Zhou, for generously sharing their knowledge about the DNAPL.

I would like to thank the fellow Parsonites: Sheila is always there to take care of everything. Friends and officemates make life here easier and more enjoyable: Rachel, Steve, Nicole, Emily, Gavin, Susan, Jingfeng, Matt, Meng-Yi, Yoshi, Yamahi, Zhenhua, Guangda...

I also like to thank George Kocur who kindly provided me a teaching assistant position to help me finish the work without worrying about the tuition.

I would like to thank my parents and my brother, who are thousands miles away but always with me. I also want to mention all friends in the Dragon soccer team. Nothing can relax me more than playing with you guys.

At last, I would like to dedicate this work to my wife, Mindy, for everything she gives me: love, support, encouragement, understanding, lunch, dinner...

# Contents

# List of Figures

# List of Tables

# Chapter 1

# Introduction

## 1.1 Background

### 1.1.1 Overview

Organic fluids that are immiscible with water, also known as nonaqueous phase liquids, or NAPLs, are common sources of groundwater contamination. As a result of widespread production, transportation, utilization and disposal of DNAPLs, which are NAPLs denser than water, there are numerous DNAPL contamination sites in North America (Cohen & Mercer, 1993). DNAPLs are introduced into subsurface systems, usually by long-term spill or disposal activities and eventually reach, and be entrapped in, a saturated zone. The lateral spreading of DNAPL is enhanced by the spatial heterogeneity/anisotropy of porous media and DNAPL source zone can extend to a scale of tens of meters or even larger at a field site (Kueper *et al.*, 1989). Previous work has shown that, as a result of slow mass transfer between the nonaqueous phase and the aqueous phase, DNAPLs can become a long-term source of groundwater contamination (Cohen & Mercer, 1993). The traditional remediation method of DNAPL spills by pump-and-treat in practice has been demonstrated to be a costly operation with low efficiency. In laboratory column experiments of centimeter scale, researchers usually observed the equilibrium concentration in effluent when pumping water through porous media with DNAPL spills. But this was rarely the case in field where the effluent concentration was found far below the effective solubility. Engineers frequently observed a long tailing in the evolution of remediation. And the groundwater sample concentration usually is less than 10% of the effective solubility.

Zhang and Brusseau (1999) numerically simulated field-scale remediation of DNAPLs by pump-and-treat and hypothesized several processes to explain the tailing effect. They concluded that the dissolution of immiscible-liquid saturation is most likely the primary cause for this observation. Miller *et al.* (1998) discussed the possible contribution of the residual saturation of DNAPL to this tailing observation and found that this rarely occurred in small-scale lab experiments with uniform DNAPL distribution. Researchers have realized that this observation can be attributed to geologic complexities in natural systems (Mackay *et al.*, 1986). While groundwater concentrations are often the basis of the health concerns and the regulated cleanup level, it is of particular importance to understand the large-scale DNAPL dissolution process in the saturated aquifer in natural porous media systems, under the impact of heterogeneity.

Organic chemists and chemical engineers have extensively investigated the mass transfer mechanics between organic chemicals and the aqueous phase. Widely accepted mass transfer models have been established (Schwarzenbach *et al.*, 1993). Mass transfer between immiscible fluids in porous media has been studied extensively in the last twenty years, primarily in laboratory experiments and numerical simulations. Laboratory experiments were mostly conducted in one-dimensional columns packed with homogeneous porous media (Miller *et al.*, 1990; Powers *et al.*, 1992; Geller and Hunt, 1993; Imhoff *et al.*, 1994; Powers *et al.*, 1994; Mayer and Miller, 1996; Powers *et al.*, 1998). Most of these studies focused on DNAPL dissolution with uniformly distributed residual saturation through columns. Dimensional analysis is applied to establish empirical models characterizing the dissolution process, which correlate the mass transfer coefficient with flow properties, DNAPL saturation and porous media characteristics.

However, it is likely that DNAPL dissolution has distinct field-scale properties from their laboratory-scale descriptions. Numerical studies can provide a tool to investigate large-scale dissolution processes including the impact of spatial heterogeneity of porous media, though it cannot provide a systematic solution to quantify the impact of heterogeneity. Another research area crucial to investigate field-scale dissolution is DNAPL saturation distribution resulted from multiphase flow. Characterization of a DNAPL source zone has proved to be a difficult task due to the heterogeneous distribution of DNAPL, low saturation and DNAPL density flow deep under the water table.

Field-scale DNAPL dissolution is more complicated as a result of difficulty of characterizing

the spatial heterogeneity of DNAPL saturation and wetting phase flow field. The nonwetting phase liquid prefers to flow in the largest pores due to the capillary effects, though under high capillary pressure this phase can penetrate into a proportion of small pores. At the balance of the capillary force with viscous and buoyancy forces, DNAPL entrapped in some proportion of the pores in a discontinuous globular state, which may exist in a single isolated pore or as ganglia occupying multiple pores (Schwille, 1988). At the scale of interest (tens to hundreds of meters), the heterogeneity of porous media has been manifested as layers or lenses with contrasting permeability, and corresponding capillary characteristics. Lenses or layers with lower permeability than the surrounding porous media act as barriers to the DNAPL. Because of these heterogeneous structures, DNAPL tends to have nonuniform distribution once spilled in a natural subsurface system. It may be trapped by capillary forces as ganglia that typically occupy 1-20% of the pore space, known as residual saturation, or pools of continuous DNAPL that may fill $>$ 50% of the pore openings. Researchers have observed that both small and large-scale heterogeneity in the pore size distribution can give rise to significant variations in the saturation of entrapped DNAPL (Illangasekare *et al.*, 1995).

This spatial heterogeneity, which significantly affects the contact area between immiscible phases, has been suspected to be a primary factor affecting large-scale dissolution. Both experimental observations and model evaluations indicated that very localized variations in the DNAPL saturation, and consequently the relative permeability, contribute to preferential flow paths and the establishment of dissolution fingers in columns packed homogeneously with uniform sand, which essentially lead to nonuniform dissolution patterns (Imhoff & Miller, 1996). Even in a relative "homogeneous" system, the effects of small-scale heterogeneities on the overall dissolution process have been observed in column experiments (Imhoff *et al.*, 1994). The scaling issue, interlinked with spatial heterogeneity and flow dimensionality, is the major factor restricting more general application of the column models to the large-scale dissolution problem with spatial heterogeneity. Quantitatively characterizing the spatial heterogeneity, including the porous media heterogeneity, DNAPL saturation distribution and wetting phase flow field, and incorporating the dissolution model is the focus of this investigation of the large-scale dissolution problem. These important characterizations are addressed in this work and the large-scale dissolution properties are obtained.

## 1.2 Related Work

A large number of laboratory experiments have been conducted to investigate the DNAPL dissolution in porous media. Some early experiments were conducted in one-dimensional columns packed with homogeneous porous media where residual DNAPL saturation was established (Imhoff *et al.*, 1994; Miller *et al.*, 1990; Powers *et al.*, 1992; Geller and Hunt, 1993; Powers *et al.*, 1994). Most of these studies focused on DNAPL dissolution with uniform distributed residual saturation through columns. By varying DNAPL species, water velocity, DNAPL initial saturation and soil types, the controlling factors of the dissolution rate coefficient were investigated in experiments. Dimensionless empirical models were established based on experimental data, which established relationships between the mass transfer coefficient and flow properties, DNAPL saturation and porous media characteristics. This scenario is elaborated in Chapter 3 where local-scale dissolution characterization is discussed in detail.

With the progress of column experiments, researchers realized that spatial heterogeneity can be important to affect the dissolution. Later research has focused on lab experiments, numerical simulations and field experiments to address the effect of geological heterogeneity on dissolution scenario on various scales. Laboratory experiments mainly studied the one-dimensional or two-dimensional DNAPL dissolution with initially non-uniform residual saturation. Usually a high-saturation DNAPL zone is established within the porous media to allow the investigation of bypassing.

Geller and Hunt (1993) conducted experiments in the column which contained a contaminated zone with high DNAPL saturation and a surrounding clean zone. They found a pronounced tailing of DNAPL concentration evolution, which is significantly different from the results of column experiments with uniform DNAPL distribution. Soerens and coworkers (1998) used two conceptual models to address the effects of nonuniform DNAPL distribution and flow bypassing on nonequilibrium mass transfer for DNAPL dissolution. This study found the apparent mass transfer kinetics of DNAPL dissolution could be accounted for by the heterogeneity of DNAPL distribution and porous media properties. Some two-dimensional experiments were conducted to incorporate the effects of heterogeneity and dimensionality, which were difficult to study in one-dimensional column experiments. Saba and Illangasekare conducted DNAPL dissolution experiments in a two-dimensional cell packed with homogeneous porous media (Saba

& Illangasekare, 2000). A contamination source was prepared outside and placed into the cell as a DNAPL pool. Compared to column experiments, they found the time scale of the dissolution process increased significantly. This work provided insight into how the heterogeneity of DNAPL distribution influences the mass transfer behavior. Powers and coworkers (1998) conducted dissolution experiments in a cell packed with fine sand surrounding imbedded coarse sand lens (Nambi & Powers, 2000). DNAPL was injected into coarse sand lenses directly to form the initial saturation. The work investigated the effect of flow conditions, DNAPL saturation and heterogeneity of porous media on the mass transfer rate. Equilibrium concentration was found in effluent extracted from the ports adjacent to the DNAPL pool. However, effluent far from the source was found far below the equilibrium concentration. The reason could be the dilution and bypassing effect caused by the nonuniform DNAPL distribution. An intermediate-scale two-dimensional flow cell experiment was conducted to study the migration of liquid Trichloroethylene (TCE) and the transport of dissolved TCE in a saturated heterogeneous porous medium (Oostrom *et al.*, 1999). It was found the nonuniform distribution of entrapped TCE was caused primarily by the heterogeneity of the porous media. A local model developed from a one-dimensional experiment cannot explain the observed effluent concentration of dissolved TCE. Also Imhoff discussed dissolution fingers due to the nonuniform flow and dissolution, even in a relatively homogeneous environment (Imhoff & Miller, 1996).

DNAPL pool dissolution was investigated broadly in laboratory experiments. Sale *et al.* (2001) established a mathematical model to calculate the dissolution rate from a DNAPL pool based on experimental results. Seagren (1999) conducted column experiments and mathematical modeling to characterize the DNAPL pool dissolution. They found the local equilibrium model represent the data well for all practical flow rates. Only in the very large flow rate (pore water velocity>18m/d) the nonequilibrium model gave a better fitting results. However, the pool in this experiment was put on top of the porous media with a confined glass wall around except on the bottom side where the pool was in contact with porous media. This kind of setup made it difficult to investigate the natural bypassing effect around the pool. Moreover, most of these studies characterize the mass transfer between the DNAPL pool and flowing water using a vertical dispersion coefficient. Such studies have the limitation that the bypassing effect caused by the heterogeneity of porous media was not included.

Table 1.1 summarizes the results and conditions of some major experimental studies. It can be seen that the correlation models derived from these studies relate the Sherwood number $Sh$ with Reynold number Re, DNAPL saturation, Schmidt number $Sc$ for aqueous phase and median size of porous media. The definitions of the dimensionless numbers are listed below:

$$Sh = \frac{\Omega d_p^2}{D_m} \tag{1.1}$$

$$Sc = \frac{\mu_a}{\rho_a D_m} \tag{1.2}$$

$$\mathrm{Re} = \frac{v_a \rho_a d_p}{\mu_a} \tag{1.3}$$

where $\Omega$ is the mass transfer rate coefficient $(T^{-1})$, $d_p$ is the particle diameter $(L)$, $\mu_a$ is the aqueous phase viscosity $\left(ML^{-1}T^{-1}\right)$, $\rho_a$ is the aqueous phase density $\left(ML^{-3}\right)$, $v_a$ is the aqueous phase velocity $\left(LT^{-1}\right)$and $D_m$ is the molecular diffusion coefficient $\left(L^2T^{-1}\right)$.

Table 1.1: Summary of Results and Conditions of Major DNAPL Dissolution Experiments

| Reference | Empirical Model | Scale length×diameter(1D) |
|---|---|---|
| Miller, C.et al. (1990) | $Sh = 12\,(\phi - \theta_n)\,\mathrm{Re}^{0.75}\,\theta_n^{0.60} Sc^{0.5}$ | 1D homogeneous 9cm×2.5cm |
| Powers, S. et al. (1991) | $Sh = 57.7\,\mathrm{Re}^{0.61}\,d_{50}^{0.64} U_i^{0.41}$ | 1D homogeneous 3-5cm×5.5cm |
| Geller, J. et al. (1993) | $Sh = 70.5\,\mathrm{Re}^{1/3}\,\theta_n^{4/9} S_{n_i}^{5/9} \phi^{-2/3} \left(\frac{d_{50}}{d_{ni}}\right)^{5/3b}$ * | 1D with one lens 15cm×5cm |
| Imhoff, P et al. (1994) | $Sh = 340\,\mathrm{Re}^{0.71}\,\theta_n^{0.87}\,(x/d_{50})^{-0.31}$ | 1D homogeneous 3cm(7cm)×8.25cm |
| Powers, S et al. (1994) | $Sh = 4.13\,\mathrm{Re}^{0.598}\,\delta^{0.673} U_i^{0.369} \left(\frac{\theta_n}{\theta_{n_i}}\right)^{\beta}$ | 1D homogeneous 3-5cm×5.5cm |
| Powers, S et al. (1998) | N/A | 2D with one lens 10cm×17.8cm |
| Saba, T et al.(1998) | $Sh = 11.34\,\mathrm{Re}^{0.2767}\,(d_{50}\theta_n/\tau L)^{1.037}\,Sc^{0.33}$ | 2D with multiple lens 2.2m×1.1m |

Note:

1.$Sh$ NAPL-aqueous phase Sherwood number; $\phi$ porosity, $\theta_n$ DNAPL volume fraction, Re aqueous phase Reynolds number, $Sc$ aqueous phase Schmidt number, $d_{50}$ median grain size diameter, $S_n$ DNAPL saturation, $U_i$ uniformity index, $d_{ni}$, $\theta_{n_i}, S_{ni}$ initial DNAPL sphere diameter, DNAPL volume fraction and DNAPL saturation before dissolution, $\delta$ normalized grain size, $\tau$ sand tortuosity, $L$ contaminated zone length, $x$ is the length of dissolution front.

2. * Formula was summarized by Miller, C. et al. 1998.

Numerical simulations were developed to address the DNAPL spill and dissolution issue on

a large scale. These studies normally simulated the DNAPL infiltration into the heterogeneous aquifer in the first step and obtained a spatial distribution of residual DNAPL saturation. Then a local mass transfer model was assumed to investigate the DNAPL dissolution evolution based on some input parameters. Guiguer presented a three-dimensional numerical simulation for the migration of DNAPL, where the dissolution process was considered as a first-order kinetics (Guiguer, 1993). This work particularly examined the effects of heterogeneities on the evolution of contaminant plumes. However, the model proposed by this work is too simplified to include some important features. Dekker recently conducted a numerical study about DNAPL entrapment in a heterogeneous aquifer and tested the sensitivity of DNAPL redistribution to various input parameters, such as the correlation scale and residual saturation (Dekker & Abriola, 2000). This work provided understanding of the control parameters of DNAPL redistribution under field conditions. Zhu studied the field-scale transport with mass transfer numerically (Zhu *et.al*, 2000). Their work found that the heterogeneity of the permeability field had the most significant influence on the mass transfer process in subsurface systems. A similar conclusion was reached in another numerical study by Mayer and Miller, who found that spatial heterogeneity was critical to study large-scale DNAPL dissolution (Mayer & Miller, 1996). On the contrary, numerical analysis by Unger and coworkers concluded that natural heterogeneity of an aquifer has less impact on the dissolution behavior in the DNAPL source zone relative to the local mass transfer characterization (Unger *et al.*, 1998). However, in that study a critical drawback existed which might make the conclusion misleading. Unger's study assigned a very large longitudinal dispersivity of 0.5 m, which is ten times more than the typical local value. This inappropriately large dispersivity gave rise to a large dispersion effect which might offset the influence of natural heterogeneity, resulting in the implausible conclusion. In addition, the Leveratt scaling applied in the study neglect the variation of the characteristic coefficient in the pressure-saturation models that represents the slope of the curve. This variation was reported significantly to affect the DNAPL flow and transport by Jacobs (1998). The exclusion of this variation will lead to the underestimation of the effect of spatial variations on the transport properties.

While mass transfer from DNAPL to aqueous phase can be kinetically controlled or at equilibrium under laboratory conditions, aqueous concentrations in the field are generally found

to be below equilibrium levels (Feenstra & Cherry, 1988). Frind *et al.* (1999) conducted a field experiment at the Borden site in Canada, using an emplaced DNAPL source to investigate the mass transfer process under field conditions. Because of the artificially-made homogeneous DNAPL source, their work was unable to study the sensitivity of the mass transfer process with respect to heterogeneity of the source zone. A similar subsequent experiment was conducted by Rivett and coworkers (Rivett *et al.*, 2001) using the emplaced source at the same site. Kueper (1993) studied DNAPL spatial distribution after spill into subsurface at the Borden site. It was found that the residual saturation of DNAPL is spatially variable and is a function not only the properties of the porous media and fluid, but also the history of the drainage. The extensive lateral spreading of DNAPL plume was observed significant. Regardless of various field-scale studies of DNAPL distribution and dissolution, a well-designed field experiment is not available yet to provide quantitative information of DNAPL dissolution under realistic conditions.

## 1.3 Motivation

Most laboratory experiments have illustrated the effect of simple heterogeneous structures on the DNAPL dissolution process. The experimental results were fitted by the empirical models obtained from column experiments, and the corresponding coefficients were obtained. Researchers intended to apply these empirical models to more general applications, such as a three-dimensional large-scale dissolution problem. However, the input properties in these models are hard to obtain in natural systems. Moreover, without using statistical information to address geological heterogeneity, the simple characterization of heterogeneity is not appropriate to study large-scale issues. Numerical investigations have the advantages that they can study more realistic large-scale problems, can incorporate complicated boundary configurations and the influence of boundary conditions for site-specific situations. However, numerical solutions cannot provide a general insight and lack the ability to identify the underlying controlling factors. Moreover, numerical simulations with overall scale of hundreds of meters require accurate characterizations at the scale of grid size, which may ranged to several meters or even tens of meters. The local scale results provided by laboratory experiments may not be suitable inputs in this case.

Based on the studies to date, there are still some unresolved problems of DNAPL dissolution.

First of all, a general study of dissolution in a nonuniform distributed DNAPL source zone in large-scale subsurface systems, incorporating natural heterogeneity, has not been available yet. As stated above, current approaches developed from the lab experiments and numerical simulations are not the adequate tools to investigate the process from a general view. Secondly, field observations have found that solute concentration was far below the equilibrium aqueous solubility of DNAPL and presented a prolonged tailing of concentration (Frind *et al.*, 1999). Which factor is responsible for the field scale kinetic observation: local mass transfer kinetics or natural heterogeneity? Therefore, theoretical investigations are needed to address DNAPL dissolution process in natural heterogeneous subsurface systems.

## 1.4 Objective and Approach

The overall objective of this research is to study field-scale DNAPL dissolution and solute transport in the entrapped DNAPL source zone with mass transfer between the DNAPL and the aqueous phase. The focus is on the effect of spatial heterogeneity of natural systems on large-scale DNAPL dissolution and solute transport. A specific focus is the bypassing effect, which is associated with diversion of water flow around zones of high DNAPL saturation as a result of low aqueous phase relative permeability. The result of the work can improve the understanding of the paradox of very low concentration frequently observed in field and equilibrium dissolution found in column experiments. Eventually we hope this analysis can provide a method to predict the mean concentration inside and outside of the source zone. More specifically, we aim:

- to provide an accurate characterization of local dissolution rate based on the affecting properties;
- to establish the statistical description of DNAPL saturation distribution and wetting phase flow field at the impact of heterogeneity;
- to develop a mathematical foundation for the processes of mass transfer between the DNAPL and the aqueous phase in the saturated zone which is based on statistical information describing properties of porous media and DNAPL saturation;
- to derive the large-scale dissolution properties which can be applied as inputs to numerical

simulations;

- to apply the theoretical solutions to field sites and predict the concentration profile in a DNAPL source at contaminated sites;
- to investigate the dominant factor controlling the field scale dissolution kinetics: spatial heterogeneity or local (small-scale) mass transfer kinetics.

In natural systems, given the complexity of the underlying mechanisms, it is practically impossible to completely characterize the spatial variability in deterministic model parameters. Numerous analyses demonstrated that natural systems and associated issues could be realistically modeled by means of stochastic concepts and methods. As a consequence, stochastic analysis can provide theoretical concepts and practical tools that can support up-scaling techniques. The objective of this analysis is to predict the large-scale mean response of the system as affected by high frequency local-scale variation. Methodologically it is a well-established approach to apply local scale results to more realistic field scale investigations (Gelhar 1993).

The spatial distribution of soil properties will be represented as the composite of two independent signals: a large-scale slowly varying deterministic mean and a high frequency random perturbation. Mean transport equations will be developed from the stochastic differential form of the local advection-dispersion equation. A linearized perturbation equation will be derived by subtracting the mean equation from the original equation. The equation derived will be utilized to describe the fluctuations of dependent variables as functions of fluctuations in soil properties and in mean flow parameters.

Stochastic analysis can capture the spatial and temporal variability of natural systems and derive the effective transport and transformation parameters, which can be compared directly with numerical results (Miralles-Wilhelm 1996, Jacobs 1998). The Eulerian approach will be applied to evaluate the stochastic partial differential equation describing solute transport. This approach is based on the assumptions that are physically meaningful and can be easily generalized to more complex transport problems (Gelhar 1993). The spectral representation will be applied to solve the stochastic differential equation. Spectral approach has the advantage that it involves relatively simple mathematical manipulations even for multidimensional systems (Gelhar 1993).

The reliability of results and their applicability under field conditions have been investigated by prior researchers. Gelhar and Axness (1983) investigated the macrodispersivity using stochastic analysis to quantify the effect of spatial variation of natural porous media on large-scale solute transport. The result has been widely used in theoretical and engineering practices since then. Miralles-Wilhelm (1996) investigated solute transport with sorption and/or biodegradation in groundwater systems incorporating the effects of natural aquifer heterogeneity. Effective properties, such as the effective retardation coefficient, were derived for the Borden and the Cape Cod sites using hydraulic parameters available. Polmann (1990) investigated the solute transport problem in the unsaturated zone. Macrodispersivity was evaluated for both transient and steady cases.

Figure 1-1 presents the major methodology and expected results of this work. As we see, the analysis is based on the transport equation within a large-scale DNAPL source zone. The local characterization provides important correlations between dissolution rate and affecting factors. DNAPL saturation distribution is characterized by statistical information and is incorporated into stochastic analysis. The derived effective properties are applied to field applications and provide accurate dissolution inputs for large-scale numerical simulations with a grid size at the scale of meters or tens of meters.

## 1.5 Thesis Overview

The major tasks of the study include local characterization of dissolution, DNAPL spatial distribution in field, development of effective properties based on stochastic analysis and applications of the theoretical results.

Chapter 2 studies the DNAPL distribution and wetting phase flow within a DNAPL source zone. This is an extension from the multiphase flow investigation by Jacobs (1998). The theoretical solutions of DNAPL saturation distribution and wetting phase flow field are obtained in forms of spatial moments of log permeability and transformation of capillary pressure saturation curve parameters.

Chapter 3 presents the local-scale dissolution characterization based on extensive laboratory column experiments reported in earlier work. The factors controlling dissolution rate have been identified and included in the partial correlation model, which is essentially equivalent with

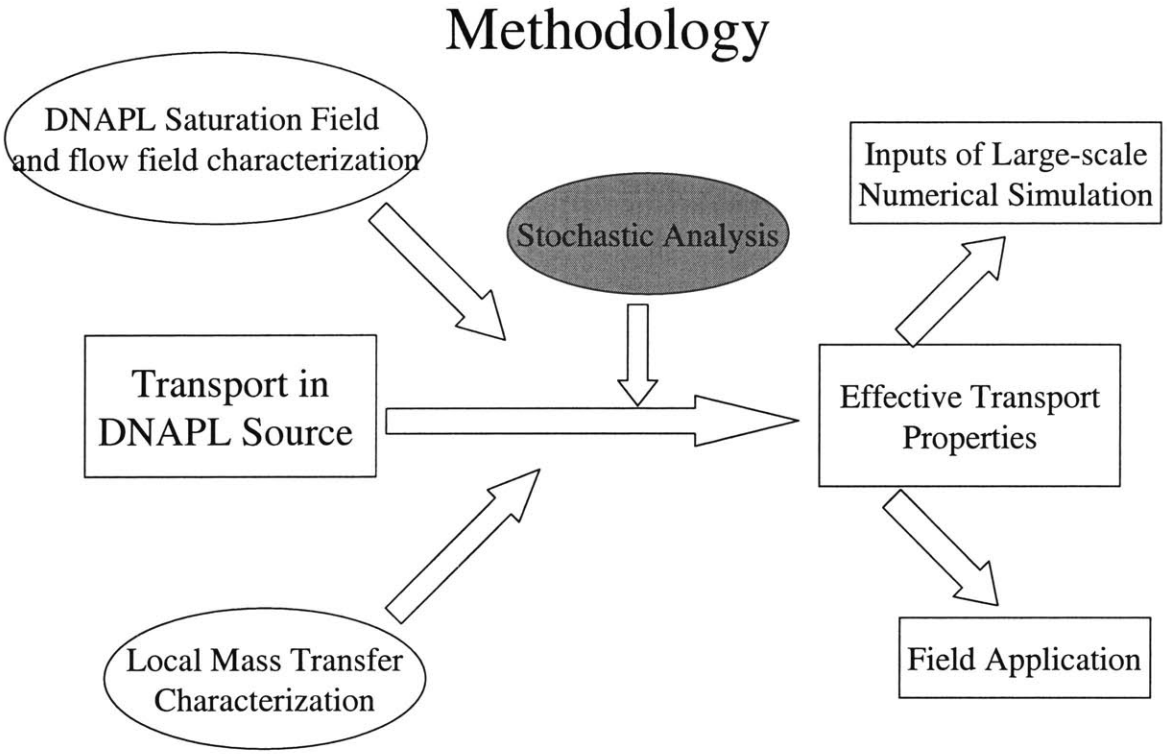


Figure 1-1: Illustration of the key methodology to investigate field-scale dissolution

the dimensionless models summarized in Table 1.1. The model is calibrated by two column experiments performed by Imhoff (1994) and Powers (1994).

Chapter 4 provides the analytical development of large-scale dissolution. The effective dissolution rate coefficient and effective dissolution distance are developed based on the stochastic analysis. The close-formed solutions are obtained by extrapolating the linearized results for large spatial variations of inputs. The impact of spatial variations of dissolution rate and bypassing effect are explicitly included in the solutions of effective properties.

In Chapter 5, a two-zone model is established to study the contribution of dissolution from two distinct DNAPL entrapment structures: DNAPL pools in lens zones and droplets in permeable zones. Moreover, by comparing the two-zone results with stochastic results at same set of inputs, the model provides an important tool to validate the extrapolation of the linearized effective properties performed in Chapter 4.

In Chapter 6, applications of the stochastic results are examined at four different sites with contrasting hydrogeological settings and extensive characterization data regarding hydraulic conductivity. Since the large-scale DNAPL contamination is not available, artificial contaminant events are established in the Borden site and the Cape Cod site. The Savannah River Site and the Hanford site are real DNAPL contaminated sites with considerable DNAPL source characterization. DNAPL concentration profiles are predicted based on theoretical solutions at the four sites. The agreement of theoretical results of concentration curve with measured data at the Hanford site reflects the plausibility of the analysis.

Chapter 7 serves as a summary and conclusion of the thesis. Primary findings and conclusions are summarized in the order of chapters. Limitations of the study are discussed and recommendations for future investigations are presented.

# Chapter 2

# DNAPL Saturation Distribution in a Source Zone

## 2.1 Introduction

### 2.1.1 Conceptual Background

DNAPL is usually introduced into subsurface systems by long-term spill or disposal activities (Cohen & Mercer, 1993). Figure 2-1 presents an illustrative diagram of DNAPL flow and distribution in the subsurface system. If enough DNAPL is released near the surface, it can migrate through the vadose zone, overcome the capillary resistance and penetrate into the saturated zone due to the density flow. Within the saturated zone, lateral spreading of DNAPL plume is promoted above finer layers and generally increases with decreasing permeability and grain size. The horizontal extent of DNAPL plumes can reach tens of meters according to field observations (Kueper *et al.*, 1993). DNAPL keeps flowing downward and spreading laterally until the source is exhausted or strong capillary resistant force is encountered. Mass transport and transfer within a large-scale DNAPL source zone is complicated by the heterogeneity nature of porous media and DNAPL distribution.

Heterogeneity is frequently observed in field and widely cited in discussions of immiscible phase field-scale transport (Kueper *et al.*, 1989). The large-scale entrapped DNAPL saturation distribution is mainly influenced by anisotropy and heterogeneity of porous media. As we can see in Figure 2-1, small-scale spatial heterogeneity determines the flow path of DNAPL and

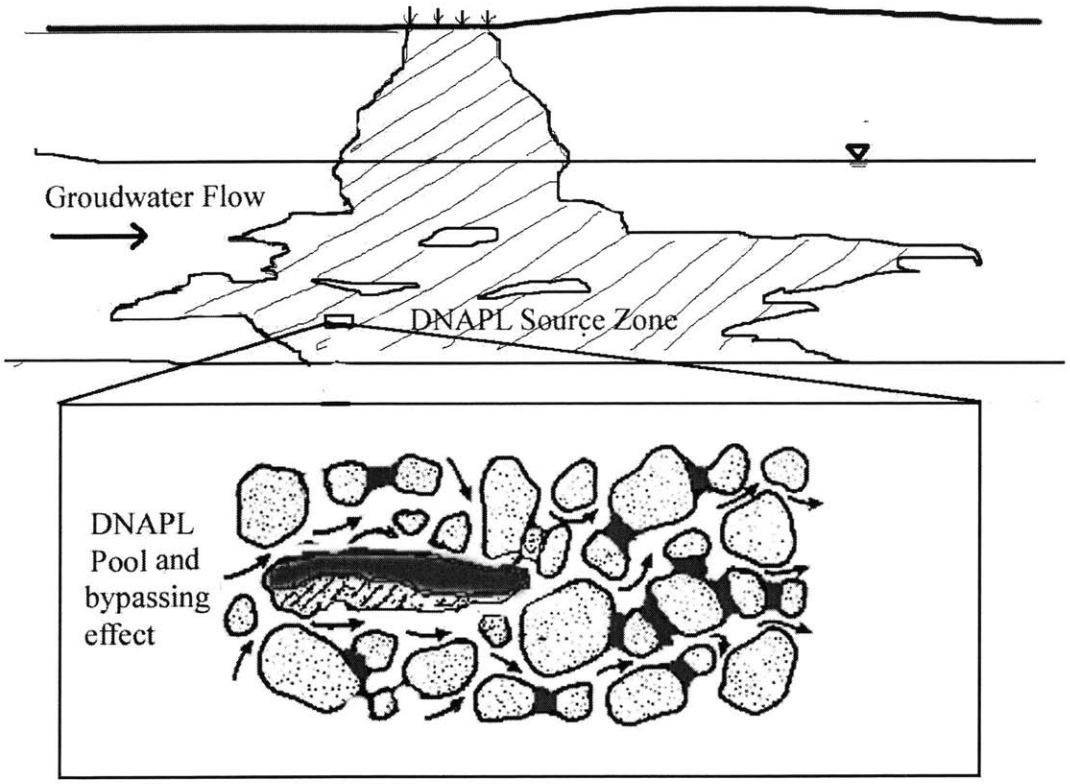


Figure 2-1: Macroscale and microscale illustration of DNAPL distribution and water flow field in a heterogeneous subsurface system

leads DNAPL occupy discontinuous lens in a relatively large saturation, called DNAPL pools. The DNAPL pools with relatively high saturation reduce the relative permeability of wetting phase flow significantly and tend to block the aqueous flow. Usually lens with DNAPL pools are with contrasting relative permeability and DNAPL saturation against regions around them. By directing the wetting phase flow to the region with larger relative permeability and less DNAPL saturation around the DNAPL pools, the portion of aqueous flow penetrating into DNAPL pools is significantly lower than those flowing around. This phenomenon is called bypassing and has been reported from local-scale and moderate-scale experiments (Nambi *et al.* 2000, Geller and Hunt 1993). Due to the impact of non-uniform distribution of DNAPL and heterogeneity of intrinsic permeability, wetting phase flow field can be highly variable in space.

DNAPL dissolves into groundwater when clean groundwater flows through the DNAPL source zone. According to numerous studies of DNAPL dissolution in porous media, it is concluded that DNAPL dissolution rate is a function of effective surface area of entrapped DNAPL exposed to flowing water and the rate of transport away the dissolved DNAPL by flowing water. Subsequently the DNAPL surface area is mainly determined by the characteristics of DNAPL saturation distribution and porous media properties. The transport rate of dissolved DNAPL is determined by the flow velocity of water around the entrapped DNAPL. In laboratory column experiments where DNAPL is distributed uniformly in a homogeneous porous media packing, the spatially invariable saturation and water velocity is assumed to characterize dissolution rate (Imhoff *et al.*, 1994). However, at the field-scale where the porous media is heterogeneous, DNAPL can be distributed in a highly non-uniform pattern in space with significant fluctuation. Similarly, due to the heterogeneous intrinsic permeability and the interrelated non-uniform DNAPL saturation distribution, the water flow may largely bypass regions of high DNAPL saturation. This gives rise to a highly variable wetting phase flow field in a heterogeneous aquifer. For example, if DNAPL presents in a saturated zone mainly in large saturation pools, then both the effective surface area and flow velocity inside the pool is significantly lower than the region where the DNAPL is distributed homogeneously with little bypassing. The field-scale dissolution rate in such a heterogeneous system can be significantly smaller than that in a homogeneous environment. Therefore, the large-scale DNAPL dissolution properties are mainly determined by the DNAPL saturation distribution structure and wetting phase flow field. The

quantitative characterization of spatial distribution of DNAPL saturation and wetting phase flow velocity, impacted by spatially variable soil properties, is a foundation to evaluate the field-scale dissolution properties.

### 2.1.2 Bypassing Effect

The bypassing effect is perceived as one of the most important factors affecting large-scale dissolution rate. Quantitatively, bypassing can be described by the correlation of flow velocity and dissolution rate. Figure 2-2 shows the illustration of bypassing and anti-bypassing effect. Figure 2-2a represents a DNAPL source zone with mainly two types of entrapment, DNAPL pools with high saturation and DNAPL droplets with low saturation. The dots represent the DNAPL droplets while the gray layers represents DNAPL pools. Due to the high saturation in pools, the relatively permeability is reduced significantly, so is the wetting phase flow rate inside the pool. On the other hand, the high saturation leads to a high dissolution rate inside a pool. On the contrary, the region containing DNAPL droplets is with relatively large flow rate but low dissolution rate due to the low saturation. Therefore, a DNAPL source of such a structure has a negative correlation between flow rate and dissolution rate, which is corresponding to the bypassing effect.

Figure 2-2b shows another structure of DNAPL source, where DNAPL is distributed as droplets in relatively permeable region. There are some impermeable lenses in the aquifer, represented by the black layer, where DNAPL can hardly penetrate into due to the extremely low permeability. Therefore little DNAPL is present in such lenses. So within the lenses, both the flow rate and the dissolution rate are low. Outside the lenses, both the flow rate and dissolution rate are relatively high due to the higher permeability and saturation. Therefore the correlation between the flow rate and the dissolution rate is positive, which is referred to anti-bypassing effect.

Figure 2-2c is a combination of the first two plots, where all three structures coexist in a source: impermeable lenses, DNAPL pools and DNAPL droplets. In such a system both the bypassing and anti-bypassing control the dissolution. So the correlation between flow rate and dissolution rate can be any value in the range of [-1,1], depending which effect is stronger. This kind of DNAPL source structure is what we often found in the subsurface systems, while the

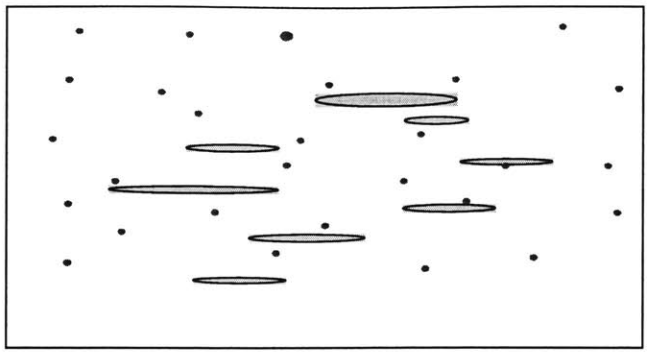

a. Strong bypassing effect with correlation between flow rate while dissolution rate is negative

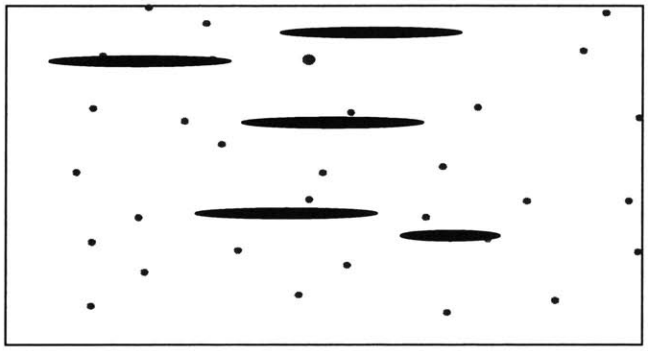

b. Strong anti-bypassing effect with correlation between flow rate while dissolution rate is positive

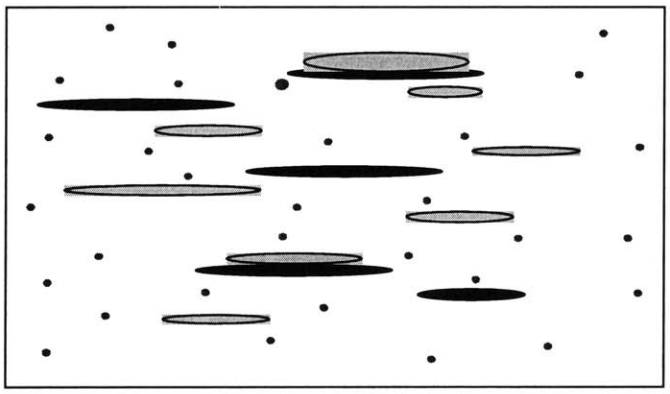

c. Effect of both bypassing and anti-bypassing effects that controls correlation between flow rate and dissolution rate appear in the range of [-1,1]

Figure 2-2: Bypassing and anti-bypassing effect in heterogeneous porous media

first two plots are just an illustration of the extreme cases. Connecting the physical structures with the parameters we have, we can elaborate the effect of bypassing and anti-bypassing on the large-scale dissolution properties.

### 2.1.3 Flow Analysis and DNAPL Saturation

For the past twenty years, understanding of multiphase flow in porous media has been enhanced by local-scale studies in laboratory experiments, numerical simulations and field experiments. Though it has been recognized that field-scale flow of DNAPL is a function of local-scale heterogeneity, there are many questions unsolved. How to quantify the spatial distribution of DNAPL and wetting phase flow at the impact of small-scale heterogeneity, expressed as a function of measurable statistics? How does soil heterogeneity impact the magnitude and distribution of DNAPL saturation? To further study a more realistic spilled DNAPL flow and distribution in a spatial variable aquifer, theoretical analysis to characterize the impact of heterogeneity on the large-scale flow process and DNAPL distribution is needed.

Recently, Jacobs performed a multi-phase flow analysis in heterogeneous porous media employing the stochastic method (Jacobs, 1998). In his work, the focus is on steady state systems of two fluid phases. The porous media is assumed with water wetting surfaces. By treating the soil properties as stationary, spatially correlated random fields, he investigated the impact of such variations on the flow of two fluid phases with density difference. The spatial distribution of soil properties and DNAPL saturation is represented by large-scale mean and high frequency random perturbation. Mean flow equations are developed from the local flow equation by a stochastic treatment. Linearized perturbation equations are derived to describe the dependence of saturation and capillary pressure on fluctuations of spatial variables. A general analytical solution was found about the effective non-wetting phase saturation, effective permeability and other effective flow properties. He concluded that the spatial variability of natural porous structures imposes a significant effect on the non-wetting phase distribution and thereafter the effective permeability of wetting phase flow. The validity of the theoretical results was demonstrated recently with numerical simulations (Zhou *et al.*, 2002).

Jacobs' work enhanced the insight of field-scale multiphase flow in heterogeneous subsurface systems and provided a theoretical tool to evaluate DNAPL distribution in an aquifer with

significant spatial variations. Extended from Jacobs' analysis, the field-scale DNAPL static saturation distribution and wetting phase flow field are obtained in this chapter. More specifically, the analytical solutions of first and second order moments of DNAPL saturation, effective permeability, as a function of mean capillary pressure and incorporated the effect of spatial variations of soil properties, can be employed as inputs for the transport analysis.

There are some key assumptions made to derive DNAPL saturation from Jacobs flow analysis. First of all, the effective properties obtained from Jacobs' analysis are based on that DNAPL is introduced in the system by a very slow vertical mean flow. Since the vertical flow rate of DNAPL used in this study is extremely small that at the order of centimeters per year, we assume that the DNAPL saturation distribution derived from this quasi-static flowing system is a good representation of the static DNAPL saturation field during the course of dissolution, when the source of flowing fluid is terminated. This method is different with the traditional method to estimate the residual saturation based on capillary number. However, the definition of residual saturation can be ambiguous and confusing in light of the fact that different definition of this concept have been encountered in different studies, though the concept is widely used. According to Mercer (1990), residual saturation is defined as the saturation at which NAPL becomes discontinuous and is immobilized by capillary forces under ambient groundwater flow conditions. So, it is a function of "ambient flow conditions". Corey (1986) defined the critical saturation that the non-wetting phase becomes entrapped and no longer interconnected and cannot be replaced simply by decreasing capillary pressure. Therefore this definition is different since the residual saturation is independent of flowing conditions. Pankow and Cherry (1996) described it as "is comprised of blobs and fingers (ganglia) of DNAPL that have been cut off and disconnected from the continuous DNAPL body by the invading water, and can be said as occluded by water".

To have a clear conceptual framework of DNAPL saturation field, it is necessary to distinguish the residual saturation $S_{nr}$ and static saturation $S_s$. Residual saturation should be defined as Corey did: " it is the saturation that cannot be reduced simply by decreasing capillary pressure". Thus it is a concept that not dependent on the ambient flow condition, and given a porous media system and immiscible fluids, it should have a fixed value. Static saturation should be that defined by Mercer *et al.* and it is a function of flowing condition. And this is the saturation

related to the saturation we are interested in for the dissolution problem. Therefore, the method used in this analysis to derive the static DNAPL saturation can avoid the confusion linked with the definition of residual saturation and related empirical models. The effect of slowly flowing DNAPL on the transport process is also evaluated in Chapter 4 and found insignificant.

Secondly, the mean DNAPL source zone is assumed uniform, which indicates that the mean DNAPL saturation is constant spatially in the source zone. This assumption is consistent with stationary assumption of DNAPL saturation in the flow analysis by Jacobs. Jacobs found that for a single DNAPL spill source, the mean DNAPL saturation varies slightly for the Borden and the Cape Cod sites vertically. For many DNAPL contaminated sites, DNAPL saturation is a result from multiple spill locations, where the mean DNAPL saturation tends to be even more stationary than that from a single source. Though more field data are necessary to provide more strict validation of the assumption, it does provide a reasonable method to simplify the otherwise extremely complicated system.

In addition, DNAPL vertical flow and saturation distribution is assumed not affected significantly by the horizontal wetting phase flow. This is discussed in detail in Section 2.3. Finally, DNAPL saturation field is assumed steady state. Jacobs applied the steady state continuity equation for different fluid phase to derive the effective flow properties. Moreover, we assume the DNAPL saturation field is not affected significantly during the course of dissolution. This is based on the observations that field-scale DNAPL dissolution rate is usually extremely low and the complete depletion time can be decades or centuries. Therefore the DNAPL saturation change is insignificant and can be regarded as steady state. This assumption is confirmed in Chapter 4 where the effective DNAPL dissolution rate coefficient is found very low in a heterogeneous DNAPL source zone.

The obtained DNAPL saturation field provides important inputs to investigate the DNAPL dissolution scenario. The derived moments of DNAPL saturation, and the wetting phase flow field will be crucial to derive the field-scale dissolution properties. The next section serves as a summary of the findings of Jacobs' study.

## 2.2 Multiphase Flow Analysis by Jacobs

### 2.2.1 Local Scale Characterization

Two local-scale models were discussed in Jacobs' work: the flow equation and the capillary pressure-saturation-relative permeability (p-s-k) model.

$$\mathbf{q}_\beta = -\frac{k\kappa_\beta}{\mu_\beta}\left(\nabla P_\beta + \rho_\beta \mathbf{g}\right) \tag{2.1}$$

The flow equation in Eq. 2.1 is based on the locally isotropic multiphase Darcy equation where

$k$ : intrinsic or saturated permeability $(L^2)$

$\kappa_\beta$ : relative permeability

$\mu_\beta$ : dynamic viscosity $(M/L/T)$

$P_\beta$ : pressure of phase $\beta$ $(M/T^2/L)$

$\rho_\beta$ : density of phase $\beta$ $(M/L^3)$

$\mathbf{g}$ : gravity vector $(L/T^2)$

The second model is the function characterizing the relationship between permeability, saturation and capillary pressure (p-s-k). Among various proposed model in this category, the van Genuchten, Brooks-Corey, Gardner characterization and Leverett scaling p-s-k models, which were discussed in Jacobs' work, are the most widely used. Here we focused on van Genuchten model of capillary pressure saturation relationship. This model is also applied in the transport analysis in Chapter 4 to be consistent:

$$S_e = \left[1 + (\alpha P_c)^{\frac{1}{1-m}}\right]^{-m} \tag{2.2}$$

where

$$S_e = \frac{\theta_w - \theta_r}{\phi - \theta_r} \tag{2.3}$$

$P_c$ : capillary pressure

$\theta_w$ : wetting phase volumetric content

$\theta_r$ : residual wetting phase volumetric content

$\phi$ : porosity

$m$ : slope parameter; $0 < m < 1$

$\alpha$ : inverse characteristic pressure; $\alpha > 0$

Mualem (1976) and Parker (1989) proposed the form of relative permeability for wetting phase and nonwetting phase in the isotropic local environment as:

$$\kappa_w = S_e^{1/2}\left[1 - \left(1 - S_e^{1/m}\right)^m\right]^2 \tag{2.4}$$

$$\kappa_o = (1 - S_e)^{1/2}\left(1 - S_e^{1/m}\right)^{2m} \tag{2.5}$$

The variables of $B$ and $L$ are defined as follows:

$$B = -\ln\alpha \tag{2.6}$$

$$L = -\ln\left(\frac{1}{m} - 1\right) \tag{2.7}$$

The introduction of these transformations of $B$ and $L$ is to avoid inadvertent, nonphysical results in the stochastic analysis when the mean of $\alpha$ or $m$ approaches its physical limit. The parameters $B$ and $L$ range from -$\infty$ to $\infty$ within the physical range of $\alpha$ and $m$, and are plausibly regarded to be Gaussian. For the field scale problem, by decomposing the parameters in the form of the sum of the mean and the perturbation, the high frequency, small-scale spatial variability was separated out from the large-scale slow varying mean process.

$$B = \overline{B} + b' \tag{2.8}$$

$$L = \overline{L} + l' \tag{2.9}$$

The spatial variability of other input parameters such as residual saturation, porosity and intrinsic permeability can be expressed in a similar way for studying a large-scale problem. The perturbations of input parameters are assumed to be partially correlated with perturbation of log intrinsic permeability $f'$, which can be written as:

$$b' = b_b f' + g'_b \tag{2.10}$$

$$l' = b_l f' + g'_l \tag{2.11}$$

where $b_b$, $b_l$ are slope coefficients and $g'_b$, $g'_l$ are zero mean residual perturbation which are not related with $f'$.

### 2.2.2 Effective Properties

Effective properties including the effective permeability of each phase and the mean DNAPL volumetric content for a large-scale system are major findings of Jacobs work. The technique includes:

- Spatially variable properties were written in the form of the sum of mean and perturbation components.
- First order approximation of the Taylor expansions about the mean parameters
- Take the expected value of the resulting expressions and derive the large-scale effective properties.

The large-scale effective relative permeability for phase $\beta$ in direction $n$ is found as follows.

$$\hat{\kappa}_{\beta,n} = \exp\left(R_\beta\left(\overline{\Gamma}\right)\right) \exp\left[\frac{E\left[\gamma'_m \gamma'_n\right]}{2}\left(\frac{\partial R_\beta}{\partial \Gamma_m}\frac{\partial R_\beta}{\partial \Gamma_n} + \frac{\partial^2 R_\beta}{\partial \Gamma_m \partial \Gamma_n}\right) + E\left[j'_{\beta,n}\gamma'_m\right]\frac{1}{J_{\beta,n}}\frac{\partial R_\beta}{\partial \Gamma_m}\right] \tag{2.12}$$

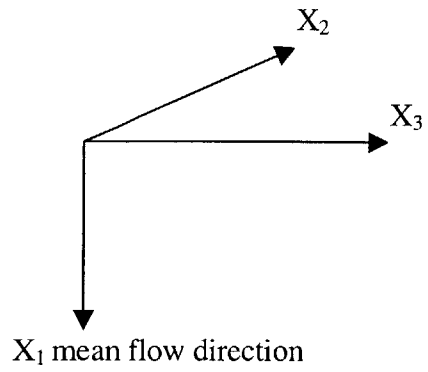


Figure 2-3: Mean flow direction aligned with principal axes for flow analysis

where

$$\begin{aligned}
\mathbf{\Phi} &= [F, B, L]\,, \text{ a vector that includes the fundamental characteristic parameters} \\
\mathbf{\Phi} &= \overline{\mathbf{\Phi}} + \boldsymbol{\phi}' \\
\mathbf{\Gamma} &= [\mathbf{\Phi}, P_c]\,, \text{ a vector that include the input variables} \\
\Gamma_m &= \overline{\Gamma}_m + \gamma'_m, \text{ the } m\text{th component of the vector } \mathbf{\Gamma} \\
R_\beta &= \ln(k\kappa_\beta) \text{ the log permeability of phase } \beta, \text{ where } k \text{ is intrinsic permeability,} \\
&\quad \kappa_\beta \text{ is the local relative permeability of phase } \beta \\
\mathbf{J}_\beta &= -\left(\nabla P_\beta + \rho_\beta \mathbf{g}\right) \text{ the hydraulic pressure gradient of phase } \beta, \\
&\quad \text{which include the gravity effects and the gradient of pressure} \\
\mathbf{J}_\beta &= \overline{J_\beta} + j'_\beta
\end{aligned}$$

and the Einstein summation convention for repeated indices has been used here. $J_{\beta,i}$ represents hydraulic pressure gradient of phase $\beta$ in direction $i$, where $i = 1$ is the mean flow direction of DNAPL vertically, $i = 2, 3$ are horizontal longitudinal and transverse direction respectively as shown in Figure 2-3. This is consistent with the notation in the two-phase flow study in Jacobs's study.

Similarly, the large-scale mean wetting phase saturation is found as:

$$\overline{S_e} = S_e\left(\overline{\mathbf{\Gamma}}\right) + \frac{E\left[\gamma'_m \gamma'_n\right]}{2} \frac{\partial^2 S_e\left(\overline{\mathbf{\Gamma}}\right)}{\partial \Gamma_m \partial \Gamma_n} \tag{2.13}$$

All the derivatives are evaluated around $\overline{\mathbf{\Gamma}}$ unless specified otherwise. The mean of transformed wetting phase saturation is:

$$\overline{W} = \ln\left(\frac{S_e\left(\overline{\mathbf{\Gamma}}\right)}{1 - S_e\left(\overline{\mathbf{\Gamma}}\right)}\right) + \frac{E\left[\gamma'_m \gamma'_n\right]}{2} \left[ \begin{array}{c} \frac{\partial^2 S_e(\overline{\mathbf{\Gamma}})}{\partial \Gamma_m \partial \Gamma_n} \left( \frac{1}{S_e(\overline{\mathbf{\Gamma}})} + \frac{1}{1 - S_e(\overline{\mathbf{\Gamma}})} \right) \\ + \frac{\partial S_e}{\partial \Gamma_m} \frac{\partial S_e}{\partial \Gamma_n} \left( -\frac{1}{S_e(\overline{\mathbf{\Gamma}})^2} + \frac{1}{(1 - S_e(\overline{\mathbf{\Gamma}}))^2} \right) \end{array} \right] \tag{2.14}$$

where

$$W = \ln\left(\frac{S_e}{1 - S_e}\right) \tag{2.15}$$

Like the transformation of $\alpha$ and $m$, to avoid problems in the estimation of the moments of $S_e$ for mean values close its natural limits, 0 and 1, a nonlinear transformation of $S_e$ is introduced. The physically reasonable domain of the transformed variables $W$ is $[-\infty, \infty]$ as $S_e \in [0, 1]$. So $W$ can be plausibly regarded as Gaussian as transformation of either wetting phase saturation or DNAPL saturation, due to the linear deterministic relationship between these two variables. The variance of transformed wetting phase saturation can be found as:

$$\sigma_w^2 = E\left[\gamma'_m \gamma'_n\right] \frac{\partial S_e}{\partial \Gamma_m} \frac{\partial S_e}{\partial \Gamma_n} \left(\frac{1}{S_e} + \frac{1}{1 - S_e}\right)^2 \tag{2.16}$$

The cross products of input variables $\gamma'_m$, $\gamma'_n$ represent the contribution from the small-scale variations of fundamental variables to the effective permeability. The random perturbation could be represented in the wave number domain using Fourier-Stieltjes Representations (FSR)

and the Spectral Representation Theorem (SRT) (Lumley and Panofsky, 1964).

$$P_c' = \int_{-\infty}^{\infty} e^{i\mathbf{k}\cdot\mathbf{x}} dZ_{P_c}(\mathbf{k}) \tag{2.17}$$

$$f' = \int_{-\infty}^{\infty} e^{i\mathbf{k}\cdot\mathbf{x}} dZ_f(\mathbf{k}) \tag{2.18}$$

$$B' = \int_{-\infty}^{\infty} e^{i\mathbf{k}\cdot\mathbf{x}} dZ_B(\mathbf{k}) \tag{2.19}$$

$$L' = \int_{-\infty}^{\infty} e^{i\mathbf{k}\cdot\mathbf{x}} dZ_L(\mathbf{k}) \tag{2.20}$$

$$q_i' = \int_{-\infty}^{\infty} e^{i\mathbf{k}\cdot\mathbf{x}} dZ_{q_i}(\mathbf{k}) \tag{2.21}$$

$$r' = \int_{-\infty}^{\infty} e^{i\mathbf{k}\cdot\mathbf{x}} dZ_r(\mathbf{k}) \tag{2.22}$$

$$W' = \int_{-\infty}^{\infty} e^{i\mathbf{k}\cdot\mathbf{x}} dZ_w(\mathbf{k}) \tag{2.23}$$

Where $dZ(\mathbf{k})$ represents a random amplitude, which is an independent process in the wave number domain where vector wave number, $\mathbf{k}$, has components $k_1$, $k_2$, $k_3$ in a Cartesian coordinates system. The perturbation process is represented in the three dimensional space. So the dot product of two vectors is

$$\mathbf{k}\cdot\mathbf{x} = k_i x_i = k_1 x_1 + k_2 x_2 + k_3 x_3 \tag{2.24}$$

In this way the cross products in the mean equations can be evaluated by the spectral method. By deriving the analytical expression of the relative permeability, the mean and variance of nonwetting phase volumetric content, the foundation for addressing the flow and transport of wetting phase within the DNAPL source zone was established. The outputs from Jacobs' study were employed to derive the wetting phase permeability and flow rate in a DNAPL source zone. These results are incorporated in the stochastic transport model in Chapter 4 to develop the transport effective properties.

## 2.3 Effect of Wetting Phase Flow on DNAPL Distribution and Effective Permeability

### 2.3.1 Background

Jacobs assumed a static wetting phase and no mean pressure gradient in the nonwetting phase in horizontal direction to obtain closed-form solutions of effective properties, though his general formula included flow of both phases. The relative permeability and effective properties of flow field are derived assuming that the horizontal wetting phase flow is absent. This assumption is plausible to derive the effective permeability field since the vertical density flow is dominant flow process compared to the horizontal wetting phase flow field. The hydraulic gradient for nonwetting phase vertical flow usually is two orders magnitude higher than that of horizontal wetting phase flow. However, in order to evaluate groundwater flow and transport properties in a DNAPL source zone, the effect of horizontal wetting phase (water) flow on DNAPL saturation field cannot be neglected. The wetting phase flow can be a significant effect to mobilize the DNAPL and affect the DNAPL saturation distribution. Therefore, in this section we investigate the influence of aqueous phase flow on the effective permeability field and DNAPL saturation. More specifically, the purpose is to study the relative importance of flowing wetting phase's effect on the effective permeability, mean and variance of DNAPL saturation. These properties are key inputs to the analysis of transport within DNAPL source zone with mass transfer. By comparing the results from the coupled process (with horizontal mean water flow) with the decoupling case, the appropriateness of applying results from Jacobs to the transport process can be evaluated.

From Jacobs (1998) Eq. 2.49, the effective permeability and the mean and variance of $W$ can be found in Eqs. 2.12, 2.14 and 2.16. By observation, we can find the key contributions in these expressions are covariance $E\left[\gamma'_m\gamma'_n\right]$ and $E\left[j'_{\beta,i}\gamma'_m\right]$. Since $E\left[\phi'_m\phi'_n\right]$ is constant which is not affected by flow condition represented as a function of capillary pressure, so we consider only the $E\left[\phi'_m P'_c\right]$, $E\left[P'_c P'_c\right]$, $E\left[j'_{\beta,i}P'_c\right]$ and $E\left[\phi'_m j'_{\beta,i}\right]$.

Since, from Jacobs (1998), the covariance terms were evaluated by spectral method using

the hole function as the input spectrum, and the results can be summarized as:

$$E\left[P_c' P_c'\right] = \int_{-\infty}^{\infty} X_m X_n^* S_{\phi_m \phi_n} dk = E\left[\phi_m' \phi_n'\right] I_{m,n}(\rho, \varepsilon) \tag{2.25}$$

$$E\left[\phi_m' P_c'\right] = \int_{-\infty}^{\infty} X_n S_{\phi_m \phi_n} dk = -E\left[\phi_m' \phi_n'\right] I_n(\rho, \varepsilon) \tag{2.26}$$

$$E\left[j_{\beta,i}' P_c'\right] = \int_{-\infty}^{\infty} Y_{m,i} X_n^* S_{\phi_m \phi_n} dk \tag{2.27}$$

$$E\left[\phi_n' j_{\beta,i}'\right] = \int_{-\infty}^{\infty} Y_{m,i} S_{\phi_m \phi_n} dk \tag{2.28}$$

where:

$$\varepsilon_{\Gamma_m,i} = l_i \left[\frac{\partial R_o}{\partial \Gamma_m} \overline{J}_{o,i} - \frac{\partial R_w}{\partial \Gamma_m} \overline{J}_{w,i}\right] \tag{2.29}$$

where $l_i$ is the correlation scale in direction $i$. This parameter represents the important flow characteristics in the direction $i$.

From Jacobs (1998), the key term of the integrands in Eqs. 2.25, 2.26 and 2.27 can be found as:

$$X_m = \frac{-il_2^2(u_i \varepsilon_{\Phi m,i}/l_n^2)\left[(\rho u_1^2 + u_2^2 + u_3^2) - il_2^2(u_i \varepsilon_{P_c,i}/l_i^2)\right]}{\left(\rho u_1^2 + u_2^2 + u_3^2\right)^2 + \left[l_2^2(u_i \varepsilon_{\Phi_i,i}/l_i^2)\right]^2} \tag{2.30}$$

where:

$$\rho = \frac{l_2}{l_1} = \frac{l_3}{l_1} \tag{2.31}$$

$$u_i \varepsilon_{\Gamma_m,i}/l_i^2 = \sum_{i=1}^{2} \frac{u_i \varepsilon_{\Gamma_m,i}}{l_i^2} \tag{2.32}$$

Therefore, $E\left[\phi_m' P_c'\right]$ can be expressed as:

$$\begin{aligned} E\left[\phi_m' P_c'\right] &= \int_{-\infty}^{\infty} X_n S_{\phi_m \phi_n} d\mathbf{k} \\ &= \int_{-\infty}^{\infty} \frac{-il_2^2(u_i \varepsilon_{\Phi_n,\, i}/l_i^2)\left[(\rho u_1^2 + u_2^2 + u_3^2) - il_2^2(u_i \varepsilon_{P_c,i}/l_i^2)\right]}{\left(\rho u_1^2 + u_2^2 + u_3^2\right)^2 + \left[l_2^2(u_i \varepsilon_{\Phi_n,i}/l_i^2)\right]^2} S_{\phi_m \phi_n} d\mathbf{u} \\ &= E\left[\phi_m' \phi_n'\right] \int_{-\infty}^{\infty}\int_{-\infty}^{\infty}\int_{-\infty}^{\infty} \frac{\left(-\rho^4 u_1^2 \varepsilon_{\Phi_n,1} \varepsilon_{P_c,1} - u_2^2 \varepsilon_{\Phi_n,2} \varepsilon_{P_c,2}\right)}{\left(\rho^2 u_1^2 + u_2^2 + u_3^2\right)^2 + \left[l_2^2\left[(u_2 \varepsilon_{P_c,2}/l_2^2) + (u_1 \varepsilon_{P_c,1}/l_1^2)\right]\right]^2} \\ &\quad \frac{4u_1^2}{\pi^2\left(1+u^2\right)^3} du_1 du_2 du_3 \end{aligned} \tag{2.33}$$

So $I_n$ in Eq. 2.26 can be found as:

$$I_n = \int_{-\infty}^{\infty}\int_{-\infty}^{\infty}\int_{-\infty}^{\infty} \frac{\left(\rho^4 u_1^2 \varepsilon_{\Phi_n,1}\varepsilon_{P_c,1} + u_2^2 \varepsilon_{\Phi_n,2}\varepsilon_{P_c,2}\right)}{\left(\rho^2 u_1^2 + u_2^2 + u_3^2\right)^2 + \left[l_2^2\left[\left(u_2\varepsilon_{P_c,2}/l_2^2\right) + \left(u_1\varepsilon_{P_c,1}/l_1^2\right)\right]\right]^2} \frac{4u_1^2}{\pi^2\left(1+u^2\right)^3} du_1 du_2 du_3 \tag{2.34}$$

### 2.3.2 Perfectly-Stratified System

Jacobs found that the derived results of effective properties of flow field are not sensitive to the perfectly-stratified assumption that $\rho \to \infty$. So we first compare the results from coupled systems to the results derived from his study assuming no wetting phase flow, which we call a decoupled system.

As for a perfectly-stratified system:

$$I_n = \int_{-\infty}^{\infty}\int_{-\infty}^{\infty}\int_{-\infty}^{\infty} \frac{u_1^2 \varepsilon_{\Phi_n,1}\varepsilon_{P_c,1}}{u_1^4 + \left(u_1\varepsilon_{P_c,1}\right)^2} \frac{4u_1^2}{\pi^2\left(1+u^2\right)^3} du_1 du_2 du_3 \tag{2.35}$$

This result is exactly the same as the decoupled case which assumes $\overline{J}_{w,i} = 0$. Therefore, the flowing wetting phase will have no effect on the covariance of $E\left[\phi'_m P'_c\right]$ as $\rho \to \infty$.

Then from Jacobs (1998), another term in integrals of Eqs. 2.27 and 2.28 can be found as:

$$Y_{m,i} = -\frac{u_i}{l_i}\frac{l_2^2}{\left(\rho u_1^2 + u_2^2 + u_3^2\right)}\left[\left(\frac{\partial R_\beta}{\partial P_c}X_m + \frac{\partial R_\beta}{\partial \Phi_m}\right)\left(\frac{u_1}{l_1}\overline{J}_{\beta,1} + \frac{u_2}{l_2}\overline{J}_{\beta,2}\right)\right] \tag{2.36}$$

So:

$$\begin{aligned} E\left[\phi'_n j'_{w,2}\right] &= \int_{-\infty}^{\infty} Y_{m,2} S_{\phi_m\phi_n} dk \\ &= -E\left[\phi'_m\phi'_n\right]\overline{J}_{w,2}\int_{-\infty}^{\infty}\frac{u_2^2}{\left(\rho u_1^2 + u_2^2 + u_3^2\right)}\left(\frac{\partial R_w}{\partial P_c}X_i + \frac{\partial R_w}{\partial \Phi_m}\right)\frac{4u_1^2}{\pi^2\left(1+u^2\right)^3} \end{aligned} \tag{2.37}$$

where

$$X_m = \frac{\left(\rho^4 u_1^2 \varepsilon_{\Phi_m,1}\varepsilon_{P_c,1} + u_2^2 \varepsilon_{\Phi_m,2}\varepsilon_{P_c,2}\right)}{\left(\rho^2 u_1^2 + u_2^2 + u_3^2\right)^2 + \left[l_2^2\left[\left(u_2\varepsilon_{P_c,2}/l_2^2\right) + \left(u_1\varepsilon_{P_c,1}/l_1^2\right)\right]\right]^2} \tag{2.38}$$

$$E\left[\phi'_n j'_{o,1}\right] = \int_{-\infty}^{\infty} Y_{m,1} S_{\phi_m \phi_n} d\mathbf{k}$$

$$= -E\left[\phi'_m \phi'_n\right] \overline{J}_{o,1} \int_{-\infty}^{\infty} \frac{\rho u_2 u_1}{\left(\rho u_1^2 + u_2^2 + u_3^2\right)} \left[\left(\frac{\partial R_o}{\partial P_c} X_m + \frac{\partial R_o}{\partial \Phi_m}\right)\right] \frac{4u_1^2}{\pi^2 \left(1+u^2\right)^3} d\mathbf{u} \quad (2.39)$$

For coupled case, $\overline{J}_{o,1}$ and $\overline{J}_{w,2}$ are nonzero simultaneously. As $\rho \to \infty, E\left[\phi'_n j'_{w,2}\right]$ doesn't contain any factors of vertical NAPL flow. Similarly $E\left[\phi'_n j'_{o,1}\right]$ is not affected by the flowing wetting phase. So the effective permeability $\hat{k}^*_{o,1}$ and $\hat{k}^*_{w,2}$ are not changed by the coupled case. Therefore, the vertical effective permeability of DNAPL will not be affected by the horizontal wetting phase flow, and vice versa. In addition, the flowing wetting phase does not affect the derivatives nor the mean input saturation $S_e\left(\overline{\Gamma}\right)$. Similar analysis can also be applied to evaluate $E\left[j'_{\beta,i} P'_c\right]$ and $E\left[P'_c P'_c\right]$. Based on Eqs. 2.25, 2.26,2.27 and 2.28, we can conclude that the covariances of $E\left[\phi'_m P'_c\right]$, $E\left[P'_c P'_c\right], E\left[j'_{\beta,i} P'_c\right]$ and $E\left[\phi'_n j'_{\beta,i}\right]$ don't change for coupled case. Thus for a perfectly-stratified system, the effect of horizontal wetting phase flow on the effective permeability and mean and variance of DNAPL saturation is demonstrated insignificant.

### 2.3.3 Imperfectly-Stratified Systems

For most of realistic sites, the aquifer is often found imperfectly-stratified, which indicates $\rho \gg 1$ but $\neq \infty$. More importantly, though for the flow analysis it was found that the results are not sensitive to the perfectly-stratified assumption, it is an important approximation to the transport analysis. It was found the classical Taylor analysis of longitudinal dispersion in a perfectly stratified system is only true when the longitudinal persistence extends in extremely large magnitude. Gelhar and Axness (1983a) discussed the large-scale solute transport in a heterogeneous aquifer and found that the layers have to be horizontally persistent for distance on the order of 10 km in order to Taylor mechanism to be dominant. Such an extensive persistence is rarely observed in realistic aquifer. Therefore, an imperfectly-stratified system, incorporating three-dimensional variations in the flow field, must be treated in the transport analysis as developed in Chapter 4, and the impact of a flowing wetting phase on the flow analysis result for such a system must be evaluated.

For an imperfectly-stratified system, the $I_m$ in Eq. 2.26 can be expressed as:

$$I_m = \int_{-\infty}^{\infty}\int_{-\infty}^{\infty}\int_{-\infty}^{\infty} \frac{\varepsilon_{\Phi_m,1}\varepsilon_{P_c,1}\left(u_1^2+u_2^2\left(\varepsilon_{\Phi_m,2}\varepsilon_{P_c,2}/\varepsilon_{\Phi_m,1}\varepsilon_{P_c,1}\rho^4\right)\right)}{\left(u_1^2+u_2^2/\rho^2+u_3^2/\rho^2\right)^2+\varepsilon_{P_c,1}^2\left[u_2\left(\varepsilon_{P_c,2}/\varepsilon_{P_c,1}\rho^2\right)+u_1\right)\right]^2}\frac{4u_1^2}{\pi^2\left(1+u^2\right)^3}du_1du_2du_3 \tag{2.40}$$

The effect of the wetting phase flow on DNAPL flow results can be neglected if the conditions below are satisfied:

$$\frac{\varepsilon_{\Phi_m,2}\varepsilon_{P_c,2}}{\varepsilon_{\Phi_m,1}\varepsilon_{P_c,1}\rho^4} \ll 1 \Longrightarrow \tag{2.41}$$

$$\frac{\left[\frac{\partial R_w}{\partial \Phi_m}\frac{\partial R_w}{\partial P_c}\right]\overline{J}_{w,2}^2}{\rho^2\left[\frac{\partial R_o}{\partial \Phi_m}\frac{\partial R_o}{\partial P_c}\right]\overline{J}_{o,1}^2} \ll 1 \tag{2.42}$$

Since the mean DNAPL saturation in a typical source zone is very small, a change of capillary pressure has much more significant influence on the DNAPL relative permeability rather water relative permeability. So when mean DNAPL saturation is small:

$$\frac{\partial R_w}{\partial \Phi_m}\frac{\partial R_w}{\partial P_c} \ll \frac{\partial R_o}{\partial \Phi_m}\frac{\partial R_o}{\partial P_c} \tag{2.43}$$

Since the hydraulic gradient of density flow usually is much higher than the natural groundwater hydraulic gradient observed, we have that

$$\overline{J}_{o,1} \geq \overline{J}_{w,2} \tag{2.44}$$

Because natural sediments typically are well stratified,

$$\rho \gg 1 \tag{2.45}$$

So the approximation in Eq. 2.42 is demonstrated to be adequate based on the above analysis. Similarly:

$$\frac{\left[\frac{\partial R_w}{\partial P_c}\right]\overline{J}_{w,2}}{\rho\left[\frac{\partial R_o}{\partial P_c}\right]\overline{J}_{o,1}} \ll 1 \Longrightarrow \tag{2.46}$$

$$\left(\varepsilon_{P_c,2}/\varepsilon_{P_c,1}\rho^2\right) \ll 1 \tag{2.47}$$

So the impact of wetting phase flow on the DNAPL saturation field and the relative permeability in an imperfectly-stratified aquifer is negligible. For the imperfectly-stratified system, the decoupled case is an appropriate assumption to calculate the effective permeability and the mean and variance of $W$. The DNAPL flow and saturation field will not be affected by the wetting phase flow. Reynolds and Kueper have conducted a numerical simulation of multiphase flow in a fractured clay/sand system and found that the rate of DNAPL loading to the lower aquifer far exceeded the rate of aqueous phase mass loading (Reynolds & Kueper, 2001). This reflected that the effect of wetting phase flow and transport on DNAPL flow is insignificant under realistic conditions.

In summary, the effect of horizontal wetting phase flow on the DNAPL vertical flow field, the consequent effective permeability and DNAPL saturation field has been studied for both perfectly-stratified systems and imperfectly-stratified systems. These effects have been demonstrated insignificant under the conditions of interest here. The theoretical analysis is consistent with the numerical simulations performed by other researchers. Therefore, the results from Jacobs work can be employed to the study of wetting phase flow and transport within the DNAPL source zone.

## 2.4 Wetting Phase Flow Field

The horizontal wetting phase flow in the DNAPL source zone is affected by the presence of DNAPL, which reduce the relative permeability of wetting phase. To evaluate the wetting phase flow field as a function of mean capillary pressure, the perturbation theory is applied here to separate the large-scale mean process with the small-scale perturbations. Using the approach applied by Jacobs, the wetting phase log hydraulic conductivity is evaluated in terms of the mean and perturbation. The spectral form of random perturbation is developed as well using Fourier-Stieltjes Representations. The perturbation of wetting phase flow rate and saturation are developed as a function of fundamental input parameters.

Here, $i = 1, 2, 3$ representing horizontal longitudinal $X_1$, horizontal transverse $X_2$ and vertical transverse $X_3$ direction as shown in Figure 2-4, which is defined differently with that for flow analysis above. This is because Jacobs' analysis focused on the DNAPL flow in the vertical direction. Here we mainly study the wetting phase flow field when the mean flow direction of

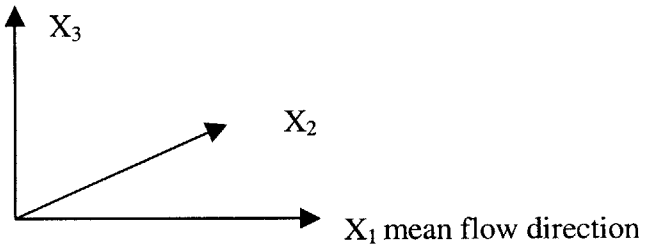


Figure 2-4: Mean flow direction aligned with principal axes for transport analysis

wetting phase is longitudinally horizontal. The coordinate system shown in Figure 2-4 is used in the rest of thesis which focuses on the transport process.

### 2.4.1 Wetting Phase Log Permeability Field

As discussed in the first section of this chapter, both the DNAPL saturation field and wetting phase flow field influence the dissolution of DNAPL at the field scale. To derive the wetting phase flow field, the mean and fluctuation of relative permeability as a function of input parameters are evaluated. The wetting phase log conductivity, $R$, can be expressed as:

$$R = lnK = \ln(\frac{kk_r\rho g}{\mu}) = \overline{R} + r' \tag{2.48}$$

Here $K$ is the hydraulic conductivity of the wetting phase. According to Jacobs (1998), for wetting phase log permeability perturbation can be found as:

$$r' = \gamma'_m \frac{\partial R}{\partial \Gamma_m} = P_c' \frac{\partial R}{\partial P_c} + f' \frac{\partial R}{\partial f} + B' \frac{\partial R}{\partial B} + L' \frac{\partial R}{\partial L} \tag{2.49}$$

By applying the Spectral Representation Theorem introduced in the first section of this chapter, the random amplitude of log permeability in the wave number domain can be written as:

$$dZ_r = \frac{\partial R}{\partial P_c} dZ_{P_c} + \frac{\partial R}{\partial f} dZ_f + \frac{\partial R}{\partial B} dZ_B + \frac{\partial R}{\partial L} dZ_L \tag{2.50}$$

This is a first order approximation based on a Taylor expansion around the mean for each of the parameters $f, B, L$; implicitly all of the partial derivatives are evaluated at the mean value of the parameters. Similar to Eq. 2.10:

$$dZ_B = b_b dZ_f + dZ_{g_b} \tag{2.51}$$

$$dZ_L = b_l dZ_f + dZ_{g_l} \tag{2.52}$$

$$dZ_{P_c} = Y_m(b_m dZ_f + dZ_{g_m}) \tag{2.53}$$

where

$$\begin{aligned}
Y_m = [ & - k^2 \left( \overline{J}_{o,i} \frac{\partial^2 R_o}{\partial \Phi_m \partial P_c} - \overline{J}_{w,i} \frac{\partial^2 R}{\partial \Phi_m \partial P_c} \right) \frac{\partial \overline{P_c}}{\partial x_i} \\
& - \left( \frac{\partial \overline{P_c}}{\partial x_i} k_i \right) k_i \left( \overline{J}_{o,i} \frac{\partial R_o}{\partial \Phi_m} \frac{\partial R}{\partial P_c} - \overline{J}_{w,i} \frac{\partial R}{\partial \Phi_m} \frac{\partial R_o}{\partial P_c} \right) \\
& + i\mathbf{k}( - k^2 \left( \overline{J}_{o,i} \frac{\partial R_o}{\partial \Phi_m} - \overline{J}_{w,i} \frac{\partial R}{\partial \Phi_m} \right) \\
& + \frac{\partial \overline{P_c}}{\partial x_i} \left( \overline{J}_{o,i} \frac{\partial^2 R_o}{\partial \Phi_m \partial P_c} \frac{\partial R}{\partial P_c} - \overline{J}_{w,i} \frac{\partial^2 R}{\partial \Phi_m \partial P_c} \frac{\partial R_o}{\partial P_c} \right) \frac{\partial \overline{P_c}}{\partial x_i} )] \\
& (k^4 + ik^2 k_i \left( - \frac{\partial R}{\partial P_c} \left( \frac{\partial \overline{P_c}}{\partial x_i} + \overline{J}_{w,i} \right) - \frac{\partial R_o}{\partial P_c} \left( \frac{\partial \overline{P_c}}{\partial x_i} - \overline{J}_{o,i} \right) \right) \\
& + k^2 \left( \overline{J}_{o,i} \frac{\partial^2 R_o}{\partial P_c^2} - \overline{J}_{w,i} \frac{\partial^2 R}{\partial P_c^2} \right) \frac{\partial \overline{P_c}}{\partial x_i} \\
& + \left( k_i \left( \overline{J}_{o,i} - \overline{J}_{w,i} - \frac{\partial \overline{P_c}}{\partial x_i} \right) \right) \left( k_i \frac{\partial \overline{P_c}}{\partial x_i} \right) \frac{\partial R}{\partial P_c} \frac{\partial R_o}{\partial P_c} \\
& + ik_i \frac{\partial \overline{P_c}}{\partial x_i} \left( \overline{J}_{w,i} \frac{\partial^2 R}{\partial P_c^2} \frac{\partial R_o}{\partial P_c} - \overline{J}_{o,i} \frac{\partial^2 R_o}{\partial P_c^2} \frac{\partial R}{\partial P_c} \right) \frac{\partial \overline{P_c}}{\partial x_i} )^{-1}
\end{aligned} \tag{2.54}$$

The index $m$ is corresponds to the three parameters $\Phi_m = (f, B, L)$. The hydraulic pressure gradient for phase $\beta$ in $i$ direction is:

$$J_{\beta,i} = - \left( \frac{\partial P_\beta}{\partial x_i} + \rho_\beta \overrightarrow{g} \right) \tag{2.55}$$

Assume the uniform mean flow $\frac{\partial \overline{P_c}}{\partial x_i} = 0$ and vertical wetting phase mean flow is negligible

$\overline{J}_{w,3} = 0$. From Jacobs result:

$$Y_m = \frac{-k_3^2 B_m B_2 - ik_3 B_m k^2}{k^4 + B_2^2 k_3^2} \tag{2.56}$$

where

$$B_m = \frac{\partial R_o}{\partial \Phi_m} \overline{J}_{o,3} \tag{2.57}$$

$$B_2 = \frac{\partial R_o}{\partial P_c} \overline{J}_{o,3} \tag{2.58}$$

So substitute Eqs. 2.51, 2.52, 2.53 and 2.56 into Eq. 2.50:

$$dZ_r = \left[\frac{\partial R}{\partial P_c} Y_m b_m + \frac{\partial R}{\partial f} + \frac{\partial R}{\partial B} b_b + \frac{\partial R}{\partial L} b_L\right] dZ_f + \frac{\partial R}{\partial P_c} Y_m dZ_{g_m} + \frac{\partial R}{\partial B} dZ_{g_b} + \frac{\partial R}{\partial L} dZ_{g_l} \tag{2.59}$$

$$dZ_r = (\varrho + \beta_m Y_m) dZ_f + \chi_b dZ_{g_b} + \chi_l dZ_{g_l} + \chi_1 dZ_{g_b} + \chi_2 dZ_{g_l} \tag{2.60}$$

where

$$\varrho = \frac{\partial R}{\partial f} + \frac{\partial R}{\partial B} b_b + \frac{\partial R}{\partial L} b_L \tag{2.61}$$

$$\beta_m = \frac{\partial R}{\partial P_c} b_m \tag{2.62}$$

$$\chi_b = \frac{\partial R}{\partial P_c} Y_b \tag{2.63}$$

$$\chi_l = \frac{\partial R}{\partial P_c} Y_l \tag{2.64}$$

$$\chi_1 = \frac{\partial R}{\partial B} \tag{2.65}$$

$$\chi_2 = \frac{\partial R}{\partial L} \tag{2.66}$$

So the wetting phase log conductivity perturbation is found explicitly as a function of perturbations of the fundamental parameters.

### 2.4.2 Wetting Phase Flow Field

By expanding the Darcy's Law to the second order, the wetting phase discharge can be represented as:

$$q_i = \exp(R)J_i = (\overline{J}_i + j_i)\exp(\overline{R} + r) \simeq (\overline{J}_i + j_i)\exp\left(\overline{R}\right)\left(1 + r + \frac{r^2}{2} + ...\right) \tag{2.67}$$

where $J_i = -\partial\Psi/\partial x_i$ and $\Psi$ is water head. Note that $J_i$ defined here is different with $J_{\beta,i}$ defined in the summary of Jacobs' work above:

$$J_i = \frac{J_{w,i}}{\rho_w g} \tag{2.68}$$

So to second order of fluctuations, the mean specific discharge is:

$$E\left[q_i\right] = \exp\left(\overline{R}\right)\left[\overline{J_i}\left(1 + \frac{\overline{r^2}}{2}\right) + \overline{j_i r}\right] \tag{2.69}$$

The perturbation is:

$$q_i = q_i - E\left[q_i\right] = \exp\left(\overline{R}\right)\left(\overline{J_i} r + j_i\right) \tag{2.70}$$

Assuming steady flow:

$$-\partial q_i/\partial x_i = 0 \tag{2.71}$$

So the flow equation becomes:

$$\frac{\partial}{\partial x_i}\left[k\kappa_w\left(\partial\Psi/\partial x_i\right)\right] = 0 \tag{2.72}$$

$$\frac{\partial^2\Psi}{\partial x_i^2} + \frac{\partial R}{\partial x_i}\frac{\partial\Psi}{\partial x_i} = 0 \tag{2.73}$$

Let

$$\Psi = \overline{\Psi} + \psi \tag{2.74}$$

Thus the mean equation is:

$$\frac{\partial^2\overline{\Psi}}{\partial x_i^2} + \frac{\partial\overline{R}}{\partial x_i}\frac{\partial\overline{\Psi}}{\partial x_i} + E\left[\frac{\partial r}{\partial x_i}\frac{\partial\psi}{\partial x_i}\right] = 0 \tag{2.75}$$

The perturbation equation becomes:

$$\frac{\partial^2 \psi'}{\partial x_i^2} + \frac{\partial \overline{R}}{\partial x_i}\frac{\partial \psi'}{\partial x_i} + \frac{\partial r'}{\partial x_i}\frac{\partial \overline{\Psi}}{\partial x_i} = -\frac{\partial r'}{\partial x_i}\frac{\partial \psi'}{\partial x_i} + E\left[\frac{\partial r'}{\partial x_i}\frac{\partial \psi'}{\partial x_i}\right] \tag{2.76}$$

By assuming the small amplitude of the perturbations, we can approximate the right side is close to zero:

$$-\frac{\partial r'}{\partial x_i}\frac{\partial \psi'}{\partial x_i} + E\left[\frac{\partial r'}{\partial x_i}\frac{\partial \psi'}{\partial x_i}\right] \simeq 0 \tag{2.77}$$

So:

$$\frac{\partial^2 \psi'}{\partial x_i^2} + \frac{\partial \overline{R}}{\partial x_i}\frac{\partial \psi'}{\partial x_i} + \frac{\partial r'}{\partial x_i}\frac{\partial \overline{\Psi}}{\partial x_i} = 0 \tag{2.78}$$

By applying the SRT, the perturbations can be represented as:

$$\psi' = \int_{-\infty}^{\infty} e^{i\mathbf{k}\cdot\mathbf{x}} dZ_\psi(\mathbf{k}) \tag{2.79}$$

Based on Eqs. 2.79 and 2.22, the random amplitude of hydraulic head can be found as a function of log permeability amplitude:

$$dZ_\psi = \frac{-ik_i \overline{J}_i}{k^2 - ik_i A_i} dZ_r \tag{2.80}$$

where

$$k^2 = k_1^2 + k_2^2 + k_3^2 \tag{2.81}$$

The spectral amplitude of log longitudinal solute velocity $v = \ln q_1$ can be found in the similar way:

$$q_1 = \exp(R) J_1 \tag{2.82}$$

$$v = R + \ln J_1 \tag{2.83}$$

Here we apply the first order approximation to the gradient $J_1$ instead of $R$ in above analysis. This approximation introduces much less error since the spatial variability of the gradient is

only secondary relative to the variability of log conductivity $R$. Let

$$v = v' + \overline{v} \tag{2.84}$$

$$R = \overline{R} + r' \tag{2.85}$$

$$J_1 = \overline{J} + j' \tag{2.86}$$

So

$$\begin{aligned} v' + \overline{v} &= \left(\overline{R} + r'\right) + \ln(\overline{J} + j') \\ &\approx \left(\overline{R} + r'\right) + \ln \overline{J} + \frac{j'}{\overline{J}} \end{aligned} \tag{2.87}$$

So:

$$\overline{v} = \overline{R} + \ln \overline{J} \tag{2.88}$$

$$v' = r' + \frac{j'}{\overline{J}} \tag{2.89}$$

Since:

$$v' = \left(r' - \frac{\partial \psi'}{\partial x_1} \frac{1}{\overline{J}}\right) \tag{2.90}$$

$$dZ_v = dZ_r - ik_i dZ_\psi \frac{1}{\overline{J}} \tag{2.91}$$

Using Eqs. 2.80, 2.91 and assuming there is no trend in the mean log conductivity, which $\frac{\partial \overline{R}}{\partial x_i} = 0$ :

$$dZ_v = \left(1 - \frac{k_1^2}{k^2}\right) dZ_r = \epsilon dZ_r \tag{2.92}$$

where $\epsilon = \left(1 - \frac{k_1^2}{k^2}\right)$. Using Eq. 2.60,

$$dZ_v = \epsilon \left[(\varrho + \beta_m Y_m) dZ_f + \chi_b dZ_{g_b} + \chi_l dZ_{g_l} + \chi_1 dZ_{g_b} + \chi_2 dZ_{g_l}\right] \tag{2.93}$$

### 2.4.3 DNAPL Saturation Field

In order to evaluate the effect of NAPL saturation on the transport and the dissolution process, cross-spectra of the transformation of DNAPL saturation with other parameters need to be

evaluated. Therefore, the spatial variability of the DNAPL phase saturation is evaluated here in terms of random perturbations and spectral amplitude.

The transformation of effective DNAPL saturation is defined in Eq. 2.15 and from Jacobs (1998) the perturbation of $W$ can be found as:

$$w' = \gamma'_m \frac{\partial S_e}{\partial \Gamma_m}\left(\frac{1}{S_e} + \frac{1}{1-S_e}\right) = D_1\left(P_c'\frac{\partial S_e}{\partial P_c} + f'\frac{\partial S_e}{\partial f} + B'\frac{\partial S_e}{\partial B} + L'\frac{\partial S_e}{\partial L}\right) \tag{2.94}$$

where

$$D_1 = \frac{1}{S_e} + \frac{1}{1-S_e} \tag{2.95}$$

Again this is a first order Taylor expansion around the mean and the derivative are all evaluated at the mean of the parameters. So the spectral representation of the perturbation can be expressed accordingly as:

$$dZ_w = D_1\left(\frac{\partial S_e}{\partial P_c}dZ_{P_c} + \frac{\partial S_e}{\partial f}dZ_f + \frac{\partial S_e}{\partial B}dZ_B + \frac{\partial S_e}{\partial L}dZ_L\right) \tag{2.96}$$

Because of Eqs. 2.51,2.52 and 2.53

$$dZ_w = [\varphi + \sigma_m Y_m]\, dZ_f + d_b dZ_{g_b} + d_l dZ_{g_l} + d_1 dZ_{g_b} + d_2 dZ_{g_l} \tag{2.97}$$

$$\varphi = D_1\left(\frac{\partial S_e}{\partial f} + \frac{\partial S_e}{\partial B}b_b + \frac{\partial S_e}{\partial L}b_L\right) \tag{2.98}$$

$$\sigma_m = D_1\frac{\partial S_e}{\partial P_c}b_m \tag{2.99}$$

$$d_b = D_1\frac{\partial S_e}{\partial P_c}Y_b \tag{2.100}$$

$$d_l = D_1\frac{\partial S_e}{\partial P_c}Y_l \tag{2.101}$$

$$d_1 = D_1\frac{\partial S_e}{\partial B} \tag{2.102}$$

$$d_2 = D_1\frac{\partial S_e}{\partial L} \tag{2.103}$$

## 2.5 Discussions

The most important findings of this chapter are the DNAPL saturation and wetting phase flow field in terms of the mean and variations based on the fundamental parameters which are statistically measurable. As will be discussed in next chapter, DNAPL saturation and water flow velocity are key factors affecting dissolution rate. Characterization of these factors as a function of basic soil properties is a central task of large-scale dissolution problem. The variations of the wetting phase flow field including the log conductivity, flow velocity and the DNAPL saturation field were derived in spectral amplitude form based on the findings of Jacobs' study. These properties will be incorporated into the large-scale transport model developed in Chapter 4 to evaluate effective dissolution properties. The effect of horizontal wetting phase flow on the DNAPL vertical flow field, the consequent effective permeability and mean DNAPL saturation field has been demonstrated to be insignificant for both perfectly-stratified systems and imperfectly-stratified systems.

# Chapter 3

# Local-scale Dissolution Characterization

## 3.1 Laboratory Findings

### 3.1.1 Introduction

As pointed out in Chapter 1, the two kinds of information needed to describe the large-scale DNAPL dissolution process are: 1. statistical information on DNAPL saturation distribution and wetting phase flow field as a function of small scale heterogeneity, 2. a local-scale dissolution model quantifying the relationship between dissolution rate with affecting factors. As the first issue was addressed in Chapter 2, this chapter focuses on the second problem. The purpose of this chapter is to establish a local-scale dissolution model that relates the dissolution rate coefficient with important affecting factors.

The local scale is a relative concept to the large-scale we refer, which extends to a scale of tens of meters and includes natural heterogeneity of porous media. In a local-scale system, the porous media and wetting phase flow field are regarded as homogeneous. DNAPL present in this system is also assumed uniformly distributed at residual saturation. The homogeneity of soil and DNAPL distribution results in a relatively uniform dissolution pattern through the system. Therefore, like the definition of Representative Elementary Volume (REV), the local scale we are referring here is small enough to assure uniform dissolution in the system, however large enough to apply transport equation. Usually the dimension of this local-scale is on the

order of a few centimeters.

The transport process with a mass transfer between DNAPL and aqueous phase in a local-scale DNAPL-aqueous-porous media system is described by the advection-dispersion equation as:

$$\frac{\partial}{\partial t}\left[\theta_a C\right] = \frac{\partial}{\partial x_i}\left[\theta_a D_{ij}\frac{\partial C}{\partial x_j}\right] - \frac{\partial}{\partial x_i}\left(q_i C\right) + \frac{\partial M}{\partial t} \tag{3.1}$$

where $C$ is the bulk aqueous concentration, $D_{ij}$ is local dispersion coefficient, $\theta_a$ is the aqueous phase volumetric content, $q_i$ is the specific discharge in direction $i$ . $\frac{\partial M}{\partial t}$ represents the mass transfer rate per unit of bulk volume to the aqueous phase. If the mass transfer is solely due to the dissolution of DNAPL and other forms of mass transfer are ignored, then we can write:

$$\frac{\partial M}{\partial t} = -\rho_n \frac{\partial \theta_n}{\partial t} \tag{3.2}$$

where $\rho_n$ is the density of DNAPL, $\theta_n$ is the DNAPL volumetric content. The term of $\rho_n \frac{\partial \theta_n}{\partial t}$ represents the mass transfer contribution from the DNAPL dissolution, which results in the DNAPL saturation decrease. Here we focus on a saturated system with DNAPL entrapped, for which the transport equation can be simplified as:

$$\frac{\partial}{\partial t}\left[\theta_a C\right] = \frac{\partial}{\partial x_i}\left[\theta_a D_{ij}\frac{\partial C}{\partial x_j}\right] - \frac{\partial}{\partial x_i}\left(q_i C\right) - \rho_n \frac{\partial \theta_n}{\partial t} \tag{3.3}$$

The characterization of dissolution of DNAPL in porous media has been studied widely in the last decade. Considerable work has been aimed at developing an appropriate mass transfer rate model for DNAPL-aqueous phase mass transfer. Traditionally local equilibrium is assumed to predict the rate of DNAPL removal. Results of recent laboratory column studies, however, demonstrated the potential limitations of such an assumption. It has been observed that mass transfer may become rate limited as DNAPL saturation is low (Powers *et al.*, 1994). The mathematical modeling of rate-limited mass transfer can be summarized as a first-order mass transfer model. More specifically, the net flux of a chemical species across the interface between DNAPL and aqueous phase results directly from the chemical potentials of that species in the respective phase. It is widely accepted that a single-resistance, linear-driving-force model is adequate to describe the rate of such interphase mass transfer (Miller *et al.*, 1990; Powers *et*

*al.*,1991). The mass transfer between aqueous phase and DNAPL is described by a lumped-parameter model in Eq. 3.4 which equates interphase mass transfer to the product of a linear driving force and a mass transfer rate coefficient:

$$-\rho_n \frac{\partial \theta_n}{\partial t} = \Omega \left( C_s - C \right) \tag{3.4}$$

where $\Omega$ is the dissolution rate coefficient which includes the effect of interfacial area and advection/diffusion mass transfer rate. Though the mass transfer is represented by a first-order kinetic process, it also includes the local equilibrium dissolution when $\Omega$ is large.

To characterize the rate coefficient both qualitatively and quantitatively, a large number of laboratory experiments have been conducted. Most of experiments were conducted in one-dimensional columns packed with homogeneous porous media where residual DNAPL saturation was established (Imhoff *et al.*, 1994; Miller *et al.*, 1990; Powers *et al.*, 1992; Geller and Hunt, 1993; Powers *et al.*, 1994).

Table 1.1 summarizes the results of major experimental studies. The scales of the experiments where correlation models were obtained are also provided in the table. The scale for the lab experiments is around 3 $cm \sim 10$ $cm$, which is regarded as a local scale. From these experimental results, we can conclude that the most apparent and important factors influencing dissolution rate coefficient are flow conditions (including flow velocity, aqueous phase diffusion coefficient, viscosity, density), porous media properties (including porosity, mean grain size, pore size distribution, uniformity) and DNAPL saturation (initial saturation and current saturation). The differences of curve-fitting coefficients obtained from various experiments are contributed from different experimental conditions, different column scales applied and different experimental methods.

Though many studies have been conducted to characterize the local mass transfer process as described in the first section, full characterization of the mass transfer coefficient is difficult due to the uncertainty of controlling factors under various conditions. Questions like whether or not the rate coefficient is a function of wetting phase flow velocity still remain unanswered. Though a lot of experiments have confirmed that the mass transfer rate is a function of water velocity, some would argue that this effect is due to the ability to transport dissolved components and keep the driving force $(C_s - C)$ large. In addition, the column averaged concentration and sat-

uration cannot provide the ground to correlate the rate constant with controlling factors due to the effect of smaller scale nonuniformity. Therefore, a well-designed column experimental study with large amount of reliable data is crucial to establish an appropriate model of mass transfer. Imhoff (1994) and Powers (1994) performed two independent column experiments studying DNAPL dissolution in homogeneous porous media. These experiments provide important data for establishing a predicative model of mass transfer.

### 3.1.2 Experiments Conducted by Imhoff and Powers

By a series of experiments, Imhoff (1994) characterized the dissolution of DNAPLs trapped at residual saturation in saturated porous media packed in one-dimensional column. The Gamma attenuation technique was applied to measure the DNAPL saturation at the resolution of 1mm layers during the dissolution experiments. This method enabled him to calculate the rate coefficient more reliably based on the saturation change, while in other studies it is determined based on effluent concentration measurement. In addition, the apparatus can measure the saturation and porosity at various locations along the column at millimeter scale. The dissolution rate at such small scale is more accurate than the column-averaged rate. Moreover, this experiment monitored the continuous change of DNAPL saturation during the dissolution, which enable them to investigate the correlation between DNAPL saturation and dissolution rate more thoroughly. More than 600 dissolution rate data were reported as well as the flow rate, and DNAPL saturation. The governing equation of Eq. 3.3 and dissolution model of Eq. 3.4 are used to derive the dissolution rate. The concentration field was regarded as steady state and the dispersion factor was ignored by Imhoff based on an order of magnitude analysis, which showed that the advective and source terms dominate for the experimental conditions. The equation determining the dissolution rate coefficient was obtained as:

$$\Omega(x,t) = \frac{\rho_n \frac{\partial \theta_n}{\partial t}(x,t)}{C(L^*,t) + \frac{\rho_n}{U}\int_x^{L^*} \frac{\partial \theta_n}{\partial t}(x',t)\,dx' - C_s} \tag{3.5}$$

where $C(L^*,t)$ is the effluent concentration out of the column with a length of $L^*$, $U$ is the flow velocity. So the dissolution rate coefficient can be calculated based on the measurements of DNAPL saturation as a function of time and the effluent concentration.

The experiments particularly evaluated the dependence of dissolution rate coefficient on the

water velocity and DNAPL saturation. Figure 3-1 and 3-2 are reprints of Figure 6 and Figure 7 in Imhoff's paper (1994). $K_l$ used in Figure 3-1 and 3-2 is the same as dissolution rate coefficient in this work $\Omega$. It was found that the dissolution rate coefficient is positively correlated with water velocity and DNAPL saturation. Larger DNAPL saturation provides more interfacial area between two phases and enhances the mass transfer. The mechanism of how the flow velocity affects the dissolution rate coefficient is not well understood yet.

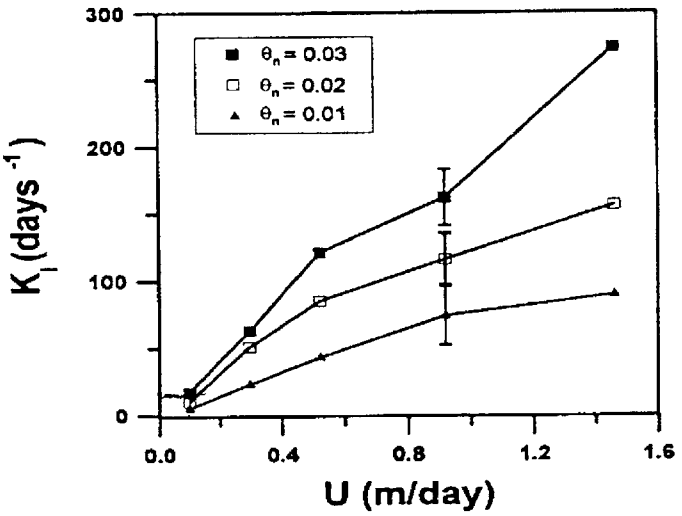


Figure 3-1: Dissolution rate coefficient changes with water velocity in Imhoff's experiments

It can be seen in Figure 3-2 that the dissolution rate is a function of locations along the column. The dissolution rate is higher at the top of the column and lower at the bottom, even at the same DNAPL saturation and water flow rate. Imhoff attributed this finding to the increasing width of the dissolution front with time as water with unsaturated concentration travel into lower regions of the column, as shown in Figure 3-3. Here Figures 3-3 to 3-5 are reprints from Imhoff (1992).

This different saturation profile at different column locations is likely attributed to two mechanisms as pointed out by Imhoff: 1. the nonuniform distribution of DNAPL along the column, 2. the growth of DNAPL fingers as a result of nonuniform dissolution as water travel through the column. DNAPL was introduced into the column by slowly replacing water in

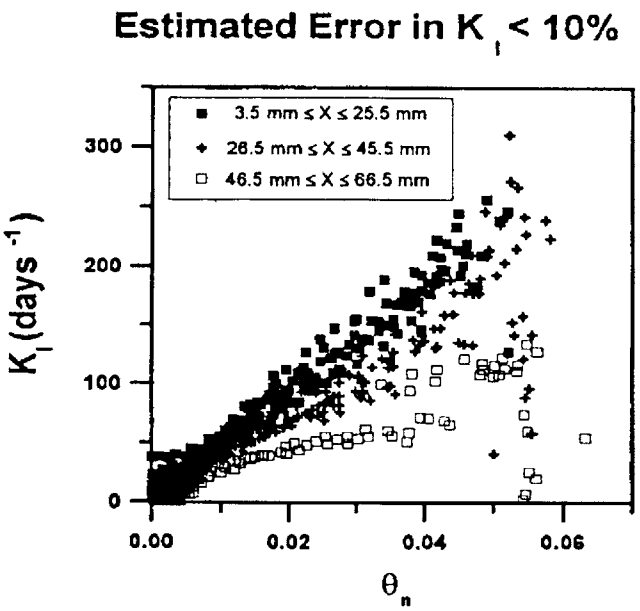


Figure 3-2: Dissolution rate coefficient changes with DNAPL saturation in Imhoff's experiments

the column as capillary pressure increased. Once the DNAPL saturation become static at a specific high capillary pressure, the saturation established is the invasion DNAPL saturation. Then water was pumped through the column at a small rate to remove the majority of DNAPL. In this way the residual DNAPL saturation was established in the column, which is defined as initial DNAPL saturation for dissolution experiments. As shown in Figure 3-4, both the DNAPL invasion saturation and initial saturation vary along the column. Imhoff attributed this variation to bypassing of both DNAPL flow and water flow when the saturation is established.

The second mechanism offered by Imhoff to explain the reduction of dissolution rate is dissolution fingering. As shown in Figure 3-5, the flow of water downward may not be uniform since DNAPL may be distributed nonuniformly over the cross-section of the column, leading to nonuniform relative permeability. As clean water front move further inside the column, the dissolution finger grows and increases the dissolution front as we see in Figure 3-3. In general, the reduced dissolution rate at the bottom of the column attributes to the nonuniform distribution of DNAPL along and cross-section of the column, which subsequently lengthens the dissolution front and reduces the saturation change rate at the bottom of the column. Though

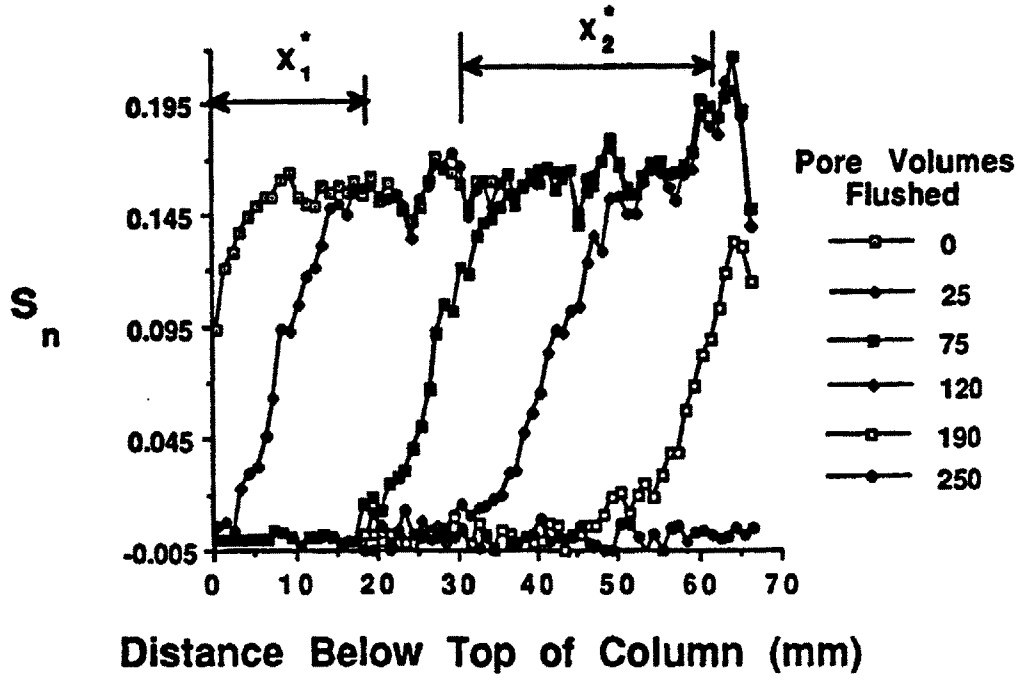


Figure 3-3: Changing DNAPL saturation profile during Imhoff's experiment. $x_1 \approx 17mm$ at 25 pore volumes to $x_2 \approx 35mm$ at 120 pore volumes.

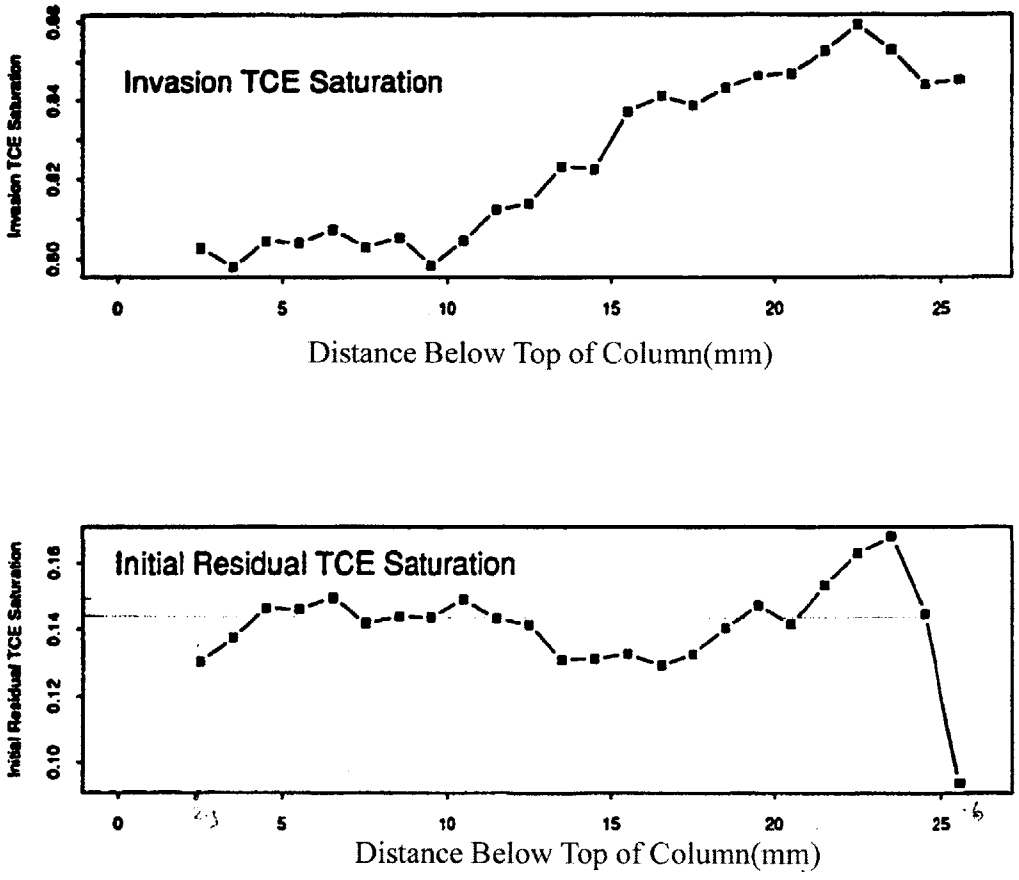


Figure 3-4: Variation of invasion DNAPL saturation and initial DNAPL saturation for Imhoff's experiment.

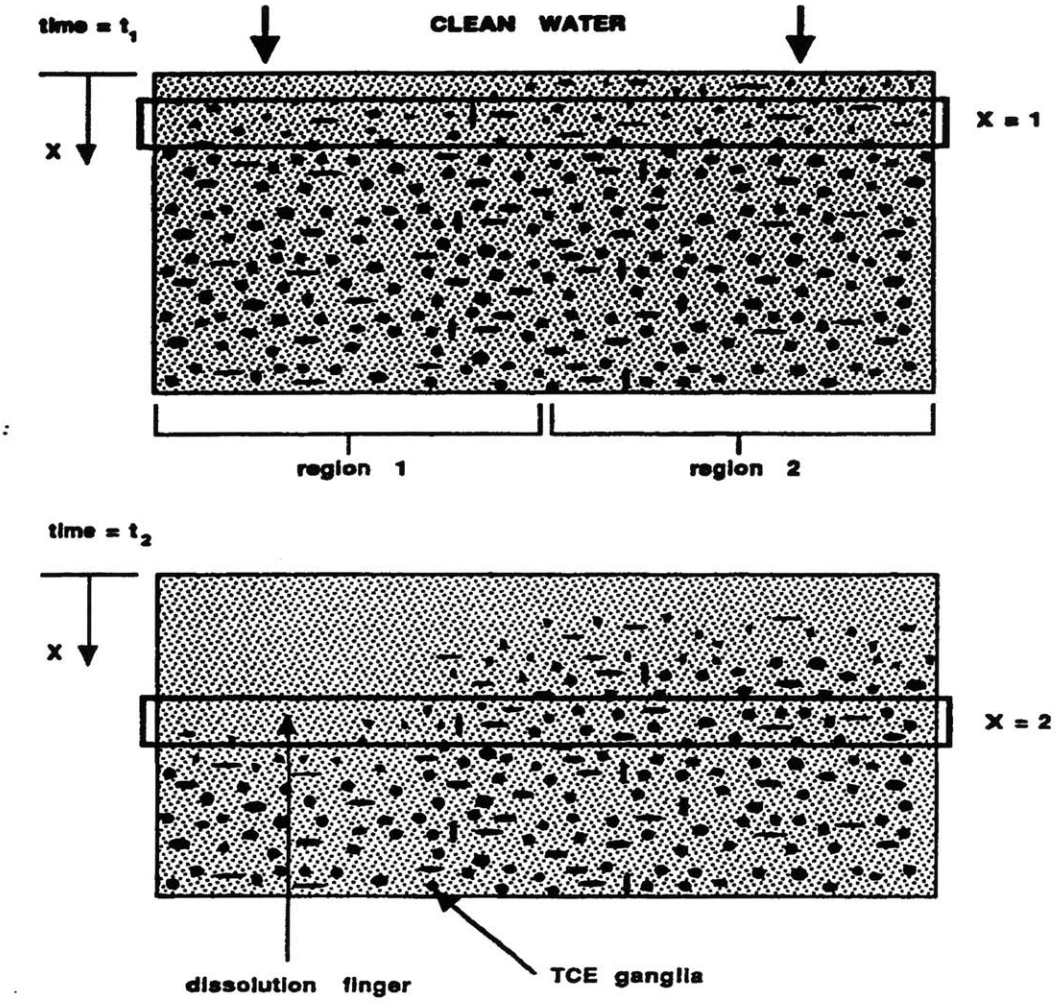


Figure 3-5: Hypothetical cross-section through the column illustrating the formation of a dissolution finger in Imhoff's experiment

such hypotheses to explain the variation of measured dissolution rate coefficient at various column locations are provided, a more thorough study of this observation is not available from Imhoff's work. Another explanation of dissolution rate coefficient behaves as a function of time and location can be that the local mass transfer model in Eq. 3.4 may not be adequate. Further study of this observation is necessary to provide more insight of local dissolution characterization.

Imhoff summarized his experimental results by establishing a dimensionless model as presented in Table 1.1:

$$Sh = 340\,\mathrm{Re}^{0.71}\,\theta_n^{0.87}\,(x/d_{50})^{-0.31} \tag{3.6}$$

Powers and coworkers performed a similar column experiment (Powers *et al.*, 1994) using different soils. They tested the dissolution rate in various porous media at various saturation and water velocity. They found that the dissolution rate is a function of soil properties such as uniformity, mean grain size etc. Based on the experimental data, the log dissolution rate is plotted against log permeability of the soil in Figure 3-6, which represents the soil characteristic properties. The negative correlation between dissolution rate and permeability reflects the fact that smaller blobs are trapped in the lower permeability zone, which provides larger interfacial area and accelerates the dissolution process. A dimensionless empirical model is established based on data from the experiments as:

$$Sh = 4.13\,\mathrm{Re}^{0.598}\,\delta^{0.673} U_i^{0.369} \left(\frac{\theta_n}{\theta_{n_i}}\right)^{\beta} \tag{3.7}$$

From these results, we can conclude that the DNAPL dissolution rate coefficient is a function of wetting phase velocity, DNAPL saturation and soil properties, such as uniformity index, mean grain size.

## 3.2 Prediction Model of Local Dissolution Rate

### 3.2.1 Model Development

The experimental results of Imhoff and other researchers suggest the possible relationship between the dissolution rate coefficient with soil properties, DNAPL residual saturation and the water flow velocity (Powers et al.,1992; Imhoff et al.,1994). The strongest affecting factor as

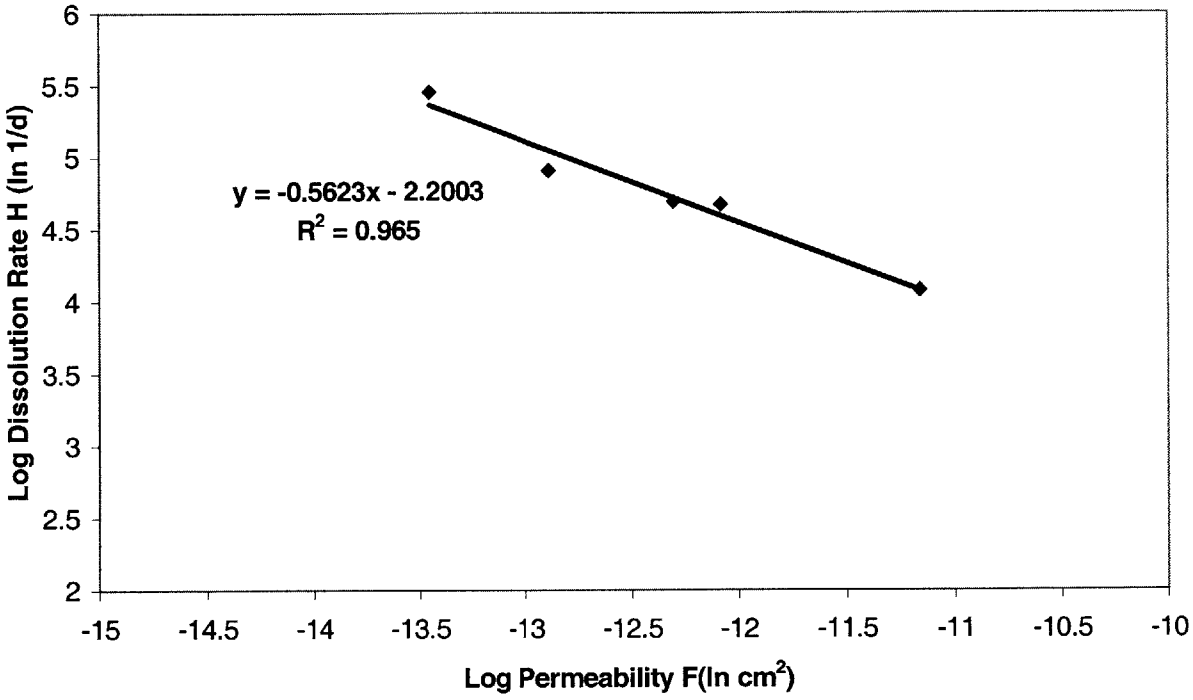


Figure 3-6: Log dissolution rate coefficient changes with permeability in Powers' experiments

shown in Figure 3-2 is DNAPL saturation, which directly affects the mass transfer source and interfacial area between DNAPL and water. The impact of properties of porous media is reflected by the shape and size of DNAPL blobs entrapped, which subsequently affect the interfacial area. Though the underlying mechanism of flow velocity's effect on dissolution rate coefficient is still unclear, the clear evidence of relationship is shown by experimental work discussed above. Therefore, a partial correlation model can be established between the mass transfer coefficient with most prominent affecting factors. Eq. 3.8 includes a correlated part with associated slope and an uncorrelated residual. The partial linear correlation between the log rate constant and controlling properties can be written as:

$$H = a + bf + cW + dv + g_h \tag{3.8}$$

where $a, b, c, d$ are slope constants, $H = \ln \Omega$ is the log dissolution rate coefficient, $f$ is the log permeability, $W$ is the transformed aqueous phase saturation, $v = \ln q_1$ is the log aqueous phase specific discharge in the mean direction $i = 1$, and $g_h$ is the uncorrelated residual. The log permeability is the parameter which represents the porous media's properties such as median size and uniformity, $W$ represents the DNAPL saturation and $v$ represents the flow velocity effect. This model can be broadly used due to its flexibility and capability to describe the relationship between $H$ and controlling factors. When the slope constants are zero, this model can describe an uncorrelated relationship. When $g_h = 0$, this is a perfect deterministic linear relationship. Such a partial correlation approach has been applied by prior researchers to represent an imperfect correlation in stochastic studies. For example, Miralles-Wilhelm (Miralles-Wilhelm & Gelhar, 1996) established a partial correlation model between the retardation coefficient and log conductivity.

The model is similar to those empirical model obtained from laboratory experiments. For example, by assuming that the uniformity index equals one, the model summarized by Powers 1994 in Eq. 3.7 can be simplified as

$$Sh = \beta_0 \, \mathrm{Re}^{\beta_1} \left( \frac{\theta_n}{\theta_{n_i}} \right)^{\beta} \tag{3.9}$$

where $\beta_0$, $\beta_1$ and $\beta$ are coefficients. By substituting Eqs. 1.1 and 1.3, Eq. 3.9 becomes

$$\Omega = \beta_0 v_a^{\beta_1} d_p^{\beta_1 - 2} \left(\frac{\theta_n}{\theta_{n_i}}\right)^{\beta} D_m \left(\frac{\rho_a}{\mu_a}\right)^{\beta_1} \tag{3.10}$$

Take logarithm of both sides of Eq. 3.10, we have:

$$H = \ln \beta_0 + \ln D_m + \beta_1 \ln \left(\frac{\rho_a}{\mu_a}\right) - \beta \ln \theta_{n_i} + \beta_1 \ln v_a + (\beta_1 - 2) \ln d_p + \beta \ln \theta_n \tag{3.11}$$

According to Kozeny-Carmen Equation, there is an empirical relationship between permeability and grain size:

$$k = \left[\frac{\phi}{(1-\phi)^2}\right] \frac{d_p^2}{180} = \beta_3 d_p^2 \tag{3.12}$$

So Eq. 3.11 becomes:

$$H = \ln \beta_0 + \ln D_m + \beta_1 \ln \left(\frac{\rho_a}{\mu_a}\right) - \beta \ln \theta_{n_i} - \beta_1 \ln \theta_a + \beta_1 \ln q_a + \beta_4 \ln k + \beta \ln \theta_n \tag{3.13}$$

where $\beta_4$ is the new coefficient. Since

$$W = \ln \frac{S_e}{1 - S_e} \tag{3.14}$$

$$\approx \ln \frac{1 - S_n}{S_n} \tag{3.15}$$

where $S_n$ is DNAPL saturation. At small DNAPL saturation, $1 - S_n \approx 1$,

$$\ln \theta_n \approx \ln \phi - W \tag{3.16}$$

So combining Eq. 3.13 and Eq. 3.16, Eq. 3.13 can be approximates as:

$$H = a' + b' f + c' W + d' v \tag{3.17}$$

where $a', b', c'$ and $d'$ are new coefficients:

$$a' = \ln \beta_0 + \ln D_m + \beta_1 \ln \left( \frac{\rho_a}{\mu_a} \right) - \beta \ln \theta_{n_i} - \beta_1 \ln \theta_a + \beta \ln \phi \quad (3.18)$$

$$b' = \beta_4 \quad (3.19)$$

$$c' = -\beta \quad (3.20)$$

$$d' = \beta_1 \quad (3.21)$$

So we can transform the empirical model obtained by Powers to the general form used in Eq. 3.8. Other empirical model presented in Table 1.1 can also be transformed in the form of Eq. 3.17 similarly. This demonstrates that the model proposed in this work in Eq. 3.8 is a generalization from the empirical model obtained from laboratory experiments. As we can see from Eq. 3.17, the constant $a'$ includes the effect of diffusivity, aqueous phase density, aqueous phase viscosity etc. Therefore, for different species of DNAPL, the effect should be reflected by the constant $a'$.

### 3.2.2 Model Calibration

The coefficients in Eq. 3.8 are determined from the selected data reported by Imhoff and Powers. The relationship between dissolution rate and DNAPL saturation is reflect in Figure 3-7 where a linear regression is established between $H$ and $W$. Because the local model we are establishing is on the basis of the uniform distribution of DNAPL and dissolution front in the small-scale, only data satisfying this condition are selected to calibrate the model in the next section. In Imhoff's experiment, this ideal situation only occurs at the top of the column where the travel distance of water is small and the growth of the dissolution finger is minimum. Here we select the data measured at the top portion of the column to establish the relationship between dissolution rate with DNAPL saturation as shown in Figure 3-2. The slope constant $c$ between $H$ and $W$ can be found is $-0.90$ as found by the linear regression result in Figure 3-7. Similarly $b$ can be determined from Powers' work which is equal to $-0.55$ based on regression results in Figure 3-6. $d$ is found around 1 from the regression of data for different DNAPL saturation at $\theta_n = 0.01$, $\theta_n = 0.02$ and $\theta_n = 0.03$, reported by Imhoff (1994) as shown in Figure 3-8.

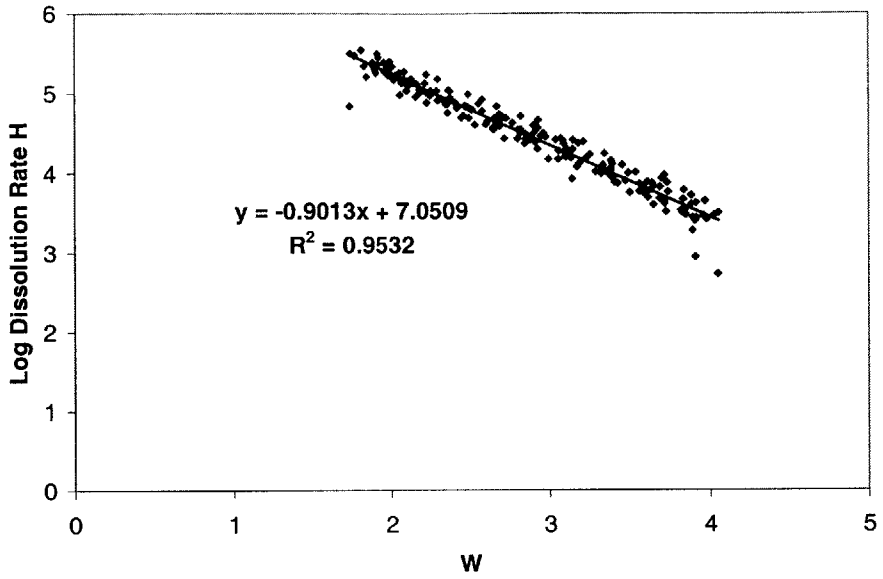


Figure 3-7: Log dissolution rate coefficient changes with transformed saturation

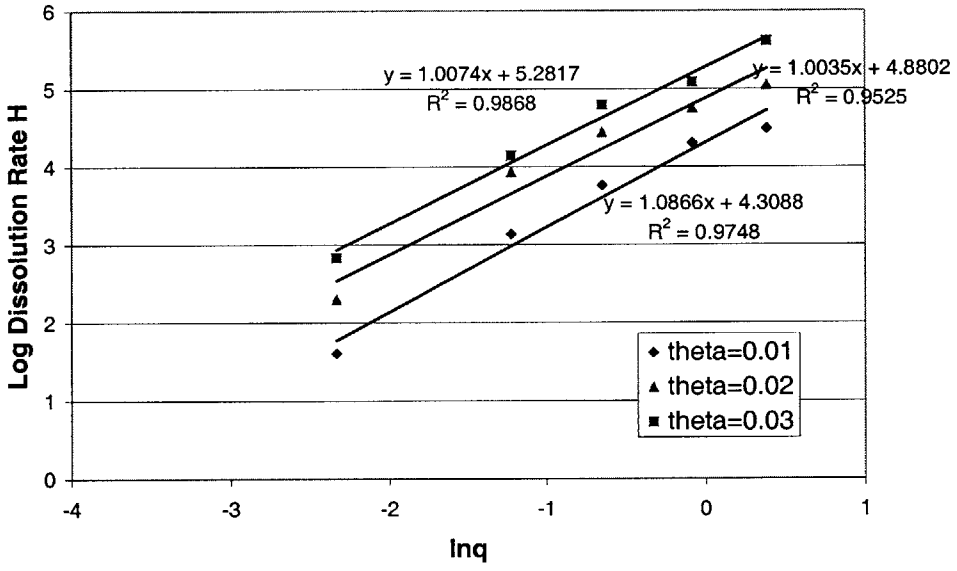


Figure 3-8: Log dissolution rate coefficient changes with log water specific discharge

$$b = -0.55 \tag{3.22}$$

$$c = -0.90 \tag{3.23}$$

$$d = 1.0 \tag{3.24}$$

Once the slope coefficients are determined, we can predict the local log dissolution rate $H$ under the conditions of flow rate $q$, DNAPL saturation transformation $W$ and intrinsic permeability $F$ based on the reference values obtained from Imhoff's work.

According to Eq. 3.8, the unknown log dissolution rate for an aquifer can be written as

$$H_o = a + bF_o + cW_o + dv_o + g_h \tag{3.25}$$

where $F_o, W_o$ and $v_o$ represent the log permeability, DNAPL saturation and aqueous velocity of the DNAPL source zone. The measured dissolution rate of reference experiments can be written as

$$H_r = a + bF_r + cW_r + dv_r \tag{3.26}$$

where $H_r$ is the reference log dissolution rate found in Imhoff's experiments. $F_r, W_r$,and $v_r$ are the properties used in Imhoff's experiments. By subtracting Eq. 3.26 from Eq. 3.25, we can find the expression for the unknown log dissolution rate based on the reference results.

$$H = H_r + b\,(F - F_r) + c\,(W - W_r) + d\,(v - v_r) + g_h \tag{3.27}$$

So the predicted value of $H$ is the expected value of above equation:

$$H_p = H_r + b\,(F - F_r) + c\,(W - W_r) + d\,(v - v_r) \tag{3.28}$$

where $F_r, W_r, v_r$ are the properties used in Imhoff's experiments closest to $F, W$ and $v$. As we can see in Eq. 3.28, using reference values provided by Imhoff's work can avoid estimating the constant $a$. In addition, Imhoff obtained the dissolution rate coefficient at different combinations of DNAPL saturation and water flow velocity as shown in Table 3.1 . Since it is necessary to

estimate the dissolution rate for widely varied conditions, it is likely that the random error can be introduced if we choose only one set of conditions in Imhoff's data as a reference, which can be significantly different with the conditions we are considering. Therefore, to minimize the random error in estimating $H_o$ in a systematic way, the reference conditions of $v_r$ and $W_r$ are chosen as closest to applied conditions $v$ and $W$. $v_r$, $W_r$ and the corresponding $H_r$ in Table 3.1 are used in Eq. 3.28 to calculate $H_p$.

Table 3.1: Reference Values from Imhoff Experiments at Different Conditions

| $q_r(m/d)$ | $v_r = \ln q_r$ | $\theta_n = 0.03$ $W_r = 2.37$ | $\theta_n = 0.02$ $W_r = 2.80$ | $\theta_n = 0.01$ $W_r = 3.53$ |
|---|---|---|---|---|
| 0.097 | $-2.33$ | $H_r = 2.83$ | $H_r = 2.30$ | $H_r = 1.61$ |
| 0.295 | $-1.22$ | $H_r = 4.14$ | $H_r = 3.93$ | $H_r = 3.14$ |
| 0.523 | $-0.65$ | $H_r = 4.80$ | $H_r = 4.44$ | $H_r = 3.76$ |
| 0.92 | $-0.08$ | $H_r = 5.09$ | $H_r = 4.75$ | $H_r = 4.30$ |
| 1.46 | 0.38 | $H_r = 5.61$ | $H_r = 5.05$ | $H_r = 4.49$ |

Note: for all DNAPL saturation and water velocity, $F_r = -14.1\left(\ln cm^2\right)$.

For example, if $q_o = 0.1m/d$, $\theta_n = 0.013$ for a given site, then from Table 3.1 the reference values should be selected as:

$$\begin{aligned} H_r &= 1.61 \\ q_r &= 0.097(m/d) \\ v_r &= \ln q_r = -2.33 \\ W_r &= 3.53 \\ F_r &= -14.1 \end{aligned}$$

To predict the mean of log dissolution rate for a certain aquifer, it can be written as:

$$\overline{H} = H_r + b\left(\overline{F} - F_r\right) + c\left(\overline{W} - W_r\right) + d\left(\overline{v} - v_r\right) \tag{3.29}$$

where $\overline{H}$ is the predicted mean log dissolution, $\overline{F}, \overline{W}$ and $\overline{q}$ are the mean properties of the DNAPL source zone.

The variance $\sigma^2_{g_h}$ of a system can be determined by the measured dissolution rate coefficient, the flow velocity and DNAPL saturation as:

$$g_h = H_m - H_p \tag{3.30}$$

$$\sigma^2_{g_h} = \overline{(H_m - H_p)^2} \tag{3.31}$$

where $H_m$ is the measured dissolution rate.

### 3.2.3 Model Validation

The model developed above is evaluated by data from another experiment performed by Imhoff (1994). For the data measured for relatively large and moderate DNAPL saturation, Figure 3-9 shows a good agreement between predicted dissolution rate and measured data. The $\sigma^2_{g_h}$ calculated by Eq. 3.31 is found around 0.024.

The model is also tested by data reported from Powers (Powers *et al.*, 1994). Powers varied flow velocity, DNAPL initial saturation and soil types in her experiment. Figure 3-10 presents the predicted log dissolution rate coefficient against the measured data. Since the directly measured dissolution rate coefficient data are not available in Powers' work, here we estimate them according to the empirical model established in her work based on the laboratory experiments. As we can see, there is are significant deviations between the model predicted values with data estimated from the experiments. The $\sigma^2_{g_h}$ calculated by Eq. 3.31 is found around 1.82. This large variation reveals the potential uncertainty of the deterministic model predictions, and underscores the importance of residual item in the model in Eq. 3.8. The deviation can attribute to the difference of experimental method, conditions, errors of experimental data, as illustrated in Table 1.1; different small-scale DNAPL dissolution column experiments can give rise to significantly different local model. Regarding Powers' experiments, the error source may come from the experimental methods used to determine the dissolution rate coefficient as an average through the column. The DNAPL saturation's effect cannot be fully accounted since only the initial saturation was measured during the experiments. In addition, the estimated value from the empirical model established from the data can also introduce error.

The applicability of the proposed dissolution model in Eq. 3.8 is limited in that some affecting factors may not be included in the model, such as uniformity of porous media. It is clear that even for a homogeneous system such as that studied in Powers' work, the deviation

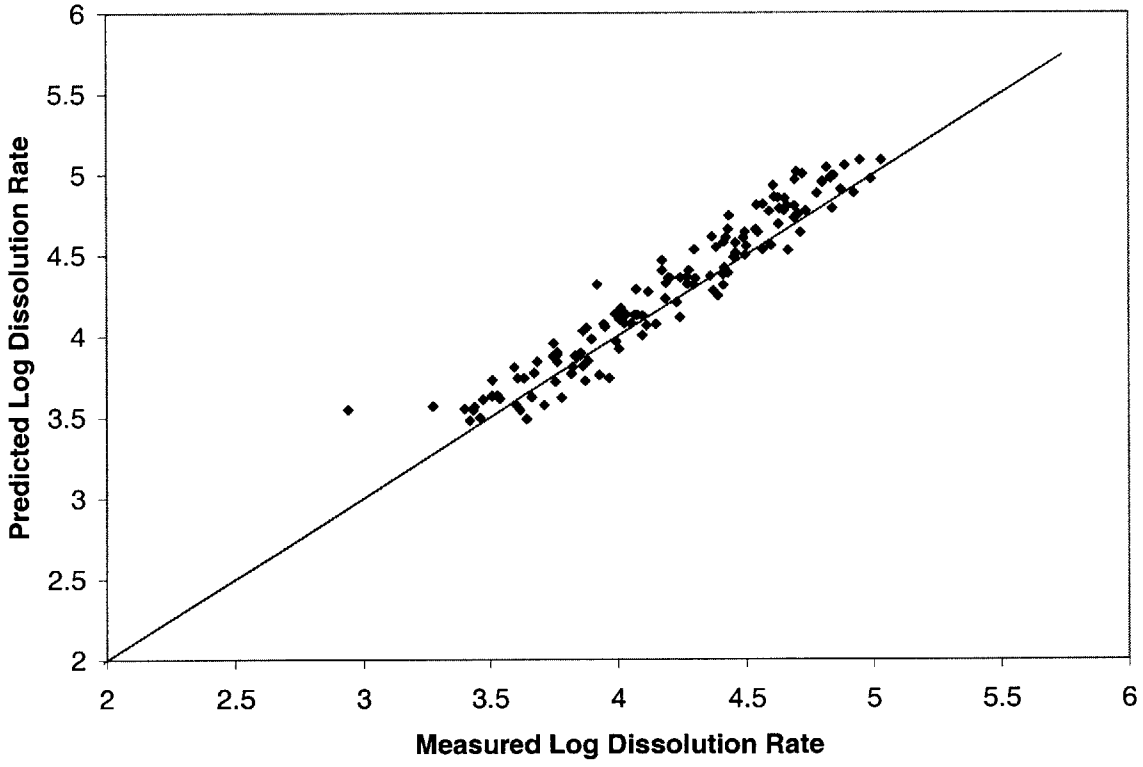


Figure 3-9: Comparison of model predicted results with measured data from Imhoff's experiment

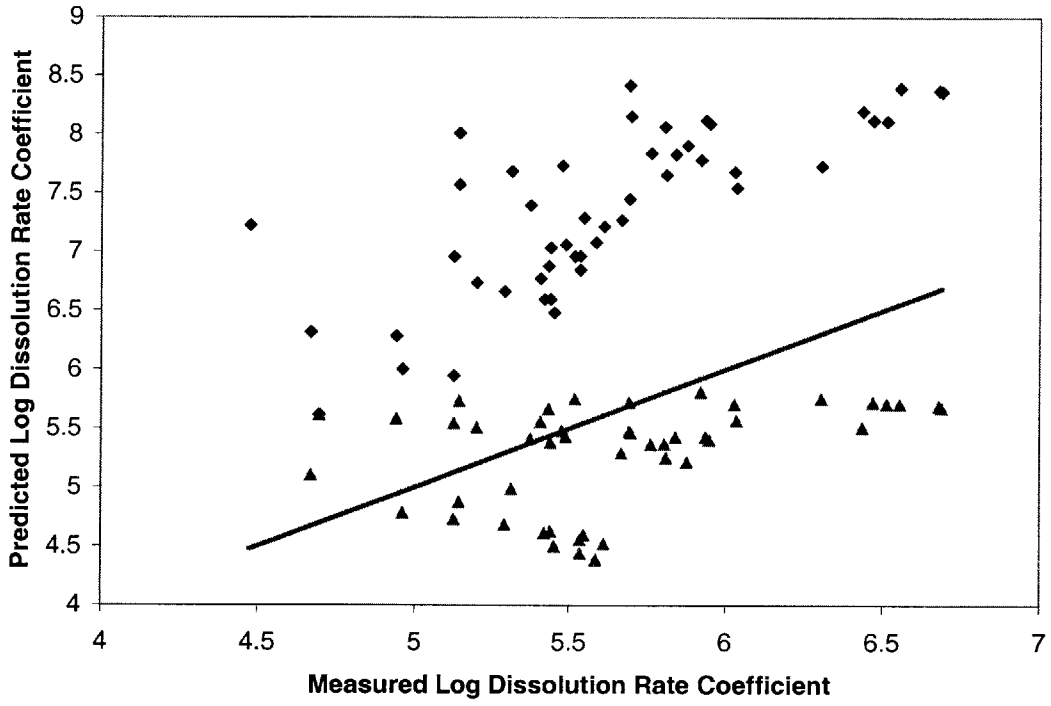


Figure 3-10: Comparison of model predicted results with measured data from Powers' experiment

between model prediction and measured data can be significant. Taking into consideration of both imperfect data available and limitations of the model, it is expected that the residual variance $\sigma^2_{g_h}$ can be large when applying the model to a field-scale, heterogeneous aquifer where DNAPL distribution can be seriously nonuniform. However, with the improvement of field data collection and measurement method, $\sigma^2_{g_h}$ can be determined exactly. This enables the local model established here to correctly predict the variance of log dissolution rate coefficient $\sigma^2_h$, which is found to be an important parameter controlling large-scale dissolution properties in Chapter 4.

## 3.3 Summary and Discussions

Based on the laboratory experimental results, a model extended from dimensionless empirical models is established to predict the local-scale dissolution rate. Dissolution rate coefficient is characterized as a partial correlation with log permeability of porous media, the transformation of saturation, and the flow velocity. This model can be broadly used due to its flexibility and capability to describe the relationship between log dissolution rate coefficient $H$ and controlling factors. When the slope constants are zero, this model can describe a uncorrelated relationship. When the uncorrelated residual equals zero, this represents a perfect linear relationship. This model can be utilized to predict the mean dissolution rate for a given site with provided mean hydrological properties and DNAPL saturation. The model was calibrated and the slope constants were obtained by experiments conducted by Imhoff *et al.* (1994). Then independent experimental data provided by Powers (1994) and Imhoff (1994) were utilized to validate the model. The model predicted dissolution rate under the experimental conditions of Imhoff' work has a good agreement with an independent data set . The residual variance was found large for the data reported by Powers. This indicates the potential uncertainty in the prediction model, especially when the data is limited and unreliable, which is often encountered in field-scale data collection. However, the local mean dissolution rate coefficient predicted by the model is demonstrated secondary affecting large-scale properties, as studied in Chapter 4. The variance of dissolution rate $\sigma^2_h$ is the dominant factor. Therefore, regardless of the uncertainty of the deterministic prediction model for the average dissolution rate, it is much more important that the model can allow us to calculate the spatial variability of dissolution rate coefficient based

on the input variability of wetting phase flow rate, DNAPL distribution and permeability, and a residual factor $\sigma^2_{g_h}$. This will be illustrated in the next chapter.

# Chapter 4

# Dissolution in a Large-scale DNAPL Source Zone

## 4.1 Introduction & Conceptual Framework

DNAPL contamination source in groundwater systems usually extends to relatively large area due to the large amount of DNAPL dumped in the waste disposal site and the lateral spreading of the DNAPL plume due to the spatial heterogeneity and anisotropy of the aquifer. Therefore, the dissolution in a DNAPL source zone usually occurs in a large scale relative to the correlation scale. As shown in Figure 4-1, clean groundwater migrates into the source zone from a pristine upgradient area. The mean groundwater concentration gradually grows as the travel distance increases due to dissolution.

Field observations reported that DNAPL concentrations measured from the sampling wells around a DNAPL source zone were far below the effective solubility, which implies the dissolution properties for large-scale heterogeneous porous media is different with that found in laboratory experiments illustrated in Chapter 3. This paradox is likely attributed to the local non-equilibrium dissolution as well as the small scale heterogeneity of an aquifer, which results in highly non-uniform DNAPL distribution and preferential flow bypassing zones with high DNAPL saturation. The quantitative analysis to characterize the large-scale dissolution aggregating effects of small-scale heterogeneity is not available so far. In this chapter we developed a stochastic analysis to evaluate the large-scale dissolution properties, on the basis of the inter-

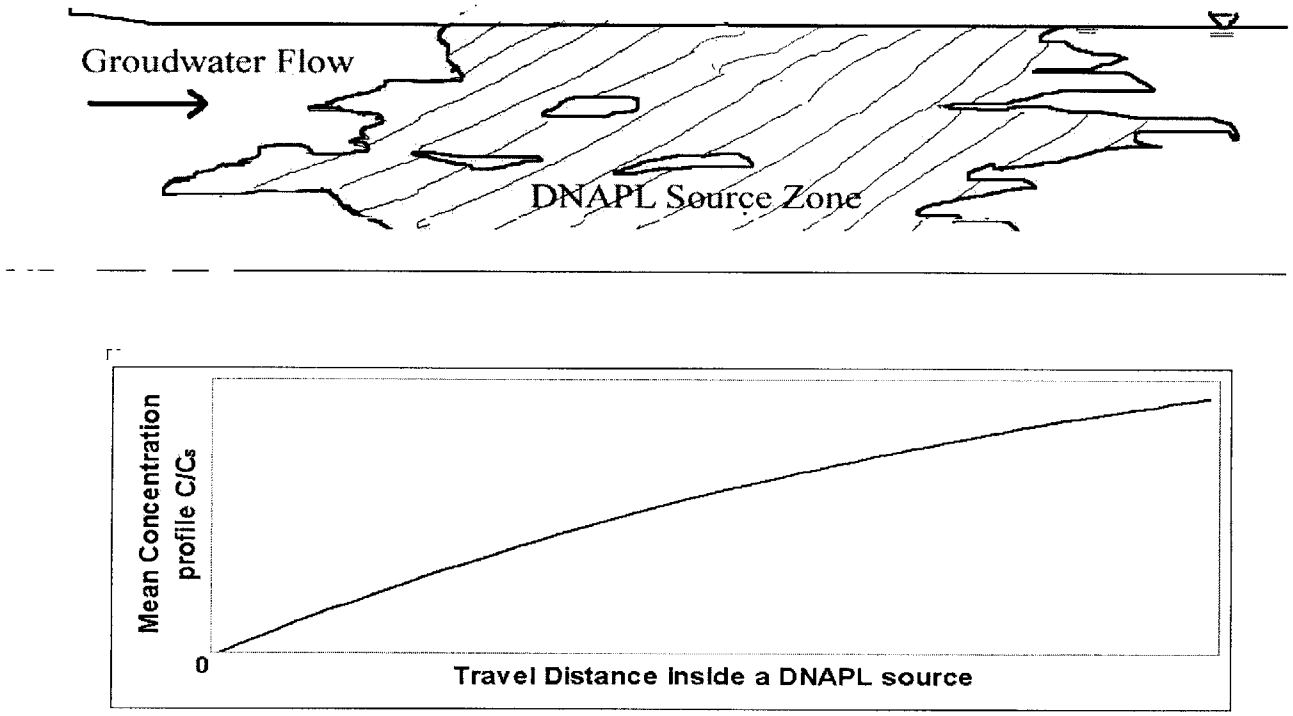


Figure 4-1: Mean DNAPL concentration as a function of groundwater travel distance inside a DNAPL source zone

related spatial distributions of flow and DNAPL saturation derived in Chapter 2, and the local dissolution model obtained in Chapter 3. The effect of spatial variability of hydrological and geochemical properties is captured by the cross products in mean equations describing the field solute transport. The coupled perturbation and mean equations are solved simultaneously to derive the effective properties, including effective dissolution rate coefficient, effective dissolution distance, effective velocity and macrodispersivity.

The DNAPL source zone is assumed stationary as the mean DNAPL saturation is invariable spatially. As pointed out by Jacobs (1998), though this assumption may not be strictly accurate at the boundary area of a DNAPL distribution, it has been shown by other researchers that it does not prevent the generation of reasonable results (Polmann, 1990). The aquifer is assumed imperfectly stratified that the horizontal correlation scale is much larger than the vertical correlation scale. This assumption has been widely applied based on the field observation, e.g. the horizontal correlation scale of the Borden Site is 20 times larger than the vertical correlation scale as reported by Sudicky (1986). Local dispersion has been demonstrated insignificant in field-scale properties by many studies (Gelhar and Axness, 1983; Polmann, 1990), e.g., Miralles-Wilhelm found that the local dispersion is negligible in studying the field-scale effective decay rate of solute (Miralles-Wilhelm & Gelhar, 1996). Therefore, the effect of local dispersion is neglected in deriving the effective properties.

It has been observed in the laboratory experiments that DNAPL depletion time could be decades and century in a heterogeneous porous media (Eberhardt & Grathwohl, 2002). As discussions in Chapter 2, the change of DNAPL saturation field and wetting phase flow field over time are assumed negligible. Since the dissolution rate is mainly determined by the DNAPL saturation field and wetting phase flow field as discussed in Chapter 3, it is assumed that the rate at which mass dissolved into the ambient groundwater over time is constant. It has also been observed that the concentration field reach to the steady state in a relatively short period compared to the depletion time scale (Eberhardt & Grathwohl, 2002). Therefore, in this study the DNAPL concentration in the aqueous phase is assumed steady-state over time.

The random input components are assumed to be stationary in the stochastic analysis, which indicates that the mean and the perturbation are spatially invariable. The nonstationarity in this analysis is evaluated by different methods. First, the mean concentration experiences an

increase along the main flowing direction within the source zone due to dissolution. The nonstationarity associated with this trend in the concentration field is recognized and transformed to a stationary problem. Secondly, the relative impact of nonstationarity at the boundary to the effective properties is evaluated. The fluctuation of the concentration at the boundary changes dramatically from zero to a non-zero value, which leads to another nonstationarity different with the downstream nonstationarity. The scale of the boundary effect is calculated based on the transfer function theory and the relative significance of the boundary effect is evaluated. In addition, the source zone is assumed wide and deep enough that the mean concentration remains constant transverse to the main flow direction.

The stochastic analysis are based on small amplitude perturbation assumption. Linearization of the governing equations is accomplished by the first order Taylor expansion, which may not be accurate for high variability. However, large variation of inputs is often encountered in field due to heterogeneous nature of the aquifer and the DNAPL distribution. An extrapolation is performed to facilitate the use of model in situation with large input variations. The extrapolation results are evaluated in Chapter 5 using results obtained from a discrete two-zone mass transfer model. Moreover, the stochastic results developed in this chapter is compared with that developed by Miralles-Wilhelm (Miralles-Wilhelm & Gelhar, 1996). Miralles-Wilhelm and Gelhar performed a study of field-scale first-order decay rate in heterogeneous aquifer. The comparison of the results from two studies can shed light on the intrinsic analogy of two studies and underscore the determining effects of field-scale mass transfer problem.

## 4.2 Methodology

### 4.2.1 Governing Equations

From Eqs. 3.3 and 3.4, the transport equation of advection and dispersion with mass transfer between DNAPL and aqueous phase in a NAPL source zone can be written in the following form:

$$\frac{\partial}{\partial t}\left[\theta_a C\right] = \frac{\partial}{\partial x_i}\left[\theta_a D_{ij}\frac{\partial C}{\partial x_j}\right] - \frac{\partial}{\partial x_i}\left(q_i C\right) + \Omega(C_s - C) \tag{4.1}$$

According to Gelhar and Axness (1983), $E_{ij} = \theta_a D_{ij}$ can be assumed constant spatially. So the governing equation becomes:

$$\frac{\partial}{\partial t}\left[\theta_a C\right] = \frac{\partial}{\partial x_i}\left[E_{ij}\frac{\partial C}{\partial x_j}\right] - \frac{\partial}{\partial x_i}\left(q_i C\right) + \Omega(C_s - C) \tag{4.2}$$

Steady state DNAPL saturation and concentration fields are assumed as:

$$\frac{\partial}{\partial x_i}\left(q_i C\right) = \frac{\partial}{\partial x_i}\left[E_{ij}\frac{\partial C}{\partial x_j}\right] + \Omega(C_s - C) \tag{4.3}$$

We define concentration deficit as the difference between the bulk concentration with the effective solubility of DNAPL in the groundwater:

$$u = C_s - C \tag{4.4}$$

Then the governing transport equation becomes:

$$\frac{\partial}{\partial x_i}\left(q_i u\right) = \frac{\partial}{\partial x_i}\left[E_{ij}\frac{\partial u}{\partial x_j}\right] - \Omega u \tag{4.5}$$

### 4.2.2 Random Field

The permeability of an aquifer is typically found to be log-normally distributed and is written as:

$$f = \ln k \tag{4.6}$$

The flow and transport variables are represented by stochastic process and decomposed in terms of the means and the perturbations:

$$f = \overline{f} + f' \tag{4.7}$$

$$u = \overline{u} + u' \tag{4.8}$$

$$q_i = \overline{q_i} + q_i' \tag{4.9}$$

$$v = \overline{v} + v' \tag{4.10}$$

$$H = \overline{H} + h' \tag{4.11}$$

$$\Omega = \overline{\Omega} + \Omega' \tag{4.12}$$

$$W = \overline{W} + W' \tag{4.13}$$

where

$$H = \ln \Omega \tag{4.14}$$

$$v = \ln q_1 \tag{4.15}$$

By taking the expectations of Eq. 3.8, we can find the mean and the perturbation of the log dissolution rate coefficient as:

$$\overline{H} = a + b\overline{f} + c\overline{W} + d\overline{v} \tag{4.16}$$

$$h' = bf' + cW' + dv' + g_h \tag{4.17}$$

### 4.2.3 Stochastic Differential Equations

The mean and the perturbation decompositions for random fields are substituted in the transport equation, and Eq. 4.5 becomes

$$\frac{\partial}{\partial x_i}\left(\overline{q_i} + q_i'\right)\left(\overline{u} + u'\right) = \frac{\partial}{\partial x_i}\left[E_{ij}\frac{\partial\left(\overline{u} + u'\right)}{\partial x_j}\right] - \left(\overline{\Omega} + \Omega'\right)\left(\overline{u} + u'\right) \tag{4.18}$$

By taking the expectation on both sides of Eq. 4.18, the mean equation is obtained as:

$$\frac{\partial}{\partial x_i}\left(\overline{q_i}\overline{u} + \overline{q_i'u'}\right) = \frac{\partial}{\partial x_i}\left[E_{ij}\frac{\partial \overline{u}}{\partial x_j}\right] - \overline{\Omega}\overline{u} - \overline{\Omega' u'} \tag{4.19}$$

Assuming unidimensional mean flow , the coordinate systems $x_i$ is aligned such the $x_1$ direction is along the directions of the mean flow.

$$\begin{aligned} q &= \overline{q_1} \\ \overline{q_i} &= 0 \text{ as } i = 2,3 \end{aligned}$$

For steady flow with no change in fluid density, conservation of mass requires that:

$$\frac{\partial}{\partial x_i}\overline{q_i} = 0, \ \frac{\partial q_i'}{\partial x_i} = 0, \ i = 1,2,3 \tag{4.20}$$

Here we also assume the source zone is wide and deep enough that the mean concentration field does not change in the directions transverse to the mean flow direction, so:

$$\frac{\partial \overline{u}}{\partial x_i} = 0 \text{ as } i = 2,3 \tag{4.21}$$

The local dispersion coefficient tensor is approximated in the form (Naff, 1978):

$$E_{ij} = \begin{bmatrix} q\alpha_L & 0 & 0 \\ 0 & q\alpha_T & 0 \\ 0 & 0 & q\alpha_T \end{bmatrix} \tag{4.22}$$

where $\alpha_L$ is the longitudinal local dispersivity, $\alpha_T$ is the transverse local dispersivity. Then the mean equation becomes unidimensional as:

$$q\frac{d\overline{u}}{dx_1} + \frac{\partial}{\partial x_1}\left(\overline{q_1'u'}\right) = \frac{d}{dx_1}\left[E_{11}\frac{d\overline{u}}{dx_1}\right] - \overline{\Omega}\overline{u} - \overline{\Omega'u'} \tag{4.23}$$

Since the rate coefficient $\Omega$ is always positive and the value is perceived of a wide distribution, I assume $H$ is Normal, i.e., $\Omega$ is lognormally distributed. Similarly $v$ is assumed Normal, or $q_1$lognormal distributed. Since $u$ is assumed normal distributed, then based on the properties of lognormal distribution in Appendix D, we can have the exact relationship as:

$$\overline{\Omega'u'} = \overline{\Omega\ h'u'} \tag{4.24}$$

$$\overline{q_1'u'} = q\ \overline{v'u'} \tag{4.25}$$

So the mean equation becomes:

$$q\frac{d}{dx_1}\overline{u}+q\frac{\partial}{\partial x_1}\overline{v'u'}=\frac{d}{dx_1}\left[E_{11}\frac{d\overline{u}}{dx_1}\right]-\overline{\Omega}\overline{u}-\overline{\Omega}\ \overline{h'u'} \tag{4.26}$$

To get the perturbation equation, subtract Eq. 4.19 from Eq. 4.18:

$$\frac{\partial}{\partial x_i}\left(q_i'\overline{u}+\overline{q_i}u'\right)+\frac{\partial}{\partial x_i}\left(q_i'u'-\overline{q_i'u'}\right)=\frac{\partial}{\partial x_i}\left[E_{ij}\frac{\partial u'}{\partial x_j}\right]-\overline{\Omega}u'-\Omega'\overline{u}+\left[\Omega'u'-\overline{\Omega'u'}\right] \tag{4.27}$$

Similar to the linearization approximation applied in Gelhar (1993), in above equation the second order items of perturbation products of $u',\Omega'$ and $u',q_1'$ are assumed small. Therefore we can approximate that

$$\frac{\partial}{\partial x_i}\left(q_i'u'-\overline{q_i'u'}\right)\approx 0 \tag{4.28}$$

$$\Omega'u'-\overline{\Omega'u'}\approx 0 \tag{4.29}$$

So the perturbation equation, to first order fluctuation, becomes:

$$q_1'\frac{d}{dx_1}\overline{u}+q\frac{\partial u'}{\partial x_1}=\frac{\partial}{\partial x_i}\left[E_{ij}\frac{\partial u'}{\partial x_j}\right]-\overline{\Omega}u'-\Omega'\overline{u} \tag{4.30}$$

Another linearization is assumed based on the assumption of small perturbation $h'$ and $\sigma_h$ and lognormal distribution of $\Omega$. The perturbation of dissolution rate coefficient can be approximated by the Taylor expansion as:

$$\Omega' = e^H-E[e^H]=e^{\bar{H}}e^{h'}-e^{\bar{H}}e^{\sigma_h^2/2}=e^{\bar{H}}[e^{h'}-e^{\sigma_h^2/2}] \tag{4.31}$$

$$\Omega' = \overline{\Omega}\left(1+\left(h'-\frac{\sigma_h^2}{2}\right)+\frac{1}{2}\left(h'-\frac{\sigma_h^2}{2}\right)^2+\ldots-1\right) \tag{4.32}$$

$$\approx \overline{\Omega}\left(1+h'-\frac{\sigma_h^2}{2}h'-1\right) \tag{4.33}$$

$$= \overline{\Omega}h'\left(1-\frac{\sigma_h^2}{2}\right) \tag{4.34}$$

Here we assume small perturbation that $\frac{\sigma_h^2}{2}\ll 1$, so we have:

$$\Omega'\approx\overline{\Omega}h' \tag{4.35}$$

Similarly the perturbation $q_1'$ can be approximated as:

$$q_1' \approx qv' \tag{4.36}$$

Therefore, the perturbation equation, 4.27, becomes:

$$qv'\frac{d}{dx_1}\overline{u} + q\frac{\partial}{\partial x_1}u' = \frac{\partial}{\partial x_i}\left[E_{ij}\frac{\partial u'}{\partial x_j}\right] - \overline{\Omega}u' - \overline{\Omega}h'\overline{u} \tag{4.37}$$

### 4.2.4 Nonstationarity Treatment

By inspection of the mean equation, we can find the mean concentration deficit demonstrates an obvious trend with distance. The nonstationarity caused by the trend limits the application of a stochastic analysis based on the stationary assumption. In this section we transform the nonstationary problem to a stationary one, which can be analyzed by a spectral representation approach.

By solving the mean transport equation, the solution of the mean concentration deficit can be written in the following form:

$$\overline{u} = C_1 e^{-\mu x_1} \tag{4.38}$$

where $C_1$ and $\mu$ are constants. $\mu$ is the exponential decay coefficient of the mean concentration deficit. $1/\mu$ represents the characteristic effective dissolution distance and is an important effective property discussed later. And similarly assuming the perturbation is exponentially dependent on the distance, then we can express the nonstationary trend in an exponential term:

$$u' = \tilde{u}e^{\beta x_1} \tag{4.39}$$

where $\tilde{u}$ is stationary concentration deficit fluctuation, and $\beta$ is a constant. So the cross covariance of the nonstationary variables can be transformed to the product of cross covariance of stationary variables and an exponential term:

$$\overline{v'u'} = e^{\beta x_1}\overline{v'\tilde{u}} \tag{4.40}$$

$$\overline{h'u'} = e^{\beta x_1}\overline{h'\tilde{u}} \tag{4.41}$$

Using Eqs. 4.38, 4.39 and 4.37, we have:

$$\begin{aligned} E_{ij}\frac{\partial u'}{\partial x_j} &= E_{ij}\frac{\partial\left(\tilde{u}e^{\beta x_1}\right)}{\partial x_j} \\ &= \beta E_{i1}\tilde{u}e^{\beta x_1} + E_{ij}e^{\beta x_1}\frac{\partial \tilde{u}}{\partial x_j} \end{aligned} \tag{4.42}$$

The perturbation equation becomes:

$$-\mu q v' C_1 e^{-\mu x_1} + q\left(\beta\tilde{u}e^{\beta x_1} + e^{\beta x_1}\frac{\partial\tilde{u}}{\partial x_1}\right) = \frac{\partial}{\partial x_i}\left[e^{\beta x_1}\left(\beta E_{i1}\tilde{u} + E_{ij}\frac{\partial\tilde{u}}{\partial x_j}\right)\right] - \overline{\Omega}\tilde{u}e^{\beta x_1} - \overline{\Omega}h' C_1 e^{-\mu x_1} \tag{4.43}$$

To remove the systematic trend in the above equation, the exponential decay coefficient of the mean and the perturbation of concentration deficit must be identical:

$$\beta = -\mu \tag{4.44}$$

Then the perturbation equation becomes:

$$-\mu q v' C_1 + q\left(-\mu\tilde{u} + \frac{\partial\tilde{u}}{\partial x_1}\right) = \frac{\partial}{\partial x_i}\left[\left(\beta E_{i1}\tilde{u} + E_{ij}\frac{\partial\tilde{u}}{\partial x_j}\right)\right] + \beta\left(\beta E_{11}\tilde{u} + E_{1j}\frac{\partial\tilde{u}}{\partial x_j}\right) - \overline{\Omega}\tilde{u} - \overline{\Omega}h' C_1 \tag{4.45}$$

Since from Eq. 4.22, $E_{ij} = 0$ for $i \neq j$ as $i = 1, 2, 3$, so above equation can be simplified as:

$$\left(q + 2E_{11}\mu\right)\frac{\partial\tilde{u}}{\partial x_1} + \tilde{u}\left(\overline{\Omega} - \mu q - \mu^2 E_{11}\right) = E_{ij}\frac{\partial^2\tilde{u}}{\partial x_i \partial x_j} + C_1\left(\mu q v' - \overline{\Omega}h'\right) \tag{4.46}$$

Let

$$\Omega^* = \overline{\Omega} - \mu q - \mu^2 E_{11} \tag{4.47}$$

$$= \overline{\Omega} - \mu q\left(1 + \mu\alpha_L\right) \tag{4.48}$$

where $\alpha_L$ is the longitudinal dispersivity. Since the typical value of exponential coefficient $\mu$ is extremely small as shown in Chapter 6 for realistic sites that $\mu^{-1}$ is at the scale of tens or hundreds of meters, and local dispersivity usually is at the order of centimeters, therefore it is appropriate to take:

$$\mu\alpha_L \ll 1 \tag{4.49}$$

and

$$\Omega^* \approx \overline{\Omega} - \mu q \tag{4.50}$$

Similarly

$$q + 2E_{11}\mu \approx q \tag{4.51}$$

So the perturbation equation is simplified as:

$$q\frac{\partial \tilde{u}}{\partial x_1} + \tilde{u}\Omega^* = \frac{\partial}{\partial x_i}E_{ij}\frac{\partial \tilde{u}}{\partial x_j} + C_1\left(\mu q v' - \overline{\Omega}h'\right) \tag{4.52}$$

So far, we have transformed the nonstationary problem of the concentration trend within a DNAPL source zone to a stationary problem, where random variables in Eq. 4.52 are all stationary. Consequently the spectral method to solve the stochastic differential equations can be applied

## 4.3 Large-scale Coefficient

### 4.3.1 General Forms

The mean equation in Eq. 4.26 and the perturbation equation in Eq. 4.52 are coupled together to solve for the large-scale transport and transfer properties. For a stationary field, the spectral approach has been used successfully to analyze the mean and perturbation equations. Based on the introduction of Fourier-Stieltjes Representations (FSR) and the Spectral Representation Theorem (SRM) (Lumley and Panofsky, 1964), the perturbation of a statistically-homogeneous

field can be represented as:

$$\tilde{u} = \int_{-\infty}^{\infty} e^{i\mathbf{k}\cdot\mathbf{x}} dZ_{\tilde{u}}(\mathbf{k}) \tag{4.53}$$

$$f' = \int_{-\infty}^{\infty} e^{i\mathbf{k}\cdot\mathbf{x}} dZ_f(\mathbf{k}) \tag{4.54}$$

$$v' = \int_{-\infty}^{\infty} e^{i\mathbf{k}\cdot\mathbf{x}} dZ_v(\mathbf{k}) \tag{4.55}$$

$$h' = \int_{-\infty}^{\infty} e^{i\mathbf{k}\cdot\mathbf{x}} dZ_h(\mathbf{k}) \tag{4.56}$$

$$W' = \int_{-\infty}^{\infty} e^{i\mathbf{k}\cdot\mathbf{x}} dZ_w(\mathbf{k}) \tag{4.57}$$

$$g_h = \int_{-\infty}^{\infty} e^{i\mathbf{k}\cdot\mathbf{x}} dZ_{g_h}(\mathbf{k}) \tag{4.58}$$

Substituting above representations into Eq. 4.52, the perturbation equation is transformed to the following equation in a spectral domain:

$$ik_1 q dZ_{\tilde{u}} + \Omega^* dZ_{\tilde{u}} = -E_{ij}k_i k_j dZ_{\tilde{u}} + C_1\left(\mu q dZ_v - \overline{\Omega} dZ_h\right) \tag{4.59}$$

The spectral amplitude of concentration deficit can be expressed as a function of the spectral amplitude of flow rate and log dissolution coefficient:

$$dZ_{\tilde{u}} = \frac{C_1\left(\mu q dZ_v - \overline{\Omega} dZ_h\right)}{\Omega^* + ik_1 q + E_{ij}k_i k_j} \tag{4.60}$$

Therefore the cross-covariance in Eq. 4.40 and 4.41 can be represented by the spectral formulations as:

$$\begin{aligned}
\overline{v'u'} &= e^{\beta x_1}\overline{v'\tilde{u}} = e^{-\mu x_1}\int_{-\infty}^{\infty} E\left[dZ_v dZ_{\tilde{u}}^*\right] \\
&= C_1 e^{-\mu x_1}\int_{-\infty}^{\infty} \frac{\left(\mu q S_{vv} - \overline{\Omega} S_{vh}\right)}{\Omega^* + ik_1 q + E_{ij}k_i k_j} d\mathbf{k} \\
&= \overline{u}\left(-\overline{\Omega} I_1 + q\mu I_2\right) \\
&= -\overline{u}\overline{\Omega} I_1 - \frac{\partial \overline{u}}{\partial x_1} q I_2
\end{aligned} \tag{4.61}$$

$$\begin{aligned}\overline{h'u'} &= e^{\beta x_1}\overline{h'\tilde{u}} = \overline{u}\int_{-\infty}^{\infty}\frac{\left(q\mu S_{hv}-\overline{\Omega}S_{hh}\right)}{\Omega^* + ik_1 q + E_{ij}k_i k_j}d\mathbf{k} \\ &= \overline{u}\left(q\mu I_1 - \overline{\Omega}I_3\right) \\ &= -\frac{\partial\overline{u}}{\partial x_1}qI_1 - \overline{u}\overline{\Omega}I_3 \end{aligned} \tag{4.62}$$

where

$$I_1 = \int_{-\infty}^{\infty}\frac{S_{vh}}{\Omega^* + ik_1 q + E_{ij}k_i k_j}d\mathbf{k} \tag{4.63}$$

$$I_2 = \int_{-\infty}^{\infty}\frac{S_{vv}}{\Omega^* + ik_1 q + E_{ij}k_i k_j}d\mathbf{k} \tag{4.64}$$

$$I_3 = \int_{-\infty}^{\infty}\frac{S_{hh}}{\Omega^* + ik_1 q + E_{ij}k_i k_j}d\mathbf{k} \tag{4.65}$$

Substituting above equations into Eq. 4.26, and the mean equation becomes:

$$\left(q - 2q\overline{\Omega}I_1\right)\frac{d}{dx_1}\overline{u} - q^2 I_2\frac{d^2\overline{u}}{dx_1^2} = -\overline{u}\left(\overline{\Omega} - \overline{\Omega}^2 I_3\right) \tag{4.66}$$

The advection terms (first-order spatial derivatives of mean concentration deficit) can be grouped together in the mean equation to produce the effective advection rate. Similarly, the coefficients of the second-order spatial derivatives can produce the effective dispersion coefficient. And the zero order terms can produce the effective rate constant.

$$q_e\frac{d}{dx_1}\overline{u} - D_e\frac{d^2\overline{u}}{dx_1^2} = -\overline{u}\Omega_e \tag{4.67}$$

where:

$$q_e = q\left(1 - 2\overline{\Omega}I_1\right) \tag{4.68}$$

$$D_e = q^2 I_2 \tag{4.69}$$

$$\Omega_e = \overline{\Omega}\left(1 - \overline{\Omega}I_3\right) \tag{4.70}$$

Here the dissolution coefficient $\mu$ controlling the exponential decay of mean concentration deficit

is found by solving the coupled Eqs. 4.67 and 4.38:

$$\mu = \frac{-q_e + \sqrt{4D_e\Omega_e + q_e^2}}{2D_e} \tag{4.71}$$

### 4.3.2 Integral Evaluation

The effective properties are obtained by evaluating the integrals of $I_1$, $I_2$ and $I_3$, where $l_1$, $l_2$ and $l_3$ are correlation scale in the direction $i = 1, 2, 3$. Then the integral of cross spectra are evaluated based on the provided input spectra. Here let us focus on one integral evaluation of cross spectrum of log flow velocity and log permeability using Eq. 4.63. By neglecting the local dispersion, Eq. 4.63 becomes:

$$I_1 = \int_{-\infty}^{\infty} \frac{S_{vh}}{\Omega^* + ik_1 q} d\mathbf{k} \tag{4.72}$$

Let $u_i = k_i l_i$, so:

$$\mathbf{k}^2 = k_1^2 + k_2^2 + k_3^2 = \frac{u_1^2}{l_1^2} + \frac{u_2^2}{l_2^2} + \frac{u_3^2}{l_3^2} = \frac{1}{l_3^2}(\frac{l_3^2}{l_1^2}u_1^2 + \frac{l_3^2}{l_2^2}u_2^2 + u_3^2) \tag{4.73}$$

Since for a imperfectly stratified system: $l_1 = l_2 \gg l_3$, so

$$\mathbf{k}^2 \approx k_3^2 \gg k_1^2 + k_2^2 \tag{4.74}$$

The input spectra function is hole type as:

$$S_{vh} d\mathbf{u} = \frac{4\overline{v'h'}u_3^2}{\pi^2 (1+u^2)^3} d\mathbf{u} \tag{4.75}$$

where

$$\mathbf{u}^2 = u_1^2 + u_2^2 + u_3^2 \tag{4.76}$$

So the integral in Eq. 4.72 can be transformed in the new domain as:

$$I_1 = \frac{\Omega^* l_1^2}{q^2} \int_{-\infty}^{\infty}\int_{-\infty}^{\infty}\int_{-\infty}^{\infty} \left[\frac{1}{[\Omega^{*2} l_1^2/q^2 + u_1^2]}\right] \frac{4\overline{v'h'}u_3^2}{\pi^2 (1+u^2)^3} du_1 du_2 du_3 \tag{4.77}$$

let

$$\zeta = \Omega^* l_1 / q \tag{4.78}$$

$$\varkappa = l_3 B_2 \tag{4.79}$$

From the definition of $\Omega^*$ in Eq. 4.50, we have:

$$\zeta = \overline{\zeta} - \mu l_1 \tag{4.80}$$

where

$$\overline{\zeta} = \frac{\overline{\Omega} l_1}{q} \tag{4.81}$$

$\overline{\zeta}$ is the dimensionless parameter representing the ratio of longitudinal correlation scale to the mean dissolution distance, which is defined as the ratio of mean flow rate to the mean dissolution rate coefficient. A large value of $\overline{\zeta}$ indicates strong local dissolution effect that the groundwater concentration reaches equilibrium in a small travel distance relative to the correlation scale. $\zeta$ is a similar parameter as $\overline{\zeta}$ except replacing $\overline{\Omega}$ by $\Omega^*$. Since $\mu$ represents the large-scale mean concentration deficit decay rate, $\zeta$ is a measure of the difference of local dissolution with the large-scale dissolution effect. For a large-scale homogeneous system, $\zeta = 0$ since there is no difference between large-scale and local-scale parameters. For a realistic heterogeneous aquifer, field observations have confirmed that there is a significant difference between local-scale with large-scale properties. Therefore, we expect $\mu \ll \overline{\zeta}$ and $\zeta \to \overline{\zeta}$ for a large-scale problem we are interested in. Since it is found that the local dissolution can be regarded as equilibrium or close to equilibrium from column experiments, it is appropriate to assume that

$$\overline{\zeta} \gg 1 \tag{4.82}$$

since the travel distance to reach equilibrium is much smaller than the longitudinal correlation scale which is at the order of meters. So it is also proper to assume that

$$\zeta \gg 1 \tag{4.83}$$

Under this assumption, the Eq. 4.77 becomes:

$$I_1 \approx \frac{\Omega^* l_1^2}{q^2} \int_{-\infty}^{\infty} \int_{-\infty}^{\infty} \int_{-\infty}^{\infty} \left[ \frac{1}{\Omega^{*2} l_1^2 / q^2} \right] \frac{4\overline{v'h'} u_3^2}{\pi^2 (1+u^2)^3} du_1 du_2 du_3 \tag{4.84}$$

Therefore, we can obtain the the result of integral of $I_1$ as:

$$I_1 \approx \frac{\overline{v'h'}}{\Omega^*} \tag{4.85}$$

Similarly, other integrals of cross-spectra are evaluated using the same method. The detailed integral evaluation can be found in Appendix A. By evaluating the cross spectra of underlying variables, the effective properties in Eq. 4.67 are found as:

$$q_e = q - 2\frac{q\overline{v'h'}}{\Phi} \tag{4.86}$$

$$A_{11} = \frac{q\sigma_v^2}{\overline{\Omega}\Phi} \tag{4.87}$$

$$\Omega_e = \overline{\Omega}\left(1 - \frac{\sigma_h^2}{\Phi}\right) \tag{4.88}$$

where

$$\overline{\zeta} = \frac{\overline{\Omega} l_1}{q} \tag{4.89}$$

$$\zeta = \frac{\Omega^* l_1}{q} \tag{4.90}$$

$$\Phi = \frac{\zeta}{\overline{\zeta}} \tag{4.91}$$

### 4.3.3 Comparison with Related Work

As mentioned in this section, Miralles-Wilhelm and coworkers studied the problem of field-scale solute transport with first-order decay by stochastic analysis (Miralles-Wilhelm & Gelhar, 1996). The governing transport equation they used is:

$$\frac{\partial C}{\partial t} = \frac{\partial}{\partial x_i}\left[D_{ij}\frac{\partial C}{\partial x_j}\right] - \frac{\partial}{\partial x_i}\left(V_i C\right) - \Omega C \tag{4.92}$$

where $\Omega$ is the first order decay rate. They focused on the unsteady solute transport produced by a pulse input source decaying in a heterogeneous aquifer. Instead of treating the mean concentration change in space as in this study, Miralles-Wilhelm analyzed the transient effect by a time scaling method. Using the perturbation method, he evaluated the effective properties. The perturbation of decay rate is assumed to be imperfectly correlated with the fluctuation of

permeability as:

$$\Omega' = bf' + \delta \tag{4.93}$$

where $\delta$ is the uncorrelated residual. The general solutions are obtained in his work as:

$$V_e = V - 2b\frac{\sigma_f^2 l_1}{\gamma}\frac{1-\exp\left[-\left(Vt/l_1\right)\left(1+\zeta\right)\right]}{1+\zeta} \tag{4.94}$$

$$A_{11} = \frac{\sigma_f^2 l_1}{\gamma^2}\frac{1-\exp\left[-\left(Vt/l_1\right)\left(1+\zeta\right)\right]}{1+\zeta} \tag{4.95}$$

$$\Omega_e = \overline{\Omega} - \frac{V\zeta}{l_1} \tag{4.96}$$

where $V$ is the mean seepage velocity, $\zeta$ is determined by the nonlinear equation:

$$\zeta^2 + \zeta - \frac{\sigma_f^2 l_1}{v^2}\left(1-\exp\left[-\left(Vt/l_1\right)\left(1+\zeta\right)\right]\right) = 0 \tag{4.97}$$

$$\gamma = \frac{\phi V}{K_g \overline{J}} \tag{4.98}$$

To compare the decay study results with results derived for the dissolution analysis in this thesis, we simplify the solutions from the two analyses by imposing the same conditions as

- large displacement that $Vt/l_1 \gg 1$;
- convert the pore velocity, decay rate and dispersivity to be consistent with those used in the dissolution study by multiplying a porosity factor in Eqs. 4.94, 4.100 and 4.96;
- saturated aquifer without DNAPL or nonwetting phase saturation;
- simple correlation model that the dissolution rate coefficient and decay rate is imperfectly correlated with log permeability as shown in Eq. 4.93;
- assume the decay rate coefficient is log normal distribution that $H = \ln\Omega$ bears normal distribution.

So the decay study gives the simplified result as we apply the above approximations:

$$q_e = q - 2\frac{\overline{q'h'}}{\Phi'} = q - 2\frac{\overline{qv'h'}}{\Phi'} \tag{4.99}$$

$$A_{11} = \frac{\sigma_q^2}{\overline{\Omega} q \Phi'} \approx \frac{q\sigma_v^2}{\overline{\Omega}\Phi'} \tag{4.100}$$

$$\Omega_e = \overline{\Omega}\left(1 - \frac{\sigma_h^2}{\Phi'}\right) \tag{4.101}$$

where

$$\Phi' = \frac{\zeta + 1}{\overline{\zeta}} \tag{4.102}$$

$$\zeta = \frac{\left(\overline{\Omega} - \Omega_e\right) l_1}{q} \tag{4.103}$$

$$\overline{\zeta} = \frac{\overline{\Omega}}{q} l_1 \tag{4.104}$$

As we can see, the results in Eqs. 4.99, 4.100 and 4.101 are equivalent to the results derived from the dissolution analysis in Eqs. 4.86, 4.87 and 4.88, except a slight difference in $\Phi'$ from $\Phi$ in the dissolution analysis, which is due to the approximation made in Eq. 4.83. Table 4.1 shows the effective properties for the dissolution analysis and decay analysis obtained by Miralles-Wilhelm.

Table 4.1: Comparison between Dissolution Analysis Results with Decay Analysis Results

| | Dissolution Analysis | Decay Analysis |
|---|---|---|
| Effective Velocity | $q_e = q - 2\frac{\overline{qv'h'}}{\Phi}$ | $q_e = q - 2\frac{\overline{qv'h'}}{\Phi'}$ |
| Macrodispersivity | $A_{11} = \frac{q\sigma_v^2}{\overline{\Omega}\Phi}$ | $A_{11} = \frac{q\sigma_v^2}{\overline{\Omega}\Phi'}$ |
| Effective Dissolution/Decay Rate | $\Omega_e = \overline{\Omega}\left(1 - \frac{\sigma_h^2}{\Phi}\right)$ | $\Omega_e = \overline{\Omega}\left(1 - \frac{\sigma_h^2}{\Phi'}\right)$ |
| Coefficient 1 | $\Phi = \frac{\zeta}{\overline{\zeta}}$ | $\Phi' = \frac{\zeta+1}{\overline{\zeta}}$ |
| Coefficient 2 | $\zeta = \frac{\Omega^* l_1}{q}$ | $\zeta = \frac{\left(\overline{\Omega}-\Omega_e\right)}{q} l_1$ |
| Coefficient 3 | $\overline{\zeta} = \frac{\overline{\Omega} l_1}{q}$ | $\overline{\zeta} = \frac{\overline{\Omega}}{q} l_1$ |

The results from the dissolution analysis is more general in terms of including the effect of DNAPL saturation, which is imbedded in the input parameters $\sigma_h^2$, $\sigma_v^2$, $corr[v,h]$. The agreement between two different studies with different methods provides a confirmation of the validity of the analysis of the more complex dissolution problem treated here.

By inspection of the integral structure in Eq. 4.77 with the equivalent integral in Miralles-Wilhelm's work, we can find a similarity between two integrals. Therefore, it is plausible to relax the approximation made in Eq. 4.83 that $\zeta \gg 1$ using solution derived in Miralles-Wilhelm's analysis. The generalization of the integral evaluation based on the decay results is suitable because of the similar structure of the integrals and the solutions. This will give rise to the new definition of $\Phi$ for the dissolution case:

$$\Phi = \frac{\zeta + 1}{\overline{\zeta}} \tag{4.105}$$

The expansion should be an adequate approximation for the full range $\zeta$ $(0 < \zeta < \infty)$. As $\overline{\zeta}$ and $\zeta$ are less than 1, it is found that the deviations of effective properties from the mean are less pronounced than that when $\zeta > 1$ and the result is not strongly dependently on $\Phi$. So the effects of the generalization are minor when $\zeta < 1$.

### 4.3.4 Results

By evaluating the cross spectra of underlying variables, the effective properties in Eq. 4.67 are found as:

$$q_e = q - 2q\frac{\overline{v'h'}}{\Phi} \tag{4.106}$$

$$D_e = \frac{\sigma_v^2}{\overline{\Omega}\Phi} q^2 \tag{4.107}$$

$$\Omega_e = \overline{\Omega}\left(1 - \frac{\sigma_h^2}{\Phi}\right) \tag{4.108}$$

$$A_{11} = \frac{\sigma_v^2}{\overline{\Omega}\Phi} q \tag{4.109}$$

where

$$\overline{\zeta} = \frac{\overline{\Omega} l_1}{q} \tag{4.110}$$

$$\zeta = \frac{\Omega^* l_1}{q} \tag{4.111}$$

$$\Phi = \frac{\zeta + 1}{\overline{\zeta}} \tag{4.112}$$

The solution expressions of effective properties in Eqs. 4.106, 4.107 and 4.108 are not dependent on the local dissolution model we developed in Chapter 2, while the evaluation of the effective properties are a function of how to derive the parameters $\overline{v'h'}$, $\sigma_v^2$ ,$\overline{\zeta}$ and $\sigma_h^2$. The impact of the spatial variability on the effective properties is represented by variance of log dissolution coefficient $\sigma_h^2$, variance of log flow rate $\sigma_v^2$ and correlation between flow rate and dissolution rate $corr[v,h]$. Here $\Phi$ is a weak function of $\overline{v'h'}$, $\sigma_v^2$ ,$\overline{\zeta}$ and $\sigma_h^2$. Therefore, each effective property is affected dominantly by different spatial variability. For example, the effective dissolution rate coefficient $\Omega_e$ is affected dominantly by $\sigma_h^2$, while the effective flow rate $q_e$ is affected dominantly by $\overline{v'h'}$. However, the three spatial variabilities are not entirely independent of each other. From Eq. 4.113 we can find that $\sigma_h^2$ includes the term of $\sigma_v^2$ and $\overline{v'h'}$. From the calculation based on the flow results, we also find that the dominant contribution to $\sigma_h^2$ is from the variability of DNAPL saturation, which is represented by $\sigma_w^2$. Also the unknown residual $\sigma_{g_h}^2$ can be significant too depending on the site characterization of the local dissolution rate. According to Eqs. 4.113 and 4.114, $\sigma_h^2$, $\overline{v'h'}$ and $\sigma_v^2$ can be derived from the results based on flow analysis developed in Chapter 2.

$$\sigma_h^2 = b^2\sigma_f^2 + c^2\sigma_w^2 + d^2\sigma_v^2 + \sigma_{g_h}^2 + 2bccov[W,f] + 2bdcov[f,v] + 2cdcov[v,W] \quad (4.113)$$

$$\overline{v'h'} = bcov[f,v] + ccov[v,W] + d\sigma_v^2 \quad (4.114)$$

When $\sigma_h^2 = 0$ in Eq. 4.108, which indicates a homogeneous dissolution environment, the effective dissolution rate equals to the mean local dissolution rate. As the variation of dissolution rate increases, the effective rate decreases in an almost linear pattern. This indicates that the strong heterogeneity contributes significantly to the effective rate decrease. In a highly heterogeneous dissolution environment, the effective rate can be far below the mean local dissolution rate. As a result, using the local dissolution rate to predict the mass transfer in a large-scale subsurface system can overestimates the mass transfer from DNAPL to water significantly.

Another important effective property is the effective dissolution distance, which represents the travel distance in the source zone for the mean concentration approaching equilibrium. The inverse of the dissolution coefficient $\mu$, according to the exponential expression of Eq. 4.38, represents the distance at which the mean concentration reaches 63% $(1-e^{-1})$ of the equilibrium value. Therefore $1/\mu$ represents a characteristic dissolution distance which is a fraction of the

distance reaching equilibrium. The parameter $\mu$ can be obtained by solving the nonlinear Eq. 4.71. This property is important to characterize the large-scale dissolution. It is found from Eqs. 4.106, 4.107 and 4.108 that the effective properties are functions of both spatial variations of $corr[v,h]$, $\sigma_v^2$ , $\sigma_h^2$ and the mean dissolution properties represented by $\overline{\zeta}$. In a homogeneous dissolution environment where the spatial variations are zero, the effective dissolution rate and flow velocity equal to the mean.

## 4.4 Boundary Effect

At the upstream boundary of the source zone, the concentration is zero (no contamination):

$$C = \overline{C} + C' = 0 \ @ \ x = 0 \tag{4.115}$$

Since the mean concentration at the boundary is zero, so the fluctuation of concentration is zero:

$$C' = 0 \Longrightarrow \sigma_c^2 = 0 \tag{4.116}$$

Consequently this boundary condition imposes nonstationarity in the concentration fluctuations at the boundary that not captured by the downstream exponential decay method used in deriving the effective properties inside a source zone. The derivation based on the nonstationary solution developed in Section 4.2 and 4.3 will not satisfy this boundary condition. Here we apply a nonstationary spectral method to evaluate the scale of the boundary affected zone and to derive a general solutions of effective parameters for the entire DNAPL source zone.

### 4.4.1 Perturbation in Boundary Zone

At the boundary, the variables $f, q, \Omega, W$ are assumed to be stationary but the concentration field is nonstationary. According the representation theorem and the nonstationary spectral method described in Li (1995), the nonstationary concentration deficit perturbation can be expressed in the form of spectral amplitude:

$$u' = \int_{-\infty}^{\infty} \phi_u(\mathbf{x}, \mathbf{k}) dZ_u(\mathbf{k})$$

where $\phi_u(\mathbf{x},\mathbf{k})$ is a transfer function which account all nonstationary effects. From the downstream stationary analysis, $dZ_u$ can be expressed in a form of the combination of $dZ_v$ and $dZ_h$ in Eq. 4.60. Therefore the perturbation of concentration deficit for the boundary zone can be expressed as:

$$u' = \int_{-\infty}^{\infty} \phi_{uv}(\mathbf{x},\mathbf{k}) dZ_v(\mathbf{k}) + \int_{-\infty}^{\infty} \phi_{uh}(\mathbf{x},\mathbf{k}) dZ_h(\mathbf{k}) \tag{4.117}$$

where $\phi_{uv}(\mathbf{x},\mathbf{k})$,$\phi_{uh}(\mathbf{x},\mathbf{k})$ are transfer functions too. As discussed in Chapter 2, it has been hypothesized that bypassing around the high DNAPL saturation zone can attribute to deviation of the large-scale dissolution properties from the local mean. Therefore we focus on the study of the bypassing effect and apply a simplified perfect negative correlation between flow rate and dissolution rate at the boundary:

$$h' = -\alpha v' \tag{4.118}$$

where

$$v' = \int_{-\infty}^{\infty} e^{i\mathbf{k}\cdot\mathbf{x}} dZ_v(\mathbf{k}) \tag{4.119}$$

So:

$$h' = -\alpha \int_{-\infty}^{\infty} e^{i\mathbf{k}\cdot\mathbf{x}} dZ_v(\mathbf{k}) \tag{4.120}$$

So:

$$u' = \int_{-\infty}^{\infty} \phi_{uv}(\mathbf{x},\mathbf{k}) dZ_v(\mathbf{k}) - \alpha \int_{-\infty}^{\infty} \phi_{uh}(\mathbf{x},\mathbf{k}) dZ_v(\mathbf{k}) \tag{4.121}$$

$$= \int_{-\infty}^{\infty} \hat{\phi}_{uv}(\mathbf{x},\mathbf{k}) dZ_v(\mathbf{k}) \tag{4.122}$$

where

$$\tilde{\phi}_{uv}(\mathbf{x},\mathbf{k}) = \phi_{uv}(\mathbf{x},\mathbf{k}) - \alpha\phi_{uh}(\mathbf{x},\mathbf{k}) \tag{4.123}$$

Since the partial differential Eq. 4.27 is only one dimensional about the $x_1$ direction, so the transfer function can be written as $\tilde{\phi}_{uv}(x_1,\mathbf{k})$. Let us decompose the transfer function by separating the stationary and nonstationary components:

$$\tilde{\phi}_{uv}(x_1,\mathbf{k}) = \hat{\phi}_{uv}(x_1,\mathbf{k}) e^{-\mu x_1} e^{i\mathbf{k}\cdot\mathbf{x}} \tag{4.124}$$

where $e^{-\mu x_1}e^{i\mathbf{k}\cdot\mathbf{x}}$ represents the transformed stationary part and $\hat{\phi}_{uv}(x_1,\mathbf{k})$ represents nonstationary kernel. The transfer function is unknown and can be solved.

Using Eqs. 4.122 and 4.124 in the perturbation equation in Eq. 4.37,

$$\begin{aligned} & q\frac{d\overline{u}}{dx_1}\int_{-\infty}^{\infty} e^{i\mathbf{k}\cdot\mathbf{x}}dZ_v(\mathbf{k}) + q\int_{-\infty}^{\infty}\frac{\partial\left[\hat{\phi}_{uv}(x_1,\mathbf{k})e^{-\mu x_1}e^{i\mathbf{k}\cdot\mathbf{x}}\right]}{\partial x_1}dZ_v(\mathbf{k}) \\ = & -\overline{\Omega}\int_{-\infty}^{\infty}\hat{\phi}_{uv}(x_1,\mathbf{k})e^{-\mu x_1}e^{i\mathbf{k}\cdot\mathbf{x}}dZ_v(\mathbf{k}) + \alpha\overline{\Omega}\overline{u}\int_{-\infty}^{\infty}e^{i\mathbf{k}\cdot\mathbf{x}}dZ_v(\mathbf{k}) \end{aligned} \tag{4.125}$$

where

$$\begin{aligned} \frac{\partial\left[\hat{\phi}_{uv}(x_1,\mathbf{k})e^{-\mu x_1}e^{i\mathbf{k}\cdot\mathbf{x}}\right]}{\partial x_1} &= e^{i(k_1x_1+k_2x_2)}\frac{\partial\left[\hat{\phi}_{uv}e^{(-\mu+ik_1)x_1}\right]}{\partial x_1} \\ &= e^{i(k_1x_1+k_2x_2)}e^{(-\mu+ik_1)x_1}\left(\frac{\partial\hat{\phi}_{uv}}{\partial x_1}+(-\mu+ik_1)\hat{\phi}_{uv}\right) \\ &= e^{i\mathbf{k}\cdot\mathbf{x}}e^{-\mu x_1}\left(\frac{\partial\hat{\phi}_{uv}}{\partial x_1}+(-\mu+ik_1)\hat{\phi}_{uv}\right) \end{aligned} \tag{4.126}$$

Since $dZ_v(\mathbf{k})$ is random, the entire integrand should equal to zero in Eq. 4.125. Therefore, to simplify Eq. 4.125:

$$q\frac{\partial\hat{\phi}_{uv}(x_1,\mathbf{k})}{\partial x_1}+(\Omega^*+iq_1k_1)\hat{\phi}_{uv}(x_1,\mathbf{k}) = -q\frac{\partial\overline{u}}{\partial x_1}e^{\mu x_1}+\alpha\overline{\Omega}\overline{u}e^{\mu x_1} \tag{4.127}$$

where $\Omega^* = \overline{\Omega} - q\mu$. Similar to the downstream analysis, let us assume that the mean concentration deficit can be expressed as:

$$\overline{u} = \widehat{u}(x_1)\,e^{-\mu x_1} \tag{4.128}$$

$$\frac{\partial\overline{u}}{\partial x_1} = e^{-\mu x_1}\left(\frac{\partial\widehat{u}}{\partial x_1}-\mu\widehat{u}\right) \tag{4.129}$$

where $\mu$ is a constant. Using Eqs. 4.129 and 4.128, perturbation equation in Eq. 4.127 becomes:

$$\frac{\partial\hat{\phi}_{uv}}{\partial x_1}+\left(\frac{\Omega^*+iqk_1}{q}\right)\hat{\phi}_{uv} = \frac{1}{q}\left(-q\frac{\partial\widehat{u}}{\partial x_1}+(\alpha\overline{\Omega}+\mu)\,\widehat{u}\right) = \frac{1}{q}\mathbf{L}(\widehat{u}) \tag{4.130}$$

where $\mathbf{L}$ is an operator as:

$$\mathbf{L}\left(\widehat{u}\right) = -q\frac{\partial \widehat{u}}{\partial x_1} + \left(\alpha\overline{\Omega} + \mu\right)\widehat{u} \tag{4.131}$$

Since we also know the cross product can be expressed as:

$$\begin{aligned}\overline{v'u'} &= E\left[\int_{-\infty}^{\infty} e^{i\mathbf{k}\cdot\mathbf{x}} dZ_v(\mathbf{k}) \int_{-\infty}^{\infty} \hat{\phi}^*_{uv}(x_1,\mathbf{k}) e^{-\mu x_1} e^{-i\mathbf{k}\cdot\mathbf{x}} dZ^*_v(\mathbf{k})\right] \\ &= \int_{-\infty}^{\infty} e^{-\mu x_1} \hat{\phi}^*_{uv}(x_1,\mathbf{k}) S_{vv} d\mathbf{k}\end{aligned} \tag{4.132}$$

$$\begin{aligned}\overline{h'u'} &= E\left[\int_{-\infty}^{\infty} e^{i\mathbf{k}\cdot\mathbf{x}} dZ_h(\mathbf{k}) \int_{-\infty}^{\infty} \hat{\phi}^*_{uv}(x_1,\mathbf{k}) e^{-\mu x_1} e^{i\mathbf{k}\cdot\mathbf{x}} dZ^*_v(\mathbf{k})\right] \\ &= -\alpha \int_{-\infty}^{\infty} e^{-\mu x_1} \hat{\phi}^*_{uv}(x_1,\mathbf{k}) S_{vv} d\mathbf{k}\end{aligned} \tag{4.133}$$

Using Eqs. 4.132 and 4.133, the mean equation in Eq. 4.26 becomes:

$$\begin{aligned}& qe^{-\mu x_1}\left(\frac{d\widehat{u}}{dx_1} - \mu\widehat{u}\right) + q\frac{\partial}{\partial x_i}\int_{-\infty}^{\infty} e^{-\mu x_1}\hat{\phi}^*_{uv}(x_1,\mathbf{k}) S_{vv} d\mathbf{k} \\ = \; & -\overline{\Omega}\widehat{u}\left(x_1\right)e^{-\mu x_1} + \overline{\Omega}\alpha\int_{-\infty}^{\infty} e^{-\mu x_1}\hat{\phi}^*_{uv}(x_1,\mathbf{k}) S_{vv} d\mathbf{k}\end{aligned} \tag{4.134}$$

By rearranging the above equation, the mean equation becomes:

$$q\frac{\partial \widehat{u}}{\partial x_1} + \Omega^*\widehat{u} = -q\frac{\partial}{\partial x_i}\int_{-\infty}^{\infty}\hat{\phi}^*_{uv} S_{vv} d\mathbf{k} + \overline{\Omega}\alpha\int_{-\infty}^{\infty}\hat{\phi}^*_{uv} S_{vv} d\mathbf{k} \tag{4.135}$$

Subject to the boundary condition:

$$\widehat{u} = C_s, \hat{\phi}_{uv} = 0 \text{ at } x_1 = 0 \tag{4.136}$$

### 4.4.2 Transfer function

From Eqs. 4.130 and 4.136, we can express the solution for the transfer function as:

$$\hat{\phi}_{uv}(x_1,\mathbf{k}) = \frac{1}{q}e^{-\left(\frac{\Omega^*+iqk_1}{q}\right)x_1}\int_0^{x_1} e^{\left(\frac{\Omega^*+iqk_1}{q}\right)\xi}\mathbf{L}\left(\widehat{u}\left(\xi\right)\right)d\xi \tag{4.137}$$

The integral in Eq. 4.137 can be written as:

$$I(x_1,k_1) = \int_0^{x_1} e^{\left(\frac{\Omega^*}{q}+ik_1\right)\xi} \mathbf{L}(\widehat{u}(\xi))\, d\xi = \int_0^{x_1} \mathbf{\Psi}(\xi)\, e^{ik_1\Theta(\xi)} d\xi \tag{4.138}$$

where

$$\mathbf{\Psi}(\xi) = e^{\frac{\Omega^*}{q}\xi} \mathbf{L}(\widehat{u}(\xi)) \tag{4.139}$$

$$\Theta(\xi) = \xi \tag{4.140}$$

Stoker studied the characteristics of such functions (Stoker, 1957). According to Stoker, when $k_1$ is large and $\mathbf{\Psi}(\xi)$ is not a rapidly oscillating function of $\xi$, the main contribution of $e^{ik_1\Theta(\xi)}$ to the integral is at the points that $\Theta(\xi)$ varies most slowly, i.e. $\Theta'(\xi) = 0$. In this study the wave number $k_1$can be regarded as large for the boundary zone since the separation is assumed small. $\mathbf{\Psi}(\xi)$ is a exponential growth function which is not a oscillating function of $\xi$. However, since $\Theta'(\xi) = 1$ for the entire domain of $\xi$, which means there is no stationary phase point. So based on the proof provided by Stoker, the integral can be written as:

$$I(x_1,k_1) = \frac{\mathbf{\Psi}(x_1)}{ik_1\Theta'(x_1)} e^{ik_1\Theta(x_1)} - \frac{\mathbf{\Psi}(0)}{ik_1\Theta'(0)} e^{ik_1\Theta(0)} - \frac{1}{ik_1}\int_0^{x_1} \mathbf{\Psi}_1(\xi)\, e^{ik_1\Theta(\xi)} d\xi \tag{4.141}$$

where

$$\mathbf{\Psi}_1(\xi) = \frac{d}{d\xi}\left(\mathbf{\Psi}/\Theta'\right) \tag{4.142}$$

Since

$$\left|\int_0^{x_1} \mathbf{\Psi}_1(\xi)\, e^{ik_1\Theta(\xi)} d\xi\right| \leq \int_0^{x_1} |\mathbf{\Psi}_1(\xi)|\, d\xi \tag{4.143}$$

So above integral is bounded as $k_1\Theta(\xi)$ is real. So $I(x_1,k)$ is of order of $1/k_1$. From 4.141, we can find the main contribution concentrates on the upper bound where $\xi = x_1$. To put it in another way, the contribution of $e^{ik_1\Theta(\xi)}$ can be regarded uniform through the domain of $\xi$. Therefore, the main contribution of the integrand is determined by $\mathbf{\Psi}(\xi)$, which has the maximum value at $\xi = x_1$. So the main contribution of the integrand is around $\xi = x_1$. So:

$$\mathbf{L}(\widehat{u}(\xi)) = \mathbf{L}(\widehat{u}(x_1)) + \frac{\partial \mathbf{L}(\widehat{u}(\xi))}{\partial x_1}_{\xi=x_1} (\xi - x_1) + ... \tag{4.144}$$

Let us take the first term and neglect the higher order terms:

$$\mathbf{L}\left(\widehat{u}\left(\xi\right)\right) \approx \mathbf{L}\left(\widehat{u}\left(x_1\right)\right) \tag{4.145}$$

The transfer function from Eq. 4.137 becomes:

$$\hat{\phi}_{uv}(x_1, \mathbf{k}) = \frac{\left(1 - e^{-\left(\frac{\Omega^* + iqk_1}{q}\right)x_1}\right)}{\Omega^* + iqk_1}\mathbf{L}\left(\widehat{u}\left(x_1\right)\right) \tag{4.146}$$

And its complex conjugate is:

$$\hat{\phi}^*_{uv}(x_1, \mathbf{k}) = \frac{\left(1 - e^{-\beta x_1}\right)}{\beta q}\mathbf{L}\left(\widehat{u}\left(x_1\right)\right) = \nu\left(x_1, k_1\right)\mathbf{L}\left(\widehat{u}\left(x_1\right)\right) \tag{4.147}$$

where

$$\beta = \frac{\Omega^* - iqk_1}{q} \tag{4.148}$$

$$\nu = \frac{\left(1 - e^{-\beta x_1}\right)}{\beta q} \tag{4.149}$$

The mean equation for the boundary zone can be obtained by inputting the transfer function into the mean equation; the right side of Eq. 4.135 becomes:

$$R = -q\frac{d}{dx_1}\int_{-\infty}^{\infty}\mathbf{L}\left(\tilde{u}\left(x_1\right)\right)\nu S_{vv}d\mathbf{k} + \overline{\Omega}\alpha\int_{-\infty}^{\infty}\mathbf{L}\left(\tilde{u}\left(x_1\right)\right)\nu S_{vv}d\mathbf{k} \tag{4.150}$$

Using Eq. 4.131, the mean equation becomes:

$$q\frac{\partial}{\partial x_1}\tilde{u} + \Omega^*\tilde{u} = -q\frac{d}{dx_1}\int_{-\infty}^{\infty}\left(-q\frac{\partial\tilde{u}}{\partial x_1} + \left(\alpha\overline{\Omega} + \mu\right)\tilde{u}\right)\nu S_{vv}d\mathbf{k} + \overline{\Omega}\alpha\int_{-\infty}^{\infty}\left(-q\frac{\partial\tilde{u}}{\partial x_1} + \left(\alpha\overline{\Omega} + \mu\right)\tilde{u}\right)\nu S_{vv}d\mathbf{k} \tag{4.151}$$

Using $\overline{u} = \widehat{u}\left(x_1\right)e^{-\mu x_1}$ according to Eq. 4.128:

$$q\frac{d}{dx_1}\overline{u} + \overline{\Omega}\overline{u} = -q\frac{d}{dx_1}\int_{-\infty}^{\infty}\left(-q\frac{d\overline{u}}{dx_1} + \alpha\overline{\Omega}\overline{u}\right)\nu S_{vv}d\mathbf{k} + \overline{\Omega}\alpha\int_{-\infty}^{\infty}\left(-q\frac{d\overline{u}}{dx_1} + \alpha\overline{\Omega}\overline{u}\right)\nu S_{vv}d\mathbf{k} \tag{4.152}$$

So the mean equation can be written as:

$$\left(q + 2q\alpha\overline{\Omega}I_1 - q^2\frac{dI_1}{dx_1}\right)\frac{d\overline{u}}{dx_1} - \frac{d}{dx_1}q^2 I_1\frac{d\overline{u}}{dx_1} = -\overline{u}\left(\overline{\Omega} + 2q\alpha\overline{\Omega}\frac{dI_1}{dx_1} - \alpha^2\overline{\Omega}^2 I_1\right) \tag{4.153}$$

where

$$I_1 = \int_{-\infty}^{\infty} \nu S_{vv} d\mathbf{k} \tag{4.154}$$

$$= \int_{-\infty}^{\infty} \frac{\left(1 - e^{-\beta x_1}\right)}{\beta q} S_{vv} d\mathbf{k} \tag{4.155}$$

This can be further simplified as:

$$q_e\frac{d\overline{u}}{dx_1} - \frac{d}{dx_1}D_e\frac{d\overline{u}}{dx_1} = -\overline{u}\Omega_e \tag{4.156}$$

where:

$$q_e = q + 2\alpha q\overline{\Omega}I_1 - q^2\frac{dI_1}{dx_1} \tag{4.157}$$

$$D_e = q^2 I_1 \tag{4.158}$$

$$\Omega_e = \overline{\Omega} - \alpha^2\overline{\Omega}^2 I_1 + 2q\alpha\overline{\Omega}\frac{dI_1}{dx_1} \tag{4.159}$$

where $\beta = \frac{\Omega^*}{q} - ik_1$. By solving the integral of $I_1$, we can obtain the effective properties for the boundary zone. The detailed development is included in the Appendix B.

### 4.4.3 General Solution

By solving the transfer function, the mean and perturbation equation for the transport at the boundary can be evaluated. The general solution of effective properties for the entire DNAPL source zone are obtained as:

$$q_e = q - 2q\frac{\overline{v'h'}}{\Phi}\left(1 - \left(1 - \frac{q\Phi}{\alpha}\right)\exp\left(-\Phi\frac{\overline{\Omega}}{q}x_1\right)\right) \tag{4.160}$$

$$D_e = \frac{q^2\sigma_v^2}{\overline{\Omega}\Phi}\left[1 - \exp\left(-\Phi\frac{\overline{\Omega}}{q}x_1\right)\right] \tag{4.161}$$

$$\Omega_e = \overline{\Omega} - \overline{\Omega}\frac{\sigma_h^2}{\Phi}\left[1 - \left(1 - \frac{q\Phi}{\alpha}\right)\exp\left(-\Phi\frac{\overline{\Omega}}{q}x_1\right)\right] \tag{4.162}$$

The general solution is not dependent on the local correlation model developed in Eq. 4.118. The effective properties are found to be a function of $\sigma_h^2$, $\sigma_v^2$ and $\overline{v'h'}$. The impact from heterogeneity on effective properties is scaled by a factor that dependent on $\Phi$, $q$, $\overline{\Omega}$ and $\alpha$ in the boundary affected zone, with an exponential convergence to the downstream values as the distance increases. The scale of the boundary affected zone can be evaluated by comparing the boundary effect distance with the horizontal correlation scale. Similar to the definition of dissolution distance, the boundary distance is defined as the inverse of the exponential coefficient:

$$\delta_b = \frac{1}{\Phi \frac{\overline{\Omega}}{q}} = \frac{q/\overline{\Omega}}{\Phi} \tag{4.163}$$

According to the definition of $\Phi$ in Eq. 4.112, the boundary distance can be written as:

$$\delta_b = \frac{l_1}{\zeta + 1} \tag{4.164}$$

So the ratio of boundary distance to the correlation scale is:

$$\frac{\delta_b}{l_1} = \frac{1}{\zeta + 1} \tag{4.165}$$

Figure 4-2 shows this ratio changes as a function of mean input $\overline{\zeta}$ under the condition listed in Table 4.2.

Table 4.2: Input Parameters to Test the Bourndary Scale

| Input Parameters | $\boldsymbol{\sigma_h^2}$ | $\mathbf{corr[v,h]}$ | $\boldsymbol{\sigma_v^2}$ |
|---|---|---|---|
| Value | 0.5 | 0.1 | 0.25 |

As we can see, the boundary distance is much smaller than the horizontal correlation scale for $\overline{\zeta} \geq 1$. Since the local dissolution equilibrium is frequently observed in the laboratory experiments, $\overline{\zeta} \geq 1$ is satisfied generally. Field observations also confirm this as discussed in Chapter 6, where we calculate the mean dissolution properties for four DNAPL contaminated sites. As the mean dissolution rate becomes larger, the boundary effect scale will influence a zone near the boundary that is only a small fraction of the longitudinal correlation scale. Since the DNAPL source zone usually spreads more than ten times of the longitudinal correlation scale, we can conclude that the boundary effect is insignificant in an extensive source zone.

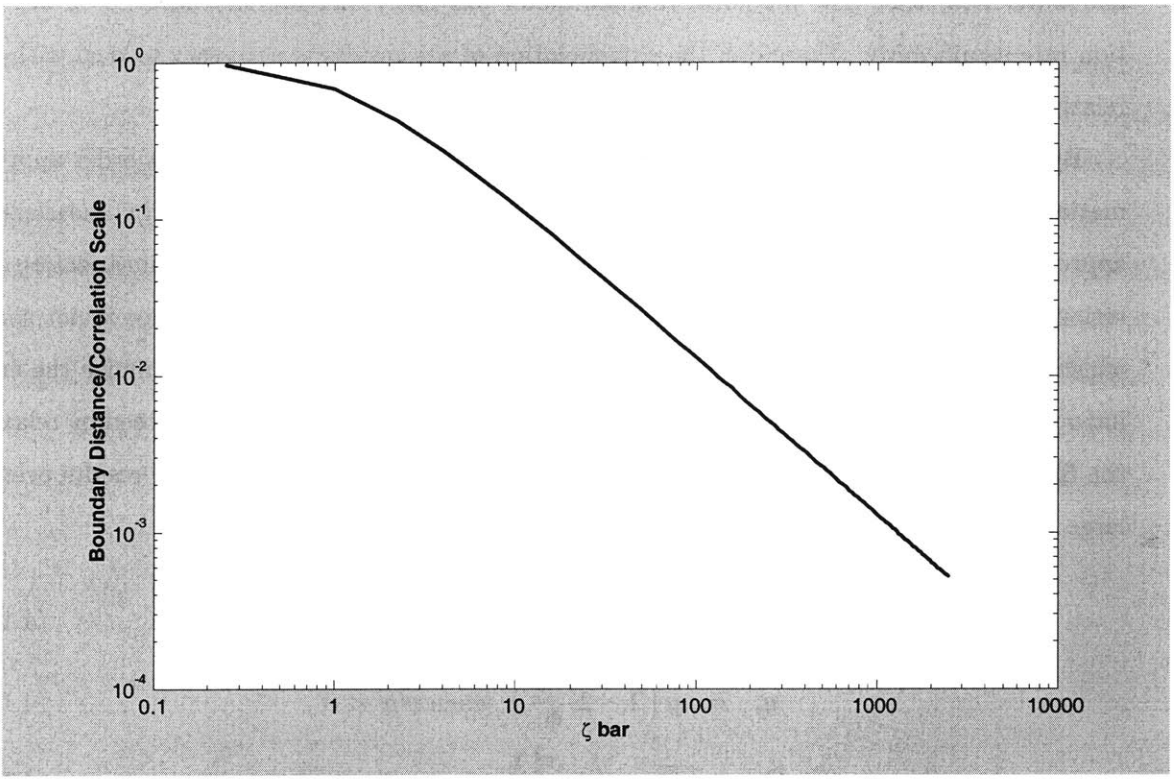


Figure 4-2: The ratio of the boundary distance to the longitudinal correlation scale as a function of the mean dissolution effect ($\zeta$ bar $= \overline{\zeta}$)

## 4.5 Extrapolation of Results

The results in Eqs. 4.106, 4.107 and 4.108 are derived based on the small perturbation assumption in Eq. 4.35 that $h'$ is small and strictly are applicable only when $\sigma_h^2 << 1$. For example, from Eq. 4.108 we find that for $\sigma_h^2 > 1$, the effective dissolution rate is negative, which is physically meaningless. However, calculation based on real site data revealed that the spatial variation of log dissolution rate could be large due to the non-uniform distribution of DNAPL and water flow field. The unknown residual factor can likely increase the variation of dissolution rate significantly. Therefore, the extrapolation of the results is necessary to deal with the relative large perturbation problem.

By inspection of the results $q_e$ and $\Omega_e$, we can find that the form is the first order approximation of the Taylor expansion of exponential. This linearized form is due to the linearization approximation in Eq. 4.31 when developing the perturbation equation. This linearization can seriously underestimate the variance of dissolution rate when the input variance is not small, which consequently results in a negative effective properties. Therefore, to minimize the error introduced by the linearization approximation, a plausible extrapolation is proposed by relaxing the linearized form to the original exponential form, which can assure positive results even at large variations. The suggested extrapolated forms of Eqs. 4.106 and 4.108 are:

$$q_e = q \exp\left(-2\frac{\overline{v'h'}}{\Phi}\right) \text{ when } \overline{v'h'} > 0 \tag{4.166}$$

$$q_e = q\left(1 - 2\frac{\overline{v'h'}}{\Phi}\right) \text{ when } \overline{v'h'} < 0 \tag{4.167}$$

$$\Omega_e = \overline{\Omega} \exp\left(-\frac{\sigma_h^2}{\Phi}\right) \tag{4.168}$$

The exponential extrapolation of effective flow velocity is only applied when the correlation between flow rate and dissolution rate is positive and the spatial variation of both are large, the circumstance that the linearized expression produce a negative result. When the correlation is negative, the linearized result in Eq. 4.106 can produce physically meaningful results and is still applied. Therefore, the effective velocity is calculated by both linearized and extrapolated expression as Eqs. 4.166 and 4.167. The effective dissolution rate experiences a exponential decay as the variation increases. At large spatial variation, the effective dissolution rate is significantly

smaller than the mean. The extrapolation of effective dissolution rate and flow rate enables us to calculate the effective properties consistently and in the entire range of spatial variations. The adequacy of the extrapolation is assessed in the next chapter where we establish an independent two-zone model to validate the results of extrapolation. Meanwhile, the theoretical results are evaluated by data measured from realistic contaminated sites in Chapter 6.

By definition of $\mu$ in Eq. 4.71, we have five equations for five unknowns including $q_e$, $D_e$, $\Omega_e$, $\mu$ and $\Phi$. Therefore the effective properties can be determined by simultaneously solving Eqs. 4.166, 4.167, 4.168, 4.107, 4.169 and 4.170.

$$\Phi = 1 - \frac{q\mu}{\overline{\Omega}} + \frac{1}{\overline{\zeta}} \tag{4.169}$$

$$D_e\mu^2 + q_e\mu - \Omega_e = 0 \tag{4.170}$$

To solve for the dissolution coefficient $\mu$ by combining above five equations with five unknowns, a nonlinear equation of $\mu$ can be derived as:

$$\frac{\sigma_v^2}{\overline{\Omega}/q\Phi}\mu^2 + \exp\left(-2\frac{\overline{v'h'}}{\Phi}\right)\mu - \frac{\overline{\Omega}}{q}\exp\left(-\frac{\sigma_h^2}{\Phi}\right) = 0 \text{ when } \overline{v'h'} > 0 \tag{4.171}$$

$$\frac{\sigma_v^2}{\overline{\Omega}/q\Phi}\mu^2 + \left(1 - 2\frac{\overline{v'h'}}{\Phi}\right)\mu - \frac{\overline{\Omega}}{q}\exp\left(-\frac{\sigma_h^2}{\Phi}\right) = 0 \text{ when } \overline{v'h'} < 0 \tag{4.172}$$

According Gelhar (1993), the conservative longitudinal macrodispersivity at infinity distance can be expressed as:

$$A_{11}^{c,\infty} = \frac{\sigma_q^2 l_1}{q^2} \approx \sigma_v^2 l_1 \tag{4.173}$$

So based on Eq. 4.109 and 4.173, the ratio of the macrodispersivity in the DNAPL source zone to the conservative macrodispersivity at infinity is:

$$\frac{A_{11}}{A_{11}^{c,\infty}} = \frac{1}{\zeta + 1} \tag{4.174}$$

The other effective results can be expressed in the ratio of the effective to the mean properties:

$$\frac{q_e}{q} = \exp\left(-2\frac{\overline{v'h'}}{\Phi}\right) \text{ when } \overline{v'h'} > 0 \tag{4.175}$$

$$\frac{q_e}{q} = \left(1 - 2\frac{\overline{v'h'}}{\Phi}\right) \text{ when } \overline{v'h'} < 0 \tag{4.176}$$

$$\frac{\Omega_e}{\overline{\Omega}} = \exp\left(-\frac{\sigma_h^2}{\Phi}\right) \tag{4.177}$$

The dissolution coefficient $\mu$ can be determined by Eq. 4.171. So the effective dissolution distance, which is the inverse of dissolution coefficient, can be obtained. Since the mean concentration deficit experiences an exponential decay according to Eq. 4.38, the effective dissolution distance represents around 20-25% of the travel distance for the mean DNAPL concentration reaching the equilibrium within the a source zone, assuming $e^{-4} \approx 0$. In another word, the effective dissolution distance reflects the travel distance for the mean concentration to reach 63% of the equilibrium concentration. Both the linearized and extrapolated results are plotted based on the inputs in Table 4.3. Large value of $\overline{\zeta}$ represents equilibrium local dissolution. Negative correlation coefficient $corr[v, h]$ indicates strong bypassing effect, while positive value represents anti-bypassing as discussed in Chapter 2.

Table 4.3: Input Parameters to Compute the Effective Properites

| Input Parameters | $\overline{\zeta}$ | $\mathbf{corr[v,h]}$ | $\sigma_v^2$ |
|---|---|---|---|
| Values | 50 | 0.5 and -0.5 | 0.25 |

Figure 4-3 shows the ratio of effective dissolution distance to the mean against $\sigma_h^2$. As we can see, the ratio increases as $\sigma_h^2$ increases, which indicates that spatial heterogeneity of dissolution rate significantly increase the effective dissolution distance. A strong bypassing has the largest effect at the same $\sigma_h^2$. This is consistent with observations that bypassing around DNAPL pools significantly affect the effective dissolution rate (Geller & Hunt, 1993). The linearized results based on Eqs. 4.106 to 4.109 are also plotted to compare with the extrapolation. As $\sigma_h^2 \ll 1$, it can be seen that the linearized results are good approximations of the extrapolated solutions. As $\sigma_h^2$ approaches 1 the linearized results increase rapidly. When $\sigma_h^2 > 1$, there are no physically meaningful solutions from the linearized results.

Figure 4-4 shows the ratio of the effective dissolution rate coefficient to the mean. For a

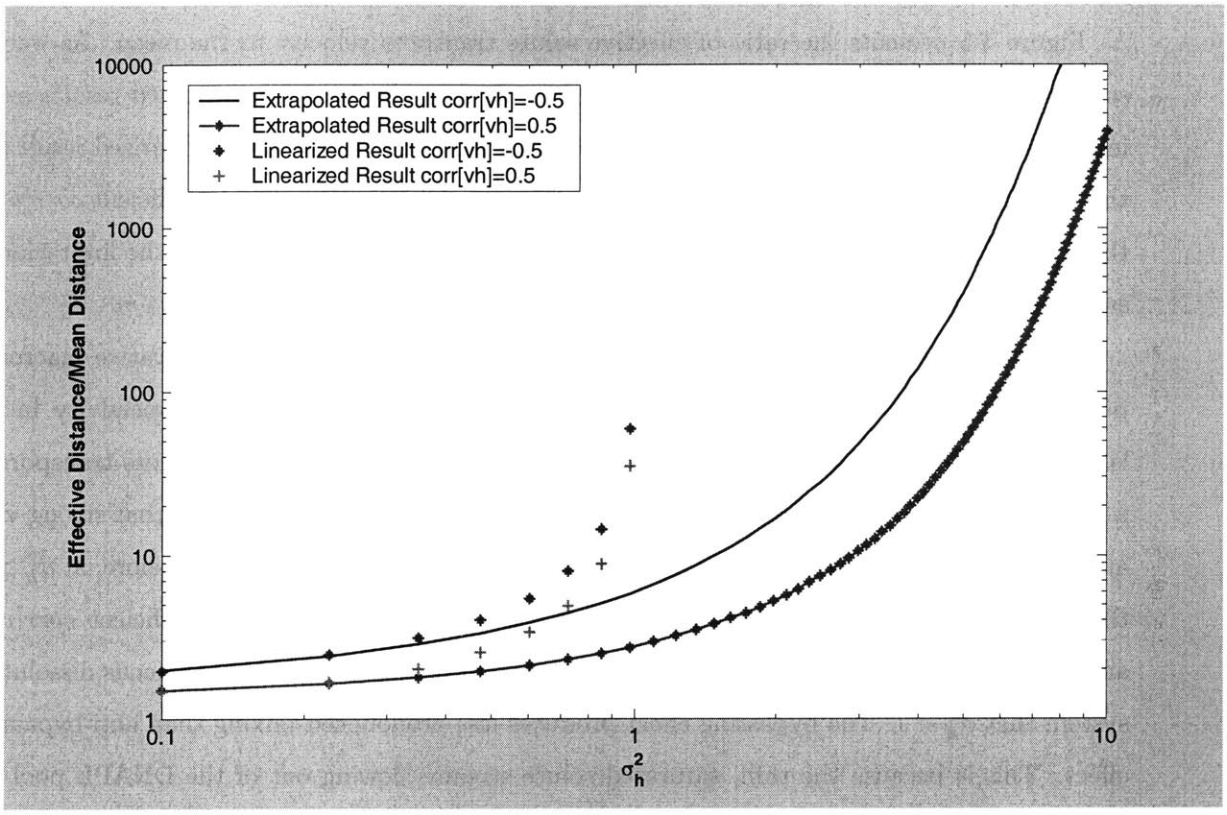


Figure 4-3: Ratio of effective dissolution distance to the mean as a function of variation of log dissolution rate coefficient and correlation between flow velocity and dissolution rate

homogeneous dissolution, while the variance of dissolution rate equals zero, the effective rate equals the mean. As heterogeneity becomes significant, the ratio decreases dramatically as $\sigma_h^2$ increases. The linearized results shows the similar pattern as Figure 4-3; for $\sigma_h^2 > 1$ there are no meaningful values from the linearized result. The effective dissolution rate is found to be insensitive to the correlation coefficient $corr[v, h]$, especially at large $\sigma_h^2$. This indicates that the dominant factor affecting effective dissolution rate is the spatial variations of local dissolution rate.

Figure 4-5 presents the ratio of effective solute transport velocity to the mean. As we can see, for a negative $corr[v, h]$, the extrapolated result deviates from the linearized results as $\sigma_h^2$ increases. As $\sigma_h^2$ approaches to zero, the exponential result converges to the linearized result and the effective flow velocity is close to the mean. For the positive correlation coefficient $corr[v, h]$, the linearized solution cannot provide a reliable solution when $\sigma_h^2 > 1$ due to the limitation of small perturbation assumption.

Figure 4-6 shows the ratio of longitudinal macrodispersivity to the conservative macrodispersivity at infinite large travel distance, as a function of $\sigma_h^2$. The macrodispersivity in the large-scale DNAPL source zone is much smaller than that of a conservative solute transport at a infinity distance. The macrodispersivity decreases as $\sigma_h^2$ increases indicating that strong variation in dissolution rate dampens the mixing effect of the plume. As we found before, at $\sigma_h^2 > 5$, the macrodispersivity is not strongly dependent on both the correlation coefficient $corr[v, h]$ and $\sigma_h^2$. The coefficient $corr[v, h]$ has significant influence only in fairly homogeneous dissolution system that $\sigma_h^2 < 1$ The bypassing effect produces less pronounced mixing than anti-bypassing effect. This is because the thin, saturated solute streams flowing out of the DNAPL pool are more difficult to mix around than large amount of unsaturated solute from the porous zone flowing in a thick plume. The effect of macrodispersion on the mean concentration distribution are limited as reflected in Figure 4-7, which compare the exact effective dissolution distance $1/\mu$ with approximate value $\frac{q_e}{\Omega_e}$ that ignores the macrodispersion. As we can see, the difference is most significant at small $\sigma_h^2$ for the positive correlation coefficient $corr[v, h]$. This is consistent with findings in Figure 4-6 that the effective dispersion effect is most significant under these conditions.

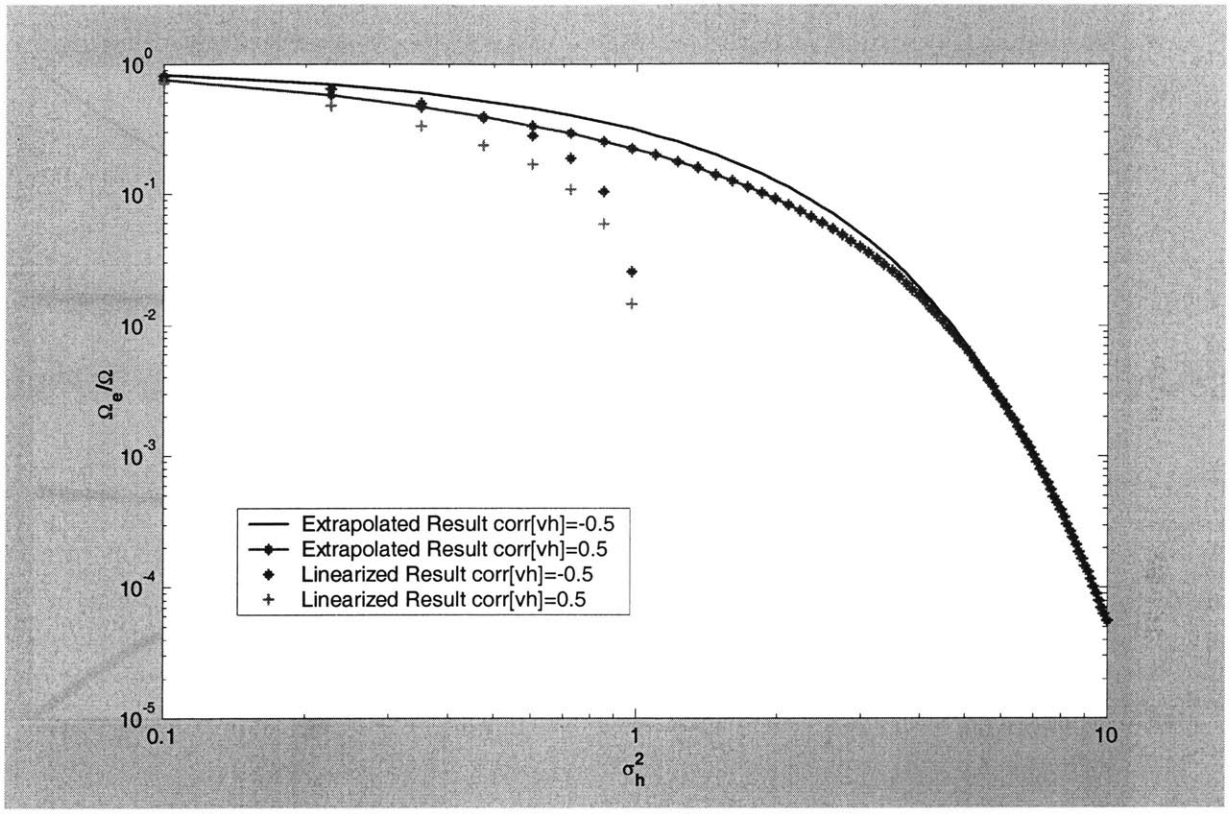


Figure 4-4: Ratio of effective dissolution rate coefficient to the mean as a function of variation of log dissolution rate coefficient and correlation between flow velocity and dissolution rate

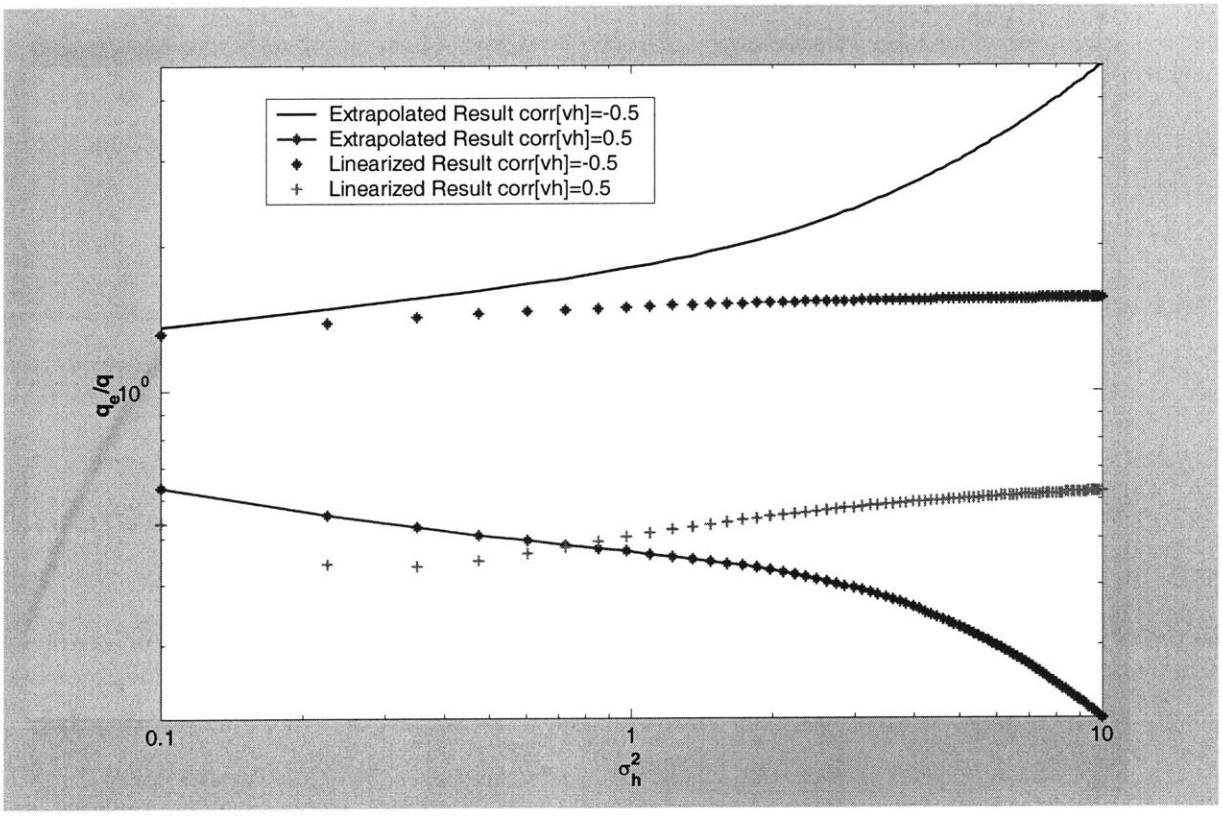


Figure 4-5: Ratio of effective flow velocity to the mean as a function of variation of log dissolution rate coefficient and correlation between flow velocity and dissolution rate

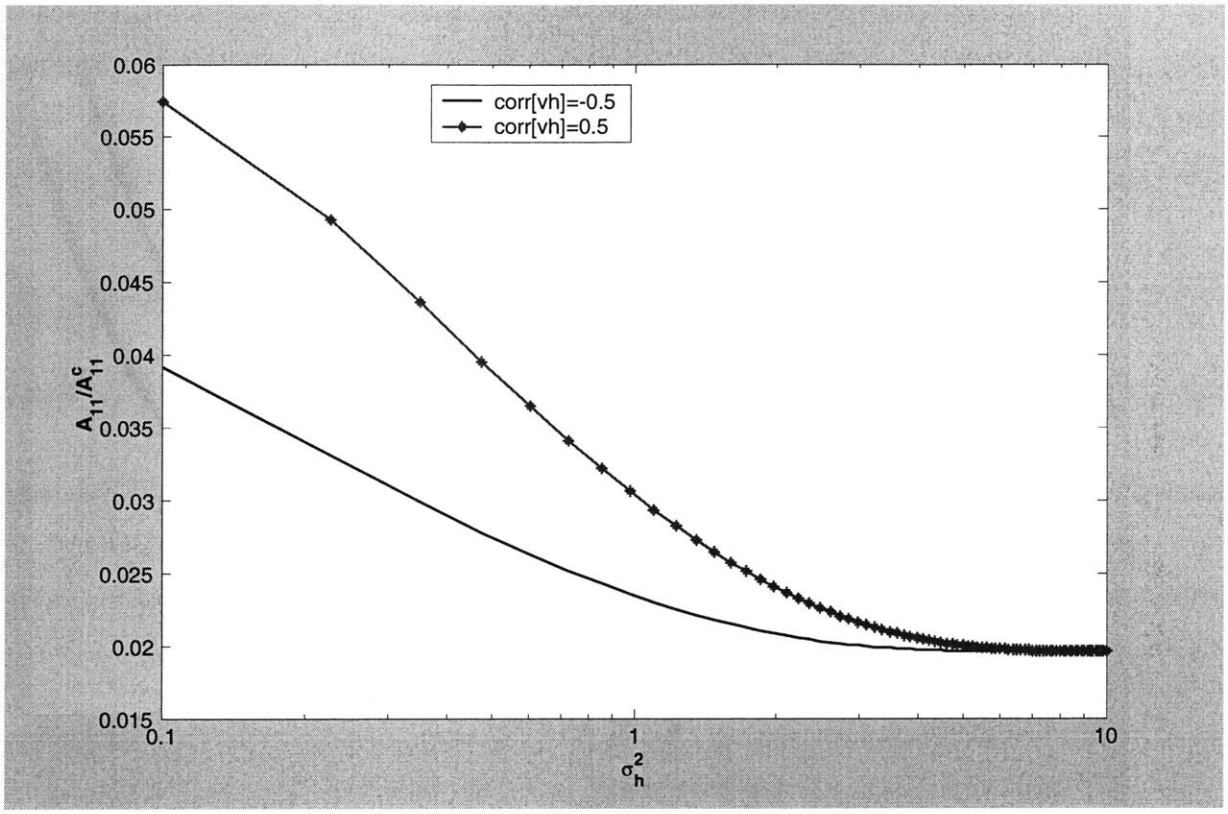


Figure 4-6: Ratio of longitudinal macrodispersivity to the conservative value at infinity distance as a function of variation of log dissolution rate coefficient and correlation between flow velocity and dissolution rate

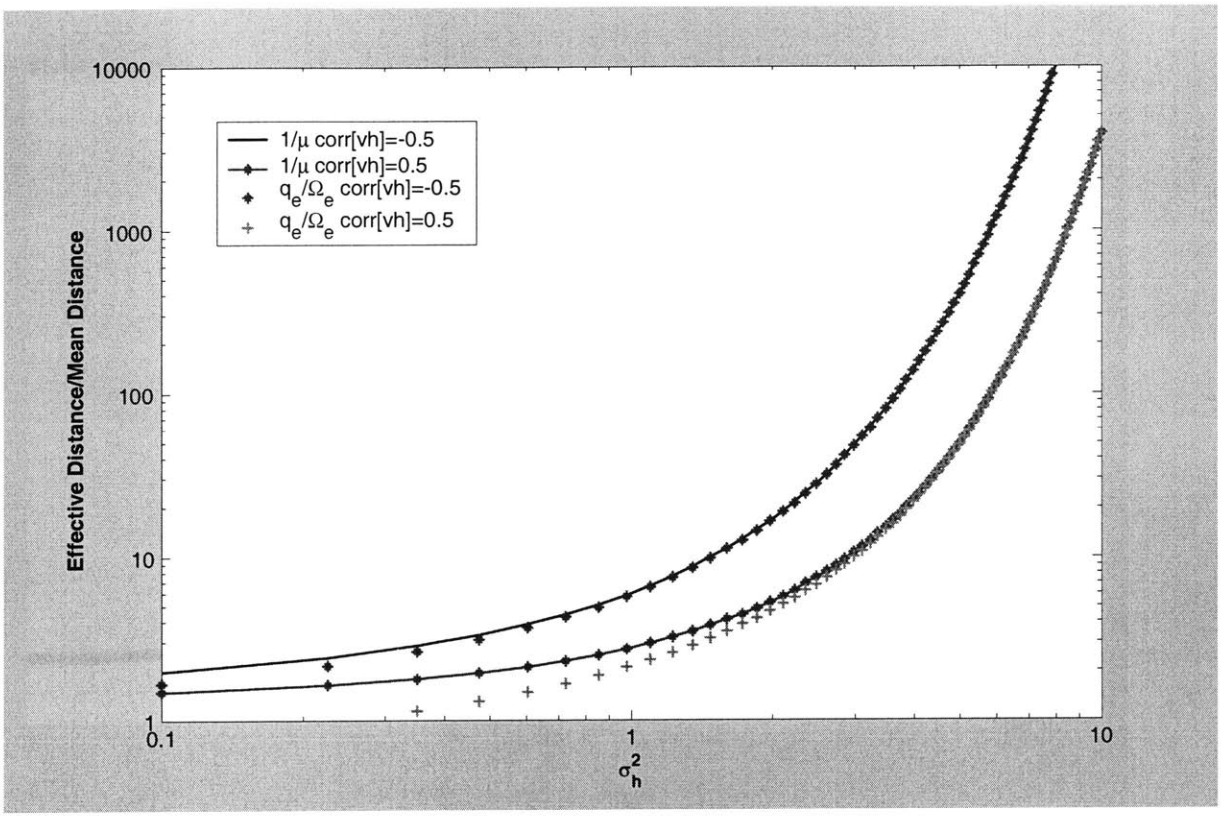


Figure 4-7: Comparison of exact effective distance ($1/\mu$) with the approximate value ($q_e/\Omega_e$) as a function of variation of log dissolution rate coefficient and correlation between flow velocity and dissolution rate

## 4.6 Discussions

### 4.6.1 DNAPL Flow along Mean Flow Direction

The transport analysis developed above is based on the static DNAPL distribution assumption. However, the DNAPL can be migrating at a very small rate in the saturated zone in both the vertical and horizontal directions. While the effect of DNAPL vertical flow has already been included in evaluating the effective transport properties, the possible horizontal migration is not considered in the above analysis. However, such a migration may have an influence on the effective properties obtained assuming a quasi-static DNAPL saturation field within a source zone. We study the effect of slowly-flowing DNAPL on the transport results developed above by adding the horizontal DNAPL hydraulic gradient in the key integrals to evaluate the effective properties. It is found that as long as two conditions are satisfied, the DNAPL horizontal movement has insignificant impact on the transport results in an imperfectly-stratified system.

$$\left|\frac{\partial R_o}{\partial P_c}\right| > \left|\frac{\partial R_w}{\partial P_c}\right| \tag{4.178}$$

$$\overline{J}_{o,3} \geq \overline{J}_{w,1} \tag{4.179}$$

The first condition represents the sensitivity of DNAPL and wetting phase relative permeability to the capillary pressure. The second condition indicates the hydraulic gradient of vertical DNAPL flow and wetting phase longitudinal flow. Since the mean DNAPL saturation at a typical source zone is very small, change of capillary pressure has much more significant influence on the DNAPL relative permeability rather water relative permeability. Therefore, it is plausible to assume $\left|\frac{\partial R_o}{\partial P_c}\right| > \left|\frac{\partial R_w}{\partial P_c}\right|$ for the DNAPL source zone at residual saturation. Also the hydraulic gradient of density flow usually is much higher than the natural groundwater hydraulic gradient. Therefore the conditions in Eq. 4.178 and 4.179 are satisfied. These conditions are also found satisfied by applying the real data from the Borden site, Canada. Therefore, it is concluded that a slowly moving DNAPL source along the mean flow direction has insignificant influence on the effective properties obtained. The detailed analysis is in Appendix C. The more general results including the impact of flowing DNAPL source can be obtained using a method of moving coordinate system. This method has been employed by Miralles-Wilhelm in the decay

study (Miralles-Wilhelm & Gelhar, 1996).

### 4.6.2 Flux Concentration Effective Properties

The effective properties obtained in this chapter are for the residence concentration field, where the concentration is calculated based on the mass in unit volume of fluid. However, field observations of concentration made using wells screened over thickness of the aquifer will not necessarily produce this depth average because water is produced preferentially from zones of higher permeability. In this case a flow weighted average should be used to establish accurate connection between theoretical predictions using effective properties and field observations. According to Gelhar (1993), the flux concentration is defined as:

$$C_f = \frac{\overline{Cq_1}}{q} = \frac{\overline{(\overline{C}+c')(q+q_1')}}{q} \tag{4.180}$$

$$= \overline{C} + \frac{\overline{c'q_1'}}{q} \tag{4.181}$$

We evaluated the effective properties for the flux concentration field and found that these properties are the same as those derived for the residence concentration above. Therefore, the effective properties derived in this chapter can be used directly to compare with field-observed concentration data. The detailed analysis is in Appendix F.

### 4.6.3 Summary of Findings

The stochastic theory developed in this study provides a framework to analyze contaminant transport in a DNAPL source zone in a three-dimensionally heterogeneous, anisotropic aquifer. The stochastic approach, which is based on a nonstationary, small-perturbation approximation, provides a systematic way of aggregating the effects of complex heterogeneities, captured in perturbation equations, into the mean equations describing field-scale mass transfer and transport. A first-order dissolution rate coefficient is employed to represent mass transfer source. The moments of spatial distribution of DNAPL saturation are incorporated in the stochastic analysis as an important contribution to the spatial variation of dissolution rate and a significant impact to the effective properties. The effective mass transfer and transport properties are obtained

from the stochastic analysis. The small-perturbation approximation is relaxed by exponential extrapolation of the effective properties. Nonstationarity at the boundary and the downstream of the plume in the source zone are transformed to stationary problem using transfer function and exponential decay method respectively.

The boundary effect was demonstrated insignificant in a DNAPL source zone with significant spreading. The field dissolution characteristics are influenced dominantly by the spatial variation of dissolution rate $\sigma_h^2$ and correlation of flow rate and dissolution rate. The field dissolution rate is always less than the mean if the dissolution is not homogeneous. The effective dissolution rate coefficient is reduced by several orders of magnitude as the variance of dissolution rate increases. The correlation coefficient between $v$ and $h$ represents the bypassing effect, which is frequently observed in the field with DNAPL pools formed on top of a relative impermeable layer. Strong negative correlation representing a strong bypassing effect reduces the field dissolution rate most. This implies a heterogeneous aquifer with lots of trapped DNAPL pools likely has the most significant effect in reducing the effective dissolution rate. Consequently, the travel distance of groundwater within a source zone to reach equilibrium concentration is increased dramatically due to the decrease of the field dissolution rate and increase of the effective solute transport velocity.

# Chapter 5

# Two-zone Model

## 5.1 Introduction

It has been realized that heterogeneities at various scales are abundant in unconsolidated aquifers (Davis *et al.*, 1997). Such media structures significantly influence DNAPL migration and distribution (Kueper *et al.*, 1989; Illangasekare *et al.*, 1995, Kueper *et al.*, 1993). Laboratory and field data from DNAPL spillage experiments have demonstrated the influence of capillary heterogeneity on DNAPL movement (Kueper *et al.*, 1993; Illangasekare *et al.*, 1995). More recently, the interaction between capillary forces and small-scale heterogeneity was shown to be important in trapping DNAPL. Two DNAPL entrapment patterns have been frequently observed: DNAPL pools within the lamina structure, and the trapped DNAPL blobs or ganglia at pore scale. For this reason, it seems quite likely that in many unconsolidated deposits DNAPL pooling is important. A recent laboratory experiment has demonstrated that DNAPL is likely trapped in small pools instead of single or multi-pore ganglia in heterogeneous media, where trichloroethylene was spilled in a cell packed with sands to reproduce facies-like geometric structures (Glass *et al.*, 2000). It was observed that small centimeter-scale pools of trichloroethylene readily formed at capillary-heterogeneity boundaries. The DNAPL distribution structure in heterogeneous porous media observed in these experiments establish a foundation to apply a simplified two-zone model to simulate the DNAPL source zone.

Two-zone model has been widely applied in studying flow, transport and mass transfer in the groundwater systems. For example, Dagan (2001) applied the framework to study the effective

conductivity of a heterogeneous porous structure by distinguishing relative high permeability zones with low permeability zones. DNAPL pool dissolution has been studied using a similar conceptual model by Sale (2001). However, most of the two-zone model studying pool dissolution is based on diffusive mass transfer, which assumes an insignificant advection effect of mass transfer from DNAPL pools. In this work we include both diffusive and advective mass transfer to characterize pool dissolution.

The main purpose of two-zone model development is to evaluate the validity of extrapolation in the stochastic model in Chapter 4, by comparing the results from the two analyses under equivalent input conditions. Moreover, the simplified model can be a valuable tool to investigate mass transfer in a DNAPL source zone with nonuniform DNAPL distribution.

## 5.2 Methodology

### 5.2.1 Conceptual Model

The two-zone concept is based on the observations in both laboratory and field experiments that DNAPL exists in subsurface systems mainly in two forms: pore-scale blobs at residual saturation, which occupy one or several pore space, and continuous pools which can extend to a scale of meters horizontally. Pools usually formed at the top of the relatively impermeable zone which DNAPL cannot penetrate due to the capillary resistant force. In our two-zone model, the DNAPL source zone is regarded as containing two composites with contrasting properties: the lens zone and permeable zone. The characteristic properties in lens zone, where high saturation of DNAPL pools, and the permeable zone, where DNAPL is entrapped, are listed in the Table 5.1.

Table 5.1: Properties Assignment in Two-zone Dissolution Model

| **Properties** | **Lens Zone** | **Permeable Zone** |
|---|---|---|
| Relative Permeability ($k_r$) | Low | High |
| DNAPL Saturation $S_n$ | High | Low |
| Water Velocity $q$ | Low | High |
| Dissolution Rate $\Omega$ | High(equilibrium) | Low(Kinetics) |
| Zone index | 1 | 2 |

As seen from the table, the lens zone is occupied by DNAPL pools with high saturation, which reduce the relative permeability of wetting phase dramatically. Consequently water velocity inside the lens is relatively low and the dissolution rate is high due to the high saturation. Therefore, the effluent concentration from the lens zone is assumed saturated. On the other hand, DNAPL is distributed in the permeable zone as residual blobs with relative low saturation compared to the lens zone, and with a high water velocity and low dissolution rate coefficient. The concentration in the permeable zone is regarded below the equilibrium concentration.

Figure 5-1 shows conceptual model the two-zone dissolution mechanism. All lens zones are idealized with same size. No interactions between lenses, which means that every lens is independent with each other. It is assumed that the effluent out of a lens does not enter another lens. The DNAPL saturation, flow rate, dissolution rate and relative permeability are regarded the same for every lens zone. Due to the relatively high mass transfer rate from the DNAPL pool inside a lens zone, a thin stream tube with equilibrium concentration exits away from the lens and contributes to the overall concentration at the downstream boundary. The overall thickness of the stream is designated as $\delta$. The concentration in the stream flowing through the permeable zone is denoted as $C$, which is a result of dissolution of DNAPL blobs trapped in the permeable zone. Figure 5-2 shows the detailed mechanism of mass transfer from a lens zone. The equilibrium concentration stream emitted from a lens is a result of two mass transfer mechanisms: longitudinal advection and transverse vertical diffusion. A thin stream with thickness $\delta_a$ is due to advection inside the lens. Since the majority of water flow bypasses the lens zone due to the relative low permeability in the lens, only a small fraction of flow enters the lens and transports mass out of the lens. Therefore, the stream due to advection is much smaller than the thickness of the lens. Mass transfer due to the vertical diffusion is reflected by the growing diffusion boundary layer on the top and the bottom of the lens along the lens. Then dissolved DNAPL at this front is then transported away from the lens due to advection. The mass transported can be regarded as a thinner layer of saturated stream with thickness $\delta_D$. So the overall mass transport from the lens can be summarized as the stream of saturated concentration with thickness of $\delta$ transported away from the lens, where

$$\delta = \delta_a + 2\delta_D \tag{5.1}$$

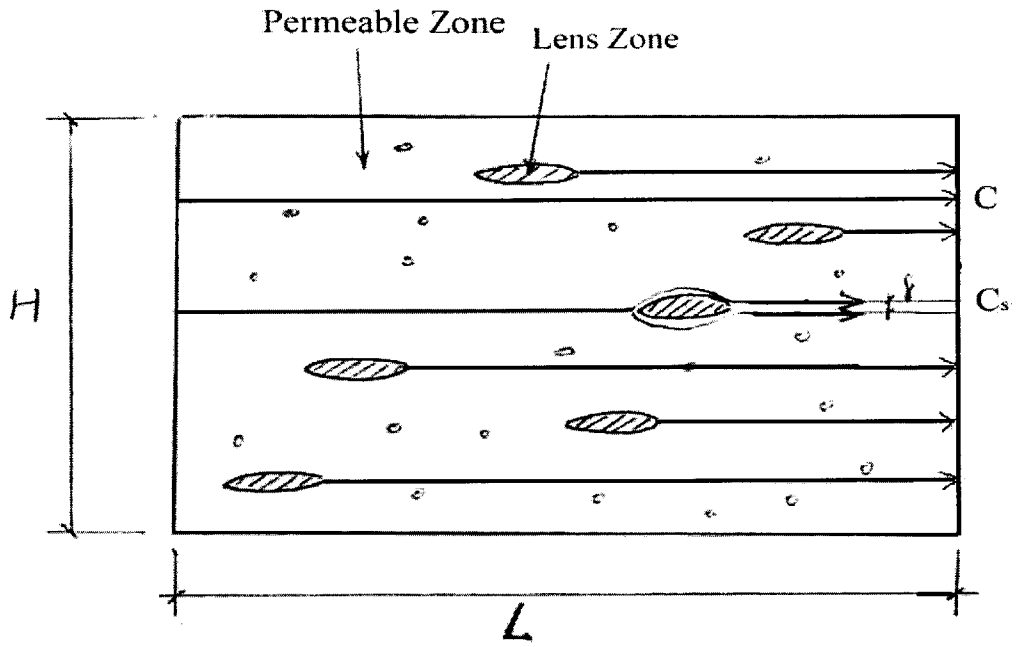


Figure 5-1: Conceptual diagram of two-zone dissolution model in a DNAPL source

### 5.2.2 Model Development

From Figure 5-1, based on mass conservation we can write:

$$WHC_e q_2 = n\delta C_s W_1 q_2 + (WH - n\delta W_1) C_2 q_2 \tag{5.2}$$

where $C_e$ is the cross-sectional effective effluent concentration, $n$ is the number of lenses, $C_s$ is the saturated concentration coming out of the lens, $C_2$ is the bulk concentration resulted from the dissolution in the permeable region, $\delta$ is the thickness of the stream transporting away from the lens with equilibrium concentration $C_s$, $q_2$ is the specific discharge in permeable zone, $W_1$ is the width of the lens, $W$ is the width of the source zone. The left side represents the overall mass flux out of the downstream boundary of the source zone in Figure 5-1. The right side represents the flux contribution from the lens zone and permeable zone. Note that $q_2\delta$ represents the flow

out of a lens while $\delta$ represents the stream thickness with specific discharge is $q_2$. So 5.2 becomes:

$$WHC_e = n\delta C_s W_1 + (WH - n\delta W_1)C_2 \tag{5.3}$$

Then we can obtain the integrated effective concentration out of the source zone:

$$C_e = \frac{n\delta}{H}\frac{W_1}{W}C_s + (1 - \frac{W_1 n\delta}{WH})C_2 \tag{5.4}$$

$$C_e = \Delta C_s + (1 - \Delta)\, C_2 \tag{5.5}$$

where

$$\Delta = \frac{n\delta}{H}\frac{W_1}{W} \tag{5.6}$$

Again the right side of Eq. 5.5 reflects the contribution from the lens zone and permeable zone, respectively. Since the flow inside the lens zone is equal to the flow in the stream in the permeable zone that comes out of the lens, so:

$$Q = K_1 J_1 H_1 = K_2 J_2 \delta_a \tag{5.7}$$

where $K_1$, $K_2$ are the hydraulic conductivity in lens zones and permeable zones, respectively. Similarly $J_1, J_2$ are hydraulic gradient within two zones, and $H_1$ is the thickness of a lens. Here I assume the hydraulic gradients within and out of the lens zone are the same as $J_1 = J_2$. So the thickness of stream out of the lens zone is:

$$\delta_a = \frac{K_1 H_1}{K_2} \tag{5.8}$$

Then we can also calculate the thickness of the diffusion layer $\delta_D$ with equilibrium concentration at the top and the bottom of the lens. Since we have:

$$\delta_D C_s = \int_0^\infty C\,(z)_{x=L_1}\, dz \tag{5.9}$$

The solution of the concentration due to diffusion is available as:

$$C(x,z) = C_s\left(1 - \text{erf}\left(\frac{z}{2\sqrt{D_T x/V_2}}\right)\right) \tag{5.10}$$

So we have:

$$\delta_D = \int_0^\infty \left(1 - \text{erf}\left(\frac{z}{2\sqrt{D_T L_1/V_2}}\right)\right) dz \tag{5.11}$$

$$\delta_D = \frac{2\sqrt{\alpha_T L_1}}{\sqrt{\pi}} \tag{5.12}$$

where

$$\alpha_T = \frac{D_T}{V_2} \tag{5.13}$$

According Eq. 5.1, the entire thickness due to mass transfer from a lens is:

$$\delta = \frac{K_1 H_1}{K_2} + 4\sqrt{\frac{\alpha_T L_1}{\pi}} \tag{5.14}$$

Using Eqs. 5.14 and 5.6, we have:

$$\Delta = n\left(\frac{K_1}{K_2} + \frac{4}{H_1}\sqrt{\frac{\alpha_T L_1}{\pi}}\right)\frac{H_1}{H}\frac{W_1}{W} \tag{5.15}$$

where $n\frac{H_1}{H}\frac{W_1}{W}$ represents the ratio of the lens area to the entire cross-sectional area. Since the effective effluent concentration deficit is

$$u_e = C_s - C_e \tag{5.16}$$

We can obtain the concentration deficit, using Eqs. 5.5 and 5.16:

$$u_e = (1 - \Delta)(C_s - C_2) \tag{5.17}$$

The transport equation in the permeable zone can be written as:

$$\frac{\partial}{\partial x}(q_2 u_2) = \frac{\partial}{\partial x}\left[E\frac{\partial u_2}{\partial x}\right] - \Omega_2 u_2 \tag{5.18}$$

where $\Omega_2$ is the dissolution rate coefficient in the permeable zone and the concentration deficit is defined as:

$$u_2 = C_s - C_2$$

Solving the differential equation by ignoring the local dispersion factor, we can derive the concentration deficit in the permeable zone as:

$$u_2 = C_s \exp(-\frac{\Omega_2}{q_2} L) \tag{5.19}$$

Using Eqs. 5.19 and 5.17, the solution of the effective concentration deficit is:

$$u_e = (1 - \Delta) C_s \exp(-\frac{\Omega_2}{q_2} L) \tag{5.20}$$

Since the effective concentration deficit could be expressed as the a function of effective properties by solving the effective transport equation:

$$u_e = C_s \exp(-\mu_T L) \tag{5.21}$$

where $\mu_T$ is the effective dissolution coefficient. So by comparing Eq. 5.20 with Eq. 5.21, we can obtain:

$$\exp(-\mu_T L) = (1 - \Delta) \exp(-\frac{\Omega_2}{q_2} L) \tag{5.22}$$

$$\mu_T = -\frac{\ln(1 - \Delta)}{L} + \frac{\Omega_2}{q_2} \tag{5.23}$$

Since we assumed above that $\Delta \ll 1$, so by applying the first order approximation of Taylor expansion, the effective coefficient can be written as:

$$\mu_T = \frac{\Omega_2}{q_2} + \frac{\Delta}{L} \tag{5.24}$$

Here I introduce a parameter $p$, which is the volumetric fraction of lens to the entire source zone.

$$p = \frac{n H_1 L_1}{H L} \frac{W_1}{W} \tag{5.25}$$

where $L_1$ is the length of the lens. So the effective dissolution coefficient can be written as:

$$\mu_T = \frac{\Omega_2}{q_2} + \left( \frac{K_1}{K_2} + \frac{4}{H_1} \sqrt{\frac{\alpha_T L_1}{\pi}} \right) \frac{p}{L_1} \tag{5.26}$$

There are two contributions to the overall two-zone dissolution model, dissolution of DNAPL blobs in the permeable zone, which is represented as $\frac{\Omega_2}{q_2}$, and dissolution of DNAPL pool in the lens zone represented as $\left( \frac{K_1}{K_2} + \frac{4}{H_1} \sqrt{\frac{\alpha_T L_1}{\pi}} \right) \frac{p}{L_1}$. In addition, there are two contributions to the DNAPL pool dissolution: advection mass transfer reflected in the ratio of permeability $\frac{K_1}{K_2}$, and the contribution from diffusion as reflected by the ratio of the diffusion layer thickness to the lens thickness $\frac{4}{H_1} \sqrt{\frac{\alpha_T L_1}{\pi}}$. The more quantitative comparison between diffusive and advective mass transfer in terms of mass transfer rate and time scale for DNAPL depletion is present in Appendix E. It is found that both mass transfer mechanisms can be important in controlling the lens zone dissolution. The contribution from permeable zones and lens zones on the right side of the equation determines the effective dissolution coefficient. The effective dissolution distance is written as:

$$\frac{1}{\mu_T} = \frac{1}{\frac{\Omega_2}{q_2} + \left( \frac{K_1}{K_2} + \frac{4}{H_1} \sqrt{\frac{\alpha_T L_1}{\pi}} \right) \frac{p}{L_1}} \tag{5.27}$$

### 5.2.3 Discrete Probability Distribution

We assume that the transport properties within the source zone distributed along with volumetric probability distribution. We know that the fraction for lens zone is $p$, while for the permeable region $1-p$. Thus the properties within the lens zone should be associated with the probability $p$. Since we assume the lognormal distribution for these properties in the continuous model, so to be consistent here I associate the logarithm of the properties with probability $p$. The properties are listed below.

$$\mathbf{\Lambda} = [v, H, R] \tag{5.28}$$

$$v = \ln q \tag{5.29}$$

$$H = \ln \Omega \tag{5.30}$$

$$R = \ln K \tag{5.31}$$

For each property of $\mathbf{\Lambda}$, there are two values $\Lambda_1$ and $\Lambda_2$ associated with the properties for the lens zone and for the permeable zone respectively. The simplified discrete probability distribution assumed in two-zone model and the underlying continuous probability distribution for parameters are shown in Figure 5-3. Because the discrete distribution model is an idealized simplification of continuous distribution, properties like $p$, $\Lambda_1$ and $\Lambda_2$ can be derived from the continuous distribution. As illustrated in Figure 5-3, once $\Lambda_c$, the critical threshold value in the continuous probability distribution to distinguish the lens and permeable properties, is determined, the probability $p$ can be determined by Eq. 5.32. $p$ is the probability that the value less then the threshold $\Lambda_c$ in the continuous distribution., while equivalently in the two-zone model $p$ represents the volumetric fraction of the lens zone to the entire control volume. The $\Lambda_1$ represents the properties for the lens zone and it is defined as the average value in the region that $\Lambda < \Lambda_c$ in the continuous distribution model as shown in Eq. 5.33. Once the critical value $\Lambda_c$ is determined, $\Lambda_1$ and $\Lambda_2$ can be found. Equations 5.32 to 5.34 provide the analytical relationship between the continuous and discrete distribution.

$$p = P\left[\Lambda < \Lambda_c\right] = \int_{-\infty}^{\Lambda_c} f_\Lambda\left(\Lambda\right) d\Lambda' \tag{5.32}$$

$$\Lambda_1 = \frac{\int_{-\infty}^{\Lambda_c} f_\Lambda\left(\Lambda\right) \Lambda d\Lambda'}{p} \tag{5.33}$$

$$\Lambda_2 = \frac{\int_{\Lambda_c}^{\infty} f_\Lambda\left(\Lambda\right) \Lambda d\Lambda'}{1-p} \tag{5.34}$$

where $f_\Lambda\left(\Lambda\right)$ is the continuous probability distribution function.

Above we introduce a generic method to determine the probability and properties of two-zone model, given the continuous distribution of the corresponding properties. However, since the critical value $\Lambda_c$ is unknown while the first and second order moments are known from stochastic results, here we use an alternative method to determine the two-zone model parameters. For the two-zone model, there are only two possible values $\Lambda_1$ and $\Lambda_2$ associated with probability $p$ and $1-p$, respectively. Two-zone probability distribution can be connected with the continuous distribution by the mean and variance of the variable. Based on the discrete probability

distribution, the mean and the variance of the properties can be written as:

$$\overline{\Lambda} = p\Lambda_1 + (1-p)\Lambda_2 \tag{5.35}$$

$$\sigma_\Lambda^2 = p\left(\Lambda_1 - \overline{\Lambda}\right)^2 + (1-p)\left(\Lambda_2 - \overline{\Lambda}\right)^2 \tag{5.36}$$

By simultaneously solving Eqs. 5.35 and 5.36, $\Lambda_1$ and $\Lambda_2$ can be expressed as a function of $\overline{\Lambda}$, $\sigma_\Lambda^2$ and $p$ :

$$\Lambda_1 = \overline{\Lambda} \mp \sqrt{\frac{1-p}{p}}\sigma_\Lambda \tag{5.37}$$

$$\Lambda_2 = \overline{\Lambda} \pm \sqrt{\frac{p}{1-p}}\sigma_\Lambda \tag{5.38}$$

The mean and variance of the flow and transport properties are known from the flow and transport analysis. Then the characteristic value in two regions $\Lambda_1$ and $\Lambda_2$ can be determined from Eqs. 5.37 and 5.38. So the dissolution rate coefficient, flow velocity and hydraulic conductivity in two zones can be expressed as:

$$\Omega_1 = e^{H_1} = \exp\left(\overline{H} + \sqrt{\frac{1-p}{p}}\sigma_H\right) \tag{5.39}$$

$$\Omega_2 = e^{H_2} = \exp\left(\overline{H} - \sqrt{\frac{p}{1-p}}\sigma_H\right) \tag{5.40}$$

$$q_1 = e^{v_1} = \exp\left(\overline{v} - \sqrt{\frac{1-p}{p}}\sigma_v\right) \tag{5.41}$$

$$q_2 = e^{v_2} = \exp\left(\overline{v} + \sqrt{\frac{p}{1-p}}\sigma_v\right) \tag{5.42}$$

$$K_1 = e^{R_1} = \exp\left(\overline{R} - \sqrt{\frac{1-p}{p}}\sigma_R\right) \tag{5.43}$$

$$K_2 = e^{R_2} = \exp\left(\overline{R} + \sqrt{\frac{p}{1-p}}\sigma_R\right) \tag{5.44}$$

## 5.3 Results and Discussions

### 5.3.1 Effective Dissolution Properties

To express the effective dissolution coefficient in Eq. 5.26 as a function of same set of input parameters of stochastic results, which are the variance of flow velocity, the variance of log dissolution rate coefficient, correlation coefficient of flow rate and dissolution rate and the mean of the dissolution rate, the right side of Eq. 5.26 for two-zone model is explored. Because the hydraulic gradient is assumed constant, so the ratio of hydraulic conductivity can be obtained using Eqs. 5.41 and 5.42:

$$\frac{K_1}{K_2} = \frac{q_1}{q_2} = \frac{\exp(\overline{v} - \sigma_v\sqrt{\frac{1-p}{p}})}{\exp\left(\overline{v} + \sigma_v\sqrt{\frac{p}{1-p}}\right)} \tag{5.45}$$

$$= \exp\left(-\sigma_v\left(\sqrt{\frac{1-p}{p}} + \sqrt{\frac{p}{1-p}}\right)\right) \tag{5.46}$$

So using the Eq. 5.42, the flow velocity in the permeable zone can be expressed as:

$$q_2 = e^{\overline{v}+\frac{\sigma_v^2}{2}} \exp\left(\sigma_v\sqrt{\frac{p}{1-p}} - \frac{\sigma_v^2}{2}\right) \tag{5.47}$$

Here I assume that $\overline{q}$ and $\overline{v}$ bear the lognormal-normal relationship as assumed in the continuous model in order to make the two models comparable. So we have:

$$q_2 = q\exp\left(\sigma_v\sqrt{\frac{p}{1-p}} - \frac{\sigma_v^2}{2}\right) \tag{5.48}$$

Similarly we assume the mean of $\Omega$ and $H$ bear the same relationship as $q$ and $v$. So the dissolution rate coefficient at the permeable zone is:

$$\Omega_2 = e^{h_2}$$

$$= \exp\left(\overline{H} - \sqrt{\frac{p}{1-p}}\sigma_h\right) \tag{5.49}$$

$$= \overline{\Omega}\exp\left(-\sqrt{\frac{p}{1-p}}\sigma_h - \frac{\sigma_h^2}{2}\right) \tag{5.50}$$

So combining Eqs. 5.46, 5.42, 5.49 and 5.26, the effective dissolution coefficient can be derived as:

$$\begin{aligned}\mu_T &= \left(\exp\left(-\sigma_v\left(\sqrt{\frac{1-p}{p}}+\sqrt{\frac{p}{1-p}}\right)\right)+\frac{4}{H_1}\sqrt{\frac{\alpha_T L_1}{\pi}}\right)\frac{p}{L_1}+\frac{\overline{\Omega}}{q}\frac{\exp\left(-\sqrt{\frac{p}{1-p}}\sigma_h-\frac{\sigma_h^2}{2}\right)}{\exp\left(\sqrt{\frac{p}{1-p}}\sigma_v-\frac{\sigma_v^2}{2}\right)} \\ &= z_1+z_2 \end{aligned} \tag{5.51}$$

where the first part $z_1$ on right side of equation represents contribution from lens zones and the second part $z_2$ from permeable zones. As we can see from Eq. 5.51, the effective dissolution distance is a function of variance of log flow velocity $\sigma_v^2$, the variance of log dissolution rate $\sigma_h^2$ and the mean of dissolution rate coefficient through $\overline{\zeta}$. The flow rate and dissolution rate is assumed perfectly negative correlated that $corr[v,h]=-1$ since the structure of the two-zone model exactly represents the strongest bypassing effect discussed in Chapter 2. So far we have derived the effective dissolution coefficient as a function of same input parameters as those in stochastic analysis, in addition to the probability and scale of a lens. The inverse of the effective coefficient is the effective dissolution distance as defined in Chapter 4. So we can compare the effective dissolution distance from two-zone model with the continuous stochastic results by applying the same inputs.

### 5.3.2 Comparison with Effective Properties from Continuous Stochastic Analysis

Table 5.2 presents the input parameters for both models. Here the thickness of the lens $H_1$ is assumed to be 10% of the length of the lens $L_1$. The parameters presented covers the range of inputs calculated for field sites of the Borden site, the Cape Cod and the Savannah River Site. The detailed calculation is demonstrated in Chapter 6.

Figure 5-4 shows the two-zone model results with different input combination of probability and length of lenses, compared with stochastic result in terms of the ratio of effective dissolution distance to the mean dissolution distance against the variance of log dissolution rate. As we can see, two-zone model results are more sensitive to the selection of probability than the length of lens. With the same input parameters, high probability indicates a high density of DNAPL pools, which subsequently implies the majority of DNAPL exists in pools. This enhances the

Table 5.2: Input Parameters for both Stochastic Model and Two-zone Model for Different Sensitivity Test

| Case Number | $\sigma_v$ | $\overline{\zeta}$ | $\frac{H_1}{L_1}$ |
|---|---|---|---|
| 1 | 0.5 | 50 | 0.1 |
| 2 | 1 | 50 | 0.1 |
| 3 | 0.5 | 10 | 0.1 |
| 4 | 0.5 | 50 | 0.2 |

bypassing effect and increase the effective dissolution distance. Different length of lenses makes two-zone model result slightly different. The agreement of results from two models is good especially at moderate input variation.

The second case we evaluate the sensitivity to the large variation coefficient of flow velocity. Figure 5-5 shows the comparison of two results. As we can see the two-zone results are now more sensitive to the probability than the first case. However, the agreement between two results is still good.

We evaluate the sensitivity of the result to the input of $\overline{\zeta}$ as the value reduces five times than that in case one. As we can see in Figure 5-6, the agreement of two models is robust at smaller variance regardless of the change of input parameters. As $\sigma_h^2$ increase, the deviation between two results becomes more noticeable.

Next we evaluate the sensitivity of results to the ratio of the thickness and the length of a lens in Figure 5-7. As the ratio increase from 0.1 to 0.2, we can find that the agreement is even better due to the less contribution from the diffusion mass transfer from the lens.

As we observed from the above tests, we find at large variance of dissolution rate, the stochastic results tend to exceed the two-zone model results. This can be attributed to the wake effect in the two-zone model. At high volumetric percentage of DNAPL pools present, it is more likely pools interfere with each other and the high-concentration stream lines from two pools overlapped. This tends to reduce the dissolution effect from the pool. We can correct this effect by dividing $z_1$ by a constant value larger than one in Eq. 5.51. Figure 5-8 shows the results of Case 1 corrected for the wake effect by a factor of 3. This means only 1/3 of pools effectively contribute to the dissolution due to the high density of pools. We see that the curve agrees with the stochastic results better than that shown in Figure 5-4.

Generally the two-zone model results are in good agreement with the stochastic result for

all cases we have evaluated. The same combination of probability and length of lenses provides robust results for different input parameters. This significantly strengthens the plausibility of the extrapolated stochastic results.

### 5.3.3 Comparison of Porous Dissolution with Lens Dissolution

From Eq. 5.26, we can identify the contributions of the dissolution from permeable zone and lens zone. Figure 5-9 shows the comparison of $z_1$ and $z_2$ for the case 1, which represents the dissolution contribution from lens zone and permeable zone respectively. The input data are listed in Table 5.3. As we can see, $z_2$ dominates $z_1$ for almost the entire range of $\sigma_h^2$. As $\sigma_h^2$ increases, the contribution from the permeable zone decreases due to the lower dissolution rate. The contribution from lens zone keeps constant with $\sigma_h^2$ since the effluent from a lens is assumed equilibrium already. This indicates that for small to moderate variability of log dissolution rate, dissolution from a DNAPL pool is not the primary contribution compared to the dissolution from the permeable zone, where DNAPL is entrapped as isolated blobs. Due to the high probability of the lens zone, the majority of the DNAPL entrapped in lens rather than in permeable zone. Though the local dissolution inside the DNAPL pool is assumed equilibrium, the mass transferred away from the DNAPL pool is very limited due to the strong bypassing effect. The overall mass transport inside a DNAPL source is controlled by the permeable zone dissolution, which is significantly nonequilibrium due to the small DNAPL saturation. So the effective dissolution distance is very high as illustrated in Figure 5-4. This is consistent with the observations that the field-scale DNAPL dissolution rate is far lower than that measured in laboratory and DNAPL contamination can be persistent for decades and century.

Table 5.3: Input Parameters for Two-zone Model to Evaluate the Contribution from Lens Zones and Permeable Zones to the Effective Dissolution

| **Case Number** | $\sigma_v$ | $\overline{\zeta}$ | $\frac{H_1}{L_1}$ | $p$ | $L_1(m)$ |
|---|---|---|---|---|---|
| 1 | 0.5 | 50 | 0.1 | 0.6 | 10 |

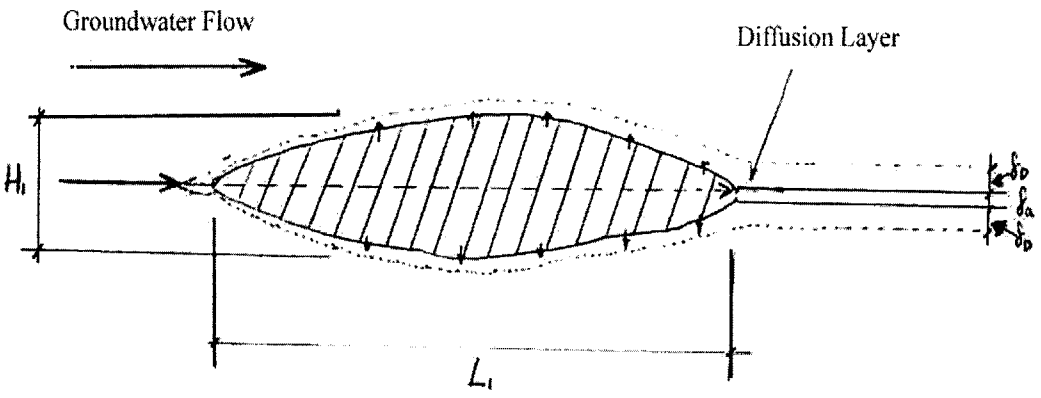


Figure 5-2: Diffusion and advection mass transfer from a lens zone

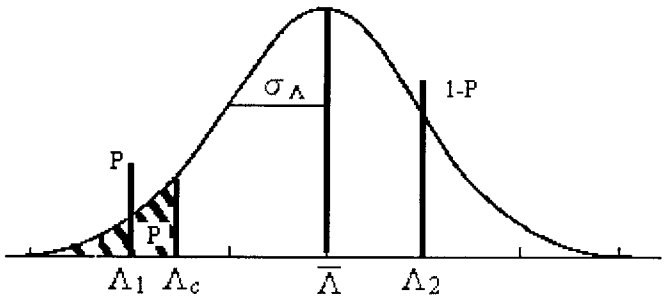


Figure 5-3: Probability distribution of two-zone model

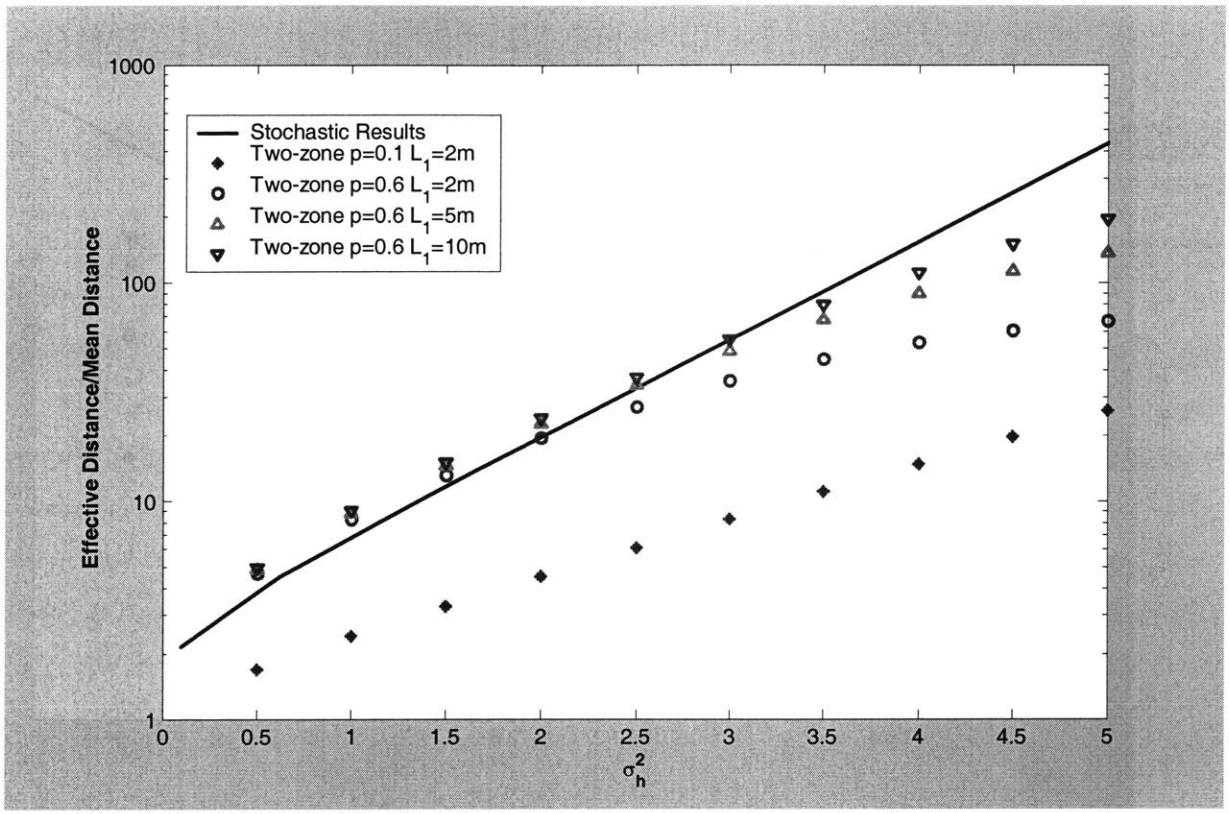


Figure 5-4: Comparison of stochastic result with two-zone model result for case 1 in Table 5.2

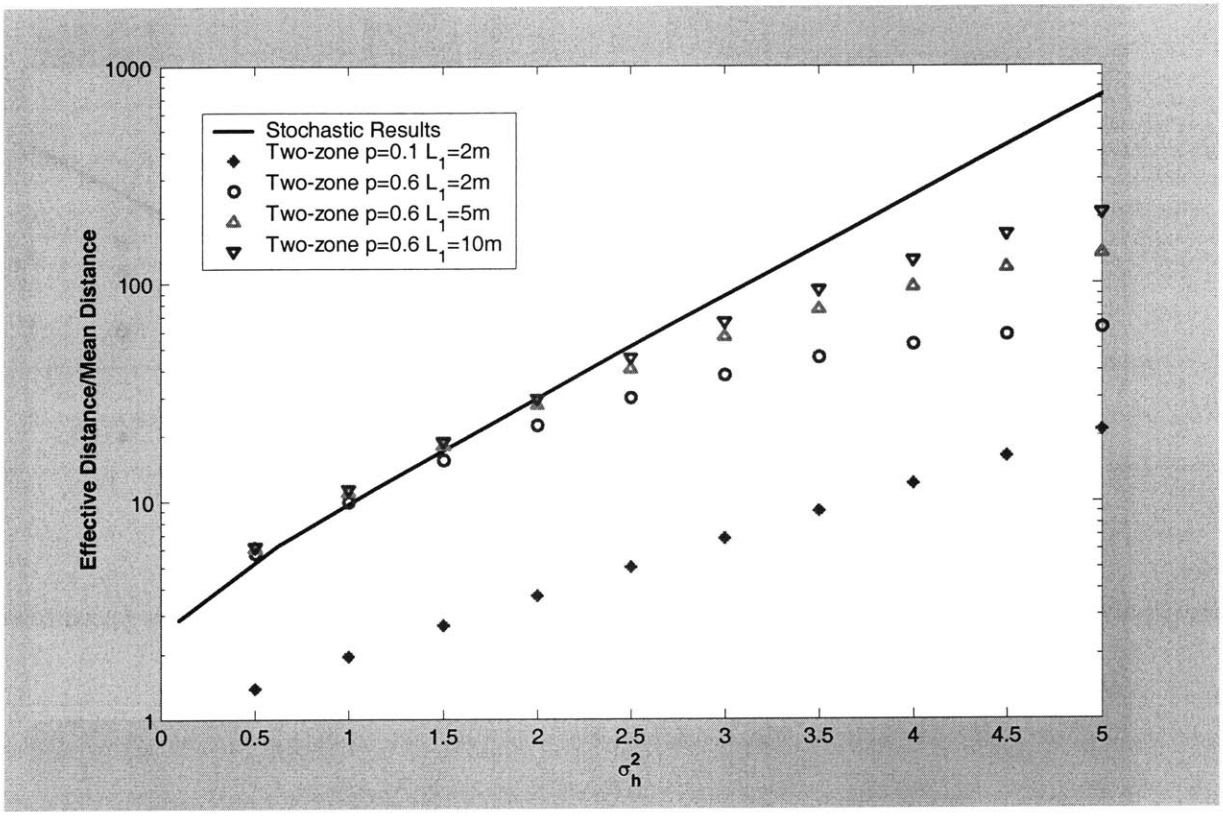


Figure 5-5: Comparison of stochastic result with two-zone model result for case 2 in Table 5.2

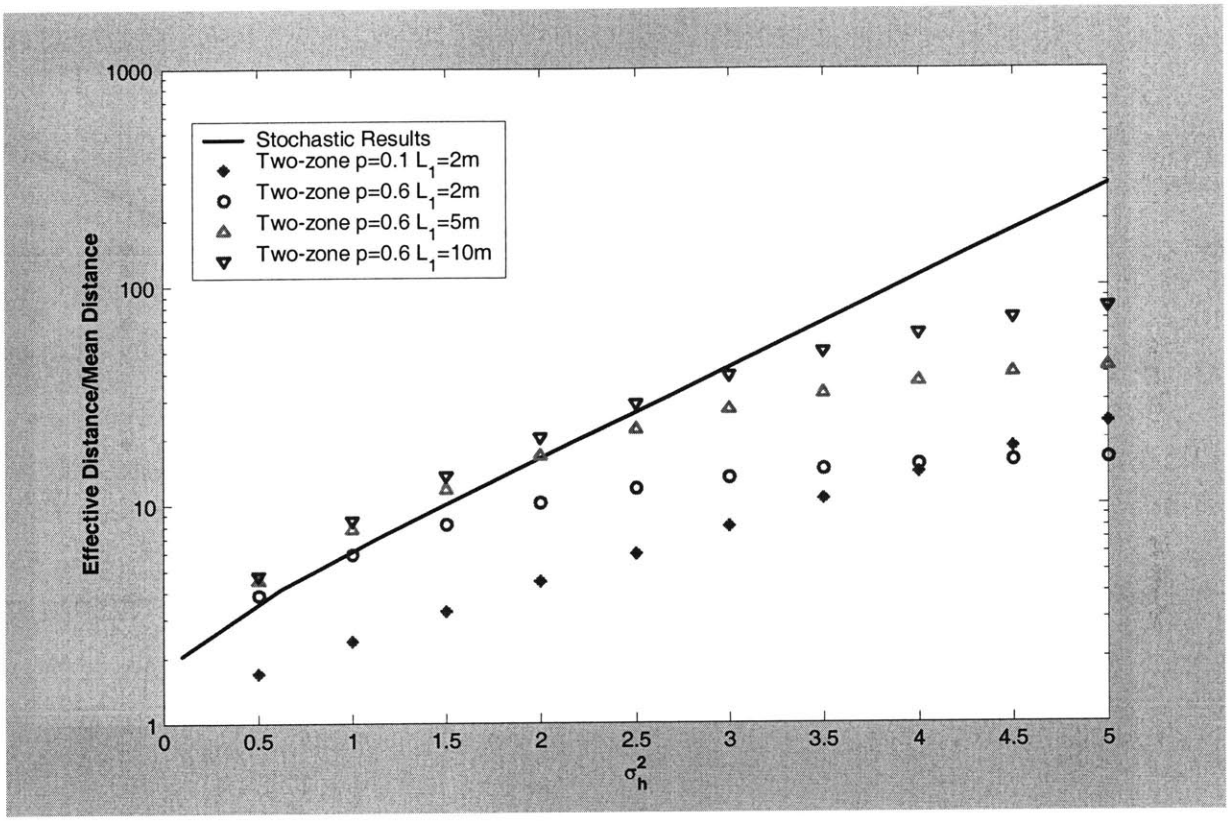


Figure 5-6: Comparison of stochastic result with two-zone model result for case 3 in Table 5.2

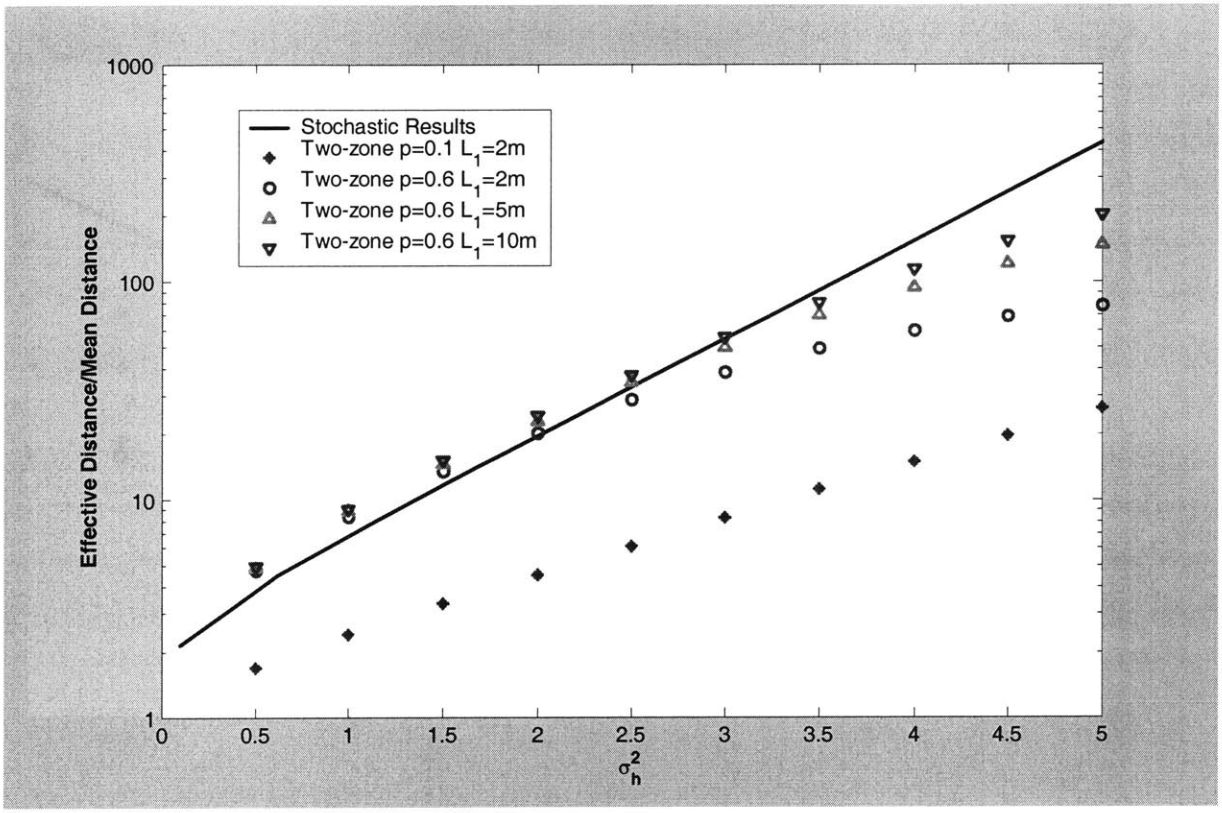


Figure 5-7: Comparison of stochastic result with two-zone model result for case 4 in Table 5.2

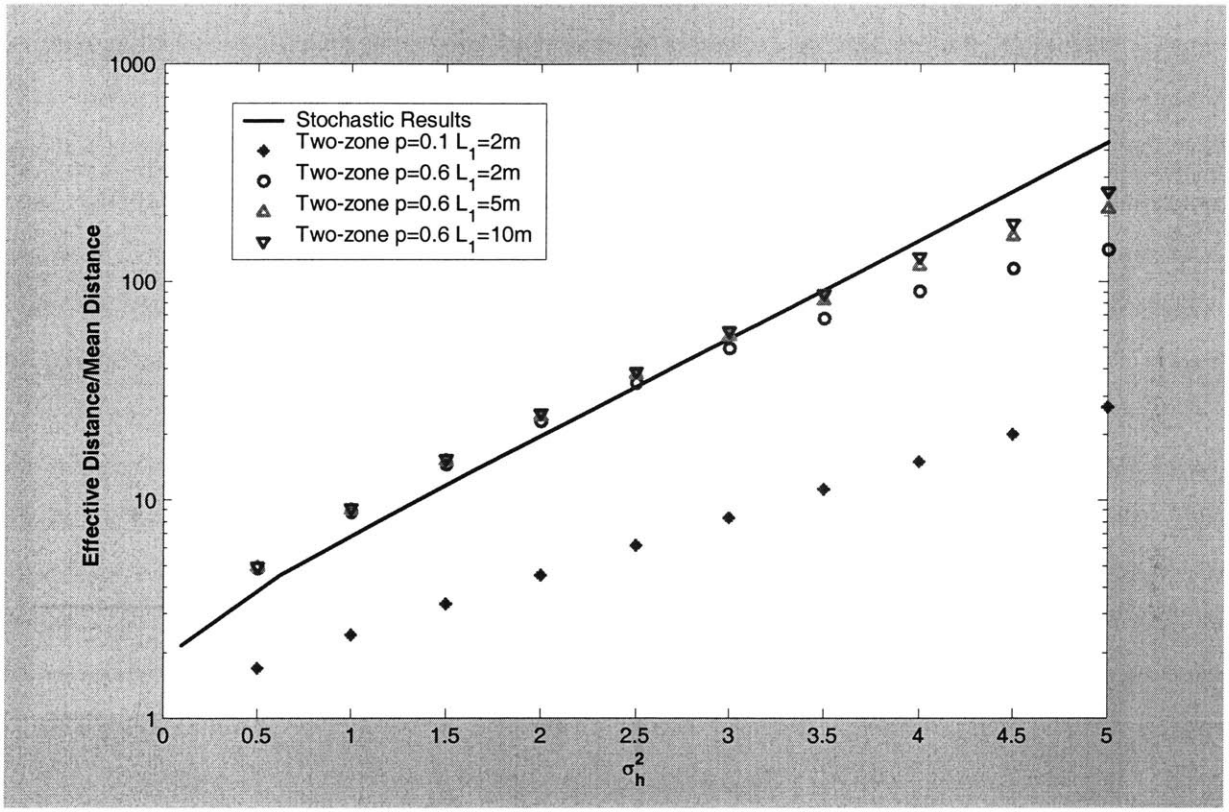


Figure 5-8: Comparison of stochastic result with two-zone model result for case 1 with wake effect by reducing the lens dissolution contribution by a factor of 3

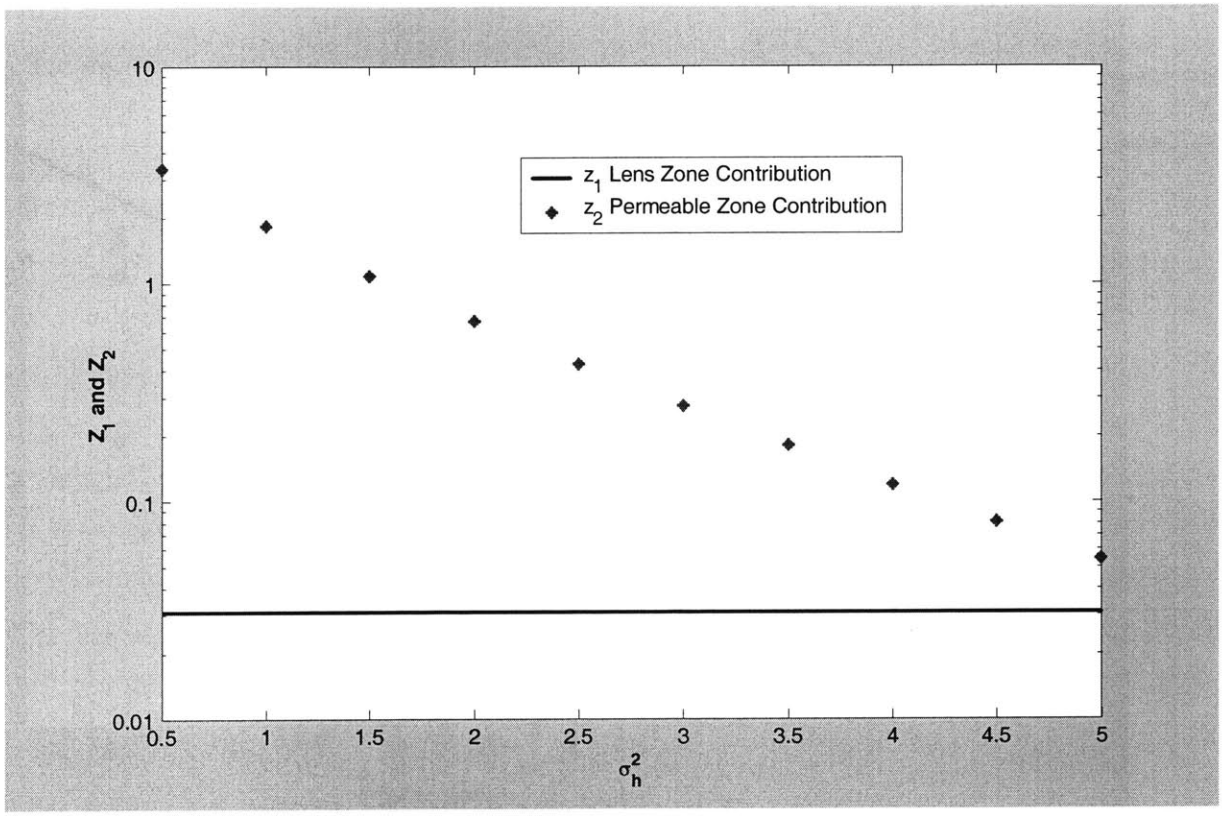


Figure 5-9: Comparison of mass transfer and transport contributions from the lens zone $z_1$ and the permeable zone $z_2$

# Chapter 6

# Field Applications

## 6.1 Overview

To demonstrate the applicability of the stochastic results, it is desirable to simulate sites with actual DNAPL contamination and available plume concentration data. Though there are hundreds of DNAPL contaminated sites in North America, most of these sites lack adequate characterization of the DNAPL source zone and/or reliable data on two-phase hydraulic characteristics. However, we have located suitable contaminated sites and created synthesized contamination events to demonstrate the feasibility of treating field-scale contamination using the effective parameters-based framework. The following four sites with contrasting geological settings are explored here: the Borden site, the Cape Cod aquifer, the Savannah River Site (SRS) and the Hanford site.

The Borden site is a glaciolacustrine sand with low bulk permeability and low variability. It is the first field site at which extensive three-dimensional hydraulic conductivity characterization was undertaken. The Borden site has been a field experimental site of groundwater contamination control and remediation since early 80s. Recently, Frind and coworkers performed a field-scale DNAPL dissolution experiment there (Frind *et al.*, 1999). In their experiment, the DNAPL source zone was made artificially by mixing DNAPL with sand before being emplaced the unit into the aquifer. Such a man-made well-mixed source gave rise to relatively homogeneous dissolution pattern. Therefore, the results of this experiment are not suitable to quantify the large-scale dissolution rate, which is a result of a naturally-formed non-uniform DNAPL

distribution. So far there is no systematic field-scale DNAPL distribution and dissolution data available at the Borden site. Using the extensive hydraulic conductivity data, here I create a hypothetical DNAPL contamination event and predict the downgradient concentration profile inside the source zone as a result.

The Cape Cod aquifer is a sand and gravel deposit described as glacial outwash of high bulk permeability and moderate variability (Springer, 1991). It is a site with detailed characterization of hydraulic conductivity and two-phase flow characteristic parameters (Jacobs, 1998). However, like the Borden site, it is not a DNAPL contaminated site and there are no field-scale DNAPL remediation experiments there. So similarly a hypothetical DNAPL contamination event is created for the Cape Cod aquifer to predict the concentration profile.

The SRS is located on Atlantic Coastal Plain and is a typical coastal plain geology, which consists interbedded sands and clayey sands separated by clay-rich beds with very low bulk permeability and high variability. It is heavily contaminated by DNAPL and considerable work has been conducted to characterize the source zone. Though DNAPL source zone is relatively well characterized, the lack of reliable groundwater concentration data and accountable multiphase flow parameters limits our ability to evaluate theoretical results at SRS. Like the Borden and the Cape Cod site, a hypothetical contamination event is created at the SRS in this work and the effective properties and concentration profile are obtained.

The Hanford site is situated within the Pasco Basin, which accumulated thick deposits of Miocene continental flood basalts and younger sediments. The aquifer formation is of low bulk permeability and extremely high variability. Significant amount of organic solvents were discharged into groundwater systems and became a continuous contamination source. Extensive investigations to characterize the contaminant source, migration, fate in subsurface systems have be performed during the last two decades (Rohay *et al.*,1994; Swanson *et al.*, 1999). Considerable data were available including hydraulic conductivity, hydraulic head and unsaturated zone capillary pressure curve characteristic parameters. Systematic concentration measurements have been conducted at 200 West Area. DNAPL concentration data are available in the area close to the disposal facility where DNAPL was discharged and became a persistent contamination source. Therefore, the Hanford site provides a unique opportunity to explore the validity of the theoretical results.

## 6.2 Site Introduction

### 6.2.1 Borden Site and Cape Cod

Several field-scale solute transport and multiphase flow experiments were conducted at the Borden site in the last two decades by researchers. Sudicky (1986) reported sampling data of the Borden site on the collection of thirty-two, 2 m long cores taken along two intersecting transects at a horizontal interval of 1 m. The cores were cut at intervals of 5 cm and estimates made of the saturated hydraulic conductivity using a falling head permeability test. The Borden site is a well-stratified deposit with the ratio of the horizontal correlation scale to the vertical correlation scale exceeds 20 (Gelhar, 1993). Kueper's field experiment of multiphase flow found that DNAPL reached the 10 m boundary with a less than 1 m vertical infiltration (Kueper *et al.*, 1993). A naturally spilled DNAPL source can reach the scale of tens of meters easily at the Borden aquifer, which is much larger than the horizontal correlation scale. Jacobs (1998) analyzed the permeability data and capillary pressure curve parameters to study the multiphase flow at the Borden site. Two-phase flow characteristics were determined using measured capillary pressure curves and saturated hydraulic conductivity for samples from the unsaturated zone at the tracer test site.

Similar to the Borden site, the Cape Cod aquifer is another site with extensive characterization in terms of hydraulic conductivity. Analysis of the statistical variability of permeability at the Cape Cod site have been performed by Springer (Springer, 1991) and Hess (Hess *et al.*, 1992). Hydraulic conductivity at the Cape Cod site was inferred along borehole transects spanning roughly 20 m horizontally in which borehole-flowmeter logging was done. Compared to the Borden site, the Cape Cod site is more permeable but also more heterogeneous. Mace (1994) performed measurements of capillary tension and saturation relationship for in 6 cores sampled from the Cape Cod at seven 8 cm intervals along each other. Capillary pressure-saturation data for the water-air system were collected and the van Genuchten and Brooks Corey model parameters were estimated. Jacobs (1998) employed this set of data and parameters as the input of his multiphase flow analysis for the Cape Cod site. In this study we use the same parameters obtained by Jacobs.

### 6.2.2 Savannah River Site

The SRS is a 800 $km^2$ site located 40 kilometers southeast of Augusta, Georgia in southwestern South Carolina adjacent to the Savannah River. SRS areas and facilities include inactive nuclear production reactors, inactive nuclear target, fuel fabrication facility, waste storage and disposal area and support, research facilities. The A/M-Area is located in the northern section of the SRS and consists of facilities that fabricated reactor fuel and target assemblies for the SRS reactors, laboratory facilities and administrative and support facilities. Operations at these facilities have resulted in the release of chlorinated solvents, primarily trichloroethylene (TCE), tetrachloroethylene (PCE) and 1,1,1-trichloroethane (1,1,1-TCA) to the subsurface. It has been estimated that 2 million pounds of chlorinated solvents were released to the M-Area Settling Basin (Jackson & Looney, 2001). Due to the high water table and the permeable near surface sediments and high density of the contaminant, DNAPL penetrated the vadose zone, with a thickness 0-40 m, and quickly reach groundwater.

The hydrogeology in A/M Area consists of three aquifers. It lies near the up-dip limit of the coastal plain deposits. The majority of the solvent contaminant present in the area is located within Steed Pond Aquifer, which is comprised of regionally defined aquifer zones including M-Area aquifer zone, the Green Clay confining zone, and the Lost Lake aquifer zone. The Lost Lake aquifer zone is the primary target of DNAPL source characterization, which was reported by previous studies (Jackson *et al.*, 2000). Considerable work has aimed at characterizing DNAPL contaminant source and understanding the extension of the DNAPL plume in the groundwater systems in the area (Jackson *et al.* 2000; Jackson and Looney 2001). Data for all sampling media including aqueous phase, soil solid and gas phase are reported. Numerical screening criteria were established to indicate the likelihood of DNAPL presence. However, systematic measurements of groundwater concentration are not available yet.

Rossabi (1999) compiled the reported measurement results of hydraulic conductivity and capillary pressure curve parameters for the M Area. Table 6.1 presents the log permeability, van Genuchten parameters of capillary pressure curve. As we can see, the aquifer in M Area is relatively impermeable with low mean log permeability. The selected data represent the middle layer ranged from 17 m to 50 m below the surface, where DNAPL most likely present as a separate phase. Due to the large pressure change step in measuring the capillary pressure curve,

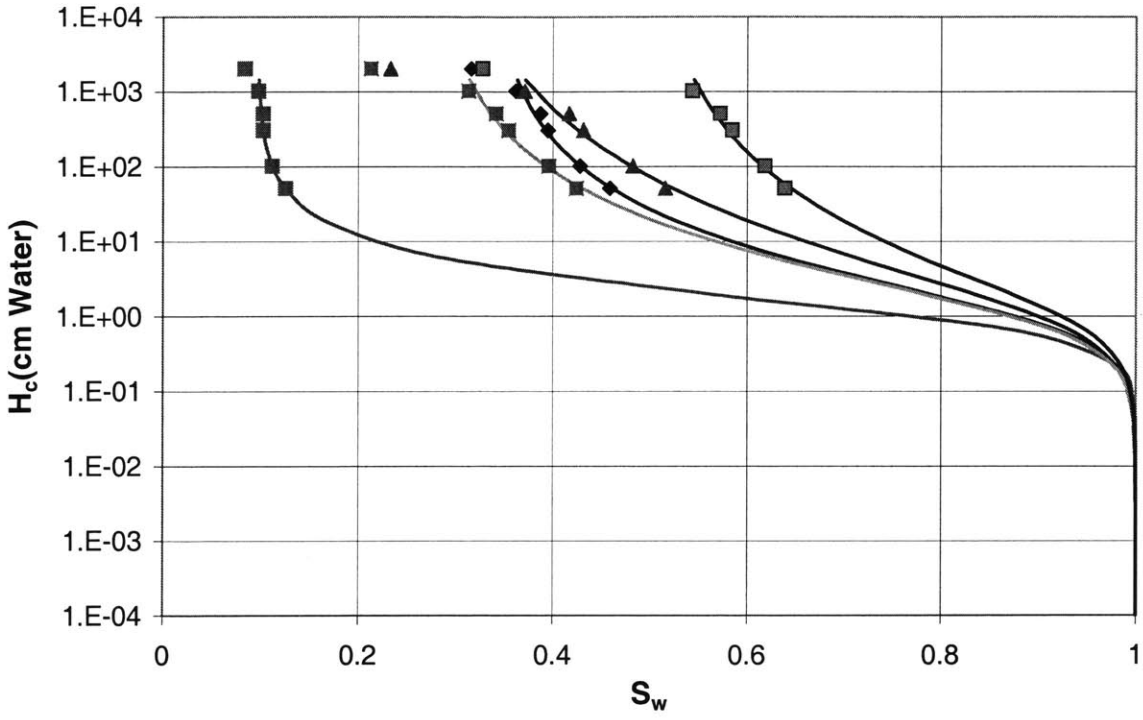


Figure 6-1: Capillary Pressure Curve for SRS Selected Mid-Layer Data

Table 6.1: Log Permeability and Transformed van Genuchten Capillary Curve Parameters at M Area of SRS

| Sample | lnk (lncm$^2$) | B (ln dynes/cm$^2$) | L |
|---|---|---|---|
| 1 | -19.02 | 6.40 | -1.33 |
| 2 | -19.33 | 6.50 | -0.10 |
| 3 | -18.33 | 6.40 | -0.87 |
| 4 | -19.00 | 6.40 | -0.95 |
| 5 | -18.08 | 6.40 | -1.20 |
| mean | -18.75 | 6.42 | -0.89 |
| variance | 0.28 | 0.00189 | 0.23 |
| correlation with lnk | - | -0.05 | -0.48 |

the saturation of nonwetting phase jumps to relative large values rapidly. So there are no data available at small nonwetting phase saturation, which is the range we are interested because DNAPL saturation is observed close to residual under field conditions. The van Genuchten model is extrapolated to the low nonwetting phase saturation zone as shown in Figure 6-1.

### 6.2.3 Hanford Site

#### Pollution History and Scale

The Hanford Site is located in south-central Washington State and has been a defense materials production complex since 1943. Carbon Tetrachloride (CTet) was used in mixtures with other organic chemicals to recover plutonium from aqueous streams and then charged into disposal facilities as a separated phase and saturated aqueous phase. During the operation of the facilities from 1955 to 1973, three disposal facilities at the 200 West Area, including 216-Z-9 trench, 216-Z-1A Tile Field and 216-Z-18 Crib, received a total of 363,000 to 580,000 liters of liquid CTet, in mixtures with other organic and aqueous phase liquids (Rohay *et al.*, 1994). Figure 6-2 shows the site map of 200 West Area where the recovery plants and disposal sites are located. As a result, approximately 750,000 kg CTet were discharged into three disposal facilities in ERA/VOC -Arid ID site (Figure 6-3) , which is at the center of 200 West Area. Due to the small aqueous solubility, around 99% of CTet mass was dumped as separate phase DNAPL, while 1% as saturated aqueous phase liquid. CTet in groundwater and soil vapor sampled in early 90s accounted for approximately 35% of the total discharged CTet. 65% of the original

inventory was believed to be in residual saturation and non-equilibrium sorption sites within vadose zone and groundwater. Based on the mass of the carbon source, Hooker *et al.* (1996) estimated that around 1% of the CTet could have transformed to chloroform by microbial decay.

As measured during 1990-1992, the plume of dissolved CTet extends over 10 $km^2$ in the unconfined aquifer underlying the 200 West Area shown in Figure 6-4. The majority of the CTet plume is concentrated in a relatively small area. As seen in Figure 6-4, 60% of CTet mass only covers 10% of the entire plume extension area. The area of highest CTet concentration lies northeast of the discharge area, which is consistent with the local gradient of the water table. However, as pointed out by (Rohay *et al.*, 1994), the centroid of the plume has not migrated significantly considering more than 20 years travel time. The zone of highest concentration still includes the 216-Z-9 Trench, which has been inactive since 1962. This suggests that the discharged CTet has been a continuous source of contamination to the groundwater.

Several hypotheses have been proposed for the observed long-term continuous high concentration in groundwater underlying the disposal area. The hypothesized CTet sources include the soil vapor in the unsaturated zone, the aqueous phase dissolved CTet and dissolution of separate phase of CTet in the groundwater. However, additional measurements in deep aquifer (>10m below the watertable) revealed that the high concentration also occurred far below the water table. As suggested by Rohay (1994), if CTet vapor were the major source of the groundwater contamination, only a thin dissolved plume would be expected at the water table. In addition, the relatively large hydraulic conductivity in 200 West Area suggested a fairly large solute transport velocity. During 30 years transport time after the shut down of the facility, the concentration peak should already travelled out of 200 West Area. The sudden jump of concentration observed in the sampling well 8 kilometers downgradient confirmed this. It has also been estimated that 6% of the original CTet is sorbed in the soil, which accounts for only 10% of the missing mass. CTet apparently exists predominantly as a separate phase at static saturation, which slowly dissolves into the flowing aqueous phase. Therefore, the presence of continuously high CTet concentrations near disposal sites is likely a result of slow dissolution of DNAPL separate phase source.

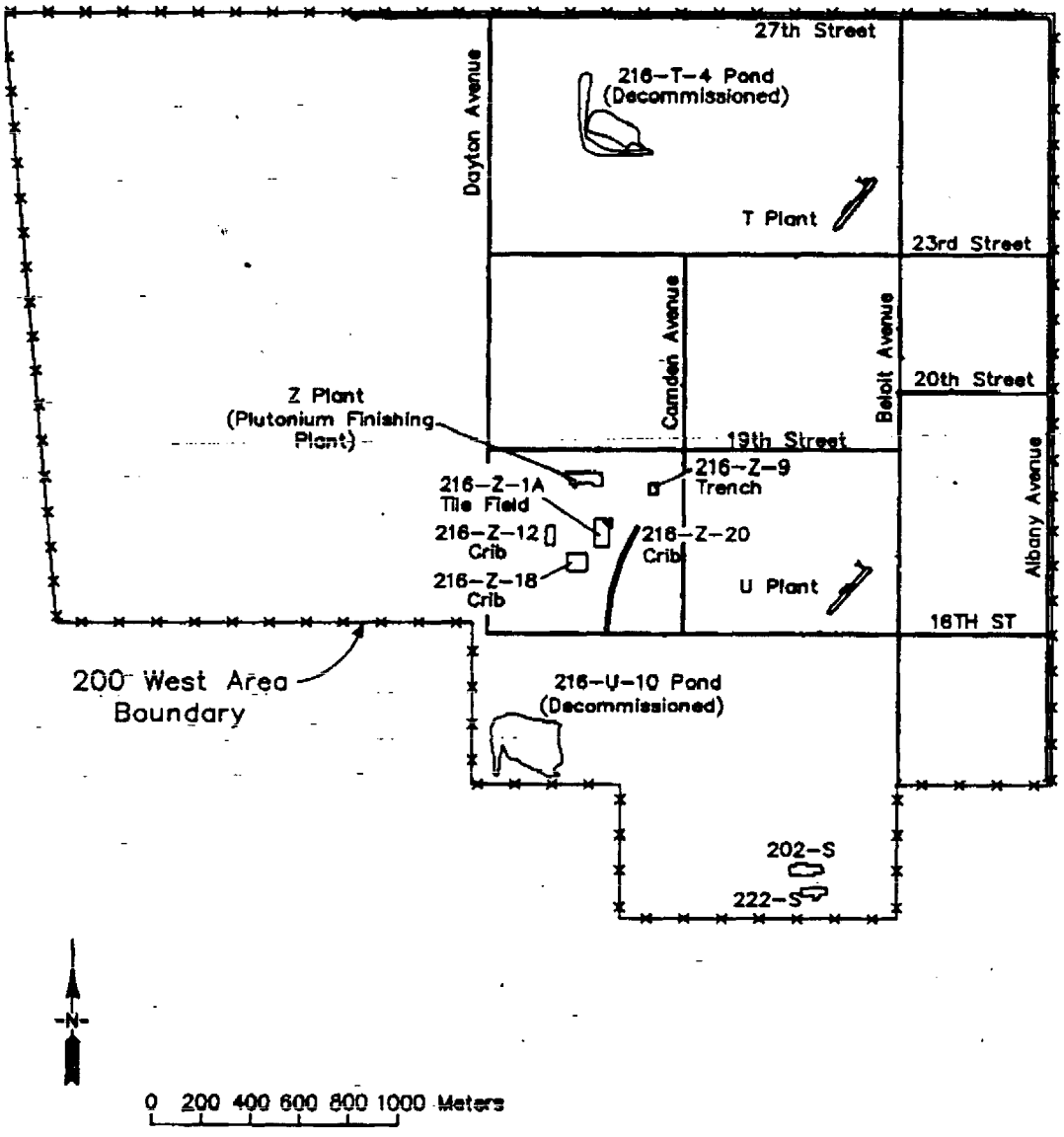


Figure 6-2: 200 West Area Site Map of the Hanford Site

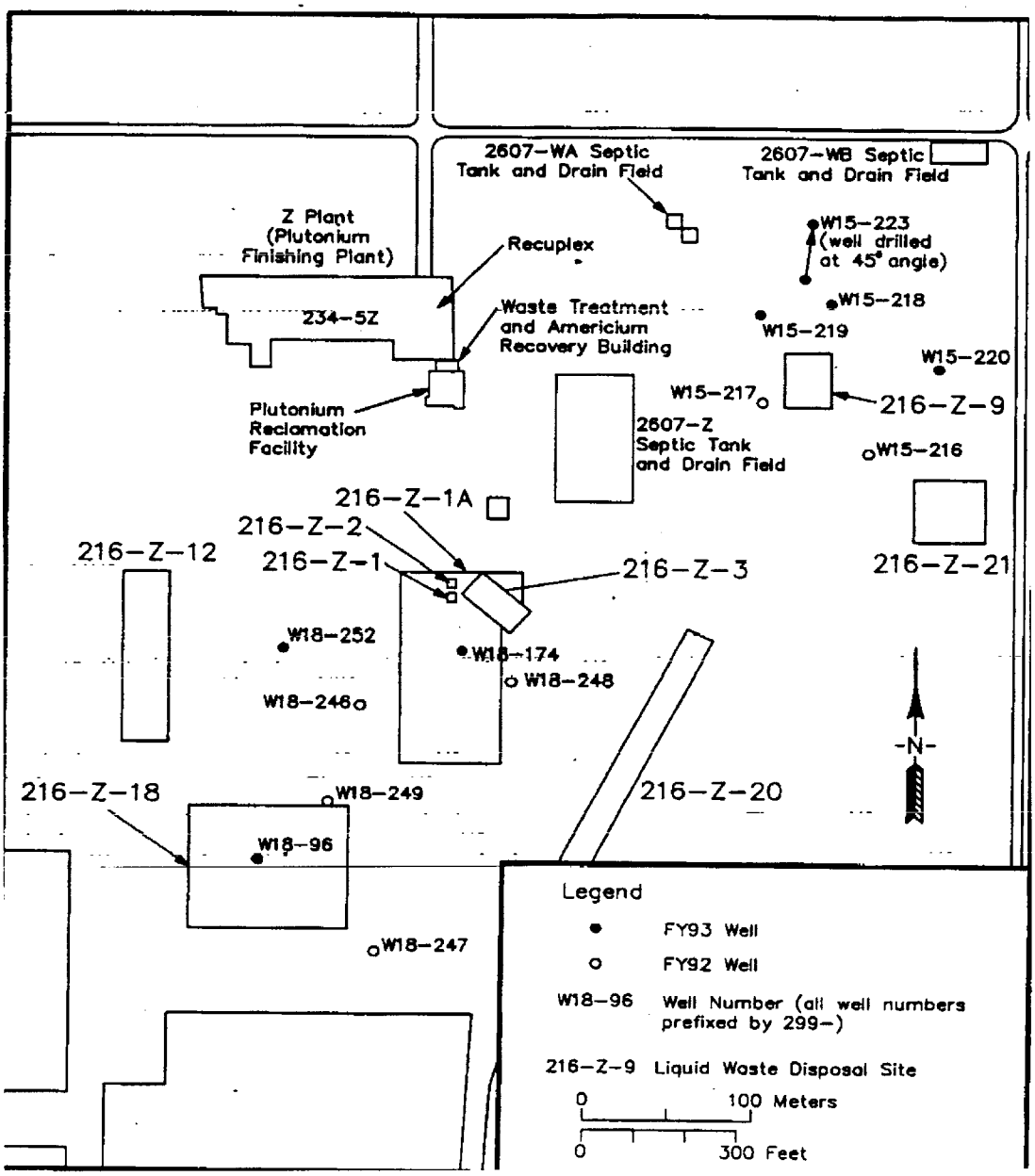


Figure 6-3: Site Map of ERA/VOC -Arid ID site of the Hanford site

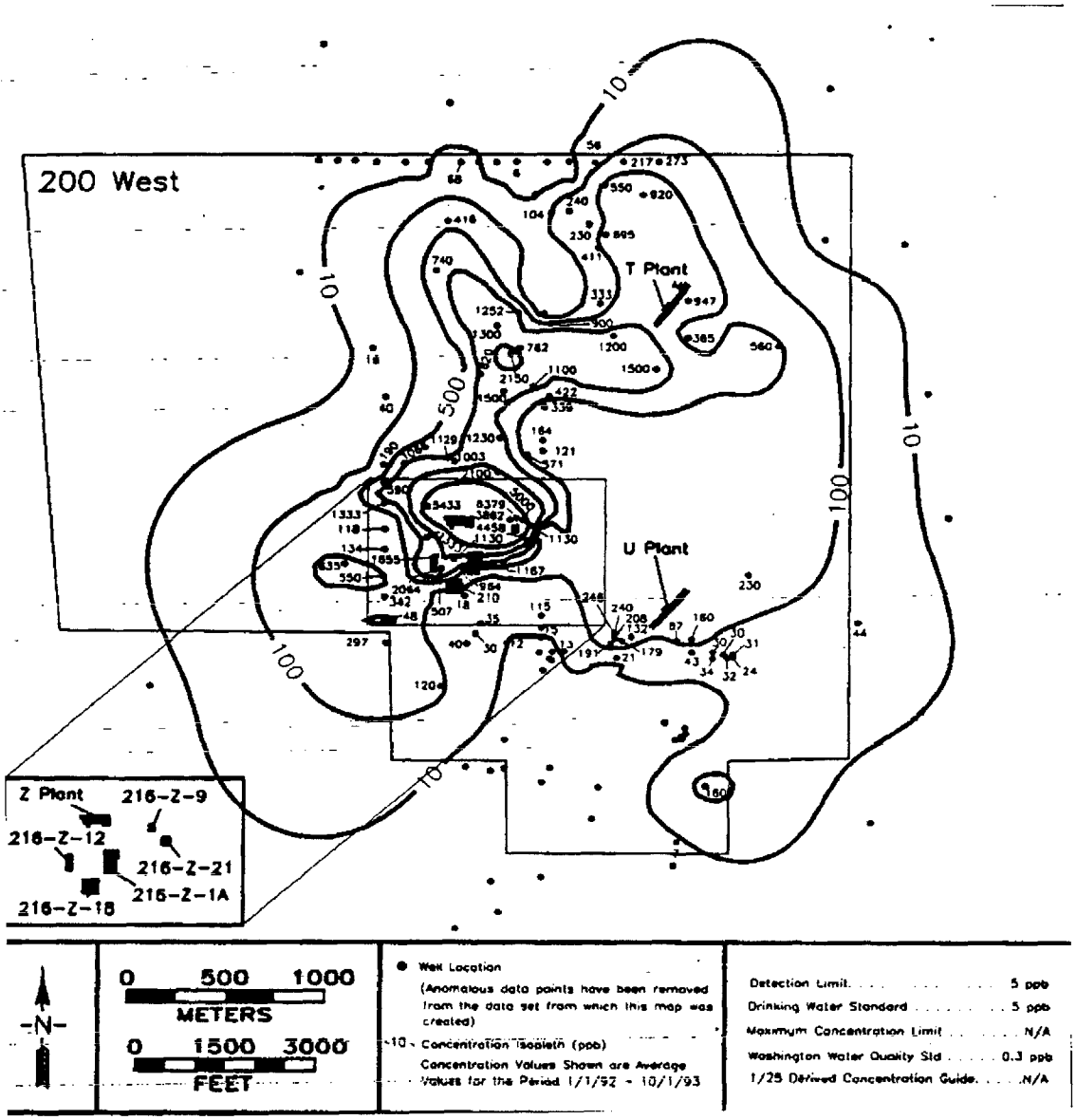


Figure 6-4: 200 West Area Carbon Tetrachloride Plume at the Hanford Site

### Environmental Setting

The site is dominated by a thick, unsaturated zone within the Hanford formation and upper Ringold Formation: an unconfined aquifer system within the Columbia River Basalt Group. The unsaturated zone underlying the CTet disposal sites ranges in thickness from 60 to 71 meters, consisting of gravel, sand and silt deposits. Groundwater underlying the 200 West Area flows within a multi-aquifer system. The uppermost aquifer beneath the area, where DNAPL is most likely present, is unconfined and lies within an unconsolidated to semi-indurated gravel and sand sequence. Hydraulic conductivity values vary by several orders of magnitude at the top of the aquifer as reported from (Rohay *et al.*, 1994). Regional groundwater flow is generally from west to east. However, due to a groundwater mound caused by past artificial recharge, the direction of groundwater flow in the vicinity of the 200 West Area is toward the northwest. A detailed summary of hydrogeological settings and data is presented in the 1994 report (Rohay *et al.*, 1994). Bjornstad (1990) and Relyea (1995) reported the hydraulic conductivity and unsaturated capillary pressure curve parameters measured at the 200 West Area. Table 6.2 shows the data reported by these two studies at upper and middle Ringold Formation where DNAPL is most likely present. Figure 6-5 shows the log permeability variation with the depth. As we can see the site is extremely heterogeneous with very large variance of lnk. Besides, the aquifer is relatively impermeable as the mean of the log permeability is low.

Table 6.2: Log Permeability and Transformed van Genuchten Capillary Curve Parameters at Hanford Site Unconfined Aquifers

| **Sample** | **lnk (lncm$^2$)** | **B (ln dynes/cm$^2$)** | **L** |
|---|---|---|---|
| 1 | -15.88 | 10.54 | -0.52 |
| 2 | -14.91 | 8.63 | -0.03 |
| 3 | -18.42 | 8.21 | -1.17 |
| 4 | -18.05 | 11.82 | -0.55 |
| 5 | -15.91 | 9.84 | -0.93 |
| 6 | -17.42 | 7.78 | -0.35 |
| 7 | -15.47 | 8.02 | -0.97 |
| mean | -16.57 | 9.26 | -0.65 |
| variance | 1.87 | 2.29 | 0.16 |
| slope with lnk | - | -0.15 | 0.10 |
| residual | | 1.50 | 0.37 |

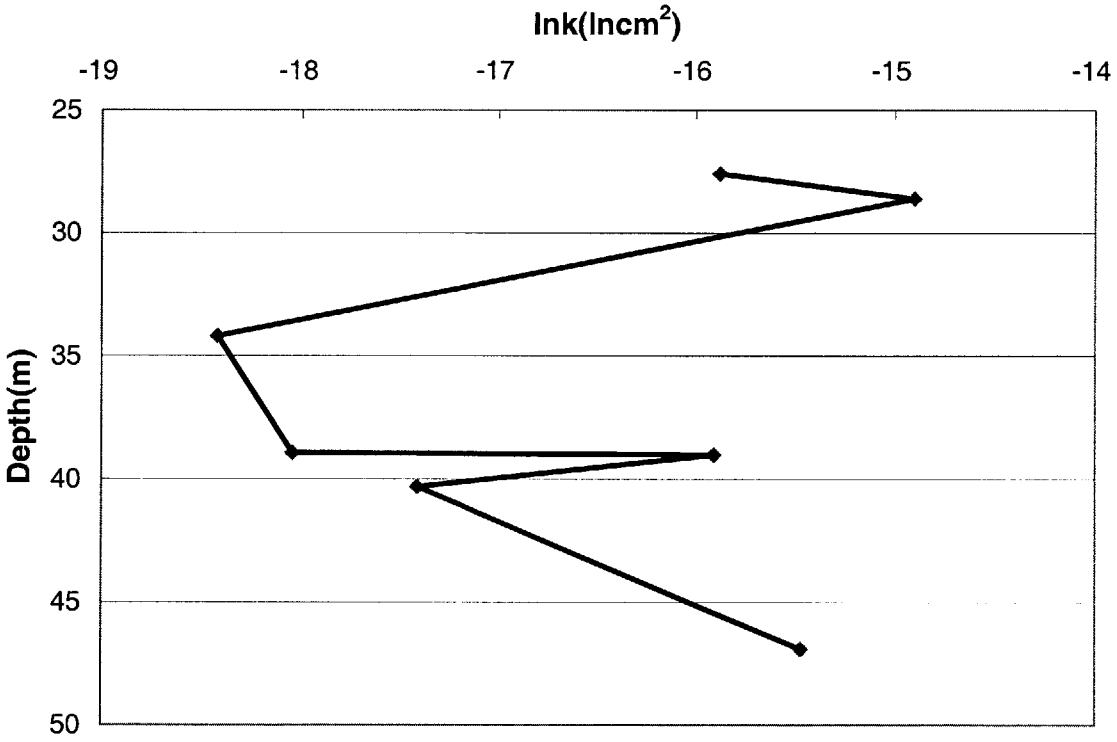


Figure 6-5: Log permeability changes with depth at the Hanford site

### 6.2.4 Summary

The key parameters used as inputs to the multiphase flow analysis for four sites are summarized in Table 6.3. As we can see, the Cape Cod site is the most permeable aquifer with relatively large mean log permeability. SRS is most impermeable site. The Hanford site as mentioned above is the most heterogeneous formations with large $\sigma_f^2$. The correlation scales in horizontal and vertical direction for SRS and the Hanford site are estimated by the empirical method cited by Talbott and Gelhar (1994) based on limited hydraulic conductivity data. For the Borden and the Cape Cod sites, these values are obtained from Jacobs (1998).

Table 6.3: Input Spatial Variables of the Borden, the Cape Cod, the SRS and the Hanford site

| **Parameters** | **Borden** | **Cape Cod** | **SRS** | **Hanford** |
|---|---|---|---|---|
| $\overline{F}$(mean log permeability) | -16.4 | -14.43 | -18.75 | -16.57 |
| $\sigma_f^2$ (variance of log permeability) | 0.123 | 0.230 | 0.276 | 1.87 |
| $\overline{B}$ (mean of p-s-k parameter transformation) | 10.4 | 8.41 | 6.42 | 9.26 |
| $\sigma_b^2$ (variance of p-s-k parameter transformation) | 0.143 | 0.15 | 0.00189 | 2.29 |
| $b_b$(slope of p-s-k parameter transformation) | -1.03 | -0.22 | -0.05 | -0.15 |
| $g_b$(residue of p-s-k parameter transformation) | 0.113 | 0.37 | 0.034 | 1.50 |
| $\overline{L}$(mean of p-s-k parameter transformation) | 1.5 | 0.53 | -0.89 | -0.65 |
| $\sigma_l^2$(variance of p-s-k parameter transformation) | 0.115 | 0.25 | 0.23 | 0.16 |
| $b_l$(slope of p-s-k parameter transformation) | -0.83 | -0.14 | -0.48 | 0.10 |
| $g_l$(residue of p-s-k parameter transformation) | 0.174 | 0.50 | 0.40 | 0.37 |
| $l_1$horizontal correlation scale (m) | 2.8 | 2.6 | 3 | 3 |
| $l_3$vertical correlation scale (m) | 0.28 | 0.44 | 0.50 | 0.27 |

## 6.3 Results

Parameters of DNAPL saturation distribution and wetting phase flow field can be calculated based on the input spatial variables in the above section. Using codes developed based on Jacobs' multiphase flow study, a DNAPL vertical flow rate is chosen to derive moments of DNAPL saturation and wetting phase flow velocity. Here we choose relatively small DNAPL flow rate to satisfy the static DNAPL saturation field assumption. Smaller infiltration rates correspond to lower mean DNAPL saturations. The mean and variation of DNAPL saturation, wetting phase flow rate, correlation between flow velocity and dissolution rate, variation of dissolution

rate and mean dissolution rate coefficient are derived based on the analysis in Chapter 2 and Chapter 3. These parameters are key inputs to calculate effective properties such as the effective dissolution rate coefficient and the effective dissolution distance as discussed in Chapter 4. The mean concentration profile is plotted against the travel distance within the DNAPL source zone.

### 6.3.1 Borden site

Four different DNAPL vertical infiltration rates are chosen to represent different DNAPL saturation conditions. The mean DNAPL volumetric content ranges from 0.48% to 4.03%. The flow velocity of DNAPL is relatively small except the first case, for which the large volumetric content of 4.03% is close to those observed in static saturation in homogeneous packings in laboratory experiments (Imhoff *et al.*, 1994). Here we listed this case just for the illustration purpose. The saturation field is regarded plausibly static at such a small flow velocity of order centimeters per year.

Table 6.4 lists the flow results including the mean and variance of transformed DNAPL saturation, DNAPL infiltration rate, wetting phase flow velocity etc. The transport properties and effective parameters are also reported in Table 6.4. The variation of dissolution rate $\sigma^2_{h\_p}$ is predicted based on the local model and does not include the residual variance $\sigma^2_{g_h}$. The residual variance of log dissolution rate coefficient $\sigma^2_{g_h}$ represents the deviation from value predicted by the local dissolution model. As discussed in Chapter 3, even for homogeneous laboratory dissolution experiments, $\sigma^2_{g_h}$ can be large. Here we assume that $\sigma^2_{g_h}$ is proportional to the model predicted value and accounts for 50% of the overall variance $\sigma^2_h$:

$$\sigma^2_{g_h}/\sigma^2_h = 50\% \tag{6.1}$$

So the variation of dissolution rate can be obtained as:

$$\sigma^2_h = \sigma^2_{h\_p} + \sigma^2_{g_h} \tag{6.2}$$

$\overline{H}$ is also calculated from the local relationship based on the mean inputs. The mean dissolution

rate coefficient is calculated based on the log normal distribution:

$$\overline{\Omega} = \exp(\overline{H} + \frac{\sigma_h^2}{2}) \tag{6.3}$$

As we can see, the relative permeability increases as the mean DNAPL saturation decreases. The variation of dissolution rate $\sigma_h^2$ increases as the mean DNAPL saturation decreases, which indicates that DNAPL source with lower mean saturation results in more heterogeneous DNAPL distribution and consequently dissolution rate. The bypassing effect, which is represented by correlation between flow rate and dissolution rate, is more prominent at large mean DNAPL saturation case. The variation of flow velocity is also large for the large mean saturation case, though the value is still relatively small due to the relatively homogeneous nature of the Borden aquifer. The effective dissolution rate coefficient is not significantly smaller than the mean at large mean saturation due to the small variation of dissolution rate, implying the effect of heterogeneity is only modest.

Figure 6-6 shows the DNAPL mean concentration curves against the travel distance within a DNAPL source zone with different DNAPL mean saturation. As we can see, lower DNAPL saturation tends to require a longer travel distance to reach the equilibrium. The enhanced spatial variation of log dissolution rate for smaller saturation contributes to the larger effective dissolution distance. Even for the smallest saturation, the equilibrium distance is only around 5 meters. On the one hand, this reveals the relatively homogeneous nature of the dissolution as a result of homogeneous geological structure at the Borden site. On the other hand, the positive correlation between flow velocity and dissolution rate, implying an anti-bypassing effect, dampen the effect of spatial variations to increase the effective dissolution distance. Relatively modest spatial variation of dissolution rate and the positive correlation between flow rate and dissolution rate cannot increase the effective dissolution distance much, as shown in Figure 6-6.

### 6.3.2 Cape Cod Site

Three different DNAPL vertical infiltration rates are chosen to represent different DNAPL saturation conditions. The mean DNAPL volumetric content ranges from 0.0017% to 0.027%. Selecting such low DNAPL saturations is to assure the DNAPL infiltration velocity in a proper range in the very permeable aquifer, which makes the static saturation assumption plausible.

Table 6.4: DNAPL Satruation Field, Water Flow Field, Transport and Transfer Properties at the Borden Site at Different Hyperthetical DNAPL Infiltration Rate

| **Flow Properties** | **Borden 1** | **Borden 2** | **Borden 3** | **Borden 4** |
|---|---|---|---|---|
| selected $q_o$ (m/y) (mean vertical DNAPL flow rate) | 0.58 | 0.088 | 0.014 | 2.20E-03 |
| $k_{rw}$ (wetting phase relative permeability) | 0.61 | 0.74 | 0.85 | 0.92 |
| $\overline{H_c}$(cm water) (mean capillary head) | 24.6 | 21.5 | 18.8 | 16.5 |
| $\overline{\theta_n}$ (mean DNAPL volumetric content) | 4.03% | 2.12% | 1.04% | 0.48% |
| $\sigma^2_{r_w}$ (variance of log permeability) | 0.30 | 0.15 | 0.12 | 0.11 |
| $\overline{W}$ (mean DNAPL saturation transformation) | 2.49 | 3.28 | 4.08 | 4.90 |
| $\sigma^2_w$ (variance of DNAPL saturation transformation) | 1.46 | 1.44 | 1.45 | 1.47 |
| $\overline{J_w}$ (wetting phase hydraulic gradient) | 0.005 | 0.005 | 0.005 | 0.005 |
| $\overline{q_w}$ $(m/d)$ (mean wetting phase flow) | 0.0233 | 0.0283 | 0.0323 | 0.0349 |
| $\sigma^2_q$ (variance of wetting phase flow) | $1.92\times10^{-4}$ | $1.30\times10^{-4}$ | $1.29\times10^{-4}$ | $1.46\times10^{-4}$ |
| **Transport Properties** | | | | |
| $\sigma^2_{h\_p}$ (calculated from local model) | 0.27 | 0.62 | 0.86 | 1.01 |
| $\sigma_v$ (standard deviation of log flow rate) | 0.35 | 0.35 | 0.35 | 0.40 |
| $corr\,[v,h]$ (correlation coefficient of flow and dissolution rate) | -0.45 | -0.20 | 0.02 | 0.15 |
| $\overline{\zeta}$ $\left(=\frac{\overline{\Omega} l_1}{q}\right.$ mean dissolution effect coefficient) | 46.66 | 39.63 | 28.86 | 17.90 |
| $\sigma^2_{g_h}$ (residual variance dissolution rate) | 0.27 | 0.62 | 0.86 | 1.01 |
| $\sigma^2_h$ (including $\sigma^2_{g_h}$) (variance of dissolution rate) | 0.54 | 1.24 | 1.72 | 2.02 |
| $\overline{\Omega}$ $(1/d)$ (mean dissolution rate coefficient) | 0.39 | 0.40 | 0.33 | 0.22 |
| $\frac{\overline{q_w}}{\overline{\Omega}}$ $(m)$ (mean dissolution distance) | 0.06 | 0.07 | 0.10 | 0.16 |
| **Effective Properties** | | | | |
| $\Omega_e$ $(1/d)$ (effective dissolution rate coefficient) | 0.18 | 0.09 | 0.05 | 0.02 |
| effective dissolution distance (m) | 0.21 | 0.38 | 0.67 | 1.19 |

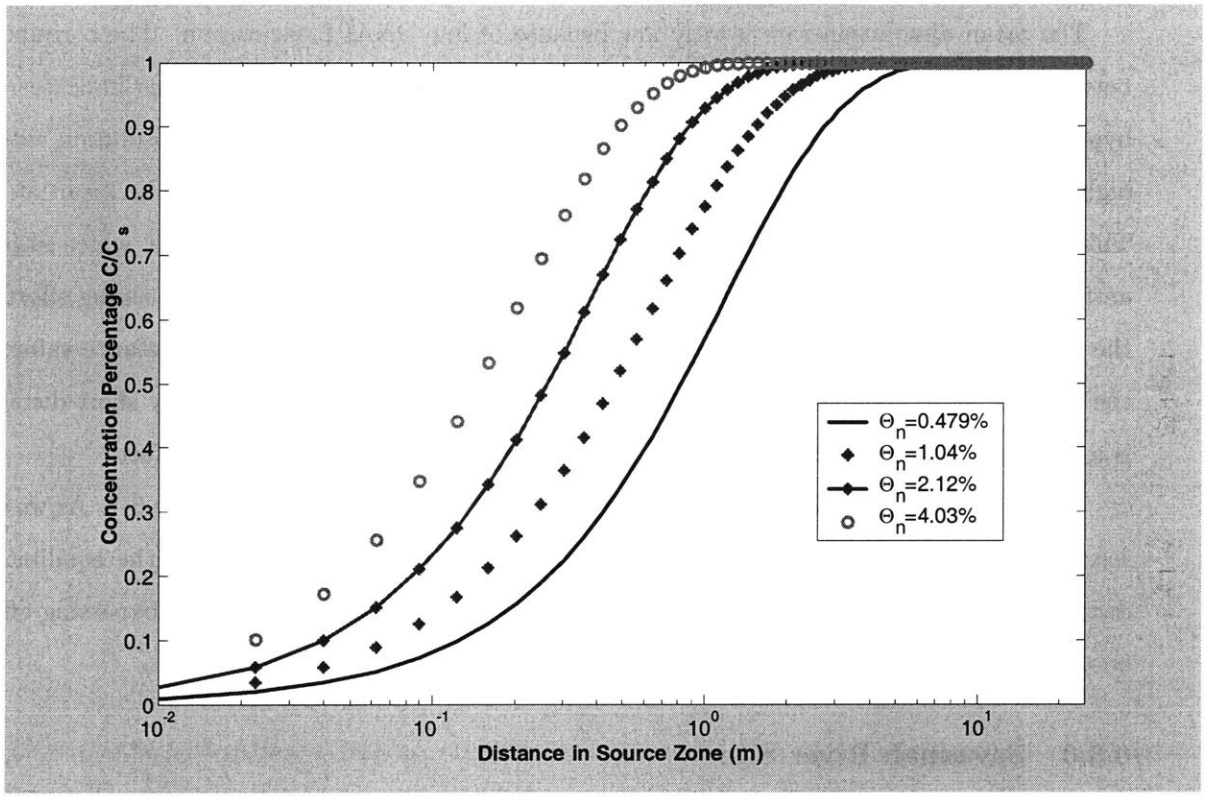


Figure 6-6: Mean concentration of DNAPL as a function of travel distance inside the source at the Borden site

Table 6.6 lists the flow results including the mean and variance of transformed DNAPL saturation, DNAPL infiltration rate, wetting phase flow velocity etc. The transport properties and effective parameters are also reported in the table. The variation of dissolution rate increases as the mean DNAPL saturation decreases, which indicates that a DNAPL source with lower mean saturation results in a more heterogeneous DNAPL distribution and consequently a lower effective dissolution rate. The residual variance of log dissolution rate coefficient $\sigma^2_{g_h}$ is estimated by the method used in the Borden site analysis above.

The mean dissolution rate is very low because of low DNAPL saturation. The correlation between flow velocity and dissolution rate, is positive for all three cases. This indicates the bypassing effect is insignificant at the Cape Cod. Though the variation of dissolution rate is higher than that at the Borden, the effective dissolution rate is not far from the mean at all. This results from the positive correlation between flow rate and dissolution rate, which implies anti-bypassing effect discussed in Chapter 2. This reflects the importance of bypassing effect on the field-scale dissolution. Therefore, we found that the effective dissolution distance value for the smallest saturation is less than 9 meters. As discussed above, this relatively short distance is a result of a relatively homogeneous porous structure with little bypassing effect.

The concentration profile within the DNAPL source zone is plotted in Figure 6-7. As we can see, even at the extremely small DNAPL mean volumetric content 0.00167%, the equilibrium distance is in the order of 10 meters. This again confirmed the importance of bypassing effect on the large-scale dissolution.

### 6.3.3 Savannah River Site

Two different DNAPL vertical infiltration rates are chosen to represent different DNAPL saturation conditions at SRS. The mean DNAPL volumetric content ranges from 0.029% to 0.072%. Table 6.6 lists the flow results including the mean and variance of transformed DNAPL saturation, DNAPL infiltration rate, wetting phase flow velocity etc., as well as the transport properties and effective parameters.

The mean dissolution rate is very low because of the low DNAPL saturation. The correlation between flow velocity and dissolution rate is negative for two cases. This indicates a relatively strong bypassing effect is present in SRS. The effective dissolution rate is significantly smaller

Table 6.5: DNAPL Satruation Field, Water Flow Field, Transport and Transfer Properties at Cape Cod at Different Hyperthetical DNAPL Infiltration Rate

| **Flow Properties** | **Cape 1** | **Cape 2** | **Cape 3** |
|---|---|---|---|
| selected $q_o$ (m/y) | 0.12 | 0.033 | 0.0087 |
| $k_{rw}$ | 0.975 | 0.987 | 0.995 |
| $\overline{\theta_n}$ | 0.027% | 0.0096% | 0.0017% |
| $\sigma^2_{r_w}$ | 0.24 | 0.24 | 0.24 |
| $\overline{W}$ | 7.17 | 7.92 | 8.69 |
| $\sigma^2_w$ | 0.93 | 1.07 | 1.21 |
| $\overline{J}_w$ | 0.0014 | 0.0014 | 0.0014 |
| $\overline{q_w}$ $(m/d)$ | 0.0787 | 0.0797 | 0.0803 |
| $\sigma^2_q$ | $1.67\times10^{-3}$ | $1.69\times10^{-3}$ | $1.70\times10^{-3}$ |
| **Transport Properties** | | | |
| $\sigma^2_{h\_p}$ | 0.64 | 0.74 | 0.85 |
| $\sigma_v$ | 0.52 | 0.52 | 0.51 |
| $corr\,[v,h]$ | 0.40 | 0.37 | 0.35 |
| $\overline{\zeta}$ | 1.65 | 0.95 | 0.54 |
| $\sigma^2_{g_h}$ | 0.64 | 0.74 | 0.85 |
| $\sigma^2_h$ (including $\sigma^2_{g_h}$) | 1.29 | 1.49 | 1.70 |
| $\overline{\Omega}$ $(1/d)$ | 0.050 | 0.029 | 0.017 |
| $\frac{\overline{q_w}}{\overline{\Omega}}$ $(m)$ (mean dissolution distance) | 1.58 | 2.74 | 4.84 |
| **Effective Properties** | | | |
| $\Omega_e$ $(1/d)$ | 0.016 | 0.011 | 0.0079 |
| effective dissolution distance (m) | 3.4 | 5.56 | 8.72 |

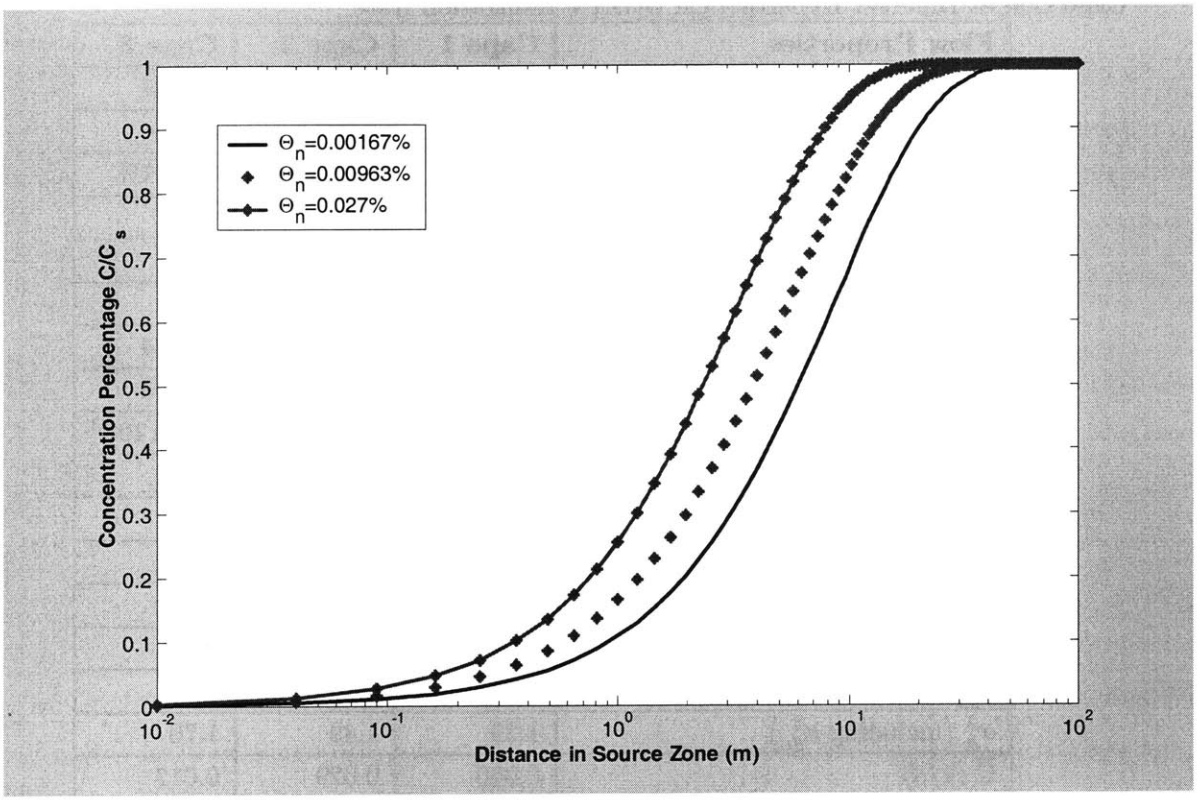


Figure 6-7: Mean concentration of DNAPL as a function of travel distance inside the source at the Cape Cod site

Table 6.6: DNAPL Satruation Field, Water Flow Field, Transport and Transfer Properties at the Savannah River Site at Different Hyperthetical DNAPL Infiltration Rate

| **Flow Properties** | **SRS 1** | **SRS 2** |
|---|---|---|
| selected $q_o$ (m/y) | 0.42 | 0.13 |
| $k_{rw}$ | 0.975 | 0.987 |
| $\overline{\theta_n}$ | 0.072% | 0.029% |
| $\sigma^2_{r_w}$ | 0.31 | 0.29 |
| $\overline{W}$ | 6.56 | 7.66 |
| $\sigma^2_w$ | 1.74 | 2.12 |
| $\overline{J}_w$ | 0.007 | 0.007 |
| $\overline{q_w}$ $(m/d)$ | 0.0034 | 0.0039 |
| $\sigma^2_q$ | $4.08\times10^{-6}$ | $5.05\times10^{-6}$ |
| **Transport Properties** | | |
| $\sigma^2_{h\_p}$ | 1.22 | 1.49 |
| $\sigma_v$ | 0.60 | 0.58 |
| $corr\,[v,h]$ | -0.43 | -0.42 |
| $\overline{\zeta}$ | 17.61 | 8.01 |
| $\sigma^2_{g_h}$ | 1.22 | 1.49 |
| $\sigma^2_h$ (including $\sigma^2_{g_h}$) | 2.44 | 2.98 |
| $\overline{\Omega}$ $(1/d)$ | 0.0118 | 0.0062 |
| $\frac{\overline{q_w}}{\overline{\Omega}}$ $(m)$ (mean dissolution distance) | 0.17 | 0.37 |
| **Effective Properties** | | |
| $\Omega_e$ $(1/d)$ | 0.001 | 0.0004 |
| effective dissolution distance (m) | 5.79 | 17.23 |

than the mean due to the large variance of dissolution rate and strong bypassing effect. The effective dissolution distance is at the order of ten meters. Compared to the Cape Cod site, even though the mean saturation of DNAPL and the mean dissolution rate is much higher here, the effective dissolution rate is much lower than that of the Cape Cod. This implies the mean property is only a secondary effect influencing the effective properties. The dominant contribution is the spatial variation and bypassing effect.

The equilibrium distance shown in Figure 6-8 is around 30 to 90 meters at different mean saturation. Compared to the Borden and the Cape Cod site, this change attributes to the relatively large spatial variation and strong bypassing effect. But still the predicted concentration is fairly high after the travel distance is beyond 10 meters. Though there are no direct concentration measurements reported from SRS aquifer, such a high concentration profile is seldom observed in other aquifers with DNAPL concentration data available, especially considering the DNAPL mean saturation is at such a low level. One possible explanation is that, for SRS, the hydraulic conductivity data is selected only from the mid-layer. So the variability of the hydraulic conductivity of the source zone is probably underestimated since the DNAPL source can extend to other layers of the aquifer. The large variation effect is explored in the Hanford site where the variance of log permeability is 1.87, which is much larger than those of the other three sites.

### 6.3.4 Hanford Site

#### Theoretical Results

The flow, transport and effective properties from stochastic analysis are listed in Table 6.7 for the Hanford site. Four DNAPL volumetric contents are chosen to be consistent with that estimated from Z-9 Trench (discussed below) with the range from 0.053% to 0.12%. The hydraulic gradient is estimated based on the head map in the 200 West area. As we can see from the table, due to the highly heterogeneous nature of the intrinsic permeability, the variations of DNAPL saturation distribution, water flow field and dissolution rate are also extremely high. The correlation between dissolution rate with flow rate are all negative indicating the bypassing effect is significant at the Hanford site. The effective dissolution rate coefficient is significantly reduced from the mean. And the effective dissolution distance is extremely large due to the

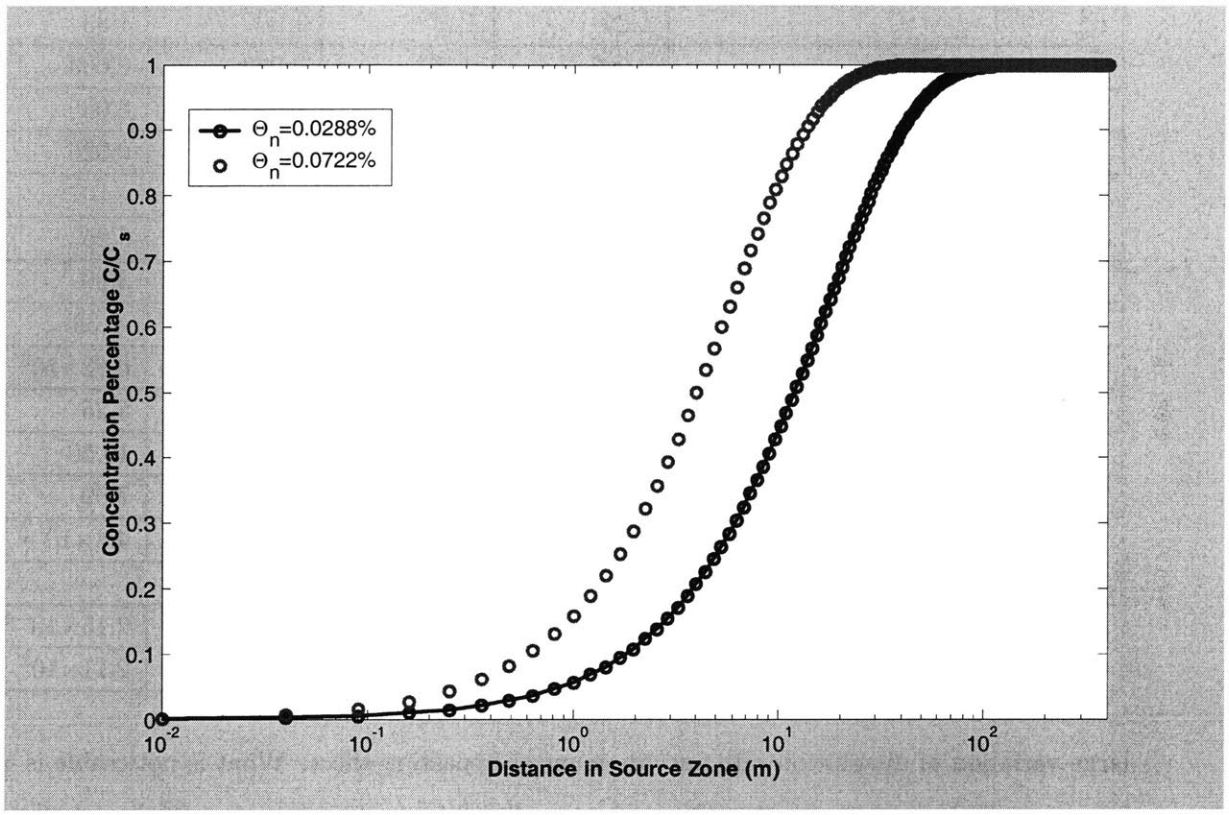


Figure 6-8: Mean concentration of DNAPL as a function of travel distance inside the source at the SRS site

Table 6.7: DNAPL Satruation Field, Water Flow Field, Transport and Transfer Properties at Hanford at Different Hyperthetical DNAPL Infiltration Rate

| **Flow Properties** | **Hanford 1** | **Hanford 2** | **Hanford 3** | **Hanford 4** |
|---|---|---|---|---|
| selected $q_o$ (m/y) | 3.64 | 2.65 | 1.92 | 1.38 |
| $k_{rw}$ | 0.99 | 0.98 | 0.99 | 0.99 |
| $\overline{\theta_n}$ | 0.12% | 0.093% | 0.071% | 0.053% |
| $\sigma^2_{r_w}$ | 2.95 | 2.83 | 2.72 | 2.63 |
| $\overline{W}$ | 5.63 | 5.95 | 6.22 | 6.49 |
| $\sigma^2_w$ | 1.25 | 1.27 | 1.30 | 1.33 |
| $\overline{J_w}$ | 0.003 | 0.003 | 0.003 | 0.003 |
| $\overline{q_w}$ $(m/d)$ | 0.045 | 0.045 | 0.045 | 0.045 |
| $\sigma^2_q$ | 0.037 | 0.032 | 0.029 | 0.026 |
| **Transport Properties** | | | | |
| $\sigma^2_{h\_p}$ | 8.28 | 6.96 | 5.98 | 5.25 |
| $\sigma_v$ | 4.25 | 3.99 | 3.78 | 3.60 |
| $corr\,[v,h]$ | -0.46 | -0.44 | -0.41 | -0.39 |
| $\overline{\zeta}$ | $3.05\times10^4$ | $6.34\times10^3$ | $1.85\times10^3$ | $6.82\times10^2$ |
| $\sigma^2_{g_h}$ | 8.28 | 6.96 | 5.98 | 5.25 |
| $\sigma^2_h$ (including $\sigma^2_{g_h}$) | 16.56 | 13.92 | 11.98 | 10.50 |
| $\overline{\Omega}$ $(1/d)$ | 343.78 | 71.52 | 20.86 | 7.69 |
| $\frac{\overline{q_w}}{\overline{\Omega}}$ $(m)$ (mean dissolution distance) | $1\times10^{-4}$ | $4.7\times10^{-4}$ | $1.6\times10^{-3}$ | $4.4\times10^{-3}$ |
| **Effective Properties** | | | | |
| $\Omega_e$ $(1/d)$ | $2.21\times10^{-5}$ | $6.46\times10^{-5}$ | $1.32\times10^{-4}$ | $2.15\times10^{-4}$ |
| effective dissolution distance (m) | $3.48\times10^4$ | $9.80\times10^3$ | $4.03\times10^3$ | $2.11\times10^3$ |

large variation of dissolution rate and pronounced bypassing effect. What is noticeable is that the case with highest mean saturation and mean dissolution rate is the one with lowest effective dissolution rate. This is because the Hanford 1 case is also with the highest dissolution rate variance, which is the controlling factor of the effective dissolution distance. This again indicates that the controlling factors affecting the effective dissolution properties are spatial variations of dissolution properties and bypassing effect. The local mean characteristics is only a secondary effect.

### Z9 DNAPL Contaminated Site

216-Z9 was the waste disposal site where CTet is most likely present in the saturated zone as a separate phase. Approximately $8.30\times10^4$ to $3.00\times10^5$ liters CTet was discharged in the Z-9 Trench. Though most of DNAPL mass was suspected to be trapped in the unsaturated zone with a thickness ranging from 60 m to 71 m, a significant amount of CTet could reach the unconfined saturated zone. An estimation of how likely the CTet liquid may have traveled through the soil column and reached the saturated zone was conducted by Rohay and coworkers (Rohay *et al.*, 1994). They concluded that the Z-9 Trench is the disposal site where CTet most likely exists as a separate phase and that the vertical migration into the saturated zone can be more than 20 meters, due to the relatively large amount of discharge and small bottom area of the facility. DNAPL most likely exists in the upper most aquifer beneath the site.

Due to the highly heterogeneous nature of hydraulic conductivity of upper and middle Ringold Formation, significant lateral spreading likely occurred after the CTet was discharged into the subsurface systems. Here the source zone in the saturated zone is assumed covering 100 $m \times 100\ m$ area horizontally and reaches the depth of 20 $m$ below the water table. Based on this control volume, the mean volumetric content of CTet is in the ranged from $\theta_n = 0.005\%$ to 0.114% in the saturated zone as a result of the Z9 discharge.

Groundwater samples were collected at the ERA/VOC-Arid ID CTet site in early 90s. Samples collected from four wells near the Z-9 Trench all contained CTet and the concentrations ranged from 6379 $\mu g/L$ in well W15-218 north of the trench to 1130 $\mu g/L$ in well W15-220 east of the trench. More concentration samples were collected recently near the Z-9 site at wells W15-1, W15-32, W15-35 and W15-38. Among the concentration measurements reported around the Z-9 trench, well W15-1, W15-6, W15-218, W15-219 and W15-220 provide the concentration data within or close to the source zone, as shown in Figure 6-9. The square boundary represents the hypothesized CTet source zone. W15-32, W15-35, W15-38 provide the concentrations out of the source region as shown in Figure 6-10. Groundwater flow is generally from southwest to northeast. The travel distance inside the source zone is measured following the stream line of the mean flow direction at $45^o$ toward northeast, from the west or south boundary to the well. Travel distance to wells outside the source is determined by the distance along the mean flow direction from one boundary to another boundary.

The concentration data measured in wells are used to calculate the ratio of concentration to the effective solubility $C_s$. The effective solubility is calculated based on the CTet molar fraction in the discharged organic liquid. It is estimated that the molar fraction of CTet ranges from 73% to 91% in the organic discharge. Here we use the molar fraction of 85% to calculate the effective solubility $C_s$. The aqueous solubility for single component CTet is 800 mg/L. The effective solubility of Ctet in multi-component DNAPL is calculated in Eq. 6.4. Dispersion is neglected for concentration measured in wells outside the source zone. As we can see, most concentration data are less than 1% of the effective solubility.

$$C_s = 800 \text{ mg/L} \times 85\% = 680 \text{ mg/L} \tag{6.4}$$

Table 6.8: Maximum Concentration of Carbon Tetrachloride Detected around Z-9 Trench at the Hanford Site

| **Well Number** | **Sample Time** | **Maximum Concentration** | **C/C$_s$** | **Travel Distance inside Source** |
|---|---|---|---|---|
| | | $(\mu g/L)$ | | **(m)** |
| W15-1 | 1999 | 7900 | 0.0116 | 85 |
| W15-6 | 1992 | 5000 | 0.0074 | 100 |
| W15-32 | 2000 | 4700 | 0.0069 | 60 |
| W15-35 | 2000 | 5400 | 0.0079 | 100 |
| W15-38 | 2000 | 4000 | 0.0059 | 90 |
| W15-218 | 1992 | 6379 | 0.0094 | 99 |
| W15-219 | 1992 | 3862 | 0.0057 | 60 |
| W15-220 | 1992 | 1130 | 0.0017 | 30 |

### Concentration Profile

Figure 6-11 shows the concentration profile against the travel distance within CTet source zone beneath the 216-Z9 disposal site. The theoretical results are plotted at four different mean saturations, which covers the estimated saturation range. Here we choose the range $\overline{\theta_n} = 0.053\%$ to 0.12% as shown in Table 6.7. The measured data were obtained from sampling wells mentioned above. The uncertainty of the travel distance inside the source zone is included in the horizontal error bar. This includes the uncertainty of DNAPL source zone size, the flow direction and

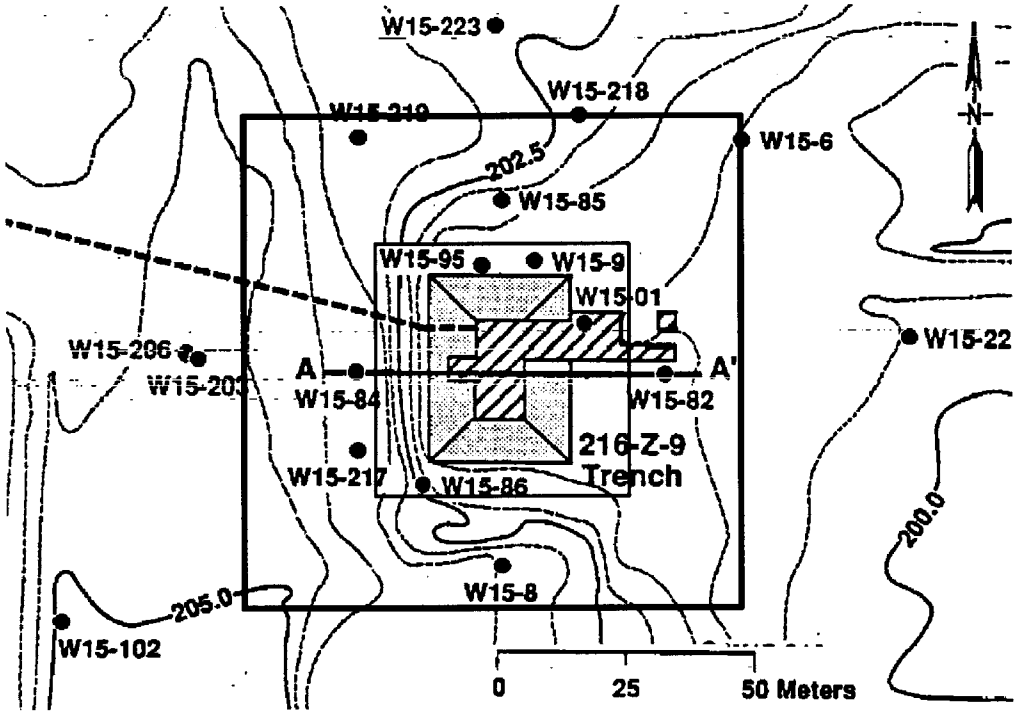


Figure 6-9: 216-Z9 Disposal Site Well Locations of the Hanford Site

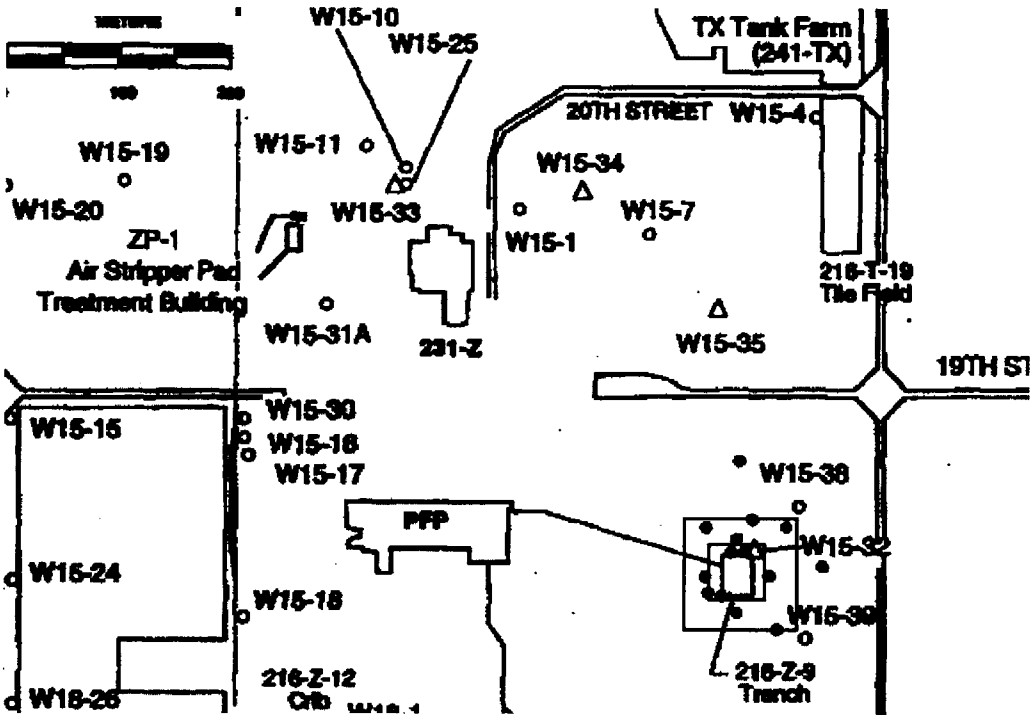


Figure 6-10: Well locations in the Disposal area of the Hanford Site

other factors affecting travel distance. The vertical error bar reflects the DNAPL component uncertainty and the error of concentration measurements. Since the wells were all screened around 10 meters within the saturated zone, the concentration data only reflect the average concentration in this range. The proportion of organic components discharged into the Z-9 Trench is estimated as a range. The figure shows that the measured concentration level is within the range predicted by theoretical analysis. The maximum observed concentration is only around 1% of effective solubility as a result of the limited travel distance inside the DNAPL source zone. This observation is attributed to the extremely heterogeneous aquifer and non-uniform distribution of CTet. Negative correlation between $v$ and $h$ indicates a strong bypassing effect, which, along with strong variation of dissolution rate, leads to an extremely large effective dissolution distance.

The level of agreement for the field data with the theoretical predictions strengthen the hypothesis that a strong bypassing effect combined with large spatial variation of dissolution rate is the dominant factor controlling the field-scale dissolution.

### Sensitivity Test

**DNAPL Source Zone Area** Due to the limited samples detecting the CTet source zone in the saturated zone, there is uncertainly regarding the size of CTet source. In above analysis we assumed the CTet source zone in the saturated aquifer spreads to an area of 100 $m \times 100$ $m$ horizontally and reaches a depth of 20 $m$. Since the bottom area of the Z9 disposal trench is 18 $m \times 9$ $m$, it is possible that the DNAPL spreading is modest and DNAPL source zone in saturated aquifer is less than that projected above. Here we evaluate the sensitivity of the result to the smaller source zone. Figure 6-12 presents the theoretical results and measured data for a DNAPL source that covers an area of 50 $m \times 50$ $m$ horizontally. As we can see, the theoretical results, which are derived from the same input parameters as above, are still in a good agreement with observed data. So the result is relatively robust for different hypothesized source zone area.

**Residual of Variance of Dissolution Rate** The theoretical result is expected to be sensitive to the residual $\sigma^2_{g_h}$. In the above analysis, the residue is assumed 50% of the entire variance $\sigma^2_h$

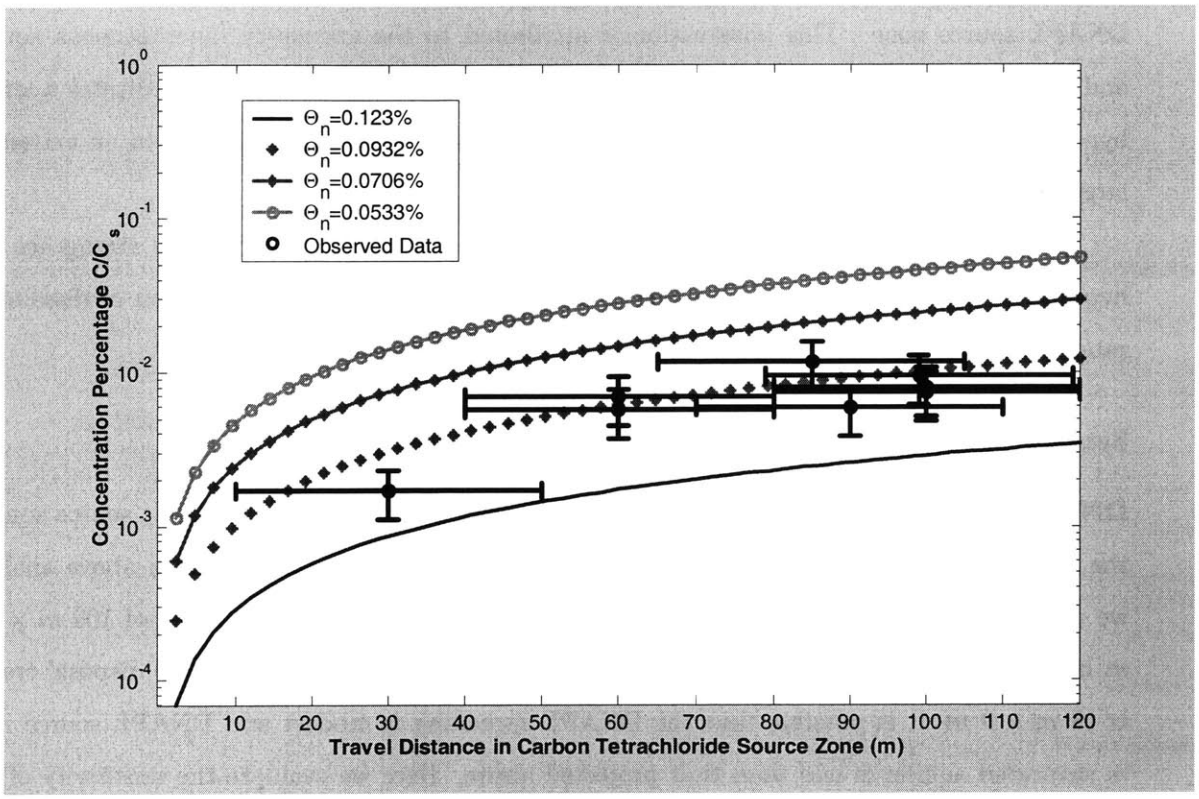


Figure 6-11: Concentration of Carbon Tetrachloride as a function of travel distance inside the source as the residue accounts 1/2 of the variance of log dissolution rate at the Hanford site

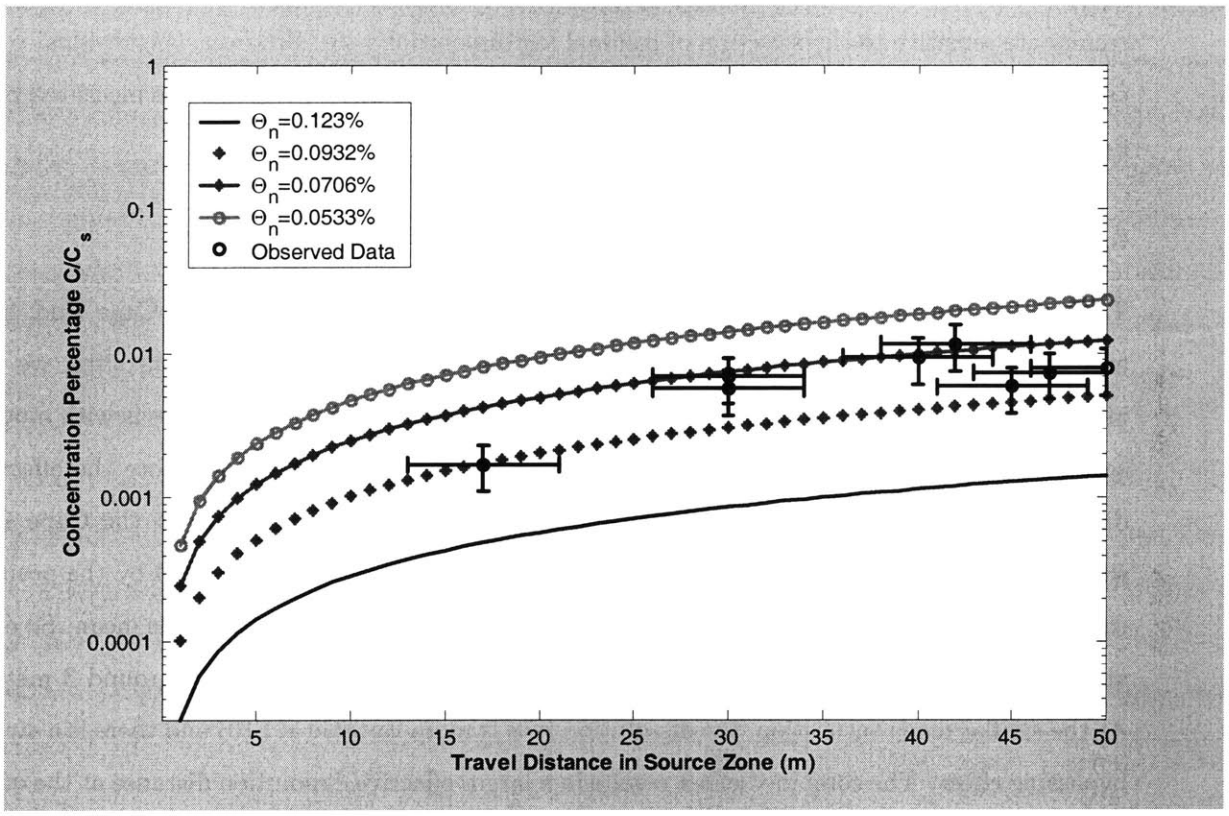


Figure 6-12: Concentration of Carbon Tetrachloride as a function of travel distance inside the smaller source as the residue accounts 1/2 of the variance of log dissolution rate at the Hanford site

as shown in Eq. 6.1. Here I evaluate the sensitivity as

$$\frac{\sigma^2_{g_h}}{\sigma^2_h} = \frac{1}{3} \tag{6.5}$$

Figure 6-13 shows the theoretical results based on Eq. 6.5 and the measured data. As we can see, concentration profiles for all four DNAPL saturations derived from the stochastic results shift up due to the smaller variance of log dissolution rate. This result indicates that the stochastic results are sensitive to the selection of residual log dissolution rate. However, this residual value can be determined as demonstrated in Chapter 3 if sufficient dissolution rate are measured from field samples.

### 6.3.5 Summary and Discussion

Table 6.9 shows the key inputs and outputs of stochastic models for Borden, Cape Cod, SRS and Hanford aquifers. By comparing the effective dissolution distance for four sites, we can identify the dominant factors controlling large-scale dissolution. The Borden site is with modest spatial variation of dissolution rate and modest anti-bypassing effect. Therefore the effective dissolution distance is relatively small, on the order of 1 meter. Similarly at the Cape Cod site the relatively small spatial variation with a strong anti-bypassing, reflected by the positive correlation, significantly reduces the deviation of the effective properties from the mean. So even at a relatively low mean saturation, the effective dissolution distance is only around 3 meters. At the similar mean saturation, the dissolution rate is more variable at SRS and there is a strong bypassing effect. The combined effect results in a larger effective dissolution distance at the order of 10 meters. The Hanford site has an extremely heterogeneous dissolution rate, as a result of the highly variable hydraulic conductivity. The strong bypassing effect plus high heterogeneity give rise to an extremely large effective dissolution distance, on the order of kilometers.

Table 6.9: Input Spatial Variations and Effective Dissolution Distance at Four Sites

| **Site** | $\overline{\theta}_n$ | $\sigma^2_h$ | $corr[v,h]$ | $\sigma_v$ | Effective Dissolution Distance (m) |
|---|---|---|---|---|---|
| **Borden** | 0.48% | 2.02 | 0.15 | 0.40 | 1.19 |
| **Cape Cod** | 0.027% | 1.29 | 0.40 | 0.52 | 3.4 |
| **SRS** | 0.029% | 2.98 | -0.42 | 0.58 | 17.23 |
| **Hanford** | 0.053% | 10.5 | -0.39 | 3.60 | 2110 |

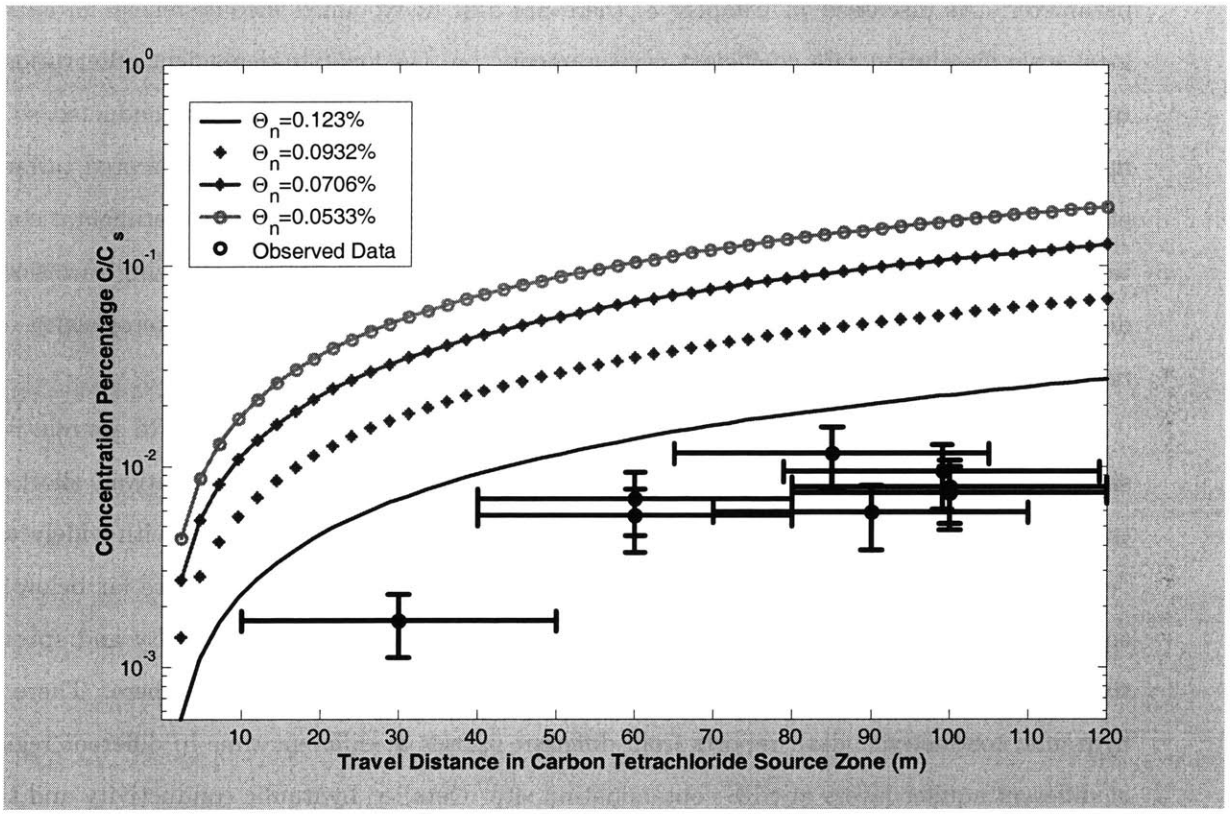


Figure 6-13: Concentration of Carbon Tetrachloride as a function of travel distance inside the DNAPL source as the residue accounts 1/3 of the variance of log dissolution rate at the Hanford site

The above analysis suggests that the heterogeneous dissolution rate with the associated bypassing effect is the main reason for the low concentration observed in the field DNAPL contaminated site. Therefore, accurate characterization of the variation of dissolution rate coefficient is central to the evaluation of the field-scale effect of small-scale heterogeneity. To achieve this goal, an optimal strategy of core sampling of the contaminated soils and specifically designed laboratory experiments are necessary to provide accurate characterization of this parameter. As discussed in Chapter 3, there are still unexplained inconsistencies in current local-scale dissolution rate coefficient measurements, i.e. the location-dependent observation in Imhoff's experiments is not adequately explained. Laboratory experiments conducted so far mainly target at characterizing the local-scale dissolution rate coefficient, with limited variation of affecting factors. The variability of dissolution rate coefficient in those experimental conditions are very limited. Therefore, laboratory experiments aiming at characterizing variation of dissolution rate coefficient are needed for evaluating the impact of spatial heterogeneity. We recommend more investment of research effort in this area.

As shown in Table 6.9, the dissolution distance for Borden, Cape Cod and SRS are relatively small so that concentration profiles reach the equilibrium concentration in a relatively short distance, compared to that of Hanford site. These predictions are not consistent with widely-used "rule of thumb" by engineers that the concentration levels observed in field are far below the equilibrium. One possible explanation is that the limitation of data availability and speculative selection of data restricts the generalization of the applications analyzed here. There are hydraulic conductivity data reports from different parties at different time in different regions at different aquifer layers at SRS contamination site. Detailed hydraulic conductivity and two-phase flow characteristic data are reported in Appendix G. By applying different data selection criteria, the calculated $\sigma_f^2$ differs significantly and can vary over two orders of magnitude. This variation can indirectly influence $\sigma_h^2$ and effective dissolution distance predicted. In this study, we use the values calculated from the data reflecting the portion of the aquifer where DNAPL most likely exists. This resulted in a low degree of spatial variation, based on the limited core sampling reports.

At a more fundamental level, the inconsistency may raise some questions about this commonly accepted "rule of thumb" that the observed/expected concentration is far below the equi-

librium concentration. So far it is not clear if any systematic analysis are available to provide the basis for such a rule. Without that, it can be regarded that it is just a case-specific conclusion based on individual experiences at limited field applications. Relatively small amount of DNAPL spilled in an aquifer, inadequate sampling work, limited horizontal spreading of DNAPL source zone could all be important to contribute to the inconsistencies here. To better understand the paradox, a systematic investigation of field experience is necessary. Considering all the uncertainties that exist, the applications here are clearly more case-specific than representative of general applications. Better understanding of DNAPL source zone, accurate characterization of input parameters, improved concentration sampling strategy and techniques are all important to effectively apply the stochastic model to field applications.

# Chapter 7

# Summary and Conclusions

## 7.1 Overview

Entrapped DNAPL in an aquifer has been recognized a long-term contaminant source to groundwater as a result of slow dissolution. Though considerable work has been performed to characterize local-scale dissolution in laboratory experiments, field-scale dissolution still remains unresolved. It has been reported the downstream concentrations within the source are significantly lower than those measured in column experiments or predicted by local-scale model. The paradox is possibly attributed to the homogeneity assumption implicit in those models. It has been observed that DNAPL distribute extremely non-uniform in a heterogeneous aquifer (Kueper *et al.*, 1993), and is likely trapped in small pools instead of single or multi-pore ganglia as in homogeneous media. The DNAPL pools, with relatively high saturation, reduce the relative permeability of wetting phase (water) flow significantly and become blocks in the flow path. Usually lens with DNAPL pools are of contrasting relative permeability and DNAPL saturation relative to region around them. By directing water flow to the region with larger relative permeability and less DNAPL saturation around the DNAPL pools, the portion of aqueous flow penetrating into DNAPL pools is significantly lower than those flowing around. This phenomenon is called the bypassing effect and has been reported from local-scale experiments. The wetting phase flow field becomes nonuniform as a result of bypassing effect, which in turn is a function of heterogenous intrinsic permeability and DNAPL distribution. The bypassing effect can be important to reduce the bulk dissolution rate at a large scale by enhancing the flow in

the region with lower DNAPL saturation around the regions of trapped DNAPL pools. However, the quantitative effects of small-scale heterogeneity and bypassing on field-scale dissolution properties are largely unexplained and unresolved.

This thesis aims at resolving the large-scale DNAPL dissolution problem, which addresses the mass transport and transfer in an extensively laterally-spreaded DNAPL source zone. This includes several key issues: 1. DNAPL saturation distribution at a field scale, 2. local dissolution characterization, 3. three-dimensional large-scale dissolution and transport properties derivation incorporating small scale heterogeneity, 4. two-zone model development, and 5. field applications of the stochastic framework. The theoretical descriptions of field-scale DNAPL saturation and wetting phase flow field obtained in Chapter 2 are the central inputs for the stochastic analysis of transport in a DNAPL zone. The local-scale dissolution model established in Chapter 3 provides essential correlations between the dissolution rate coefficient and affecting factors, which enables us to calculate the first and second moments of local dissolution rate based on results from Chapter 2. Stochastic analysis is developed in Chapter 4 to derive effective properties as influenced by small-scale heterogeneity. Then the two-zone model is established to provide an independent method to validate the extrapolation of effective properties in stochastic analysis at large spatial variations. Finally the theoretical results are applied to simulate the real contamination sites or to create contamination events at sites with extensive statistical information of hydraulic properties.

## 7.2 Summary

### 7.2.1 Field-scale DNAPL Saturation

DNAPL is introduced into subsurface systems usually by long-term spill or disposal activities from either single or multiple point sources. It has been reported from field observations that heterogeneity of porous media leads to an extremely heterogeneous distribution of DNAPL saturation (Poulsen & Kueper, 1992). DNAPL was also observed spreading laterally in an extensive scale due to heterogeneous strata in aquifers. As found by laboratory experiments, DNAPL dissolution rate is a strong function of DNAPL saturation (Imhoff *et al.*, 1994). At field-scale, where the porous media is heterogeneous, DNAPL can be distributed in a highly non-uniform

pattern in space with significant fluctuations. Bypassing can occur to affect the dissolution properties due to the spatial variation of DNAPL saturation. Therefore, the quantitative characterization of spatial distribution of DNAPL saturation and wetting phase flow, impacted by spatially variable soil properties, is a foundation to evaluate the field-scale dissolution properties.

Considerable numerical and experimental studies have been conducted in studying multiphase flow and DNAPL residual saturation. However, many analyses are not directly relevant to the static DNAPL saturation we are interested in due to the conceptually unresolved subject related to "residual saturation" in their studies. The analysis developed by Jacobs (1998) systematically studied the effect of small-scale heterogeneity on large-scale multiphase flow. The saturation characteristics for both phases are obtained. This quasi-static saturation field of the nonwetting phase can be a good representation of the static DNAPL saturation to study field-scale dissolution problem, considering it incorporates the impact of small-scale heterogeneity of soil properties and two-phase flow characteristics.

In Chapter 2, a steady-state, quasi-static DNAPL saturation distribution in a source zone is derived based on an extension of the Jacobs' work. The DNAPL saturation is assumed static considering the extremely small vertical DNAPL flow rate applied. DNAPL saturation distribution is found not affected significantly by the horizontal water flow. The mean DNAPL source zone is assumed uniform, which indicates that the mean DNAPL saturation is constant spatially in the source zone. Finally, DNAPL saturation field is assumed steady state, which is not affected significantly during the course of dissolution. This assumption is confirmed in Chapter 4 where the effective DNAPL dissolution rate coefficient is found very low in a heterogeneous DNAPL source zone. The effect of small-scale heterogeneity is expressed as second order moments of permeability and capillary curve properties.

The obtained DNAPL saturation field provides important inputs to investigate the DNAPL dissolution properties. The derived moments of DNAPL saturation, and the wetting phase flow field are crucial to derive the field-scale dissolution properties.

### 7.2.2 Local Dissolution Model

In Chapter 3 a local-scale dissolution model is established based on the extensive laboratory experimental results. It is a generalization of the empirical models derived from these experiments.

An imperfect correlation model is established between the local mass transfer rate coefficient and affecting factors including flow velocity, DNAPL saturation, permeability and an uncorrelated residual. The model is calibrated and the slope coefficients are found by laboratory experimental data reported by Imhoff (1994) and Powers (1994). The model predicted dissolution rate shows reasonable agreement with an independent data set. It is found that the residual random term in the local model is important to describe the deviation between model predicted values with observed data. Even in the homogeneous dissolution environment, the random residual can be large considering the limitation of the model and the possible data error. So it is expected that for the field-scale heterogeneous aquifer the random variance can be significant and this random error cannot be captured by the local-scale empirical models established in other studies.

The model can be utilized to calculate the mean and variance of log dissolution rate coefficient for a DNAPL source, provided by hydraulic conductivity data and two-phase flow characteristics. The local model also provides a basis to determine the other statistical parameters, such as the correlation between dissolution rate with flow rate, based on the soil properties, flow and DNAPL saturation inputs, which are functions of statistical information of aquifer permeability. These parameters represent small-scale heterogeneity and bypassing effects and are important to determine the effective properties.

### 7.2.3 Effective Transport Properties

Prediction of the solute concentration downstream of the source is of considerable interest in DNAPL contamination control research. Correctly estimating the dissolution rate in a field-scale DNAPL source is essentially important to predict the concentration profile. However, it also has been observed that the dissolution rate in DNAPL source is far smaller than those measured in laboratory experiments. In Chapter 4 we developed a stochastic analysis to evaluate the large-scale dissolution properties, on the basis of the interrelated spatial distributions of flow and DNAPL saturation derived in Chapter 2, and the local dissolution model obtained in Chapter 3.

We assume that the concentration field is steady state within the DNAPL source zone during the long dissolution process, which can last several decades. Linear theory is applied to derive the effective properties based on the spectral method, modified to treat the nonstationarity

of the concentration field. A linearized solution for effective properties is obtained due to the small perturbation amplitude limitation. Due to the relative large spatial variation of flow and transport variables encountered in field, an extrapolation is performed to relax the small amplitude perturbation assumption and derive the general results addressing the entire range of spatial variation. The extrapolated result is exponentially dependent on the input spatial variations instead of a linear dependence. The extrapolation is evaluated by the two-zone discrete model established independently in Chapter 5, though numerical studies may be necessary to provide further proof.

The closed form analytical solutions of effective properties are derived as a function of small-scale variations of transport properties. These spatial variations of transport properties, which are represented in forms of correlation coefficient between log flow rate and log dissolution rate coefficient $corr[v, h]$, variance of log flow rate $\sigma_v^2$ and variance of log dissolution rate coefficient $\sigma_h^2$, have significant impact on the large-scale effective properties including dissolution rate, plume advection rate, macrodispersivity and effective dissolution distance. $corr[v, h]$ reflects the bypassing effect. A negative correlation between flow velocity and dissolution rate implies a strong bypassing effect. The variation of flow rate is due to the intrinsic permeability heterogeneity and nonuniform DNAPL saturation distribution, which results in a heterogeneous relative permeability. Variance of log dissolution rate coefficient represents the variability of dissolution rate which is affected by the spatial variations of flow field and DNAPL saturation field.

The effective dissolution rate is found to be less than the mean and presents an exponential decrease as the spatial variation of dissolution rate increases. The negative correlation between solute velocity and dissolution rate make the effective dissolution rate lower. The variation of solute velocity has relatively small effect on the effective dissolution rate.

The effective dissolution distance increases dramatically as variation of dissolution rate coefficient increases and is found much larger than the mean. This indicates the dominant effect of variability of dissolution rate on the effective dissolution distance and the concentration profile of a solute plume. The bypassing effect is another important factor to increase this distance.

The effective solute velocity is dominantly affected by the correlation between log flow rate and log dissolution rate coefficient $corr[v, h]$. Positive correlation decreases the solute velocity

while the negative correlation increase it. On the other hand, mean dissolution rate has little influence on the downstream effective velocity. Higher variation of flow rate leads to a higher deviation of effective velocity from the mean. The ratio of macrodispersivity to the conservative one decreases as variation of dissolution rate coefficient increase, which means the heterogeneity of dissolution rate leads to a significant smaller macrodispersivity.

The stationary assumption is studied for two cases: downstream concentration decay and nonstationary concentration field at the boundary. By separating the nonstationary component of the downstream concentration field from the stationary component, the Spectral Representative Theory (SRT) can be applied to the stationary concentration field and effective properties are derived using spectral method. The nonstationary effect at the boundary is found insignificant under field conditions.

Miralles-Wilhelm and Gelhar studied solute transport with first-order decay in a heterogeneous aquifer with plug flow as the boundary condition (Miralles-Wilhelm & Gelhar, 1996). Instead of treating the mean concentration increasing trend in space as in this study, they analyzed the transient effect by a time scaling method. They derived the effective transport properties including the effective decay rate, effective solute transport velocity and macrodispersivity. The results obtained from his analysis are compared with those derived from this study at the context of same input conditions. The effective properties of both studies are found equivalent. The equivalence between two different studies with different methods reveals the similar dominant impact of spatial heterogeneity on the large-scale mass transfer and transport process in groundwater systems and confirms the plausibility of the results derived in this work for the more complex dissolution problem.

### 7.2.4 Two-zone Model

The two-zone model is a straightforward way to describe the bypassing effect, which corresponds to highly negative correlation between $v$ and $h$ in the stochastic model. The two-zone model is developed in the work primarily to provide an independent method to evaluate the extrapolation of linearized stochastic solutions.

Observations from experiments confirmed that the spilled DNAPL is often present in a subsurface system in forms of pools, which are formed due to the contrasting permeability and capil-

lary properties, and droplets which are entrapped in fairly homogeneous porous media (Kueper *et al.*, 1993). The dissolution process for these two types of DNAPL are found significantly different (Sale & McWhorter, 2001). A discrete two-zone model is established to represent the spatial variations of soil properties and the DNAPL distribution in a DNAPL source zone. The two zones have contrasting properties of permeability, DNAPL saturation, dissolution rate and flow rate. The lens zone represents the area with a high DNAPL saturation, a high dissolution rate and a low water flow velocity, while a relatively low DNAPL saturation, a low dissolution rate and a high flow velocity occur in the permeable zone. The effluent from the lens zone is assumed to reach the equilibrium concentration due to the slow water flow velocity through a DNAPL pool and a large dissolution rate due to the high saturation. A discrete probability distribution is assigned to describe the spatial distribution of permeability, dissolution rate and water flow rate. The unique feature of this model is that it takes into account the advective effect from lens zones, in addition to the diffusive mass transfer which is commonly considered.

The inputs of two-zone model are the volumetric probability of lens zones and the length of the lens. By applying the transport model to each zone, we derived the relationship between the effective dissolution distance and the contributions from each zone. There are two contributions to the overall two-zone dissolution distance, dissolution of DNAPL blobs in the permeable zone, which is a function of dissolution rate and flow rate in this zone, and dissolution of DNAPL pool in the lens zone. In addition, there are two contributions to the DNAPL pool dissolution: advection mass transfer reflected by the ratio of permeability of two zones, and the contribution from diffusion as reflected by the ratio of the diffusion layer thickness to the lens thickness.

It is found that the two-zone model results are of a good agreement with stochastic results when flow velocity and dissolution rate are perfectly negative correlated, representing a strong bypassing effect. The effective dissolution distance increases as the spatial variation of dissolution increases. The results agree with each other well for different input parameters. The probability and the length of lens are found independent with the spatial variations and the mean dissolution properties, which confirmed that the exponential extrapolation of stochastic results is appropriate.

### 7.2.5 Applications

To demonstrate the applicability of the stochastic results, we locate suitable contaminated sites and create synthesized contamination events to demonstrate the feasibility of treating field-scale contamination using the effective parameters-based framework. The following four sites with contrasting geological settings are explored: the Borden site, the Cape Cod aquifer, the Savannah River Site (SRS) and the Hanford site. Extensive data on hydraulic conductivity and multiphase flow parameters are available for these sites. Stochastic flow and transport models are applied by inputting statistical hydraulic information reported from other studies. DNAPL saturation distribution and effective flow and transport properties are derived. Concentration profiles are plotted within the source zone for four sites.

The effect of heterogeneity can be reflected in the mean concentration profile curves for the Hanford site, the Borden site, the Cape Cod site and SRS. Due to highly variable nature of permeability and capillary properties of soil, the effective dissolution distance is much higher than the mean which is at a scale of centimeters. The predicted mean concentration profile is in good agreement with data measured within or around the source zone at Z9 area of the Hanford site. It is found that spatial heterogeneity is a significant factor affecting the large-scale dissolution. The bypassing effect, which is represented by the negative correlation between flow and dissolution rate, magnifies this effect. Spatial variability of dissolution rate without significant bypassing effect leads to only a modest increase of effective dissolution distance from the mean. This finding emphasizes the impact of bypassing effect and spatial variation on the large-scale mass transfer process, which make the effect of mean dissolution rate secondary.

One of the strength of this study is that it is able to deal with large variation problem by exponential extrapolation. This can substantially increase the applicability of the results since highly heterogeneous aquifers are not rare when studying DNAPL contamination sites. The variance of dissolution rate coefficient is determined by the intrinsic permeability variation and subsequent variability of DNAPL saturation and flow field. The Hanford site appears to be a highly heterogeneous aquifer with variance of log permeability equals 1.87. This large spatial variability of permeability leads to a significant non-uniform DNAPL distribution. Subsequently it results in a highly variable dissolution rate with large $\sigma_h^2$ and strong bypassing effect. The predicted concentration level downstream of the source zone is only 1% of the solubility, which

is in accordance with observed field data. The agreement of predicted results with field data significantly enhances the applicability and accountability of the theoretical solutions.

The concentration in the Borden aquifer reaches equilibrium in a distance of one to ten meter at various mean DNAPL saturations. This is due to the relatively homogeneous nature of the aquifer permeability which leads to relative homogeneous dissolution rate. Compared to the Borden aquifer, the Cape Cod aquifer is more permeable but also more heterogeneous. The effective dissolution distance is in the range of 10 meters and changes as a function of DNAPL saturation. Heterogeneity does not increase the effective dissolution distance due to the strong anti-bypassing effect at the Cape Cod site. Even though the mean DNAPL saturation is low, resulting in an extreme low mean dissolution rate, the effective dissolution distance is not large. This confirms that the effect of the mean dissolution rate is only a secondary effect compared to the spatial heterogeneity and bypassing effect. SRS is the most impermeable aquifer among the four sites. The effective dissolution distance there is on the order of tens of meters due to the strong bypassing effect.

Compared to the commonly used empirical model from column experiments, the effective dissolution distances predicted for these sites are almost two orders of magnitude higher. This indicates that by using the empirical model results or only considering the kinetic effects without taking heterogeneity in account, the dissolution rate coefficient of DNAPL and DNAPL concentration level in aqueous phase is significantly overestimated. Though the large-scale dissolution is controlled by both the mean dissolution and transport properties, as well as spatial variations of soil properties, DNAPL saturation, and the wetting phase flow field, the significant spatial variation of dissolution rate with strong bypassing effect is found a dominant impact on effective dissolution distance. Considering all the uncertainties that exist in terms of limitation of data availability and the speculation of DNAPL source zone, the applications here are clearly more case-specific than representative of general applications. Better understanding of DNAPL source zone, accurate characterization of input parameters, improved concentration sampling strategy and techniques are all important to effectively apply the stochastic model to field applications.

## 7.3 Conclusions

The major conclusions of this study are listed below:

1. The field-scale spatially-variable aqueous flow field and the theoretical quasi-static nonuniform DNAPL distribution is derived from stochastic framework. The quasi-static DNAPL saturation is produced by a very low steady DNAPL infiltration rate and taken as a good representation of static DNAPL saturation. The DNAPL vertical flow is not influenced significantly by horizontal water flow, and the impact of DNAPL flow on the transport result is negligible.

2. A local dissolution model is established based on a partial correlation between the local mass transfer rate coefficient and affecting factors including flow velocity, DNAPL saturation, permeability and an uncorrelated residual. The mean and variance of log dissolution rate coefficient can be derived from the model based on the input statistical properties of an aquifer and the DNAPL distribution.

3. A linearized stochastic analysis of solute transport is applied to derive the large-scale effective dissolution properties as affected by small-scale spatial heterogeneity, based on the obtained nonuniform DNAPL saturation field and water flow field. An extrapolation, which aims to relax the linearization limitation during the derivation, is performed to accommodate the large variability of dissolution and transport properties, which is frequently encountered under field conditions.

4. The variability of dissolution rate and the bypassing effect resulted from spatial heterogeneity are found the most important factors affecting the effective dissolution distance. Effective dissolution rate decreases exponentially as the spatial variability increases. The effective dissolution distance is several orders of magnitude higher than the mean when the spatial variation of dissolution rate is large.

5. A two-zone model, including both advective and diffusive mass transfer effects, provides a unique approach to simulate the dissolution in a heterogeneous DNAPL source zone. The relative importance of dissolution from permeable zones and lens zones is also demonstrated. The two-zone model particularly represents the strong bypassing in the large-scale dissolution process. The agreement of two-zone results with stochastic results supports adequacy of extrapolation hypothesized in the stochastic study.

6. Theoretical predictions agree well with the concentration profile measured at the Hanford

Site in Washington, US, but uncertainties regarding the input parameters and DNAPL source zone are present. The effective dissolution distances at the Borden, the Cape Cod and the Savannah River Site are found significantly larger than those predicted by the mean. The derived effective properties help to explain the paradox that the observed concentration levels at contaminated field sites are typically far below those predicted by the parameters derived from homogeneous porous media in a small-scale laboratory apparatus.

## 7.4 Limitations

- Extrapolation of linearized stochastic results for large variation problem is an aspect of this work requiring further evaluation. To apply the stochastic framework to sites like the Hanford site with extremely large spatial variation of permeability, extrapolations of both flow and transport analysis are necessary. Since the traditional stochastic technique is based on the small-amplitude perturbation assumption, potential errors can be introduced when the extrapolation technique is applied.

- The widely used van Genuchten model of local relationship of capillary pressure saturation curve may not be accurate for some soils and could produce significant errors. Tse (1997) found that errors of several orders of magnitude are frequently encountered using the van Genuchten relationship to predict wetting phase permeability. However, this relationship is employed in this study to derive the DNAPL saturation and wetting phase relative permeability field. Future work to develop more accurate empirical model of two-phase flow characteristics is necessary.

- Experimental and numerical techniques to better understand DNAPL distribution in subsurface systems are not available yet. Current studies of DNAPL distribution estimation cannot capture the small-scale heterogeneity effect or cannot provide a definite model relate the DNAPL saturation distribution with controlling factors. At most field sites the systematic sampling work to determine DNAPL saturation distribution are not available. This limits the validation test of DNAPL saturation results derived in this study.

- Hydraulic conductivity data for SRS and the Hanford sties are selected from the layer

and formations that DNAPL most likely exists. Originally reported data are composed data measured by different parties at different location at different time with different methods. These data as a whole are extremely widely distributed and the variance of log permeability can be larger than 10. Concentration measurement data at the Hanford site are also with limitations due to the vertical averaged value along the screen in sampling wells. More systematic and well-designed measurements of hydraulic conductivity, two-phase flow characteristics, DNAPL source zone characterization and DNAPL concentration are necessary to provide a better understanding of the DNAPL dissolution problem and a better tool to evaluate stochastic results.

## 7.5 Recommended Future Work

- Numerical simulation of DNAPL dissolution in a source zone should be performed to provide a measure to confirm the theoretical results. Though the plausibility of the extrapolation introduced in deriving the effective dissolution properties at large variance has been confirmed by the two-zone model results, further evaluation using numerical simulations is necessary.

- Well designed field experiments to investigate the dissolution and monitor the solute transport from a DNAPL contamination site are needed. Though the contaminant concentration data are provided for the Hanford Site as well as hydrological parameters, the lack of observation of DNAPL presence in saturated aquifer and the uncertainty of the DNAPL source zone limit the applicability of these field data. A well-designed field experiment with a well-characterized DNAPL source zone, careful measurements of aqueous phase concentration and hydrological parameters is needed.

# References


Bjornstad, B.N. 1990. *Geohydrology of the 218-W-5 Burial Ground, 200 West Area, Hanford Site. PNL-7336.* Tech. rept. Pacific Northwest Laboratories, Richland, Washington,US.

Cohen, R.M., & Mercer, J.W. 1993. *DNAPL Site Evaluation.* C.K.SMOLEY, Boca Raton, Florida, USA.

Corey, A.T. 1986. *Mechanics of ImmiscibleFluids in Porous Media.* Water Resource Publications, Littleton, Colorado, USA.

Dagan, G., & Lessoff, S.C. 2001. Solute transport in heterogeneous formations of bimodal conductivity distribution 1.Theory. *Water Resources Research*, **37**(3), 465–472.

Davis, J.M., Wilson, J.L., Phillips, F.M., & Gotkowitz, M.B. 1997. Relationship between fluvial bounding surfaces and the permeability correlation structure. *Water Resources Research*, **33**(8), 1843–1854.

Dekker, T.J., & Abriola, L.M. 2000. The influence of field-scale heterogeneity on the infiltration and entrapment of dense nonaqueous phase liquids in saturated formations. *Journal of Contaminant Hydrology*, **42**(3), 187–218.

Eberhardt, C., & Grathwohl, P. 2002. Time scales of organic contaminant dissolution from complex source zones: coal tar pools vs. blobs. *Journal of Contaminant Hydrology*, **59**(2002), 45–66.

Feenstra, S., & Cherry, J.A. 1988. Subsurface contamination by dense non-aqueous phase liquid (DNAPL) chemicals.

Frind, E.O., Molson, J.W., & Schirmer, M. 1999. Dissolution and mass transfer of mul-

tiple organics under field conditions: The Borden emplaced source. *Water Resources Research*, **35**(3), 683–694.

Gelhar, L.W. 1993. *Stochastic Subsurface Hydrology.* Prentice Hall, Englewood Cliffs, New Jersey, USA.

Gelhar, L.W., & Axness, C.L. 1983. Three-dimensional stochastic analysis of macrodispersion in aquifers. *Water Resources Research*, **19**(1), 161–180.

Geller, J.T., & Hunt, J.R. 1993. Mass Transfer From Nonaqueous Phase Organic Liquids in Water-Saturated Porous Media. *Water Resources Research*, **29**(4), 833–845.

Glass, R.J., Gonrad, S.H., & Peplinski, W. 2000. Gravity-destabilized nonwetting phase invasion in macroheterogeneous porous media: Experimental observations of invasions dynamics and scale analysis. *Water Resources Research*, **36**(11), 3121–3137.

Guiguer, N. 1993. *Dissolution and mass transfer processes for residual organics in the saturated groundwater zone: numerical modeling.* Ph.D. thesis, University of Waterloo, Waterloo, Ortario, Canada.

Hess, K.M., Wolf, S.H., & Celia, M.A. 1992. Large-scale natural gradient trancer test in sand and gravel, 3,Hydraulic conductivity variability and calculated macrodispersivities. *Water Resources Research*, **28**(8), 2011–2027.

Hooker, B.S., Truex, M.J., Clement, T.P., & Skeen, R.S. 1996. Preliminary Validation of Intrinsic Remediation of Carbon Tetrachloride at the Hanford Site, Presented at the Intrinsic Remediation Conference, April 1996, Salt Lake City, Utah, USA.

Illangasekare, T.H., III, E.J. Armbruster, & Yates, D.N. 1995. Nonaqueous phase fluids in heterogeneous aquifers-Experimental study. *Journal of Environ. Eng.*, **121**(8), 571–579.

Imhoff, P.T. 1992. *Dissolution of a nonaqueous phase liquid in saturated porous media.* Ph.D. thesis, Princeton University, Princeton, NJ, USA.

Imhoff, P.T., & Miller, C.T. 1996. Dissolution fingering during the solubilization of nonaqueous phase liquids in saturated porous media 1. Model predictions. *Water Resources Research*, **32**(7), 1919–1928.

Imhoff, P.T., Jaffe, P.R., & Pinder, G.F. 1994. An experimental study of complete dissolution of a nonaqueous phase liquid in saturated porous media. *Water Resources Research*, **30**(2), 307–320.

Jackson, D.G., & Looney, B.B. 2001. *Evaluating DNAPL Source and Migration Zones: M-Area Setting Basin and the Western Sector of A/M Area, Savannah River Site(U) WSRC-TR-2001-00198.* Tech. rept. Westinghouse Savannah River Company, Aiken, South Carolina,US.

Jackson, D.G., Noonkester, J.V., Vangelas, K.M., & Brigmon, R.L. 2000. *Characterization Activity to Evaluate Chlorinated Solvent Discharges to TImes Branch from the A/M Area of the Savannah River Site(U) WSRC-TR-2000-00472.* Tech. rept. Westinghouse Savannah River Company, Aiken, South Carolina,US.

Jacobs, B. 1998. *Effective Properties of Multiphase Flow in Heterogeneous Subsurface Systems.* Ph.D. thesis, Massachusetts Institute of Technology, Cambridge, Massachusetts, USA.

Kueper, B.H., Abbot, W., & Farquhar, G. 1989. Experimental observations of multiphase flow in heterogeneous porous media. *Journal of Contaminant Hydrology*, **5**(1), 83–95.

Kueper, B.H., Redman, D., Starr, R.C., Reitsma, S., & Mah, M. 1993. A Field Experiment to Study the Behavior of Tetrachloroethylene Below the Water Table: Daptial Distribution of Residual and Pooled DNAPL. *Water Resources Research*, **31**(5), 756–766.

Li, S-G, & McLaughlin, D. 1995. Using the nonstationary spectral method to analyze flow through heterogeneous trending media. *Water Resources Research*, **31**(3), 541–551.

Mace, R.E. 1994. *Steady flow and non-reactive transport in unsaturated sand gravel cores.* M.Phil. thesis, University of Waterloo, Waterloo, Canada.

Mackay, D.M., Freyberg, D.L., Roberts, P.V., & Cherry, J.A. 1986. A Natural Gradient Experiment on Solute Transport in a Sand Aquifer 1. Approach and Overview of Plume Movement. *Water Resources Research*, **22**(13), 2017–2029.

Mayer, A.S., & Miller, C.T. 1996. The influence of mass transfer characteristics and porous media heterogeneity on nonaqueous phase dissolution. *Water Resources Research*, **32**(6), 1551–1567.

Mercer, J.W., & Cohen, R.M. 1990. A Review of Immiscible Fluids in the Subsurface: Properties, Models, Characterization and Remediation. *Journal of Contaminant Hydrology*, **6**(1990), 107–163.

Miller, C.T., Poirier-McNeill, M.M., & Mayer, A.S. 1990. Dissolution of Trapped Nonaqueous Phase Liquids: Mass Transfer Characteristics. *Water Resources Research*, **26**(11), 2783–2796.

Miller, C.T., G. Christakos, P.T. Imhoff, McBride, J.F., Pedit, J.A., & Trangenstein, J.A. 1998. Multiphase flow and transport modeling in heterogeneous porous media: challenges and approaches. *Advances in Water Resources*, **21**(2), 77–120.

Miralles-Wilhelm, F., & Gelhar, L.W. 1996. Stochastic Analysis of Transport and Decay of a Solute in Heterogeneous Aquifers. *Water Resources Research*, **32**(12), 3451–3459.

Mualem, Y. 1976. A new model for predicting the hydraulic conductivity of unsaturated porous media. *Water Resources Research*, **12**(3), 513–522.

Nambi, I.M., & Powers, S.E. 2000. DNAPL dissolution in heterogeneous systems: an experimental investigation in a simple heterogeneous system. *Journal of Contaminant Hydrology*, **44**(2000), 161–184.

Oostrom, M., Hofstee, C., Walker, R.C., & Dane, J.H. 1999. Movement and remediation of trichloroethylene in a saturated heterogeneous porous media 1. Spill behavior and initial dissolution. *Journal of Contaminant Hydrology*, **37**(1999), 159–178.

Pankow, J.F., & Cherry, J.K. 1996. *Dense Chlorinated Solvents in Groundwater: History, Behavior, and Remediation.* Waterloo Press, Waterloo, Canada.

Parker, J.C. 1989. Multiphase flow and transport in porous media. *Review of Geophysics*, **27**(3), 311–328.

Polmann, D.J. 1990. *Application of Stochastic Models to Transient Flow and Transport in Heterogeneous Unsaturated Soils.* Ph.D. thesis, Massachusetts Institute of Technology, Cambridge, Massachusetts, USA.

Poulsen, M., & Kueper, B.H. 1992. A field experiment to study the behaviour of tetrachloroethylene in unsaturated porous media. *Environmental Science and Technology*, **26**(5), 889–895.

Powers, S.E., Loureiro, C.O., Abriola, L.M., & W.J. Weber, Jr. 1991. Theoretical Study of the Significance of Nonequilibrium Dissolution of Nonaqueous Phase Liquids in Subsurface Systems. *Water Resources Research*, **27**(4), 463–477.

Powers, S.E., Abriola, L.M., & W.J. Weber, Jr. 1992. An Experimental Investigation of Nonaqueous Phase Liquid Dissolution in Saturated subsurface system: Steady State Mass Transfer Rates. *Water Resources Research*, **28**(10), 2691–2705.

Powers, S.E., Abriola, L.M., & W.J. Weber, Jr. 1994. An Experimental Investigation of nonaqueous phase liquid dissolution in saturated subsurface system: Transient mass transfer rates. *Water Resources Research*, **30**(2), 321–332.

Powers, S.E., Nambi, I.M., & Jr., G.W. Curry. 1998. Non-aqueous phase liquid dissolution in heterogeneous systems: Mechanisms and a local equilibrium modeling approach. *Water Resources Research*, **34**(12), 3293–3302.

Relyea, J. 1995. *Laboratory Reports, Project Files for WHC-EP-0883,Rev.0.* Tech. rept. Westinghouse Hanford Company, Richland, Washington,US.

Reynolds, D.A., & Kueper, B.H. 2001. Multiphase flow and transport in fractured clay/sand sequences. *Journal of Contaminant Hydrology*, **51**(1).

Rivett, M.O., Feenstra, S., & Cherry, J.A. 2001. A controlled field experiment on groundwater contamination by a multicomponent DNAPL: creation of the emplaced-source and overview of dissolved plume development. *Journal of Contaminant Hydrology*, **49**(2001), 111–149.

Rohay, V.J., Swett, K.J., & Last, G.V. 1994. *1994 Conceptual Model of the Carbon Tetrachloride Contamination in the 200 West Area at the Hanford Site, WHC-SD-EN-TI-248, Rev.0.* Tech. rept. Westinghouse Hanford Company, Richland, Washington,US.

Rossabi, J. 1999. *The Influence of Atmosphere Pressure Bariations on Subsurface Soil Gas and the Implications for Environmental Characterization and Remediation.* Ph.D. thesis, Clemson University, Clemson,South Carolina, USA.

Saba, T., & Illangasekare, T.H. 2000. Effect of groundwater flow dimensionality on mass transfer from entrapped nonaqueous phase liquid contaminants. *Water Resources Research*, **36**(4), 971–979.

Sale, T.C., & McWhorter, D.B. 2001. Steady state mass transfer from single-component dense nonaqueous phase liquids in uniform flow fields. *Water Resources Research*, **37**(2), 393–404.

Schwarzenbach, R.P., Gschwend, P.M., & Imboden, D.M. 1993. *Environmental Organic Chemistry.* John Wiley and Sons, New York City, New York, USA.

Schwille, F. 1988. *Dense Chlorinated Solvents in Porous and Fractured Media (translated by J.Pankow).* Lewis Publishers, Chelsea,Michigan, USA.

Seagren, E.A., Rittmann, B.E., & Valocchi, A.J. 1999. An experimental investigation of NAPL pool dissolution enhancement by flushing. *Journal of Contaminant Hydrology*, **37**(1).

Soerens, T.S., Sabatini, D.A., & Harwell, J.H. 1998. Effects of flow bypassing and nonuniform NAPL distribution on the mass transfer characteristics of NAPL dissolution. *Water Resources Research*, **34**(7), 1657–1673.

Springer, K.R. 1991. *Application of an Improved Slug Test Analysis to the Large-Scale Characterization of Heterogeneity in a Cape Cod Aquifer.* M.Phil. thesis, Massachusetts Institute of Technology, Cambridge, MA, USA.

Stoker, J.J. 1957. *Water Waves.* Interscience Publishers, Inc., New York City, New York, USA.

Sudicky, E.A. 1986. A natural gradient experiment on solute transport in a sand aquifer: Saptial variability of hydraulic conductivity and its role in the dispersion process. *Water Resources Research*, **22**(13), 2069–2082.

Swanson, L. C., Rohay, V.J., Faurote, J.M., & Inc, CH2M Hill Hanford. 1999. *Hydrogeologic Conceptual Model for the Carbon Tetrachloride and Uranium/Technetium Plumes in the 200 West Area: 1994 Through 1999 Update BHI-01311, Rev.0.* Tech. rept. Bechtel Hanford Inc., Richland, Washington,US.

Talbott, M.E., & Gelhar, L.W. 1994. *Performance Assessment of a Hypothetical Low-Levl Waste Facility.* Tech. rept. U.S. Nuclear Rgulatory Commission, Washington,DC, US.

Tse, R. 1997. *A Critical Assessment of Two Phase Flow Characterization of Soils.* M.Phil. thesis, Massachusetts Institute of Technology, Cambridge, MA, US.

Unger, A.J.A., Forsyth, P.A., & Sudicky, E.A. 1998. Influence of alternative dissolution models and subsurface heterogeneity on DNAPL disappearance times. *Journal of Contaminant Hydrology*, **30**(1998), 217–242.

Zhang, Z., & Brusseau, M.L. 1999. Nonideal transport of reactive solutes in heterogeneous porous media 5. Simulating regional-scale behavior of a trichloroethene plume during pump-and-treat remediation. *Water Resources Research*, **35**(10), 2921–2935.

Zhou, Q., Gelhar, L.W., & Jacobs, B. 2002. Comparison of field-scale effective properties of two-phase flow in heterogeneous porous media. *Pages 389–392 of:* Findikakis, A. N. (ed), *Proceedings of the International Groundwater Symposium on Bridging the Gap Between Measurement and Modeling In Heteroegeneous Media,Berkeley, CA, March 25-28, 2002.* International Association for Hydraulic Research.

Zhu, J., & Sykes, J.F. 2000. Stochastic simulations of DNAPL mass transport in variably saturated heterogeneous porous media. *Transport in Porous Media*, **39**, 289–314.

# Appendix A

# Integral Evaluation

The integral evaluation present in Chapter 4 is the direct way to obtain the effective properties. Here I present an alternative approach to evaluate the integrals using the local dissolution model to decompose the cross covariance between dissolution rate with other properties. From Eq. 4.17, we have:

$$dZ_h = bdZ_f + cdZ_W + ddZ_v + dZ_{g_h} \tag{A.1}$$

## A.1 Evaluation of $I_1$

We can decompose the cross-spectrum $S_{vh}d\mathbf{k}$ in Eq. 4.63 as:

$$\begin{aligned} S_{vh}d\mathbf{k} &= E\left[dZ_v dZ_h^*\right] && \text{(A.2)} \\ &= dZ_v\left(bdZ_f^* + cdZ_W^* + ddZ_v^* + dZ_{g_h}^*\right) && \text{(A.3)} \\ &= bS_{vf}d\mathbf{k} + cS_{vW}d\mathbf{k} + dS_{vv}d\mathbf{k} && \text{(A.4)} \end{aligned}$$

So:

$$I_1 = A_1 + A_2 + A_3 \tag{A.5}$$

where

$$A_1 = b\int_{-\infty}^{\infty} \frac{S_{vf}}{\Omega^* + iqk_1 + E_{ij}k_ik_j} d\mathbf{k} \tag{A.6}$$

$$A_2 = c\int_{-\infty}^{\infty} \frac{S_{vW}}{\Omega^* + iqk_1 + E_{ij}k_ik_j} d\mathbf{k} \tag{A.7}$$

$$A_3 = d\int_{-\infty}^{\infty} \frac{S_{vv}}{\Omega^* + iqk_1 + E_{ij}k_ik_j} d\mathbf{k} \tag{A.8}$$

### A.1.1 $A_1$ Evaluation

From Eq. 2.93, we have:

$$S_{vf}d\mathbf{k} = E\left[dZ_v dZ_f^*\right] \tag{A.9}$$

$$= \epsilon[\varrho + \beta_m Y_m]S_{ff}d\mathbf{k} \tag{A.10}$$

so:

$$A_1 = b\int_{-\infty}^{\infty} \frac{S_{vf}}{\Omega^* + iqk_1 + E_{ij}k_ik_j} d\mathbf{k} = b\int_{-\infty}^{\infty} \frac{\epsilon[\varrho + \beta_m Y_m]}{\Omega^* + iqk_1 + E_{ij}k_ik_j} S_{ff}d\mathbf{k} \tag{A.11}$$

For uniform mean nonwetting phase vertical flow ($\nabla\overline{P_c} = 0$) from Jacobs result in Eq. 2.56. Putting $Y_m$ into $A_1$and canceling the odd functions of $\mathbf{k}$:

$$A_1 = b\int_{-\infty}^{\infty} \epsilon\left[\varrho\frac{(\Omega^* + E_{ij}k_ik_j)}{\left[(\Omega^* + E_{ij}k_ik_j)^2 + q^2k_1^2\right]} - \frac{\beta_m B_m B_2 k_3^2\left(\Omega^* + E_{ij}k_ik_j\right)]}{\left(k^4 + B_2^2k_3^2\right)\left[(\Omega^* + E_{ij}k_ik_j)^2 + q^2k_1^2\right]}\right] S_{ff}d\mathbf{k} \tag{A.12}$$

Neglecting the local dispersion,

$$A_1 = b\int_{-\infty}^{\infty} \frac{\epsilon\Omega^*[\varrho\left(k^4 + B_2^2k_3^2\right) - \beta_m B_m B_2 k_3^2]}{\left(k^4 + B_2^2k_3^2\right)\left[\Omega^{*2} + q^2k_1^2\right]} S_{ff}d\mathbf{k} \tag{A.13}$$

and let $u_i = k_il_i$, so:

$$k^2 = k_1^2 + k_2^2 + k_3^2 = \frac{u_1^2}{l_1^2} + \frac{u_2^2}{l_2^2} + \frac{u_3^2}{l_3^2} = \frac{1}{l_3^2}(\frac{l_3^2}{l_1^2}u_1^2 + \frac{l_3^2}{l_2^2}u_2^2 + u_3^2) \tag{A.14}$$

Since for an imperfect stratified layer system: $l_1 = l_2 >> l_3$, so

$$k^2 = k_3^2 >> k_1^2 + k_2^2 \tag{A.15}$$

Thus $A_1$ is approximated as:

$$A_1 = b\Omega^*\int_{-\infty}^{\infty}\left[\frac{\varrho}{\left(\Omega^{*2} + q^2k_1^2\right)} - \frac{\beta_m B_m B_2}{\left(k_3^2 + B_2^2\right)\left[\Omega^{*2} + q^2k_1^2\right]}\right] S_{ff}d\mathbf{k} \tag{A.16}$$

Using the three-dimensional hole-type spectrum in Eq. A.17:

$$S_{ff}d\mathbf{k} = \frac{4\sigma_f^2 l_1 l_1 l_3^3 k_3^2}{\pi^2\left(1+l_1^2k_1^2+l_2^2k_2^2+l_3^2k_3^2\right)^3}d\mathbf{k} = \frac{4\sigma_f^2 u_3^2}{\pi^2\left(1+u^2\right)^3}d\mathbf{u} \tag{A.17}$$

the integral becomes:

$$A_1 = \frac{b\Omega^* l_1^2}{q^2}\int_{-\infty}^{\infty}\left[\frac{\varrho}{\left[\Omega^{*2}l_1^2/q^2+u_1^2\right]} - \frac{l_3^2\beta_m B_m B_2}{\left(u_3^2+l_3^2B_2^2\right)\left[\Omega^{*2}l_1^2/q^2+u_1^2\right]}\right]\frac{4\sigma_f^2 u_3^2}{\pi^2\left(1+u^2\right)^3}d\mathbf{u} \tag{A.18}$$

with

$$\zeta = \Omega^* l_1/q \tag{A.19}$$

$$\varkappa = l_3 B_2 \tag{A.20}$$

Changing to spherical coordinate

$$u_1 = r\sin\psi\cos\theta \tag{A.21}$$

$$u_2 = r\sin\psi\sin\theta \tag{A.22}$$

$$u_3 = r\cos\psi \tag{A.23}$$

$$du_1 du_2 du_3 = r^2\sin\psi dr d\psi d\theta \tag{A.24}$$

$$A_1 = b\Omega^*\frac{4\sigma_f^2}{\pi^2}\int_0^{2\pi}\int_0^{\pi}\int_0^{\infty}\frac{l_1^2[\varrho\left(r^2\cos^2\psi+\varkappa^2\right)-l_3^2\beta_m B_m B_2]}{\left(r^2\cos^2\psi+\varkappa^2\right)\left[\Omega^{*2}l_1^2+q^2r^2\sin^2\psi\cos^2\theta\right]}\frac{r^2\cos^2\psi}{\left(1+r^2\right)^3}r^2\sin\psi dr d\psi d\theta \tag{A.25}$$

integrate about $\theta$

$$A_1 = b\Omega^* l_1^2\frac{4\sigma_f^2}{\pi^2}\int_0^{\pi}\int_0^{\infty}\frac{[\varrho\left(r^2\cos^2\psi+\varkappa^2\right)-l_3^2\beta_m B_m B_2]}{\left(r^2\cos^2\psi+\varkappa^2\right)}\frac{r^4\cos^2\psi\sin\psi}{\left(1+r^2\right)^3}\frac{2\pi}{\Omega^{*2}l_1^2\sqrt{1+\left(\frac{1/\Omega^*}{l_1/q}\right)^2 r^2\sin^2\psi}}dr d\psi \tag{A.26}$$

By assuming $\zeta = \Omega^* l_1/q >> 1$, so the result can be simplified as:

$$A_1 = b\frac{8\sigma_f^2}{\pi}\frac{\overline{\zeta}/\overline{\Omega}}{\zeta}\int_0^{\pi}\int_0^{\infty}\frac{[\varrho\left(r^2\cos^2\psi+\varkappa^2\right)-l_3^2\beta_m B_m B_2]}{\left(r^2\cos^2\psi+\varkappa^2\right)}\frac{r^4\cos^2\psi\sin\psi}{\left(1+r^2\right)^3}dr d\psi \tag{A.27}$$

where

$$\overline{\zeta} = \overline{\Omega} l_1 / q \tag{A.28}$$

let $t = \cos\psi$,

$$A_1 = b\frac{8\sigma_f^2}{\pi}\frac{\overline{\zeta}/\overline{\Omega}}{\zeta}\int_{-1}^{1}\int_{0}^{\infty}\left[\varrho - \frac{l_3^2\beta_m B_m B_2}{(r^2t^2+\varkappa^2)}\right]\frac{r^4t^2}{(1+r^2)^3}drdt \tag{A.29}$$

$$\begin{aligned}
A_1 &= b\frac{8\sigma_f^2}{\pi}\frac{\overline{\zeta}/\overline{\Omega}}{\zeta}\left(\frac{\pi}{8}\varrho - l_3^2\beta_m B_m B_2\int_{-1}^{1}\int_{0}^{\infty}\frac{1}{(r^2t^2+\varkappa^2)}\frac{r^2t^2}{(1+r^2)^3}r^2drdt\right) && \text{(A.30)}\\
&= b\frac{8\sigma_f^2}{\pi}\frac{\overline{\zeta}/\overline{\Omega}}{\zeta}\left(\frac{\pi}{8}\varrho - l_3^2\beta_m B_m B_2\int_{0}^{1}\frac{\pi}{16}\frac{2t^2(3\varkappa^4+6\varkappa^2t^2-t^4+8\varkappa^3t)}{(\varkappa^2-t^2)^3}dt\right) && \text{(A.31)}\\
&= b\sigma_f^2\frac{\overline{\zeta}/\overline{\Omega}}{\zeta}\left(\varrho - l_3^2\beta_m B_m B_2\frac{8}{\pi}\frac{\pi}{16}\frac{2}{(1-\varkappa)^2}\right) && \text{(A.32)}\\
&= b\sigma_f^2\frac{\overline{\zeta}/\overline{\Omega}}{\zeta}\left(\varrho - l_3^2\beta_m B_m B_2\frac{1}{(1-\varkappa)^2}\right) && \text{(A.33)}\\
&= b\sigma_f^2\frac{\overline{\zeta}/\overline{\Omega}}{\zeta}In_1 && \text{(A.34)}
\end{aligned}$$

Where:

$$In_1 = \varrho - l_3^2\beta_m B_m B_2\frac{1}{(1-\varkappa)^2} \tag{A.35}$$

### A.1.2 $A_2$ Evaluation

$$A_2 = c\int_{-\infty}^{\infty}\frac{S_{vw}}{\Omega^* + iqk_1 + E_{ij}k_ik_j}d\mathbf{k} \tag{A.36}$$

Since using Eqs. 2.97 and 2.93, so:

$$S_{vw}d\mathbf{k} = E\left[dZ_v dZ_w^*\right] = \epsilon(\varrho+\beta_m Y_m)(\varphi+\sigma_m Y_m)^* S_{ff}d\mathbf{k} \tag{A.37}$$

$$+\epsilon\left[(d_b+d_1)(\chi_b+\chi_1)^* S_{g_bg_b} + (d_l+d_2)(\chi_l+\chi_2)^* S_{g_lg_l}\right]d\mathbf{k} \tag{A.38}$$

Neglecting the local dispersion

$$A_2 = c\int_{-\infty}^{\infty} \frac{\epsilon(\varrho+\beta_m Y_m)(\varphi+\sigma_m Y_m)^* S_{ff}}{\Omega^* + iqk_1} d\mathbf{k} \tag{A.39}$$

$$+ c\int_{-\infty}^{\infty} \frac{\epsilon\left[(d_b+d_1)(\chi_b+\chi_1)^* S_{g_b g_b} + (d_l+d_2)(\chi_l+\chi_2)^* S_{g_l g_l}\right]}{\Omega^* + iqk_1} d\mathbf{k} \tag{A.40}$$

$$= I + II \tag{A.41}$$

**Term $I$**

Using Ea. 2.56, we can write:

$$(\beta_m Y_m)(\sigma_m Y_m)^* = \left[(\beta_m Y_m)\frac{-k_3^2 B_2 - ik_3 k^2}{k^4 + B_2^2 k_3^2}\right]\left[(\sigma_m B_m)\frac{-k_3^2 B_2 + ik_3 k^2}{k^4 + B_2^2 k_3^2}\right] \tag{A.42}$$

$$= (\beta_m Y_m)(\sigma_m B_m)\frac{k_3^4 B_2^2 + k_3^2 k^4}{\left(k^4 + B_2^2 k_3^2\right)^2} \tag{A.43}$$

Putting $Y_m$ into $I$, canceling the odd function of $\mathbf{k}$:

$$I = c\int_{-\infty}^{\infty} \frac{\epsilon\Omega^*}{\left[\Omega^{*2} + q^2 k_1^2\right]}\left[\varrho\varphi - \frac{\eta_m B_m B_2 k_3^2}{\left(k^4 + B_2^2 k_3^2\right)} + \frac{(\beta_m B_m)(\sigma_m B_m)\left(B_2^2 k_3^4 + k_3^2 k^4\right)}{\left(k^4 + B_2^2 k_3^2\right)^2}\right] S_{ff} d\mathbf{k} \tag{A.44}$$

where $\eta_m = \varrho\sigma_m + \varphi\beta_m$. let $u_i = k_i l_i$, so:

$$k^2 = k_1^2 + k_2^2 + k_3^2 = \frac{u_1^2}{l_1^2} + \frac{u_2^2}{l_2^2} + \frac{u_3^2}{l_3^2} = \frac{1}{l_3^2}\left(\frac{l_3^2}{l_1^2}u_1^2 + \frac{l_3^2}{l_2^2}u_2^2 + u_3^2\right) \tag{A.45}$$

Since for a imperfect stratified layer system: $l_1 = l_2 >> l_3$, so:

$$k^2 = k_3^2 >> k_1^2 + k_2^2 \tag{A.46}$$

So similarly to the evaluation of $A_1$ :

$$I = c\int_{-\infty}^{\infty} \frac{\Omega^*}{\left[\Omega^{*2} + q^2 k_1^2\right]}\left[\varrho\varphi - \frac{\eta_m B_m B_2}{\left(k_3^2 + B_2^2\right)} + \frac{(\beta_m B_m)(\sigma_m B_m)\left(B_2^2 + k_3^2\right)}{\left(k_3^2 + B_2^2\right)^2}\right] S_{ff} d\mathbf{k} \tag{A.47}$$

$$I = c\int_{-\infty}^{\infty} \frac{\Omega^*\left[\varrho\varphi\left(k_3^2 + B_2^2\right) - \eta_m B_m B_2 + (\beta_m B_m)(\sigma_m B_m)\right]}{\left[\Omega^{*2} + q^2 k_1^2\right]\left(k_3^2 + B_2^2\right)} S_{ff} d\mathbf{k} \tag{A.48}$$

put $u_i = k_i l_i$ in using Eq. A.17, the integral becomes:

$$I = c\Omega^* l_1^2 \int_{-\infty}^{\infty} \frac{1}{\left[l_1^2\Omega^{*2} + q^2 u_1^2\right]} \left[\varrho\varphi + \left[-\eta_m B_m B_2 + (\beta_m B_m)(\sigma_m B_m)\right] \frac{l_3^2}{\left(u_3^2 + l_3^2 B_2^2\right)}\right] \frac{4\sigma_f^2 u_3^2}{\pi^2 \left(1+u^2\right)^3} \quad \text{(A.49)}$$

$$I = c\sigma_f^2 \frac{\overline{\zeta}/\overline{\Omega}}{\zeta} \left[\varrho\varphi - \frac{\left(\eta_m B_m B_2 l_3^2 - l_3^2 \left(\beta_m B_m\right)(\sigma_m B_m)\right)}{\left(1-\varkappa\right)^2}\right] \quad \text{(A.50)}$$

$$= c\sigma_f^2 \frac{\overline{\zeta}/\overline{\Omega}}{\zeta} In_2 \quad \text{(A.51)}$$

where

$$In_2 = \left[\varrho\varphi - \frac{\left(\eta_m B_m B_2 l_3^2 - l_3^2 \left(\beta_m B_m\right)(\sigma_m B_m)\right)}{\left(1-\varkappa\right)^2}\right] \quad \text{(A.52)}$$

**Term** $II$

$$II = c \int_{-\infty}^{\infty} \frac{\epsilon \left[\left(d_b + d_1\right)\left(\chi_b + \chi_1\right)^* S_{g_b g_b} + \left(d_l + d_2\right)\left(\chi_l + \chi_2\right)^* S_{g_l g_l}\right]}{\Omega^* + iqk_1} d\mathbf{k} \quad \text{(A.53)}$$

$$= i + ii \quad \text{(A.54)}$$

Let us look at the first item $i$. Since:

$$\chi_b d_b = \frac{\partial R_w}{\partial P_c} Y_b D_1 \frac{\partial S_e}{\partial P_c} Y_b^* \quad \text{(A.55)}$$

$$= E_1 \left(Y_b Y_b^*\right) \quad \text{(A.56)}$$

where

$$Y_b = B_b \frac{-k_3^2 B_2 - ik_3 k^2}{k^4 + B_2^2 k_3^2} \quad \text{(A.57)}$$

$$E_1 = D_1 \frac{\partial R_w}{\partial P_c} \frac{\partial S_e}{\partial P_c} \quad \text{(A.58)}$$

$$Y_b Y_b^* = \left[B_b \frac{-k_3^2 B_2 - ik_3 k^2}{k^4 + B_2^2 k_3^2}\right] \left[B_b \frac{-k_3^2 B_2 + ik_3 k^2}{k^4 + B_2^2 k_3^2}\right] \quad \text{(A.59)}$$

$$= B_b^2 \frac{k_3^4 B_2^2 + k_3^2 k^4}{\left(k^4 + B_2^2 k_3^2\right)^2} \quad \text{(A.60)}$$

So:

$$i = c\int_{-\infty}^{\infty} \frac{\epsilon\left(\chi_b d_b + \chi_b^* d_1 + \chi_1 d_b + \chi_1 d_1\right) S_{g_b g_b}}{\Omega^* + iqk_1} d\mathbf{k} \tag{A.61}$$

$$= c\int_{-\infty}^{\infty} \epsilon \frac{\left(E_1\left(Y_b Y_b^*\right) + d_1 \frac{\partial R_w}{\partial P_c} Y_b^* + \chi_1 D_1 \frac{\partial S_e}{\partial P_c} Y_b + \chi_1 d_1\right) S_{g_b g_b}}{\Omega^* + iqk_1} d\mathbf{k} \tag{A.62}$$

$$= c\sigma_{g_b}^2 \frac{\overline{\zeta}/\overline{\Omega}}{\zeta}\left(\frac{E_1 B_b^2 l_3^2}{\left(1-\varkappa\right)^2} - \frac{\left(d_1 \frac{\partial R_w}{\partial P_c} + \chi_1 D_1 \frac{\partial S_e}{\partial P_c}\right) l_3^2 B_b B_2}{\left(1-\varkappa\right)^2} + \chi_1 d_1\right) \tag{A.63}$$

$$= c\sigma_f^2 \frac{\overline{\zeta}/\overline{\Omega}}{\zeta} In_3 \tag{A.64}$$

where:

$$In_3 = \left(\frac{E_1 B_b^2 l_3^2}{\left(1-\varkappa\right)^2} - \frac{\left(d_1 \frac{\partial R_w}{\partial P_c} + \chi_1 D_1 \frac{\partial S_e}{\partial P_c}\right) l_3^2 B_b B_2}{\left(1-\varkappa\right)^2} + \chi_1 d_1\right) \nu_b \tag{A.65}$$

where

$$\nu_b = \frac{\sigma_{g_b}^2}{\sigma_f^2} \tag{A.66}$$

Similarly for term $ii$ :

$$\chi_l d_l = \frac{\partial R_w}{\partial P_c} Y_l D_1 \frac{\partial S_e}{\partial P_c} Y_l^* \tag{A.67}$$

$$= E_1\left(Y_l Y_l^*\right) \tag{A.68}$$

$$ii = c\frac{\sigma_{g_l}^2}{\Omega^*}\left(\frac{E_1 B_l^2 l_3^2}{\left(1-\varkappa\right)^2} - \left(d_2 \frac{\partial R_w}{\partial P_c} + \chi_2 D_1 \frac{\partial S_e}{\partial P_c}\right) l_3^2 B_l B_2 \frac{1}{\left(1-\varkappa\right)^2} + \chi_2 d_2\right) \tag{A.69}$$

$$= c\sigma_f^2 \frac{\overline{\zeta}/\overline{\Omega}}{\zeta} In_4 \tag{A.70}$$

where:

$$In_4 = \left(\frac{E_1 B_l^2 l_3^2}{\left(1-\varkappa\right)^2} - \left(d_2 \frac{\partial R_w}{\partial P_c} + \chi_2 D_1 \frac{\partial S_e}{\partial P_c}\right) l_3^2 B_l B_2 \frac{1}{\left(1-\varkappa\right)^2} + \chi_2 d_2\right) \nu_l \tag{A.71}$$

$$\nu_l = \frac{\sigma_{g_l}^2}{\sigma_f^2} \tag{A.72}$$

So:

$$II = i + ii = c\sigma_f^2 \frac{\overline{\zeta}/\overline{\Omega}}{\zeta} (In_3 + In_4)$$

So:

$$A_2 = I + II = c\sigma_f^2 \frac{\overline{\zeta}/\overline{\Omega}}{\zeta} (In_2 + In_3 + In_4) \tag{A.73}$$

### A.1.3 $A_3$ Evaluation

$$A_3 = d \int_{-\infty}^{\infty} \frac{S_{vv}}{\Omega^* + iqk_1 + E_{ij}k_ik_j} d\mathbf{k} \tag{A.74}$$

Since

$$dZ_v = \epsilon \left[ (\varrho + \beta_m Y_m) dZ_f + \chi_m dZ_{g_m} + \chi_1 dZ_{g_b} + \chi_2 dZ_{g_l} \right] \tag{A.75}$$

so:

$$S_{vv} d\mathbf{k} = E\left[dZ_v dZ_v^*\right] = \epsilon^2 (\varrho + \beta_m Y_m)(\varrho + \beta_m Y_m)^* S_{ff} d\mathbf{k} \tag{A.76}$$

$$+ \epsilon^2 \left[ (\chi_b + \chi_1)(\chi_b + \chi_1)^* S_{g_b g_b} + (\chi_l + \chi_2)(\chi_l + \chi_2)^* S_{g_l g_l} \right] d\mathbf{k} \tag{A.77}$$

$$A_3 = d \int_{-\infty}^{\infty} \frac{\epsilon^2 (\varrho + \beta_m Y_m)(\varrho + \beta_m Y_m)^* S_{ff}}{\Omega^* + iqk_1 + E_{ij}k_ik_j} d\mathbf{k} \tag{A.78}$$

$$+ d \int_{-\infty}^{\infty} \frac{\epsilon^2 \left[ (\chi_b + \chi_1)(\chi_b + \chi_1)^* S_{g_b g_b} + (\chi_l + \chi_2)(\chi_l + \chi_2)^* S_{g_l g_l} \right]}{\Omega^* + iqk_1 + E_{ij}k_ik_j} d\mathbf{k} \tag{A.79}$$

$$= I + II \tag{A.80}$$

**Term $I$**

Putting $Y_m$ in Eq. 2.56 into $I$, canceling the odd function of $\mathbf{k}$:

$$I = d \int_{-\infty}^{\infty} \frac{\epsilon^2 (\Omega^* + E_{ij}k_ik_j)}{\left[ (\Omega^* + E_{ij}k_ik_j)^2 + q^2 k_1^2 \right]} \left[ \varrho^2 - \frac{2\varrho\beta_m B_m B_2 k_3^2}{(k^4 + B_2^2 k_3^2)} + \frac{(\beta_m B_m)^2 (B_2^2 k_3^4 + k_3^2 k^4)}{(k^4 + B_2^2 k_3^2)^2} \right] S_{ff} d\mathbf{k} \tag{A.81}$$

So, this is very similar to the form $I$ in evaluation of $A_2$, only replace $\varphi, \sigma_m$ by $\varrho$, $\beta_m$ respectively, so:

$$I = d\sigma_f^2 \frac{\overline{\zeta}/\overline{\Omega}}{\zeta} In_2' \tag{A.82}$$

where

$$In_2' = \varrho^2 - \left[2\varrho\beta_m B_m B_2 l_3^2 + l_3^2(\beta_m B_m)^2\right] \frac{1}{(1-\varkappa)^2} \tag{A.83}$$

Similarly, the 2nd part $II$ is very similar to the $II$ in evaluation of $A_2$, so:

$$II = d\int_{-\infty}^{\infty} \frac{\epsilon^2 \left[(\chi_b+\chi_1)(\chi_b+\chi_1)^* S_{g_b g_b} + (\chi_l+\chi_2)(\chi_l+\chi_2)^* S_{g_l g_l}\right]}{\Omega^* + iqk_1 + E_{ij}k_i k_j} d\mathbf{k} \tag{A.84}$$

$$= i + ii \tag{A.85}$$

$$\chi_b^2 = \frac{\partial R_w}{\partial P_c} Y_b \frac{\partial R_w}{\partial P_c} Y_b^* \tag{A.86}$$

$$= E_2 Y_b Y_b^* \tag{A.87}$$

where

$$E_2 = \left(\frac{\partial R_w}{\partial P_c}\right)^2 \tag{A.88}$$

$$i = d\frac{\sigma_{g_b}^2}{\Omega^*}\left(\left[l_3^2 E_2 B_b^2 - 2\frac{\partial R_w}{\partial P_c}\chi_1 l_3^2 B_b B_2\right]\frac{1}{(1-\varkappa)^2} + \chi_1^2\right)\nu_b \tag{A.89}$$

$$= d\frac{\sigma_f^2}{\Omega^*} In_3' \tag{A.90}$$

$$In_3' = \left(\left[l_3^2 E_2 B_b^2 - 2\frac{\partial R_w}{\partial P_c}\chi_1 l_3^2 B_b B_2\right]\frac{1}{(1-\varkappa)^2} + \chi_1^2\right)\nu_b \tag{A.91}$$

Similarly:

$$ii = d\sigma_{g_l}^2 \frac{\overline{\zeta}/\overline{\Omega}}{\zeta}\left(\left(l_3^2 E_2 B_l^2 - 2\frac{\partial R_w}{\partial P_c}\chi_2 l_3^2 B_l B_2\right)\frac{1}{(1-\varkappa)^2} + \chi_2^2\right) \tag{A.92}$$

$$= d\sigma_f^2 \frac{\overline{\zeta}/\overline{\Omega}}{\zeta} In_4' \tag{A.93}$$

$$In_4' = \left(\left(l_3^2 E_2 B_l^2 - 2\frac{\partial R_w}{\partial P_c}\chi_2 l_3^2 B_l B_2\right)\frac{1}{(1-\varkappa)^2} + \chi_2^2\right)\nu_l \tag{A.94}$$

So:

$$A_3 = I + II = d\sigma_f^2 \frac{\overline{\zeta}/\overline{\Omega}}{\zeta}(In_2' + In_3' + In_4') \tag{A.95}$$

So,

$$I_1 = A_1 + A_2 + A_3 = b\sigma_f^2 \frac{\overline{\zeta}/\overline{\Omega}}{\zeta} In_1 + c\sigma_f^2 \frac{\overline{\zeta}/\overline{\Omega}}{\zeta}(In_2 + In_3 + In_4)$$
$$+ d\sigma_f^2 \frac{\overline{\zeta}/\overline{\Omega}}{\zeta}(In_2' + In_3' + In_4') \quad \text{(A.96)}$$
$$= \sigma_f^2 \frac{\overline{\zeta}/\overline{\Omega}}{\zeta}\left[bIn_1 + c\left(In_2 + In_3 + In_4\right) + d\left(In_2' + In_3' + In_4'\right)\right] \quad \text{(A.97)}$$

And

$$I_2 = A_3/d = \sigma_f^2 \frac{\overline{\zeta}/\overline{\Omega}}{\zeta}(In_2' + In_3' + In_4') \quad \text{(A.98)}$$

## A.2 Evaluation of $I_3$

According to Eq. A.1,

$$S_{hh}d\mathbf{k} = E\left[dZ_h dZ_h^*\right] = E\left(bdZ_f + cdZ_W + ddZ_v + dZ_{g_h}\right)\left(bdZ_f^* + cdZ_W^* + ddZ_v^* + dZ_{g_h}^*\right) \quad \text{(A.99)}$$
$$= \left(b^2 S_{ff} + c^2 S_{WW} + d^2 S_{vv} + S_{g_h g_h} + 2bcS_{fW} + 2bdS_{fv} + 2cdS_{vW}\right)d\mathbf{k} \quad \text{(A.100)}$$

So:

$$I_3 = A_4 + A_5 + A_6 + A_7 + A_8 + A_9 + A_{10} \quad \text{(A.101)}$$

where

$$A_4 = b^2 \int_{-\infty}^{\infty} \frac{S_{ff}}{\Omega^* + iqk_1 + E_{ij}k_i k_j} d\mathbf{k} \quad \text{(A.102)}$$

$$A_5 = c^2 \int_{-\infty}^{\infty} \frac{S_{WW}}{\Omega^* + iqk_1 + E_{ij}k_i k_j} d\mathbf{k} \quad \text{(A.103)}$$

$$A_6 = d^2 \int_{-\infty}^{\infty} \frac{S_{vv}}{\Omega^* + iqk_1 + E_{ij}k_i k_j} d\mathbf{k} = dA_3 \quad \text{(A.104)}$$

$$A_7 = \int_{-\infty}^{\infty} \frac{S_{g_h g_h}}{\Omega^* + iqk_1 + E_{ij}k_i k_j} d\mathbf{k} \quad \text{(A.105)}$$

$$A_8 = 2bc \int_{-\infty}^{\infty} \frac{S_{fW}}{\Omega^* + iqk_1 + E_{ij}k_i k_j} d\mathbf{k} \quad \text{(A.106)}$$

$$A_9 = 2bd \int_{-\infty}^{\infty} \frac{S_{fv}}{\Omega^* + iqk_1 + E_{ij}k_i k_j} d\mathbf{k} = 2dA_1 \quad \text{(A.107)}$$

$$A_{10} = 2cd \int_{-\infty}^{\infty} \frac{S_{vW}}{\Omega^* + iqk_1 + E_{ij}k_ik_j} d\mathbf{k} = 2dA_2 \tag{A.108}$$

Since:

$$A_4 = b^2 \int_{-\infty}^{\infty} \frac{S_{ff}}{\Omega^* + iqk_1 + E_{ij}k_ik_j} d\mathbf{k} \tag{A.109}$$

This is very similar to the part $II$ of $A_2$, so:

$$A_4 = b^2\sigma_f^2 \frac{\overline{\zeta}/\overline{\Omega}}{\zeta} \tag{A.110}$$

According to Eq. 2.97, we can write:

$$\begin{aligned} S_{ww}d\mathbf{k} &= (\varphi + \sigma_m Y_m)(\varphi + \sigma_m Y_m)^* S_{ff}d\mathbf{k} + (d_b + d_1)(d_b + d_1)^* S_{g_bg_b}d\mathbf{k} + (d_l + d_2)(d_l + d_2)^* S_{g_lg_l}d\mathbf{k} \\ &= I + II + III \end{aligned} \tag{A.112}$$

So, this is very similar to the form $I$ in evaluation of $A_2$, only let $\varphi$ replace $\varrho, \sigma_m$ replace $\beta_m$ here, so :

$$I = c^2 \frac{\sigma_f^2}{2} \frac{\overline{\zeta}/\overline{\Omega}}{\zeta} In_2'' \tag{A.113}$$

Similarly, the 2nd part $II$ is very similar to the $II$ in evaluation of $A_2$, so:

$$d_b d_b^* = D_1 \frac{\partial S_e}{\partial P_c} Y_b D_1 \frac{\partial S_e}{\partial P_c} Y_b^* \tag{A.114}$$

$$= E_3 Y_b Y_b^* \tag{A.115}$$

$$E_3 = D_1^2 \left( \frac{\partial S_e}{\partial P_c} \right)^2 \tag{A.116}$$

So:

$$A_5 = c^2\sigma_f^2 \frac{\overline{\zeta}/\overline{\Omega}}{\zeta} (In_2'' + In_3'' + In_4'') \tag{A.117}$$

where

$$In_2'' = \left( \varphi^2 - 2\varphi(\sigma_m B_m) B_2 l_3^2 \frac{1}{(1-\varkappa)^2} + (\sigma_m B_m)^2 l_3^2 \frac{1}{(1-\varkappa)^2} \right) \tag{A.118}$$

$$In_3'' = \nu_b \left[ \frac{E_3 B_b^2 l_3^2}{(1-\varkappa)^2} - 2D_1^2 \frac{\partial S_e}{\partial P_c} \frac{\partial S_e}{\partial B} B_b B_2 l_3^2 \frac{1}{(1-\varkappa)^2} + d_1^2 \nu_b \right] \tag{A.119}$$

$$In_4'' = \nu_l \left[ \frac{E_3 B_l^2 l_3^2}{(1-\varkappa)^2} - 2D_1^2 \frac{\partial S_e}{\partial P_c} \frac{\partial S_e}{\partial L} B_l B_2 l_3^2 \frac{1}{(1-\varkappa)^2} + \nu_l d_2^2 \right] \tag{A.120}$$

And $A_6$ is obtained from the result of $A_3$ :

$$A_6 = d^2 \int_{-\infty}^{\infty} \frac{S_{vv}}{\Omega^* + iqk_1 + E_{ij}k_i k_j} d\mathbf{k} = dA_3 = d^2 \sigma_f^2 \frac{\overline{\zeta}/\overline{\Omega}}{\zeta} (In_2' + In_3' + In_4') \tag{A.121}$$

$$A_7 = \int_{-\infty}^{\infty} \frac{S_{g_h g_h}}{\Omega^* + iqk_1 + E_{ij}k_i k_j} d\mathbf{k} = \sigma_f^2 \frac{\overline{\zeta}/\overline{\Omega}}{\zeta} \nu_h \tag{A.122}$$

where $\nu_h = \sigma_{g_h}^2 / \sigma_f^2$

$$A_8 = 2bc \int_{-\infty}^{\infty} \frac{S_{fW}}{\Omega^* + iqk_1 + E_{ij}k_i k_j} d\mathbf{k} \tag{A.123}$$

very similar to $A_1$, only $\varrho = \varphi, \beta_m = \sigma_m$

$$A_8 = bc\sigma_f^2 \frac{\overline{\zeta}/\overline{\Omega}}{\zeta} In_1' \tag{A.124}$$

$$A_9 = 2bd \int_{-\infty}^{\infty} \frac{S_{fv}}{\Omega^* + iqk_1 + E_{ij}k_i k_j} d\mathbf{k} = 2dA_1 = bd\sigma_f^2 \frac{\overline{\zeta}/\overline{\Omega}}{\zeta} In_1 \tag{A.125}$$

$$A_{10} = 2cd \int_{-\infty}^{\infty} \frac{S_{vW}}{\Omega^* + iqk_1 + E_{ij}k_i k_j} d\mathbf{k} = 2dA_2 = 2cd\sigma_f^2 \frac{\overline{\zeta}/\overline{\Omega}}{\zeta} (In_2 + In_3 + In_4) \tag{A.126}$$

So:

$$I_3 = \sigma_f^2 \frac{\overline{\zeta}/\overline{\Omega}}{\zeta} \begin{bmatrix} 2bcIn_1' + 2bdIn_1 + c^2(In_2'' + In_3'' + In_4'') \\ +d^2(In_2' + In_3' + In_4') + 2cd(In_2 + In_3 + In_4) + \nu_h + b^2 \end{bmatrix} \tag{A.127}$$

Since:

$$I_1 = \sigma_f^2 \frac{\overline{\zeta}/\overline{\Omega}}{\zeta} \left[ bIn_1 + c\left(In_2 + In_3 + In_4\right) + d\left(In_2' + In_3' + In_4'\right) \right] \tag{A.128}$$

$$I_2 = \sigma_f^2 \frac{\overline{\zeta}/\overline{\Omega}}{\zeta} (In_2' + In_3' + In_4') \tag{A.129}$$

$$q_e = q - \frac{\overline{\zeta}/\overline{\Omega}}{\zeta} F_1 \tag{A.130}$$

$$D_e \approx \frac{\overline{\zeta}/\overline{\Omega}}{\zeta} F_2 \tag{A.131}$$

$$\Omega_e = \overline{\Omega} - \frac{\overline{\zeta}/\overline{\Omega}}{\zeta} F_3 \tag{A.132}$$

$$F_1 = 2\overline{\Omega}\sigma_f^2 \left(bIn_1 + c(In_2 + In_3 + In_4) + d(In_2' + In_3' + In_4')\right) \tag{A.133}$$

$$= 2\overline{\Omega v' h'} \tag{A.134}$$

$$F_2 = \sigma_f^2 \left(In_2' + In_3' + In_4'\right) \tag{A.135}$$

$$= \sigma_v^2 \tag{A.136}$$

$$F_3 = \sigma_f^2 \overline{\Omega}^2 \left[ \begin{array}{c} \nu_h + b^2 + bcIn_1' + bdIn_1 + c^2(In_2'' + In_3'' + In_4'') + \\ d^2(In_2' + In_3' + In_4') + 2cd(In_2 + In_3 + In_4) \end{array} \right] \tag{A.137}$$

$$= \overline{\Omega}^2 \sigma_h^2 \tag{A.138}$$

So:

$$q_e = q - \frac{2q\overline{v'h'}}{\Phi} \tag{A.139}$$

$$D_e = \frac{q^2 \sigma_v^2}{\overline{\Omega}\Phi} \tag{A.140}$$

$$\Omega_e = \overline{\Omega}\left(1 - \frac{\sigma_h^2}{\Phi}\right) \tag{A.141}$$

where

$$\Phi = \frac{\zeta}{\overline{\zeta}} \tag{A.142}$$

So the results based on the decomposition of the cross spectra using local model are exactly the same as that derived directly in Chapter 4. This confirms the accuracy of the analysis results based on the spectral method.

# Appendix B

# Boundary Integral Evaluation

The effective properties at the boundary affecting zone can be evaluated by the integral presented in Eq 4.155, so we can express $I_1$ using Eq. 4.148 as:

$$I_1 = M_1 - M_2 \tag{B.1}$$

where

$$M_1 = \int_{-\infty}^{\infty} \frac{S_{vv} d\mathbf{k}}{\Omega^* - iq_1 k_1} \tag{B.2}$$

$$M_2 = \int_{-\infty}^{\infty} \frac{\exp(-\beta x_1)}{\Omega^* - iq_1 k_1} S_{vv} d\mathbf{k} \tag{B.3}$$

$$= \int_{-\infty}^{\infty} \frac{\exp\left(-\frac{\Omega^* - iqk_1}{q} x_1\right)}{\Omega^* - iq_1 k_1} S_{vv} d\mathbf{k} \tag{B.4}$$

Since:

$$\exp\left(-\frac{\Omega^* - iqk_1}{q} x_1\right) = \exp\left(-\frac{\Omega^*}{q} x_1\right) \exp(ik_1 x_1) \tag{B.5}$$

$$= \exp\left(-\frac{\Omega^*}{q} x_1\right) [\cos(k_1 x_1) + i \sin(k_1 x_1)] \tag{B.6}$$

So:

$$M_2 = \exp\left(-\frac{\Omega^*}{q}x_1\right)\int_{-\infty}^{\infty}\frac{S_{vv}}{\Omega^* - iq_1k_1}\left[\cos\left(k_1x_1\right) + i\sin\left(k_1x_1\right)\right]d\mathbf{k} \tag{B.7}$$

Cancel the odd term about $k_1$:

$$\begin{aligned} M_2 &= \exp\left(-\frac{\Omega^*}{q}x_1\right)\int_{-\infty}^{\infty}\frac{\left[\Omega^*\cos\left(k_1x_1\right) - q_1k_1\sin\left(k_1x_1\right)\right]}{\left(\Omega^{*2} + q^2k_1^2\right)}S_{vv}d\mathbf{k} & \text{(B.8)}\\ &= \exp\left(-\frac{\Omega^*}{q}x_1\right)\left(I_A - I_B\right) & \text{(B.9)}\end{aligned}$$

where

$$\begin{aligned} I_A &= \int_{-\infty}^{\infty}\frac{\Omega^*\cos\left(k_1x_1\right)}{\left(\Omega^{*2} + q^2k_1^2\right)}S_{vv}d\mathbf{k} & \text{(B.10)}\\ I_B &= \int_{-\infty}^{\infty}\frac{qk_1\sin\left(k_1x_1\right)}{\left(\Omega^{*2} + q^2k_1^2\right)}S_{vv}d\mathbf{k} & \text{(B.11)}\end{aligned}$$

Let $k_1 = \frac{u_1}{l_1}$,after evaluating the integral in terms of $u_2$ and $u_3$, we have:

$$\begin{aligned} I_A &= Const\int_{-\infty}^{\infty}\frac{\cos\left(\frac{u_1}{l_1}x_1\right)}{\left[\zeta^2 + u_1^2\right]}\frac{1}{\left(1 + u_1^2\right)}du_1 & \text{(B.12)}\\ &= Const\frac{\pi}{\zeta^2 - 1}\left[\exp\left(-\frac{x}{l_1}\right) - \frac{1}{\zeta}\exp\left(-\frac{x}{l_1}\zeta\right)\right] & \text{(B.13)}\end{aligned}$$

$$\begin{aligned} I_B &= Const\frac{q}{\Omega^* l_1}\int_{-\infty}^{\infty}\frac{u_1\sin\left(\frac{u_1}{l_1}x_1\right)}{\left[\zeta^2 + u_1^2\right]}\frac{1}{\left(1 + u_1^2\right)}du_1 & \text{(B.14)}\\ &= Const\frac{1}{\zeta}\frac{\pi}{\zeta^2 - 1}\left[\exp\left(-\frac{x}{l_1}\right) - \exp\left(-\frac{x}{l_1}\zeta\right)\right] & \text{(B.15)}\end{aligned}$$

Since the corresponding core integral in $M_1$ gives:

$$\begin{aligned} M_1 &= Const\int_{-\infty}^{\infty}\frac{1}{\left[\zeta^2 + u_1^2\right]}\frac{1}{4\left(1 + u_1^2\right)}du_1 & \text{(B.16)}\\ &= Const\frac{\pi}{\zeta(\zeta + 1)} & \text{(B.17)}\end{aligned}$$

So:

$$M_2 = \exp\left(-\frac{\Omega^*}{q}x_1\right)(I_A - I_B) \tag{B.18}$$

$$= \exp\left(-\frac{\Omega^*}{q}x_1\right)\frac{\zeta}{\zeta-1}\begin{pmatrix}\left[\exp\left(-\frac{x}{l_1}\right)-\frac{1}{\zeta}\exp\left(-\frac{x}{l_1}\zeta\right)\right]\\ -\frac{1}{\zeta}\left[\exp\left(-\frac{x}{l_1}\right)-\exp\left(-\frac{x}{l_1}\zeta\right)\right]\end{pmatrix}M_1 \tag{B.19}$$

$$= \exp\left(-\frac{\Omega^*}{q}x_1\right)\frac{\zeta}{\zeta-1}\left[\exp\left(-\frac{x}{l_1}\right)-\frac{1}{\zeta}\exp\left(-\frac{x}{l_1}\right)\right]M_1 \tag{B.20}$$

$$= \exp\left(-\frac{\Omega^*}{q}x_1\right)\exp\left(-\frac{x}{l_1}\right)M_1 \tag{B.21}$$

$$= M_1\exp\left(-\left(\frac{\Omega^*}{q}+\frac{1}{l_1}\right)x_1\right) \tag{B.22}$$

So:

$$I_1 = M_1 - M_2 \tag{B.23}$$

$$= M_1\left[1-\exp\left(-\eta x_1\right)\right] \tag{B.24}$$

where

$$\eta = \frac{\Omega^*}{q}+\frac{1}{l_1} = \frac{\zeta+1}{l_1} = \Phi\frac{\overline{\Omega}}{q} \tag{B.25}$$

So:

$$I_1 = M_1\left[1-\exp\left(-\left(\zeta+1\right)\frac{x_1}{l_1}\right)\right] \tag{B.26}$$

So the boundary effect is determined by $\Omega^*, q$ and $l_1$ where

$$\zeta = \frac{\Omega^* l_1}{q} \tag{B.27}$$

So:

$$I_1 = M_1\left[1-\exp\left(-\left(\zeta+1\right)\frac{x_1}{l_1}\right)\right] \tag{B.28}$$

Since the effective flow rate at the boundary can be obtained as in Eq. 4.157 and:

$$\frac{dI_1}{dx_1} = \frac{d}{dx_1}\left[M_1\left[1-\exp\left(-\eta x_1\right)\right]\right] \tag{B.29}$$

$$= -M_1\left(-\eta\right)\exp\left(-\eta x_1\right) \tag{B.30}$$

$$= M_1\eta\exp\left(-\eta x_1\right) \tag{B.31}$$

So:

$$q_e = q - 2q\frac{\overline{v'h'}}{\Phi}\left(1-\left(1-\frac{q\Phi}{\alpha}\right)\exp\left(-\eta x_1\right)\right) \tag{B.32}$$

Similarly $D_e$ and $\Omega_e$ can be derived using the same method:

$$D_e = \frac{q^2\sigma_v^2}{\overline{\Omega}\Phi}\left[1-\exp\left(-\eta x_1\right)\right] \tag{B.33}$$

$$\Omega_e = \overline{\Omega} - \overline{\Omega}\frac{\sigma_h^2}{\Phi}\left[1-\left(1-\frac{q\Phi}{\alpha}\right)\exp\left(-\eta x_1\right)\right] \tag{B.34}$$

# Appendix C

# Coupled Process for Transport

Here we evaluate the relative impact of a positive DNAPL hydraulic gradient in the mean water flow direction on the transport results. The integrals in Eqs. 4.63 to 4.65 are reevaluated by applying a positive DNAPL gradient in the term of $Y_m$.

## C.1 $Y_m$

$Y_m$ is the key parameter to evaluate the multiphase flow properties in the source zone. From Jacobs 1998, the general form is given in Eq. 2.54. By assuming uniform mean flow $\frac{\partial \overline{P_c}}{\partial x_i} = 0$ :

$$\begin{aligned} Y_m &= \frac{ik_i\left(-k^2 B_{m,i}\right)}{k^4 + ik^2 k_i B_{2,i}} = \frac{ik_i\left(-B_{m,i}\right)}{k^2 + ik_i B_{2,i}} \\ &= \frac{-i\left(k_1 B_{m,1} + k_2 B_{m,2} + k_3 B_{m,3}\right)}{k^2 + i\left(k_1 B_{2,1} + k_2 B_{2,2} + k_3 B_{2,3}\right)} \end{aligned} \tag{C.1}$$

where

$$B_{m,i} = \overline{J}_{o,i}\frac{\partial R_o}{\partial \Phi_m} - \overline{J}_{w,i}\frac{\partial R_w}{\partial \Phi_m} \tag{C.2}$$

$$B_{2,i} = \overline{J}_{o,i}\frac{\partial R_o}{\partial P_c} - \overline{J}_{w,i}\frac{\partial R_w}{\partial P_c} \tag{C.3}$$

Eq. C.1 becomes:

$$Y_m = \frac{-\left(k_1 B_{m,1} + k_2 B_{m,2} + k_3 B_{m,3}\right)\left(k_1 B_{2,1} + k_2 B_{2,2} + k_3 B_{2,3}\right) - ik^2\left(k_1 B_{m,1} + k_2 B_{m,2} + k_3 B_{m,3}\right)}{k^4 + \left(k_1 B_{2,1} + k_2 B_{2,2} + k_3 B_{2,3}\right)^2} \tag{C.4}$$

for horizontal flow, uniform mean flow means

$$\overline{J}_{o,1} = \overline{J}_{w,1} \tag{C.5}$$

where

$$\begin{aligned} B_{m,1} &= \overline{J}_{o,1}\frac{\partial R_o}{\partial \Phi_m} - \overline{J}_{w,1}\frac{\partial R_w}{\partial \Phi_m} \\ &= \overline{J}_{w,1}\left(\frac{\partial R_o}{\partial \Phi_m} - \frac{\partial R_w}{\partial \Phi_m}\right) \qquad \text{(C.6)} \\ &= c_m \overline{J}_{w,1} \qquad \text{(C.7)} \end{aligned}$$

and

$$c_m = \frac{\partial R_o}{\partial \Phi_m} - \frac{\partial R_w}{\partial \Phi_m} \tag{C.8}$$

Assuming mean flow in the horizontal transverse direction for both phase are zero:

$$\overline{J}_{o,2} = \overline{J}_{w,2} = 0 \tag{C.9}$$

So

$$B_{m,2} = 0 \tag{C.10}$$

For uniform mean vertical flow and assume $\overline{J}_{w,3} << \overline{J}_{o,3}$

$$\overline{J}_{o,3} = -\triangle \rho g \tag{C.11}$$

where $\triangle \rho = \rho_{o-}\rho_w$.

$$B_{m,3} = \overline{J}_{o,3}\frac{\partial R_o}{\partial \Phi_m} \tag{C.12}$$

Similarly:

$$B_{2,1} = c_2 \overline{J}_{w,1} \tag{C.13}$$

where

$$c_2 = \frac{\partial R_o}{\partial P_c} - \frac{\partial R_w}{\partial P_c} \tag{C.14}$$

$$B_{2,2} = 0 \tag{C.15}$$

$$B_{2,3} = \overline{J}_{o,3} \frac{\partial R_o}{\partial P_c} \tag{C.16}$$

Using Eqs. C.7, C.10, C.12, C.13, C.15, C.16 and C.4

$$Y_m = \frac{-\left(k_1 B_{m,1} + k_3 B_{m,3}\right)\left(k_1 B_{2,1} + k_3 B_{2,3}\right) - ik^2\left(k_1 B_{m,1} + k_3 B_{m,3}\right)}{k^4 + \left(k_1 B_{2,1} + k_3 B_{2,3}\right)^2} \tag{C.17}$$

$$= \frac{A_m + E_m i}{D} \tag{C.18}$$

where

$$D = k^4 + \left(k_1 B_{2,1} + k_3 B_{2,3}\right)^2 \tag{C.19}$$

$$A_m = -\left(k_1 B_{m,1} + k_3 B_{m,3}\right)\left(k_1 B_{2,1} + k_3 B_{2,3}\right) \tag{C.20}$$

$$E_m = -k^2\left(k_1 B_{m,1} + k_3 B_{m,3}\right) \tag{C.21}$$

## C.2 Evaluation of $A_1$

$A_1$ in Eq. A.6 is one of the integrals evaluated to study the effective parameters for transport process. Since all integrals are evaluated using similar techniques and approximations, $A_1$ can be a good representation of all integrals.

Since

$$A_1 = b\int_{-\infty}^{\infty} \frac{S_{vf}}{\Omega^* + iqk_1 + E_{ij}k_i k_j} dk = b\int_{-\infty}^{\infty} \frac{\epsilon[\alpha + \beta_m Y_m]}{\Omega^* + iqk_1 + E_{ij}k_i k_j} S_{ff} dk \tag{C.22}$$

Let us look at

$$int = \frac{[\alpha + \beta_m Y_m]}{\Omega^* + iqk_1 + E_{ij}k_i k_j} = \frac{[\alpha + \beta_m \frac{A_m + E_m i}{D}]}{G + Hi} \tag{C.23}$$

$$= \frac{(\alpha D + A_m \beta_m) G + \beta_m E_m H + [\beta_m E_m G - (\alpha D + A_m \beta_m) H] i}{D(G^2 + H^2)} \tag{C.24}$$

Let us look at $D$ and let $k_1 = \frac{u_1}{l_1}, k_3 = \frac{u_3}{l_3}$ :

$$D = k^4 + (k_1 B_{2,1} + k_3 B_{2,3})^2 \tag{C.25}$$

$$= \left( \left( \frac{u_1}{l_1} \right)^2 + \left( \frac{u_2}{l_2} \right)^2 + \left( \frac{u_3}{l_3} \right)^2 \right)^2 + \left( \frac{u_1}{l_1} B_{2,1} + \frac{u_3}{l_3} B_{2,3} \right)^2 \tag{C.26}$$

For imperfectly stratified system: $\delta = \frac{l_3}{l_1} = \frac{l_3}{l_2} << 1$, so if $B_{2,1} < or \approx B_{2,3}$ (The validity of the approximation is shown at the end of the development.), then

$$D = \frac{u_3^4}{l_3^4} + \frac{1}{l_3^2 l_1^2} u_3^2 \hat{B}_{2,3}^2 \tag{C.27}$$

$$D = k_3^4 + k_3^2 B_{2,3}^2 \tag{C.28}$$

Similarly:

$$A_m = -(k_1 B_{m,1} + k_3 B_{m,3}) k_3 B_{2,3} \tag{C.29}$$

$$E_m = -k_3^2 (k_1 B_{m,1} + k_3 B_{m,3}) \tag{C.30}$$

So put Eq. C.28 into Eq. C.24. Since the integral is from $-\infty$ to $\infty$, so cancel the odd function of $\mathbf{k}$. so Eq. C.24 becomes:

$$int = \frac{\alpha D G + \beta_m A_m G}{D(G^2 + H^2)} \tag{C.31}$$

put Eq. C.31 into Eq. C.22 and neglect the dispersion. Then

$$A_1 = b\int_{-\infty}^{\infty} \frac{\Omega^*\epsilon[\alpha\left(k_3^4 + k_3^2 B_{2,3}^2\right) - \beta_m\left(k_1 B_{m,1} + k_3 B_{m,3}\right) k_3 B_{2,3}]}{\left(\Omega^{*2} + q^2 k_1^2\right)\left(k_3^4 + k_3^2 B_{2,3}^2\right)} S_{ff} dk \tag{C.32}$$

$$= b\int_{-\infty}^{\infty} \frac{\Omega^*\epsilon[\alpha\left(k_3^4 + k_3^2 B_{2,3}^2\right) - \beta_m B_{m,3} B_{2,3} k_3^2]}{\left(\Omega^{*2} + q^2 k_1^2\right)\left(k_3^4 + k_3^2 B_{2,3}^2\right)} S_{ff} dk \tag{C.33}$$

This integral is exactly the same as the decoupling case. Similarly by applying similar analysis to the other integrals, the same result can be obtained. So the inclusion of horizontal DNAPL hydraulic gradient has little impact on the effective properties obtained assuming static DNAPL saturation field. This can prove the approximation of decoupling is appropriate for transport process based on imperfect stratified assumption. The transport process within DNAPL source zone is not affected significantly by slowly flowing DNAPL in the mean flow direction in terms of effective properties.

## C.3 Key Assumption

The assumption of $|B_{2,3}| > or \approx |B_{2,1}|$ is the key to have above conclusion plausible according to the analysis given. Be noted that the $B_{2,3}$ here is $B_2$ in decoupling case. And $B_{2,1} = 0$ in decoupled case for $\overline{J}_{w,1} = 0$.

$$B_{2,1} = \left(\frac{\partial R_o}{\partial P_c} - \frac{\partial R_w}{\partial P_c}\right)\overline{J}_{w,1} \tag{C.34a}$$

$$= \left(\frac{\partial R_o}{\partial h_c} - \frac{\partial R_w}{\partial h_c}\right)\frac{\overline{J}_{w,1}}{\rho_w g} \tag{C.34b}$$

$$B_{2,3} = \overline{J}_{o,3}\frac{\partial R_o}{\partial P_c} = \frac{\overline{J}_{o,3}}{\rho_w g}\frac{\partial R_o}{\partial h_c} \tag{C.35}$$

where

$$h_c = P_c/\rho_w g \tag{C.36}$$

According to Eq. 2.55

$$J_{\beta,i} = -\left(\frac{\partial P_\beta}{\partial x_i} + \rho_\beta \overrightarrow{g}\right) \tag{C.37}$$

Since uniform mean flow, so:

$$\overline{J}_{o,3} = \overline{J}_{w,3} - \triangle\rho g \simeq -\triangle\rho g \tag{C.38}$$

Applying the Borden site mean parameters: $\frac{\partial R_o}{\partial h_c} \simeq 7.84(1/cm)$, $\frac{\partial R_w}{\partial h_c} \simeq -0.035(1/cm)$, $\overline{J}_{o,3}/\rho_w g = -\frac{\triangle\rho g}{\rho_w g} = -0.6$, So:

$$B_{2,3} = \frac{\overline{J}_{o,3}}{\rho_w g}\frac{\partial R_o}{\partial h_c} = -0.6 \times 7.84 = -4.7(1/cm) \tag{C.39}$$

Since $\overline{J}_{w,1}/\rho_w g = 0.005$

$$B_{2,1} = \left(\frac{\partial R_o}{\partial h_c} - \frac{\partial R_w}{\partial h_c}\right)\frac{\overline{J}_{w,1}}{\rho_w g} \tag{C.40a}$$

$$= (7.84 + 0.035) \times 0.005 \tag{C.40b}$$

$$= 0.039(1/cm) \tag{C.40c}$$

So $|B_{2,3}| >> |B_{2,1}|$. And the approximation is appropriate here.

# Appendix D

# Derivation of Relationship Between Covariance of Lognormal and Normal Distributed Random Variables

Assume $Y$ is normal distributed and $X$ is lognormal

$$H = \ln \Omega \tag{D.41}$$

and:

$$H = \overline{H} + h' \tag{D.42}$$

$$\Omega = \overline{\Omega} + \Omega' \tag{D.43}$$

Assume $\Omega$ is lognormal distributed, so:

$$\Omega' = \Omega - \overline{\Omega} = e^{\overline{H}}(e^{h'} - e^{\frac{\sigma_h^2}{2}}) \tag{D.44}$$

$$= \overline{\Omega}\left(e^{h' - \frac{\sigma_h^2}{2}} - 1\right) \tag{D.45}$$

$$= \overline{\Omega} X \tag{D.46}$$

where

$$X = e^{h'-\frac{\sigma_h^2}{2}} - 1 \tag{D.47}$$

$$= \widehat{X} - 1 \tag{D.48}$$

where

$$\widehat{X} = e^{h'-\frac{\sigma_h^2}{2}} \tag{D.49}$$

Since $\overline{\Omega}$ is a constant, so $X$ and $\widehat{X}$ bear lognormal distribution too. Assuming $u$ bears normal distribution and both $X$ and $u$ are with zero mean:

$$\overline{X} = 0 \tag{D.50}$$

$$\overline{u} = 0 \tag{D.51}$$

so:

$$X = x' \tag{D.52}$$

$$u = u' \tag{D.53}$$

So:

$$\overline{x'u'} = E[X,u] = E\left[\widehat{X},u\right] \tag{D.54}$$

Since:

$$E\left[\widehat{X},u\right] = \int_{-\infty}^{\infty}\int_{0}^{\infty} \widehat{x}u \; f_{\widehat{X},u}(\widehat{x},u)\, d\widehat{x}du \tag{D.55}$$

Since let

$$M = \ln \widehat{X} = h - \frac{\sigma_h^2}{2} \tag{D.56}$$

So:

$$E\left[\widehat{X},u\right] = \int_{-\infty}^{\infty}\int_{-\infty}^{\infty} e^{M}u \; f_{M,u}(m,u)\, dmdu \tag{D.57}$$

$$= e^{-\frac{\sigma_h^2}{2}} \int_{-\infty}^{\infty}\int_{-\infty}^{\infty} e^{h}u \; f_{H,u}(h,u)\, dhdu \tag{D.58}$$

Now the joint distribution is Gaussian as:

$$f_{H,u}(h,u) = \frac{\exp\left[-\frac{1}{2(1-\rho^2)}\left[\frac{h^2}{\sigma_h^2} - 2\rho\frac{hu}{\sigma_u\sigma_h} + \frac{u^2}{\sigma_u^2}\right]\right]}{2\pi\sigma_u\sigma_h(1-\rho^2)^{1/2}} \tag{D.59}$$

Using Eq. D.59, we can evaluate the integral in Eq D.58. The evaluation in terms of $u$ first is

$$\int_{-\infty}^{\infty} u \exp\left[-\frac{1}{2(1-\rho^2)}\left[\frac{h^2}{\sigma_h^2} - 2\rho\frac{hu}{\sigma_u\sigma_h} + \frac{u^2}{\sigma_u^2}\right]\right] du \tag{D.60}$$

$$= \exp\left(\frac{-h^2}{2\sigma_h^2}\right)\sigma_u^2\rho\frac{h}{\sigma_h}\sqrt{2(1-\rho^2)}\sqrt{\pi} \tag{D.61}$$

Substituting the integration result D.61 into D.58, we have

$$E\left[\widehat{X},u\right] = \frac{e^{-\frac{\sigma_h^2}{2}}}{2\pi\sigma_u\sigma_h(1-\rho^2)^{1/2}}\int_{-\infty}^{\infty}\exp\left(\frac{-h^2}{2\sigma_h^2}\right)\sigma_u^2\rho\frac{e^h h}{\sigma_h}\sqrt{2(1-\rho^2)}\sqrt{\pi}dh \tag{D.62}$$

$$= \frac{e^{-\frac{\sigma_h^2}{2}}\sigma_u\rho}{\sqrt{2}\sqrt{\pi}\sigma_h^2}\int_{-\infty}^{\infty} h\exp\left(h - \frac{h^2}{2\sigma_h^2}\right)dh \tag{D.63}$$

$$= \frac{\sigma_u\rho}{\sqrt{2}\sqrt{\pi}\sigma_h^2}\int_{-\infty}^{\infty} h e^{-\frac{\left(h-\sigma_h^2\right)^2}{2\sigma_h^2}}dh \tag{D.64}$$

Let

$$v = \frac{(h-\sigma_h^2)}{\sqrt{2}\sigma_h} \tag{D.65}$$

$$h = \sqrt{2}\sigma_h v + \sigma_h^2 \tag{D.66}$$

$$dh = \sqrt{2}\sigma_h dv \tag{D.67}$$

So:

$$E\left[\widehat{X},u\right] = \frac{\sigma_u\rho}{\sqrt{\pi}\sigma_h}\int_{-\infty}^{\infty}\left(\sqrt{2}\sigma_h v + \sigma_h^2\right)e^{-v^2}dv \tag{D.68}$$

$$= \frac{\sigma_u\rho\sigma_h}{\sqrt{\pi}}\int_{-\infty}^{\infty} e^{-v^2}dv \tag{D.69}$$

$$= \frac{\sigma_u\rho\sigma_h}{\sqrt{\pi}}\sqrt{\pi} = \rho\sigma_u\sigma_h = \overline{h'u'} \tag{D.70}$$

So:

$$\overline{x'u'} = \overline{h'u'} \tag{D.71}$$

under the zero mean conditions for $X$ and $u$. Then according to Eqs. D.46 and D.52, we have:

$$\overline{\Omega'u'} = \overline{\Omega}\ \overline{h'u'} \tag{D.72}$$

# Appendix E

# Diffusion and Advection Mass Transfer from DNAPL Pools

Here we compare the mass transfer from a DNAPL pool by diffusion and advection, in terms of mass transfer rate and DNAPL depletion time. The factors controlling the two mass transfer rate are identified.

## E.1 diffusive Mass Transfer

Figure E-1 illustrates the conceptual model of diffusive mass transfer from a DNAPL pool to the ambient groundwater. The governing equation of steady-state two-dimensional transport with one dimensional flow is written as:

$$V_2 \frac{\partial C}{\partial x} = D_T \frac{\partial^2 C}{\partial z^2} \tag{E.1}$$

with boundary condition:

$$C = C_s \quad x > 0, z = 0 \tag{E.2}$$

$$C = 0 \quad x = 0 \tag{E.3}$$

$$C = 0 \quad z = \infty \tag{E.4}$$

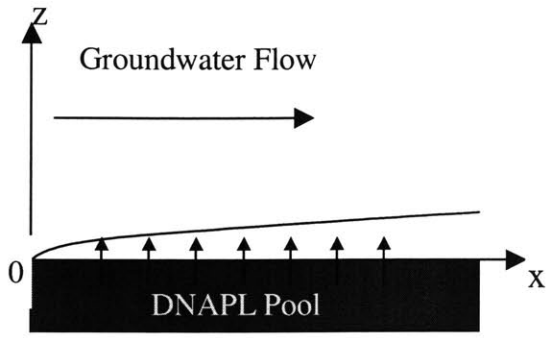


Figure E-1: Diffusion mass transfer from a DNAPL pool to the ambient groundwater water

where $D_T$ is the vertical diffusion coefficient and $V_2$ is the water velocity outside the pool, $C$ is the bulk concentration outside the DNAPL pool. The solution is obtained as:

$$C(x,z) = C_s\left(1 - \operatorname{erf}\left(\frac{z}{2\sqrt{D_T x/V_2}}\right)\right) \tag{E.5}$$

The vertical mass flux transport from the pool can be obtained as according to the boundary condition E.2:

$$J(x)_{z=0} = -D_T \frac{\partial C}{\partial z}_{z=0} = C_s\phi\sqrt{V_2 D_T/(x\pi)}$$

We can derive the mass transfer rate from a pool by diffusion as:

$$\frac{\partial M}{\partial t} = W_1 \int_0^{L_1} J(x)_{z=0}\, dx$$

where $L_1$, $W_1$ are length and width of the DNAPL pool. So $L_1 W_1$ represents the area of pool bottom. $M$ represents the mass of DNAPL in the pool. So the mass transfer rate is:

$$\frac{\partial M}{\partial t} = 2\phi C_s\sqrt{\frac{L_1 V_2 D_T}{\pi}} W_1 \tag{E.6}$$

Since the total mass of DNAPL can be expressed as:

$$M = V\phi S_n \rho_n$$

where $V$ is the volume of the pool zone, $\phi$ is the porosity, $S_n$ is DNAPL saturation inside the pool and $\rho_n$ is the density of DNAPL. So the time scale of mass depletion in a pool by diffusion can be found as:

$$T_D = \frac{M}{\frac{\partial M}{\partial t}} \tag{E.7}$$

$$T_D = S_n \frac{\rho_n}{C_s} \frac{H_1}{2} \sqrt{\frac{L_1 \pi}{V_2 D_T}} \tag{E.8}$$

where $H_1$ is the thickness of the pool.

## E.2 Advection Mass Transfer

The advection effect from a pool is illustrated in Figure 5-2 that a thin stream of water flow transport DNAPL out of the pool. Due to the high saturation, slow flow rate and high dissolution rate inside the pool, the concentration of the effluent from a pool is assumed to be at equilibrium. So the mass transfer rate from a pool is

$$\frac{\partial M}{\partial t} = C_s q_1 W_1 H_1 \tag{E.9}$$

The depletion time by the advection can be expressed similarly as diffusion case as:

$$T_a = \frac{M}{\frac{\partial M}{\partial t}}$$

$$T_a = \phi S_n \frac{\rho_n}{C_s} \frac{L_1}{q_1} \tag{E.10}$$

Table E.1: Input Parameters and Output Result of comparison of diffusion Mass Transfer with Addvection Mass Transfer from a Pool

| $\mathbf{L_1}(m)$ | $H_1(m)$ | $\mathbf{q_1/q_2}\,(m/d)$ | $\phi$ | $D_m\,(m^2/d)$ | $q_2\,(m/d)$ | $\tilde{\alpha}_T$ **(m)** | $\frac{T_D}{T_a}$ |
|---|---|---|---|---|---|---|---|
| 1 | 0.1 | 0.1 | 0.35 | $8\times10^{-5}$ | 0.3 | $2.7\times10^{-4}$ | 0.3 |

## E.3 Comparison of Time Scale by Two Mass Transfer Mechanism

By comparing the time scale for the deletion of DNAPL in a pool by two mass transfer mechanisms, the controlling mass transfer mechanism can be identified. The ratio of the diffusion time to the advection time is:

$$\frac{T_D}{T_a} = \frac{S_n \frac{\rho_n}{C_s} \frac{H_1}{2} \sqrt{\frac{L_1 \pi}{V_2 D_T}}}{\phi S_n \frac{\rho_n}{C_s} \frac{L_1}{q_1}} \tag{E.11}$$

$$= \frac{H_1 q_1}{2\phi L_1} \sqrt{\frac{L_1 \pi}{V_2 D_T}} \tag{E.12}$$

Since $V_2$ represents the pore velocity of wetting phase outside a pool and the local dispersion coefficient can be expressed as:

$$V_2 = q_2/\phi \tag{E.13}$$

$$D_T = q_2 \tilde{\alpha}_T = D_m \tag{E.14}$$

where $q_2$ is the specific discharge outside a pool, $D_m$ is molecular diffusion coefficient. Here we assume there is no mechanical dispersion at the boundary of the pool. So $\tilde{\alpha}_T$ is defined as

$$\tilde{\alpha}_T = \frac{D_m}{q_2} \tag{E.15}$$

So the ratio can be simplified as:

$$\frac{T_D}{T_a} = \frac{H_1}{2L_1} \frac{q_1}{q_2} \sqrt{\frac{L_1 \pi}{\phi \tilde{\alpha}_T}} \tag{E.16}$$

Typical values of a DNAPL pool and flow velocity are estimated in Table E.1.

The mass transfer due to the diffusion and advection is a function of the size of the DNAPL

pools, the transverse dispersivity, the ratio of the flow velocity inside and outside of pools. Under different situation, different mass transfer mechanism can dominate or both are important. Based on a set of typical values of input parameters listed in Table E.1, we can calculate the ratio of the depletion time of two mass transfer mechanism. The diffusion mass transfer can be dominant when the relative permeability inside a pool is significantly reduced due to high DNAPL saturation that the ratio of the velocity is really small, in addition of small pool thickness.

# Appendix F

# Flux Concentration Based Development

Since

$$\overline{C} = C_f - \frac{\overline{q'c'}}{q} \tag{F.1}$$

where $C_f$ is the flux concentration weighted by flows. So the concentration deficit can be written as:

$$\overline{u} = C_s - C_f + \frac{\overline{q'c'}}{q} \tag{F.2}$$

$$= u_f + \frac{\overline{q'c'}}{q} \tag{F.3}$$

where

$$u_f = C_s - C_f \tag{F.4}$$

Since

$$c' = -u' \tag{F.5}$$

So:

$$\overline{u} = u_f - \frac{\overline{q'u'}}{q} \tag{F.6}$$

$$= u_f - \overline{v'u'} \tag{F.7}$$

According to Eq. 4.61:

$$\overline{v'u'} = \overline{u}\left(-\overline{\Omega}I_1 + q\mu I_2\right) \tag{F.8}$$

So:

$$\begin{aligned} u_f &= \overline{u} + \overline{v'u'} = \overline{u} - \overline{u}\left(-\overline{\Omega}I_1 + \mu I_2\right) && \text{(F.9)} \\ &= \overline{u}\left(1 + \overline{\Omega}I_1 - \mu I_2\right) && \text{(F.10)} \end{aligned}$$

So:

$$\overline{u} = \tau u_f \tag{F.11}$$

where

$$\tau = \frac{1}{1 + \overline{\Omega}I_1 - \mu I_2} \tag{F.12}$$

Using Eq. F.11 and the mean equation in Eq. 4.67, we have

$$q_e \frac{\partial}{\partial x_1}\left(\tau u_f\right) - D_e \frac{\partial^2\left(\tau u_f\right)}{\partial x_1^2} = -\tau u_f \Omega_e \tag{F.13}$$

Since $I_1$ and $I_2$ are integral results which are independent with $x$ and $\overline{\Omega}$ is constants, so $\tau$ is not a function of $x_1$ and can be cancel out on both sides:

$$q_e \frac{\partial}{\partial x_1} u_f - D_e \frac{\partial^2 u_f}{\partial x_1^2} = -u_f \Omega_e \tag{F.14}$$

So we find that the effective properties obtained for the resident concentration field are unchanged for the flux concentration. So the effective results can be directly used to compare the observed concentration data from field samples.

# Appendix G

# Hydraulic Conductivity and Two-phase Flow Characteristic Data Reported at Savannah River Site

**Soil Moisture/Capillary Pressure Data for T2VOC Modeling**

| Name | Type | Depth (feet) | Sm | alphagw m-1 | alphagn m-1 | alphanw m-1 | n | k m2 | Ref. |
|---|---|---|---|---|---|---|---|---|---|
| MHB-4T | sandy clay | 40-42 | 0.05 | 16.7 | 38.2 | 25.5 | 1.09 | 4.60E-16 | Bramblett Thesis |
| MHB-1T | sandy clay | 40-42 | 0.15 | 29.4 | 57.9 | 38.2 | 1.012 | 4.00E-17 | Bramblett Thesis |
| MHB-1T | sand | 80-82 | 0.15 | 50 | 118 | 75.5 | 1.23 | 1.70E-12 | Bramblett Thesis |
| sand1 | sand | | 0.15 | 0.00099967 | 0.001 | 3 | 0.1 | 1.00E-12 | T2VOC |
| atmos | | | 0.15 | 0.00099967 | 0.001 | 3 | 0.05 | | T2VOC |
| clay1 | clay | | 0.35 | 0.00099967 | 0.001 | 3 | 0.25 | 1.00E-15 | T2VOC |
| Drainage | | | | | | | | | |
| **MOX-2A** | **Sand w/silt** | **67-69** | **0.3751** | **20.0572** | **46.1380** | **32.5252** | **1.3451** | **2.40E-12** | Law Engineering |
| MOX-2B | Silty Clayey Sand | 107-109 | 0.2000 | 16.2450 | 37.3687 | 26.3432 | 1.4849 | 1.50E-16 | Law Engineering |
| MOX-2C | Sand w/silt | 127-129 | 0.0805 | 2.0121 | 4.6284 | 3.2628 | 4.4483 | 2.60E-13 | Law Engineering |
| MOX-2D | Silty Sand | 137-139 | 0.0500 | 1.5787 | 3.6316 | 2.5601 | 2.1117 | 1.80E-15 | Law Engineering |
| MOX-3A | Sand w/silt | 107-109 | 0.2000 | 1.8567 | 4.2710 | 3.0109 | 1.2536 | 9.80E-14 | Law Engineering |
| MOX-3B | Sand w/silt | 127-129 | 0.4150 | 1.5163 | 3.4880 | 2.4589 | 4.4195 | 3.40E-13 | Law Engineering |
| MOX-5 | Silty Sand | 155-157 | 0.2000 | 1.1327 | 2.6055 | 1.8368 | 1.6363 | 5.20E-15 | Law Engineering |
| Drainage | | | | | | | | | |
| MHB-1Ta | clayey sand | 31-33 | 0.2088 | 2.1964 | 5.0524 | 3.5617 | 1.5548 | 1.80E-17 | |
| MHB-1Tb | sandy clay | 40-42 | 0.9686 | 0.8384 | 1.9285 | 1.3595 | 1.9567 | 3.50E-17 | |
| MHB-1Tc | silty sand | 56-58 | 0.2517 | 9.5390 | 21.9428 | 15.4687 | 1.3654 | 3.30E-13 | |
| **MHB-1Td** | **sand w/silt** | **80-82** | **0.2726** | **5.7561** | **13.2410** | **9.3343** | **1.3219** | **1.50E-12** | |
| MHB-1Te | sand w/silt | 100-102 | 0.2654 | 100.0000 | 230.0319 | 162.1622 | 1.2657 | 5.50E-13 | |
| MHB-1Tf | sandy clay | 110-112 | 0.0967 | 90.7280 | 208.7034 | 147.1265 | 1.9023 | 4.00E-13 | |
| MHB-1Tg | sand w/silt | 130-131.3 | 0.3314 | 100.0000 | 230.0319 | 162.1622 | 1.4179 | 1.10E-12 | |
| MHB-4Ta | sandy clay | 40-42 | 0.2000 | 2.3120 | 5.3183 | 3.7492 | 1.1108 | 4.00E-16 | |
| MHB-4Tb | clayey sand | 60-62 | 0.2707 | 100.0000 | 230.0319 | 162.1622 | 1.3865 | 5.60E-13 | |
| **MHB-4Tc** | **clayey sand** | **70-72** | **0.4695** | **6.1529** | **14.1537** | **9.9777** | **1.3664** | **4.00E-14** | |
| MHB-4Td | sand w/silt | 80-82 | 0.4871 | 100.0000 | 230.0319 | 162.1622 | 1.2999 | 1.40E-12 | |
| **MHB-4Te** | **sandy clay** | **110-112** | **0.9012** | **3.1387** | **7.2201** | **5.0898** | **1.3369** | **6.20E-18** | |
| **MHB-8Ta** | **silty sand** | **155-157** | **0.6065** | **0.2369** | **0.5448** | **0.3841** | **3.1271** | **3.40E-16** | |
| MHB-8Tb | clayey sand | 170-171 | 0.2000 | 0.5576 | 1.2827 | 0.9043 | 1.3110 | 4.00E-16 | |
| MHT-10B | sand w/silt | 201-201.7 | 0.5733 | 0.5318 | 1.2233 | 0.8624 | 2.1030 | 4.30E-14 | |
| MHT-11Ca | clayey sand | 165-167.75 | 0.2000 | 36.0571 | 82.9428 | 58.4709 | 1.0940 | 1.90E-16 | |
| MHT-11Cb | sand w/silt | 200-202.4 | 0.3347 | 2.8388 | 6.5301 | 4.6034 | 1.6728 | 2.50E-13 | |
| MHT-12C | sand | 200-202.2 | 0.1423 | 2.6315 | 6.0532 | 4.2672 | 2.1937 | 3.80E-13 | |

Figure G-1: Hydaulic conductivity and two-phase flow characteristic data reported at the Savannah River Site